https://theses.gla.ac.uk/

Theses Digitisation:

https://www.gla.ac.uk/myglasgow/research/enlighten/theses/digitisation/

This is a digitised version of the original print thesis.

Copyright and moral rights for this work are retained by the author

A copy can be downloaded for personal non-commercial research or study, without prior permission or charge

This work cannot be reproduced or quoted extensively from without first obtaining permission in writing from the author

The content must not be changed in any way or sold commercially in any format or medium without the formal permission of the author

When referring to this work, full bibliographic details including the author, title, awarding institution and date of the thesis must be given

Enlighten: Theses
https://theses.gla.ac.uk/
research-enlighten@glasgow.ac.uk

AN OPTO-ELECTRONIC STAND-OFF SENSOR FOR ROBOTICS

HUSSEIN ALI ABDULLAH

(BSc Baghdad)

SUBMITTED AS A THESIS FOR THE DEGREE

OF

MASTER OF SCIENCE

IN ENGINEERING

DEPARTMENT OF MECHANICAL ENGINEERING

FACULTY OF ENGINEERING

UNIVERSITY OF GLASGOW

© Hussein Ali Abdullah

September 1988

ProQuest Number: 10998024

All rights reserved

INFORMATION TO ALL USERS
The quality of this reproduction is dependent upon the quality of the copy submitted.

In the unlikely event that the author did not send a complete manuscript
and there are missing pages, these will be noted. Also, if material had to be removed,
a note will indicate the deletion.

ProQuest 10998024

Published by ProQuest LLC (2018). Copyright of the Dissertation is held by the Author.

All rights reserved.
This work is protected against unauthorized copying under Title 17, United States Code
Microform Edition © ProQuest LLC.

ProQuest LLC.
789 East Eisenhower Parkway
P.O. Box 1346
Ann Arbor, MI 48106 – 1346

TO MY FATHER, MOTHER AND AWSAF

WITH ALL MY LOVE

ACKNOWLEDGEMENTS

I wish to express may thanks to my supervisors Mr. Finlay D. Buchan and Prof. Brian F. Scott for their guidance, advice and constant encouragement throughout this research.

Thanks are also due to the staff of the Mechanical Engineering Department especially: Mrs. L. McCormick, Mrs. C. Carmichael, Mr. Duncan Robertson, Mr. Cameron Millar and Mr. George Falconer.

Special thanks are due to my family for their patience and support.

Finally, thanks are reserved for the Government of the Republic of Iraq for their financial and moral support.

SUMMARY

This thesis presents an opto-electronic stand-off sensor and actuation system developed for robotic applications. The measuring principle is based on an on-axis method of detecting variation in a beam reflected from a surface. The sensor utilizes two photodiodes to measure the difference in beam power falling through two pinholes, to estimate the distance between the workpiece surface and incident focused beam waist. The output voltage from the differential stage is normalized to negate the effects of surface reflectivity, colour, and texture.

Two mathematical models are presented which simulate the device. The first depends only on the theory of propagation of gaussian beams, whilst the second relies upon simulating the reflected beam using geometrical optics to calculate the radiometric distribution at the detecting pinholes.

A set of experiments were performed to analyze and optimize the performance of a number of sensor configurations. The experimental results are bounded between gaussian and radiometric model results. A comparison of the results of the three models, conclusions regarding sensor performance and principles for optimally designing such systems are given.

A proportional control circuit for one sensor servo combination was designed and tested using a solenoid as an actuator. The predicted performance of the complete servo system was modelled utilizing the ACSL language. While an experimental rig was built and experiments designed to analyze the output of the system in response to a step input.

The results of this show that the stand-off system gives varying response to different materials indicating that the electronic method of normalizing the sensor output is insufficient. The results also show that the device is sensitive to controller gain and behaves in a non-linear fashion as predicted. The actual response is generally faster than the predicted response.

Conclusions and recommendations for further work and development are given.

CONTENTS

Page no.

Acknowledgements i

Summary ii

Contents iii

List of figures vii

List of graphs x

Nomenclature xii

Chapter 1 : Introduction 1

1.1-Introduction 2

1.2-General sensor specification 3

1.3-Scheme chosen 4

1.4-Robotic sensors 4

1.4.1 Optical sensors 7

1.5-Profilometer 10

1.5.1 Optical profilometer 11

Chapter 2: Propagation of gaussian beams and associated radiometric theory 15

2.1-Introduction 16

2.2-Gaussian theory 16

2.2.1 Propagation through free space 17

2.2.2 Propagation through non-truncating thin lens 23

2.3-Radiometric theory 28

2.3.1 Radiometric units 28

2.3.2 Point sources 31

2.3.3 Lambertian sources 33

2.4-Summary of theoretical results 35

Chapter 3 : Mathematical modelling 37

3.1-Introduction 38

3.2- Measuring principle 38

3.2.1 The differential photodiode method 40

3.3-Gaussian modelling 44

3.3.1 Gaussian analysis 44

3.3.2 Gaussian modelling program 49

3.3.3 Results of simulation 51

3.4-Radiometric modelling 55

3.4.1 Radiometric analysis 55

3.4.2 Radiometric modelling program 62

3.4.3 Results of simulation 62

Chapter 4 : Experimental Modelling 67

4.1-Introduction 68

4.2-Experimental apparatus 68

4.2.1 Optical system 69

4.2.1.1 Alignment of optical components 71

4.2.2 Transducers and signal conditioning system 71

4.2.2.1 The differential amplifier 72

4.3-Experimental procedure 74

4.4- Results 75

4.5-Comparison between mathematical and experimental modelling 79

Chapter 5 : Closed loop stand-off system design and operational characteristics 105

5.1-Introduction 106

5.2-Control issues 106

5.3-Actuation 108

5.4-The control circuit 110

5.4.1 System model 112

5.5-Predicted performance 114

5.6-Operational characteristics 116

5.6.1 Results 119

Chapter 6 : Conclusion 133

6.1-Discussion and conclusions 134

6.2-Further work and development 137

Appendices 138

Appendix (A1) General definition, classification and application of robots 139

Appendix (A2) Robot internal sensors 145

Appendix (A3) Robot external sensors 148

Appendix (A4) Review of work conducted in the field of a gaussian beam generation, transmission and modification 153

Appendix (A5) Derivation of formula for the total power with in a gaussian geam 154

Appendix (A6) Derivation of gaussian beam divergence 156

Appendix (A7) Gaussian beam simulation program 157

Appendix (A8) Derivation of the total power transmitted through a pinhole 170
Appendix (A9) Gaussian-radiometric simulation program 172
Appendix (A10) Alignment procedure 186
Appendix (A11) Block diagram representation and mathematical modelling 188
Appendix (A12) Robotic actuators 196
Appendix (A13) ACSL control program 198
Appendix (A14) Gaussian radiometric subroutine for control simulation 200

References 204

LIST OF FIGURES

Figure no.		Page no.
1.1	Robot sensor classification	5
1.2	Robot sensing architecture	6
2.1	The intensity profile of a gaussian beam of radius W	18
2.2	Propagation of a gaussian beam in free space	20
2.3	Near-field Far-field distances	21
2.4	Plot of the radius of curvature (R) versus the distance (Z) from the beam waist	22
2.5	Gaussian beam transformed by a lens	24
2.6	The solid angle Ω for the area dA on a sphere of radius R	30
2.7	Radiant intensity of a point source with solid angle Ω	31
2.8	Radiance of an extended source to an area making an angle θ with the normal	33
2.9	Radiant intensity from a point source to an area making an angle θ with the normal	34
3.1	The measurement principle	39
3.2a	One photodiode output	42
3.2b	Output of two photodiodes offset from Z'=0 by a distance ±l	42
3.2c	Output of photodiodes after amplification and subtraction	42
3.3a	Principle of differential photodiode method	43
3.3b	The differential signal	43
3.4	One arm of the optical system for the gaussian model	45
3.5	The flow chart of the gaussian modelling program	50
3.6	Gaussian simulation results for 75mm lens	52
3.7	Gaussian simulation results for 120mm lens	53
3.8	Gaussian simulation results for Dobosz parameters	54
3.9	Diagram showing radiometric method of modelling	56

Figure no.		Page no.
3.10	The total power emitted from the beam spot on the workpiece surface toward a pinhole	60
3.11	The flow chart of the radiometric modelling program	63
3.12	Radiometric simulation results for 75mm lens	64
3.13	Radiometric simulation results for 120mm lens	65
3.14	Radiometric simulation results for Dobosz parameters	66
4.1	The experimental components	70
4.2	The circuit diagram of the amplifier	73
4.3	The front view of the amplifier	74
4.4	Overlapping of photodiode output voltages	76
5.1	Block diagram of a closed-loop control system	107
5.2	Block diagram of a unity feed-back control system	107
5.3	Block diagram of open-loop control system	108
5.4	Schematic diagram for solenoid	109
5.5	Block diagram of the control system using a solenoid	111
5.6	The solenoid current model	112
5.7	Output results of the predicted performance	115
5.8	Schematic diagram of apparatus used in control experiments	117
5.9	Circuit diagram of the proportional controller	118
A1.1	Cartesian configuration	141
A1.2	Spherical configuration	141
A1.3	Cylindrical configuration	142
A1.4	Anthropomorphic configuration	142
A1.5	SCARA configuration	143
A2.1	A rotary potentiometer	146
A2.2	A linear variable differential transformer (LVDT)	146
A3.1	The organization of a robot vision system	148

Figure no.		Page no.
A3.2	Range sensing by triangulation	149
A3.3	The design of a time flight sensor	149
A3.4	Sensor utilizing a structured light approach	150
A3.5	Tactile array sensor	151
A3.6	Slip sensor	152
A5.1	On axis view of a gaussian beam intensity distribution	154
A8.1	The total power emitted from the beam spot on the workpiece surface toward a pinhole	170
A8.2	The pinhole elemental cross sectional area dA	170
A8.3	The source elemental cross sectional area dS	170
A11.1	Block diagram representation	188
A11.2	Signal arrows	188
A11.3	A junction point	189
A11.4	Block diagram of a comparator	189
A11.5	Spring characteristics	190
A11.6	Viscous damper characteristics	190
A11.7	Inertial characteristics of an accelerating mass	191
A11.8	Mass-spring-damper combination	192
A11.9	Representation of resistor	192
A11.10	Representation of inductor	193
A11.11	Representation of capacitor	193
A11.12	Resistor, inductor and capacitor series circuit	194
A11.13	Block diagram of the charge Q for series RLC circuit	194
A12.1	Double action hydraulic actuator	196

LIST OF GRAPHS

Graphs no.		Page no.
4.1	Effect of the pinhole offset distance (75mm lens)	82
4.2	Effect of the pinhole offset distance (120mm lens)	83
4.3	Effect of the pinhole size (75mm lens)	84
4.4	Effect of the pinhole size (120mm lens)	85
4.5	Effect of the distance between laser and main lens (75mm lens)	86
4.6	Effect of the distance between laser and main lens (120mm lens)	87
4.7	Effect of the angle of the workpiece (75mm lens)	88
4.8	Effect of the angle of the workpiece (120mm lens)	89
4.9	Effect of increasing the distance between the main and image lenses (75mm lens)	90
4.10	Effect of increasing the distance between the main and image lenses (120mm lens)	91
4.11	Effect of reducing the distance between main and image lenses (75mm lens)	92
4.12	Effect of reducing the distance between main and image lenses (120mm lens)	93
4.13	Effect of different main and image lenses	94
4.14a	Effect of pinhole offset distance (75mm lens)	95
4.14b	Effect of pinhole offset distance (120mm lens)	95
4.15a	Effect of pinhole size (75mm lens)	96
4.15b	Effect of pinhole size (120mm lens)	96
4.16a	Effect of distance between laser and main lens (75mm lens)	97
4.16b	Effect of distance between laser and main lens (120mm lens)	97
4.17a	Effect of distance between the main and image lenses (75mm lens)	98
4.17b	Effect of distance between the main and image lenses (120mm lens)	98
4.18	Gaussian and radiometric normalized output for Dobosz parameters	99

Graphs no.		Page no.
4.19	Gaussian and radiometric normalized output for 10mm main lens and 30mm image lens	100
4.20	Gaussian and radiometric normalized output for 10mm main lens and 230mm image lens	101
4.21	Effect of laser wavelength	102
4.22	Effect of initial beam waist radius	103
4.23	Effect of changing the distance between laser and main lens	104
5.1	Step response for Mild steel	123
5.2	Step response for Galvanised steel	124
5.3	Step response for Formica	125
5.4	Step response for Mild steel	126
5.5	Step response for Mild steel	127
5.6	Forward and backward step responses for Mild steel	128
5.7	Different step responses for Mild steel	129
5.8	Different theoretical step responses	130
5.9	Profile of three different materials	131
5.10	Response time for mild steel with different gain	132
5.11	Steady state error for mild steel with different gain	132

<u>NOMENCLATURE</u>

Symbol	Definition	Unit
(for gaussian propagation)		
W_o	Beam waist radius	m
d_o	Beam waist diameter	m
W_z	Beam radius at distance (Z)from the beam waist	m
θ_f	Full angle beam divergence	radian
θ_h	Half angle beam divergence	radian
Z_R	Rayleigh range	m
R	Phase front Radius of curvature	m
I_o	Maximum beam intensity	W/m^2
I_r	Intensity at radius (r) from the beam axis	W/m^2
f	Lens focal length	m
m	Lens magnification	
λ	Wavelenght of light	m
d_i	Axial distance between beam waist and centre of the lens (i)	m
P_T	Total beam power	W
ρ	Aperture radius	m
(for radiation propagation)		
ϕ_e	Radiant flux or (power)	W
Q_e	Radiant energy	J
U_e	Radiant density	J/m^3
M_e	Radiant emittance	W/m^2
I_e	Radiant intensity	W/sr
Ω	Solid angle	sr

E_e	Irradiance	W/m^2
L_e	Radiance	W/m^2sr

(for mathamatical models)

L_1	Main lens	
L_2	Unfolded Image of the main lens	
L_3	Image lens	
F	Object focal point of a lens	
F'	Image focal point of a lens	
f	Object focal length of a lens	m
f'	Image focal length of a lens	m
D	Distance between the focal plains of object and image lens.	
m	Lens magnification (gaussian model)	
n	Medium refractive index	
Z_2	Offset distance of the workpiece surface	m
d_P	Offset distance of the pinhole	m
P_P	Total power in front of the pinhole	W
P_{PN}	Total power transmitted through the pinhole	W
R_P	Radius of the pinhole	m
W_P	Beam radius in front of the pinhole	m
K_P	Photodiode sensitivity	
V_P	Photodiode output voltage	volt
V_T	Normalized output voltage	volt
K_A	Amplifier gain	
P_s	Total power falling on the workpiece surface	W

W_s	Beam radius on the workpiece surface	m
DP	Distance between the beam waist and Lens for the radiometric model	m
MP	lens magnification (radiometric model)	
D_s	Distance between main lens and the surface	m

(for system design)

K	Spring stiffness	N/m
B	Damping cofficient	N.s/m
m	Mass	kg
F	Force	N
X	Displacement	m
R	Electrical resistance	ohm
I	Electrical current	ampere
C	Electrical capacitance	farad
V	Applied voltage	volt
L	Inductance	henry
K_c	Controller gain	
V_c	Controller voltage	volt
V_e	Error voltage	volt
I_{sol}	Solenoid current	ampere
K_{sol}	Solenoid constant	N/ampere

CHAPTER 1
INTRODUCTION

CHAPTER 1: INTRODUCTION

1.1 Introduction:

The aim of the work presented is the design and development of an opto-electronic stand-off sensor for use in robotic applications. That is a noncontact instrument capable of measuring the distance between an end effector and a workpiece (stand-off distance).

The stand-off distance sensor developed is shown to be both accurate and sensitive with a variable range of acquisition. Additionally the level of signal processing required is simpler and faster than more complex methods, such as those required by a vision system.

Stand-off sensors are used in a large number of applications including: seam tracking, range, height and proximity sensing. If the stand-off distance, can be accurately measured and the robot's end effector can be made to accurately follow a workpiece profile, then robots can accomplish tasks, such as laser welding or slitting, surface inspection, or dimensional measurement successfully, whilst ensuring safe operation.

A general definition of robots including: basic components, classification and application is given in appendix (A1).

To perform the applications described robots must be: accurate, reliable and cost effective and in order to achieve these goals robots must be aided by sensors. Sensory systems impart the capacity for the robot to respond to variables in its environment. Much of robotics research has been and is still concerned with how to equip robots with more effective sensors and it is to this goal that the research detailed in this thesis is aimed.

The structure of this thesis is as follows :

A review of robot sensors generally and optical sensors in particular is given. Chapter 2 presents a review of the propagation of gaussian beams and radiometric theory, supported by mathematical analysis. In chapter 3 the structure of the mathematical modelling of the chosen sensor is detailed and modelling programmes together with results of simulations are presented. Chapter 4 describes the experimental modelling undertaken including: experimental apparatus, procedures used and experimental results. A comparison of the mathematical and experimental results is given in chapter 4. In chapter 5 the design of a

complete stand-off system is presented and control issues are introduced. Simulation of the control circuit is described and the results obtained from simulation are compared with experimental results. The last chapter draws conclusions, discusses the work and makes recommendations for future research

1.2 General Sensor Specification:

Generally, to design a sensor for robotics, the designer should know the general required characteristics of that sensor. A generic design can then be produced containing many parameters affecting the sensor output, which may be calculated later to achieve optimal performance for a specific sensor task.

The general sensor specification, around which this work is based can be stated in the following design requirements for a robot sensor.

1. Noncontact, no physical contact with the object.
2. The ability to range a variety of materials and surfaces, with different colour, profile and texture, without recalibration.
3. The ability to determine its present position, with regard to the correct position, in order that a control signal can be generated.
4. The ability to measure the depth of holes with an aspect ratio of around 10.
5. Wide ranging sensitivity, giving a measurement accuracy as high as possible commensurate with the range of the signal acquisition.
6. Rapid response time.
7. Small size, compatible with being mounted on a robot arm or end effector.
8. The total cost of building, installing and operating to be low in comparison with other visual sensors.
9. The transduced signal should not require expensive processing techniques.
10. A sensor output compatible with a wide variety of control systems.

1.3 Scheme Chosen:

Since, the general specification has been stated in the previous section, the chosen scheme should be selected from all the techniques available and should be the one which fits the sensor specification most closely.

To satisfy the first, fourth and eighth requirements, an optical sensor employing an on-axis principle was chosen as being most suitable. A normalized differential photodiode method of detection was used, to satisfy the second, third, ninth and tenth criteria. This method and the measuring principle of the sensor are described in more details in chapter 3. The fifth requirement is satisfied as the current devices can be operate over a range of ±12mm, this could quite easily be increased to ±20mm, by minor modifications. By using a collimated diode laser and reducing the optical focal lengths and diameters, point seven can be demonstrated.

A feed back control loop using a proportional controller was chosen to satisfy the sixth requirement.

1.4 Robotic Sensors:

Robots are designed to carry out predetermined tasks and sensors are needed to optimally accomplish these. Sensors recover information from the robotic environment and pass this to the robot controller either directly in digital (bi-stable or word) form or through an A/D converter.

Robot sensing can be defined as in Refs.(6,7) as the translation of relevant characteristics or relational object properties into the information required to perform a given robot function. The object properties are basically mechanical, optical, electrical and magnetic.

Robot sensors may be classified as external and internal sensors fig.(1.1). Internal sensors send information as to the state of the robot itself, such as joint speed, acceleration

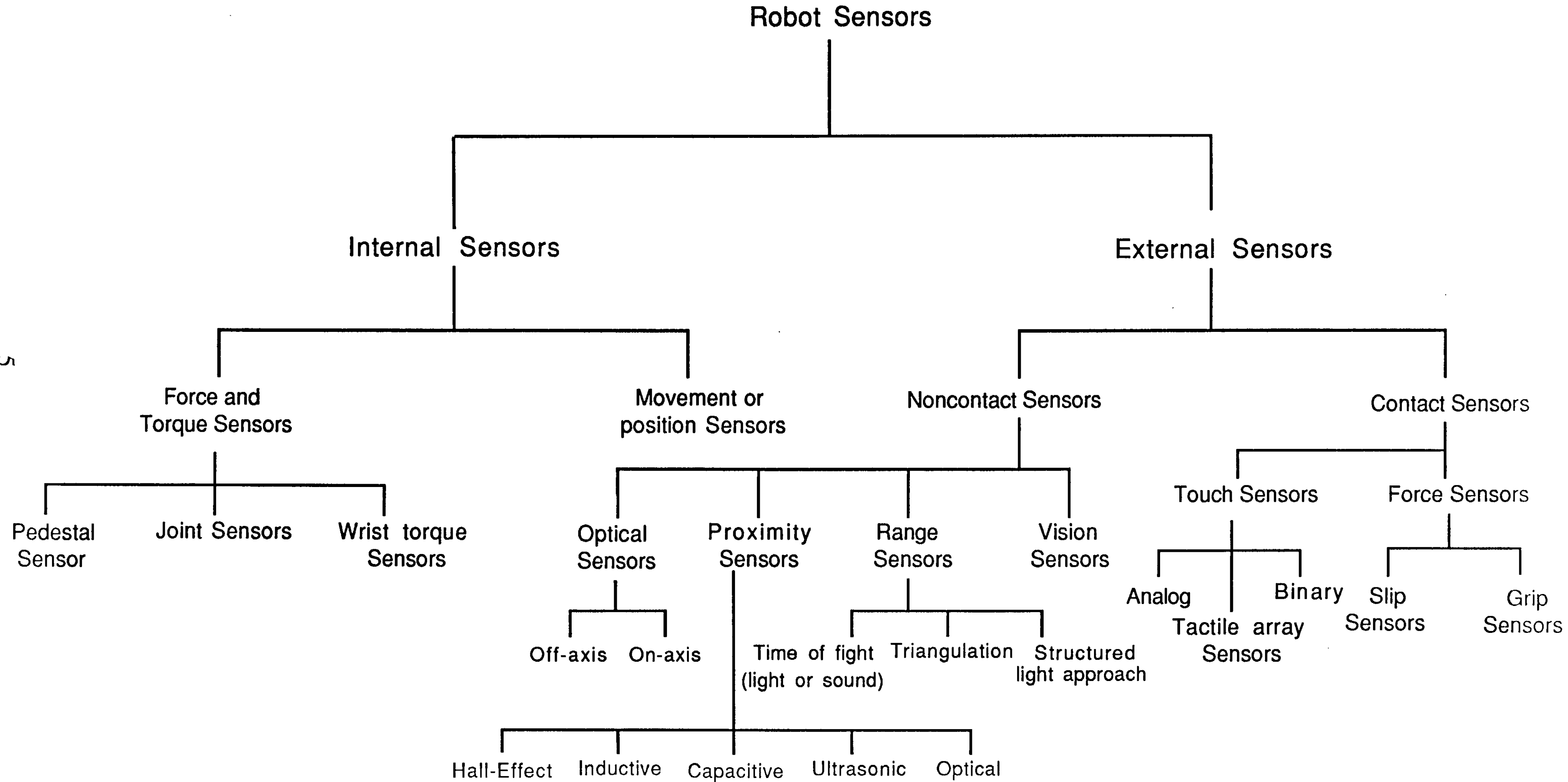

Figure 1.1 Robot sensor classification

and position, to the controller. Internal sensors can be divided into the following categories: force or torque sensors and movement or position sensors see appendix (A2). External sensors are used to sense the environment in which the robot operates. These may be classified as noncontact or contact see appendix (A3) on their basis of information acquisition. Noncontact sensors operate without requiring direct physical contact with the object being sensed and as a result, are less exposed to the risk of physical damage.

Robot sensors can also be classified as active or passive devices Ref.(6,7).

The study of sensor requirement, sensor function and data analysis techniques is a growing area in robotics, with novel categories of sensor still under research.

A robot sensing architecture is shown in fig.(1.2). The output of the acquisition stage is a signal either in digital or analog form. A digital signal may be fed directly to robot controller. Analog signals require to be conditioned and converted into digital words by A/D converters before being directed to a robot controller. Interpretation of data takes place within the controller where control function is generated. Unwanted data are either discarded or stored for later use. Control signals are then fed to the robot actuation system to drive the manipulator to perform a robot function.

The sensor described in this thesis is an external sensor used to acquire environmental status, designed to the general specifications presented later in section 1.4..

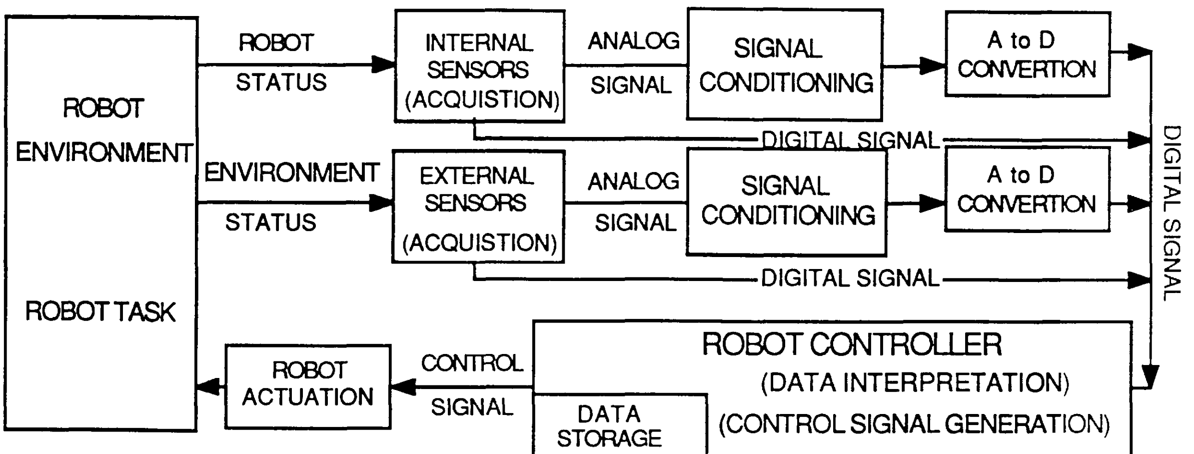

Figure 1.2 Robot sensing architecture

1.4.1 Optical Sensors :

An Optical sensor is by definition a noncontact sensor, which uses visible or invisible light as a medium for information transfer. Associated optical and opto-electronic components are used to modulate and measure returned data. Generally, the principle of operation is based on the focusing of a light beam on an object and the detection of the returned light by means of a photodetector. Optical sensors are used in sensing the location, presence or absence, distance and orientation of an object surface.

Simple (binary) optical proximity sensors are designed to sense the reflection of diffuse light from a surface physically close to the sensor, or the interruption of a light beam between source and sensor. More complex devices, known as range sensors, [see appendix (A3)] are fixed on the end of a manipulator to keep a specific distance from a surface while performing machining or inspection tasks these being termed stand-off sensors. Other devices directly inspect the machined surface properties of components.

A wide variety of optical sensors are available making use of different methods of: propagation and collection techniques, optical measurement schemes and photodetector layouts. Indeed it is difficult to separate vision systems from optical sensors since both relay upon optical information transfer.

Optical sensors are often preferred in robotics application for the following advantages :

- No physical contact is required.
- Sensitive and accurate devices can be manufactured inexpensively.
- Both smooth and rough surfaces can be detected.
- Both solid and liquid states can be detected.
- They can be made physically small.
- Their total cost is less than computer based visual systems.
- The physical characteristics of the object, such as its thickness, or the near presence of edges, holes or cracks do not affect signal integrity.
- Only low level processing of the output signal is required.

In response to these advantages research have been conducted within this field to

develop and demonstrate optical sensors suitable for robot applications. The following brief review presents some of these according to the following application areas: seam tracking, range, height and proximity sensing.

For seam tracking applications Porsander T. and Sthen T. in 1983 Ref.(11) designed an adaptive torch positioner (seam finder). This consisted of an optical sensor and integrated microcomputer which interpreted sensor data and sent an appropriately formatted error signal to the robot controller. The optical sensor was mounted on the welding torch holder of an ASEA robot to form a measuring spot approximately 20mm ahead of the welding area. The sensor system was located about 175mm above the surface and utilized an off-axis principle of spot projection.

Bjorkelund M. in 1986 presented a paper for a seam-tracker sensor for arc welding robots Ref.(11), based on the same measuring principles as the previous seam finder. With the reflected light being electronically analyzed to determine the welding profile.

Another example of a tracking sensor is a real time optical sensor integrated into a PUMA robot end effector Ref.(12). This demonstrated the ability to follow a two dimensional tracking path by correcting the position of the robot arm. It consisted of an imaging system and four quadrant position sensing spot detector.

An optical range sensor for measuring distance and orientation at a range of four to five centimeters was developed by Kanade T. and Sommer T. M. in 1983 Ref.(13). The sensor utilized multiple infrared LEDs as the light source and a PIN-diode area sensor chip for detecting spot position. The sensor generated about 1000 reading of distance and orientation per second with a precision of 70μm and 1.5^{o} over the range of 40mm to 50mm and $+30^{o}$ to -30°.

A group of investigators in Stanford University developed an optical sensor for range and depth measurement using an optical microscope Ref.(14), This has a resolution of the order of 2μm at a distance of 10-20cm. Two techniques were employed, the first determined for the maximum reflected amplitude, observed at the upper and lower surface of a transparent reflecting film. Whilst the second determined the film thickness from the

phase shift in the reflected beam.

One height sensor Ref.(15), which employed a diode laser light source was mounted on a three dimensional laser cutting machine (MELCUT-3DCM). This consisted of: diode laser, projecting and focusing lenses, protection glass, optical filter, position sensitive device (PSD), A/D converter and high speed processor. An off-axis principle was utilized to measure and control the stand-off distance between laser head and workpiece.

Optical devices have been used as a noncontact alternative to contact probing. One such device consisted of a (Unimate PUMA 560 MK2) robot, Addison Lasermike (type 8050), laser micrometer and Apple II microcomputer Ref.(16) and was used to inspect the external dimensions of turned components.

Optical sensors can be classified upon their reflected beam path: off-axis and on-axis. If the reflected beam in the sensor module returns along a different path to that of the initial probe beam, then it is sorted into the off-axis class. Conversely if the reflected beam returns along the same path as the inspection beam the sensor may be classed as on-axis.

It should be noted at this point that the vast majority of techniques researched to date have been based on off-axis principles.

1.5 Profilometer:

As apposed to optical sensors where the output is used to achieve a control function, profilometers are purely recording devices. This section examines different types of profilometers, including their measuring and operating principles and highlights the optical profilometer.

A profilometer is an instrument used to measure and inspect the profile of a machined surface and to translate it into an output identifying surface characteristics. Generally, profilometers can be classified into contact types such as, mechanical profilometers and noncontact profilometers based on pneumatic, optical or capacitive principles.

- Mechanical profilometer : This is the most widely used profilometer (commonly known as a Talysurf), utilizing a stylus in mechanical contact with the surface under inspection to perform a profile measurement. The disadvantages of this method are the need for mechanical contact, which causes wear of the stylus and damage to the measured surface and the restriction to hard solids. On the other hand, it is mechanically vigorous, simple and cheap.

- Capacitive or Inductive profilometers utilize changes in electrical properties between a probe tip and a surface. The output is amplified and linearized to produce a signal proportional to the distance between the tip and surface. Such methods are restricted in application to conductive or inductive materials and the presence of edges and holes or changes in material thickness cause erroneous outputs.

- Pneumatic profilometer : The operational principle used is to direct a gas jet flow from a nozzle at a surface and to measure the back pressure, this being a function of the distance between nozzle and surface. The disadvantage of this instrument is that it can only be used for scanning solid materials and the presence of holes or slits cause unpredictable behavior and as such is clearly not suitable for such processes such as, the slitting, drilling or joining of sheets.

1.5.1 Optical profilometer:

An optical profilometer is a noncontact device which makes use of light reflected from a surface to determine the profile of the surface under inspection. Such devices are fabricated from optical components such as, lenses, filters and beam splitters, which are used to condition and direct the light beam. Optical devices have the favorable features of being: inherently noncontacting, versatile in their range of application and suitable for miniaturization and in-line real time operation due to their rapid response Ref.(18).

Through out the literature three main themes can be observed as classifying optical profilometers:

1. Type of light source (laser, normal light) used.

2. Method of detection of the reflected beam including the number and type of the detectors (photodiode, photocell, astigmatic lens).

3. Path of the return beam (on-axis, off-axis).

One of the earliest studies of optical profilometers was carried out to enable micro displacements in vibrating surfaces to be measured without contact Ref.(19). The instrument consisted of: microscope lens, light source and focus analyzer. The operational principle was based on on-axis methods of focusing the light and analysis of the reflected light from the object. Two method of focus analysis were studied to determine the position of the surface. The first used the difference in modulation factors at planes located on either side of an image, so the output signal of the receptor (detector) gave an indication as to whether the correct focusing plane was obtained or not. A second method used the variation of the energy surrounding the refocused image of a point or slot.

The physical implementation of two receptors (detectors), two diaphragms and the bifurcation of the reflected beam was later utilized in another investigation Ref.(20), but with a laser providing the light source and an alternative method of mathematical analysis. The output of a differential amplifier was fed into a translation stage used to position the object surface. This method indicated a sensitivity of the order of 0.1μm with a spatial resolution of 2μm. The mathematical analysis performed used the developed method of

Operator Algebra and the characteristics of the Wigner distribution function.

A similar design was forwarded in 1983 by Dobosz Ref.(21), although the measuring principle was similar to the previous work, an alternative (and simpler) mathematical analysis based on the theory of propagation of gaussian laser beams was used. This work showed that instruments could be fabricated to perform measurement in three ranges: up to 1μm with resolution of ≈2nm, up to 200μm with a resolution of ≈0.1μm and up to several millimeters with a resolution of ≈0.1μm. The resolution of ≈2nm over 1μm range was experimentally demonstrated. The detection stage again made use of a two photodiode method utilizing a differential amplifier.

Later in 1985 Kleinknecht H. P. and Meter H. Ref.(22), published the design of an optical profilometer for measuring surface contours up to 150μm in profile based upon the differential photodiode method. This used a high-power microscope objective to focus a laser beam. Whilst the output signals of the two photodiodes were employed to drive a servo-motor to reposition the microscope objective lens.

Arecchi F. T., Bertani D. and Ciliberto S. described an optical profilometer for measuring roughness in the submicron range up to several tens of microns Ref.(23). The reflected laser beam was collected and focused upon a single pinhole with a photodetector placed behind it. The maximum output of the photodetector occurred when the focus of the objective lens coincided with the surface plane.

Other studies also utilized laser light sources ,but with alternative detection techniques. One of these methods was presented by Whitefield R. J., in 1975 Ref.(24), where he demonstrated an optical device utilizing diffraction analysis. The diffraction amplitude was obtained by using a chain of fourier transformation lenses, spatial filters and apertures. The reflected beam was trifurcated: one path being used for alignment of the illumination optics, one used to determine the reflected intensity from the surface and the third path used to conduct diffraction analysis, whereby the fourier transformed reflected beam was detected by x-y detector to form a signal representing a surface profile.

An alternative approach of profile detection is to make use of an astigmatic imaging

approach. This can generate a position error signal (PES), which can be used to drive the focusing lens back into the focal plane. This technique has been widely investigated Ref.(25) and utilizes an on-axis principle, where the returning beam is directed to an astigmatic measurement system. The astigmatic system consisted of: a quadrant detector placed at the midpoint of the two focal planes of an astigmatic lens combination. The PES is derived by taking the difference between the sum of the signals from the four parts of the quadrant detector. This technique is widely employed in compact disk players to maintain optimal focussing of the read head Ref.(26).

Other on-axis profilometers exploit incoherent (spectrally mixed or white) light sources for their operation. Quercioli F., Tiribilli B. and Molesini G. Ref.(27) designed and investigated a prototype of a noncontacting electro-optical probe for surface characterization. The optical apparatus consisted of: collimating lens, cube beam splitter, main focussing lens, dispersing element (prism) and image lens to focus a returned light beam on a linear photodiode array. The instrument employs a white light source to exploit the monotonic longitudinal chromatic aberration of a lens upon which its measuring principle is based. Accordingly the main lens is designed to have a back focal length that varies monotonically as a function of wavelength. The output signal from the photodiode array is converted to digital format and is monitored by a micro computer. The output signal takes a form of bell-shape and its peak position indicates which particular wavelength is in focus on the sample surface. As the probe scans the sample surface, the peak location shifts according to the variation in the height between the optical head and surface under test.

All the previous methods outlined are based on on-axis principles. An alternative technique is to make use of off-axis triangulation. One advantage gained by utilizing this technique is that there is no need to split the returned reflected beam out of the main laser beam. On the other hand, it is restricted in depth and hole measurement, as well as the tilt angle of the workpiece which limits the range of application.

One typical implementation of an off-axis method was a fast optical profilometer

presented in Ref.(28) which utilized an incandescent source. The light beam generated was collimated and focused by an objective lens on a test surface. The reflected light returned to an image lens along a different path where its position was sensed by a photodiode array, made more accurate by the use of a differential method of detection.

CHAPTER 2
PROPAGATION OF GAUSSIAN BEAMS AND ASSOCIATED RADIOMETRIC THEORY

CHAPTER 2: PROPAGATION OF GAUSSIAN BEAMS AND ASSOCIATED RADIOMETRIC THEORY

2.1 Introduction:

Laser light is a suitable source for many optical experiments because of a number of unique and useful properties, these include: high directionality, high brightness, monochromaticity and spatial and temporal coherence.

Because the power emitted from a laser is concentrated into a highly directional beam (whereas other sources of light are emitted in all directions from an extended source), even diffuse reflection, which have to pass through several air-glass interfaces, are sufficiently bright to be detectable with inexpensive sensors.

Laser light is commonly employed as a medium for the transmission of data in optical sensors. Since such optical sensors rely upon the propagation, reflection and detection of near gaussian beams. It is necessary that these elements can be sythesised, analysed and optimized to their desired function.

This chapter outlines the basic theory of propagation of gaussian beams through free space and non-truncating lens systems. Mathematical equations are presented which can be used to calculate required beam parameters. Additionally some principles of radiometry and how they are used to calculate intensity distributions of radiating sources are presented.

These theories are based upon the investigations of previous authors (referenced later). A summary of the equations derived is given for use in mathematical modelling.

2.2 Gaussian Theory:

A laser resonator can be considered as a light storage device in which the output mirror allows part of the stored energy to leak out. The resonator mode characterises the spatial distribution of stored light energy between the laser mirrors.

A laser may operate in one or many transverse electromagnetic modes(TEM). A beam with fundamental TEM_{oo} mode has a circular cross section with maximum intensity on the

beam axis decreasing radially away from the centre. In theory this profile is similar to a gaussian radial intensity variation, so the TEM_{00} mode output is often called a gaussian beam. In practice the intensity curve of a fundamental mode laser is not exactly of gaussian shape, but for the vast majority of modelling it may be taken as such.

Fundamental TEM_{00} mode of operation is desired for the following significant characteristics. The gaussian radial intensity distribution, has the highest possible intensity for a given diameter, the lowest divergence and provides spatial coherence. It has several names "gaussian beam", "diffraction limited mode". Low power lasers can be designed to operate in the TEM_{00} mode. While very high power lasers generally oscillate in higher - order modes(TEM_{mn}).

Many researchers have worked in the field of the gaussian beam theory. Its structure, profile, behavior and generation through the mode of oscillation is well described. Many formulas for tracing the characteristics of spherical gaussian beams through free space and lenses have been generated. Others have detailed methods for the measurement of the beam waist and its location. Previous research work has developed the theory of diffraction of gaussian beams to a high level and a short review highlighting a number of these works is given in appendix (A4).

Clearly, the design of an optical system utilizing a near gaussian beam, requires knowledge and understanding of its propagation through free space and its transformation through a thin lens, as a model of any non-truncating optical system may be constructed using these two basic units.

2.2.1 Propagation Through Free Space:

A beam having a circular cross section with a gaussian intensity distribution along a line perpendicular to the propagation axis, as in fig.(2.1) is commonly known as a gaussian beam. The intensity profile of a gaussian beam is given by Refs.(29,30,31) :

$$I_r = I_o\, e^{-2(r^2/W^2)} \qquad (2.1)$$

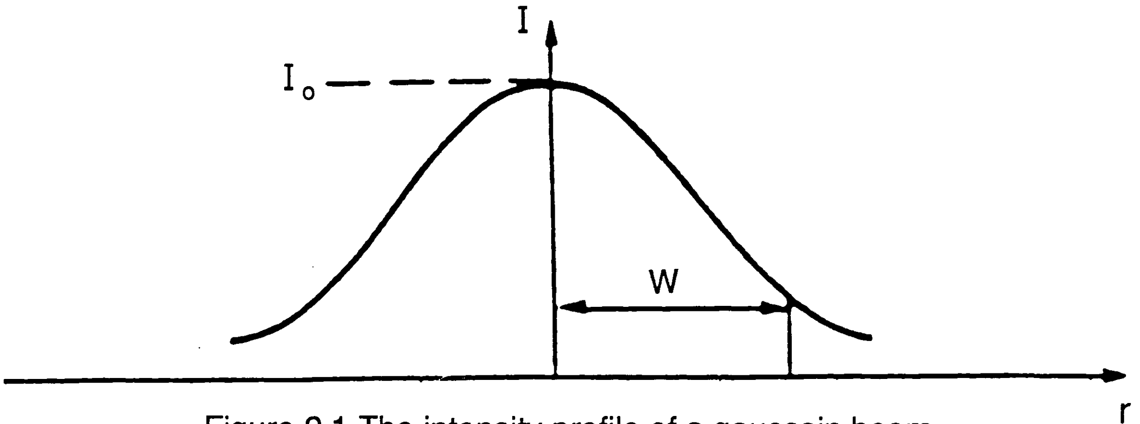

Figure 2.1 The intensity profile of a gaussain beam of radius W

Where I_o is the maximum intensity which occurs on the axis of the beam, r is the radius from the axis and (W) the characteristic beam radius at which the intensity is $1/e^2$ times that on the axis. The result of integrating the irradiance over a cross section of the gaussian beam is the total power (P_T) falling with in this area.

$$P_T = \int_A I \, dA \qquad (2.2)$$

Solving this equation as in appendix (A5) for an infinite radius gives the total power transmitted by the beam :

$$P_T = [\, I_o\, \pi\, W^2] / 2 \qquad (2.3)$$

When a gaussian beam passes through a circular aperture of radius ρ the total power transmitted through the aperture (P) is : appendix (A5)

$$P = P_T\, [1 - e^{-2(\rho^2/W^2)}] \qquad (2.4)$$

The area inside a circle with a radius defined as that when the intensity has fallen to $(1/e^2)$ of that on the axis, centered on the beam axis will receive 86.5% of the total power. The remaining 13.5% of the power lies in the edge of the beam beyond this arbitrarily chosen distance.

Truncation effects occur when a gaussian beam passes through any aperture like a pinhole or lens. If the beam after passing through an optical system maintains a near gaussain intensity profile, then the system is termed a non-truncating optical system. While if the transverse intensity profile is changed significantly, then truncation effects are present and the beam can no longer be considered as gaussian.

Safe truncation can be assumed when as the radius of any aperture is least twice the $(1/e^2)$ radius of the gaussian beam at the aperture . It should be noted that the radius of a focused truncated beam is greater than that of the nontruncated beam and correspondingly the centre intensity I_o of the focused truncated beam is less than that of the nontruncated beam.

Dickson in Ref.(32) proved that if a beam has an initial gaussian radial intensity distribution it will remain gaussian as it propagates through free space. However, gaussian beams diverge as they are travel away from their sources and converge when focused through a lens to a small radius called the beam waist (a plane where the wave front is flat) as in fig.(2.2). The amount of divergence or convergence can be quantified by the full-angle beam divergence θ_f. This is the rate at which the beam diameter diverges as measured at the $(1/e^2)$ contour. Some articles deal with a half-angle θ_h, represented by the angle between the beam axis and the $(1/e^2)$ contour.

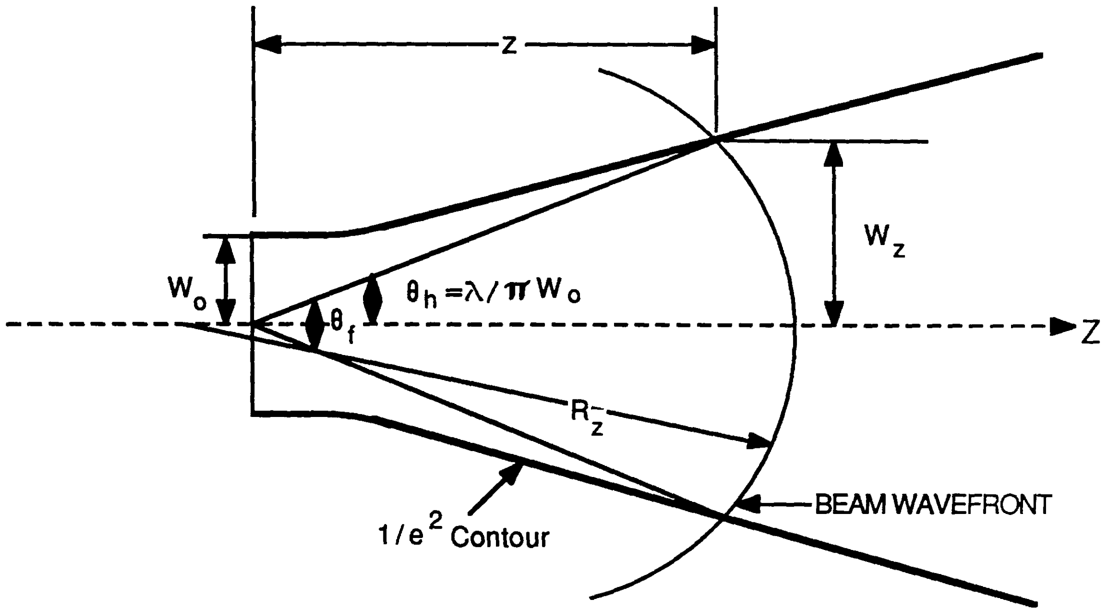

Figure 2.2 Propagation of a gaussian beam in free space

As a gaussian beam is symmetrical about its waist, the rate of convergence is equal to the divergence. This divergence however varies with distance from the beam waist. In general beam behavior can be classified into two regions: the far-field and the near-field as in fig.(2.3). These have been loosely defined Refs.(33,34) as :

$$\text{Far - field} \qquad Z > \pi\, d_o^2/4\,\lambda \tag{2.5}$$

$$\text{Near - field} \qquad Z < \pi\, d_o^2/4\,\lambda \tag{2.6}$$

Where Z is the distance from the beam waist and d_o is the beam waist diameter. $\pi d_o^2/4\lambda$ is known as the Rayleigh range Z_R. This is the distance from the beam waist to the point where the $(1/e^2)$ radius of the beam is $(\sqrt{2})$ times that at the beam waist and can be expressed as : Refs.(29,32,33,35,36)

$$Z_R = \pi\, W_o^2 / \lambda \tag{2.7}$$

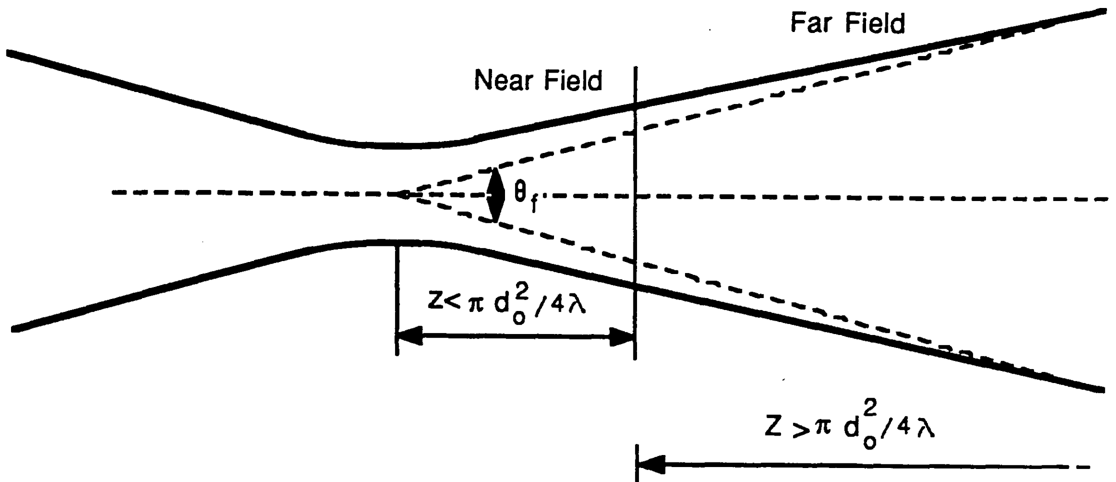

Figure 2.3 Near-field and Far-field distances

The far-field full angle beam divergence is as in Ref.(34) and derived in appendix (A6) is given by :

$$\theta_f = 4\ \lambda/\pi\ d_o \qquad (2.8)$$

Where λ is the wavelength of the laser light.

The far-field half angle is as in Refs.(33,37,38,39)

$$\theta_h = \lambda\ /\ \pi\ W_o \qquad (2.9)$$

The other parameter that characterizes a gaussian beam as it propagates is the radius of curvature of the phase front (R), which can be expressed as :

$$R_z = Z\ [\ 1 + (\pi W_o{}^2/\ \lambda Z\ )^2\ ] \qquad (2.10)$$

Where Z is the distance from the plane where the beam's wavefront is flat (the beam waist). An alternative form of the equation using the Rayleigh range Refs.(33,36)

$$R_z = Z\,[\,1 + (Z_R/\,Z\,)^2]\qquad(2.11)$$

Figure (2.4) shows the radius of curvature of the beam's wavefront with respect to the axial distance away from the waist. This is infinite at large distances, passes through minimum values at $Z = \pm Z_R$ and returns to infinity at the beam waist.

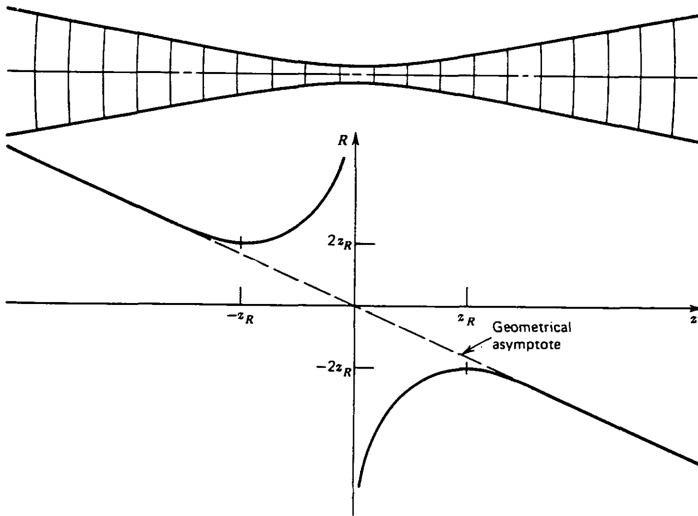

Figure 2.4 Plot of the radius of curvature (R) versus the distance (Z) from the beam waist Ref(34)

The beam radius W changes as the beam propagates and can be expressed as a function of distance Z from the beam waist as:

$$W_z^2 = W_o^2\,[\,1 + (\,\lambda Z/\pi W_o^2)^2\,]\qquad(2.12)$$

This equation is symetrical for Z i.e the beam is symetrical about the beam waist. This can be also expressed in the form:

$$W_z^2 = W_o^2[\,1 + (\,Z/Z_R\,)^2\,]\qquad(2.13)$$

After dividing eq.(2.12) by eq.(2.10)

$$\pi W_z^2 / \lambda R = Z \lambda / \pi W_o^2 \qquad (2.14)$$

Then the beam waist radius and the distance in terms of W_z and R may be expressed as:

$$W_o^2 = W_z^2 / [1 + (\pi W_z^2 / \lambda R)^2] \qquad (2.15)$$

$$Z = R / [1 + (\lambda R / \pi W_z^2)^2] \qquad (2.16)$$

2.2.2 Propagation Through a Non-truncating Thin Lens:

A raw laser beam must be modified to employ it in the vast majority of applications. One way to modify the beam is to use the transforming property of a lens. The thin lens equation from geometrical optics is given by :

$$1/S + 1/S' = 1/f \qquad (2.17)$$

where S and S' are the object and image distance respectively from the centre of the lens.

When a gaussian beam passes through a nontruncating, diffraction limited lens it remains gaussian, as the radial intensity is not affected by the lens. Clearly, the beam radius just after the lens plane is equal to that just before the lens.

If the axis of the propagated beam coincides with the axis of the lens and is perpendicular to the lens surface. The beam radius of curvature is changed through the lens by an amount $(1/f)$ as in the geometrical optics case Refs.(33,37,38,39,40) :

$$1/ R_2 = 1/R_1 - 1/f \qquad (2.18)$$

Where R_1, R_2 are the radius of curvature at the left and the right of the lens respectively. The initial gaussian beam is transformed into a new gaussian beam as in fig.(2.5).

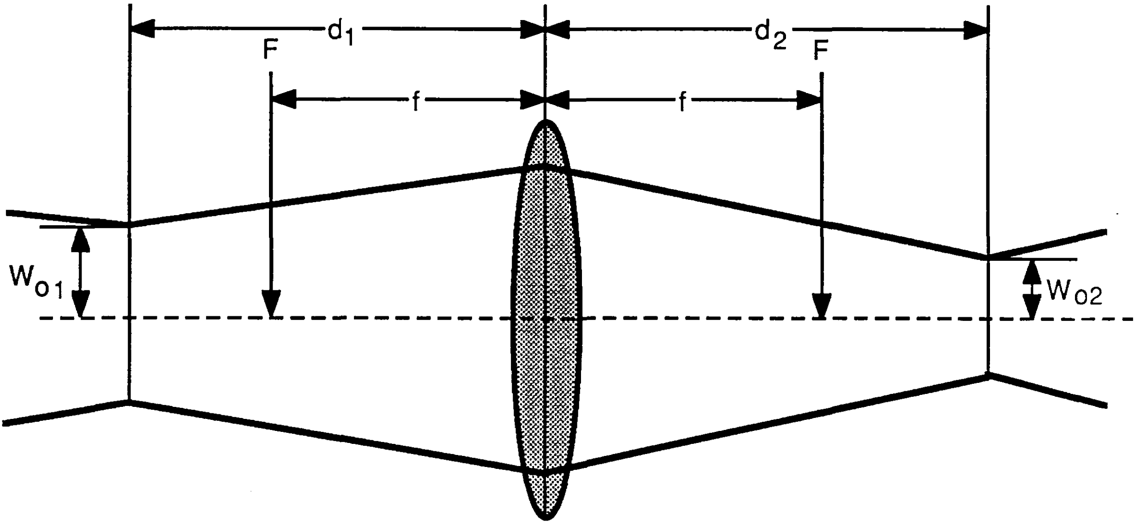

Figure 2.5 Gaussian beam transformed by a lens

A gaussian beam with initial beam waist W_{01} at a distance d_1 from the lens, passes through a lens with focal length f, a new beam waist W_{02} will be formed at a distance d_2 from the lens. The relation between these parameters can be derived from (2.18) and may be stated as Refs.(34,38,39) :

$$(d_2 - f)/(d_1 - f) = W_{02}^2 / W_{01}^2 \tag{2.19}$$

or alternatively as Refs.(34,38,39)

$$(d_1 - f)\,(d_2 - f) = f^2 - f_o^2 \tag{2.20}$$

where f_o Ref.(34) is a term introduced to account for diffraction sometimes termed the matching length Refs.(38,41) and defined as : Refs.(37,38,39,41)

$$f_o = \pi W_{01} W_{02}/\lambda \tag{2.21a}$$

Or Ref.(34) :

$$f_o = Z_R Z_R' \tag{2.21b}$$

Where Z_R' is the new Rayleigh range.

The magnification of a lens is the ratio of the (output/input) beam waist radii :

$$m = W_{02}/ W_{01} \tag{2.22a}$$

or Refs.(32,33,34,39,40)

$$m^2 = f^2/ [(d_1 - f)^2+(\pi W_{01}^2/ \lambda)^2] \tag{2.22b}$$

By substitution with eq.(2.7):

$$m^2 = f^2 / [(d_1 - f)^2 + Z_R^2] \tag{2.22c}$$

From eqs.(2.19, 2.22a) the location of the new beam waist d_2 is:

$$d_2 = f + m^2 (d_1 - f) \tag{2.23}$$

The mode matching formulae as in: Refs.(37,38,39,41)

$$|(d_1 - f)| = W_{01}/W_{02} (f^2 - f_o^2)^{0.5} \tag{2.24}$$

$$|(d_2 - f)| = W_{02}/W_{01} (f^2 - f_o^2)^{0.5} \tag{2.25}$$

For large distance Z fig.(2.2)

$$W_z \approx \lambda Z / \pi W_o \tag{2.26}$$

If such a beam is focused, the beam waist will be formed near the focal point of the lens so ($d_2 \approx f$) then :

$$W_{o2} = \lambda f / \pi W_{1L} \tag{2.27}$$

Where W_{1L} is the beam radius at the focussing lens. Substitution of eq.(2.9) gives :

$$W_{o2} = f\,\theta_h \tag{2.28}$$

So for any given beam the focused spot size W_{o2} is directly proportional to the focal length of the lens, whether or not the lens is in the far-field of the incident beam. From equation (2.22a) the new beam waist radius is proportional to the magnification, which is proportional to the focal length as in eq.(2.22b). So the formation of a small spot size requires a lens with a short focal length. The new beam divergence is inversely proportional to the new beam waist radius, while the Rayleigh range is proportional to the new waist radius. By dividing equation (2.23) by the focal length f the result is :

$$\frac{d_2}{f} = 1 + m^2\left[\frac{d_1}{f} - 1\right] \tag{2.29}$$

By substituting the quantity of the magnification m^2 from eq. (2.22c):

$$\frac{d_2}{f} = 1 + \frac{f^2\,[(d_1/f) - 1]}{[d_1 - f]^2 + Z_R^2} \tag{2.30}$$

$$\frac{d_2}{f} = 1 + \frac{[(d_1/f) - 1]}{[(d_1/f) - 1]^2 + [Z_R/f]^2} \qquad (2.31)$$

2.3. Radiometric Theory:

Any optical system will produce an image with a certain intensity distribution. To design an optical instrument based upon the measurement of such a distribution it is necessary to understand the sciences related to intensity and power measurement.

Photometry deals with the propagation and measurement of the visible part of the electromagnetic spectrum and uses units based on the response of the human eye. Radiometry is a more general science concerned with the propagation and measurement of all electromagnetic radiation. The fundamental photometric unit is the lumen (lm), while radiometry uses the watt (W). Radiometric values can be converted into photometric values by taking account of the relative visibility of the radiation. For more information see Refs.(34,42,43,44,45).

2.3.1 Radiometric Units:

This section gives the definition, symbols and nomenclature of fundamental radiometric quantities. The International System of units uses the same set of symbols for both radiometric and photometric quantities with different subscripts beings used to distinguish between them. Table 2.1 gives a summary of these quantities together with their units.

The total amount of radiant energy transferred per unit time is the radiation power ϕ_e, also called radiant flux. Refs.(45,46) :

$$\phi_e = dQ_e / dt \tag{2.32}$$

Where the radiation or more precisely radiant energy Q_e is the total energy emitted transmitted or collected in a radiation process. The radiant density U_e which is the radiant

Radiometry Quantity	Symbol	Unit
Radiant power or flux	ϕ_e	Watt (W)
Radiant energy	Q_e	Joule (J)
Radiant density	U_e	Joule per cubic metre (J/m^3)
Radiant emittance (exitance)	M_e	Watt per square metre (W/m^2)
Radiant intensity	I_e	Watt per steradian (W/sr)
Irradiance	E_e	Watt per square metre (W/m^2)
Radiance	L_e	Watt per steradian and square metre (W/sr m^2)
Photometry quantity	**Symbol**	**Unit**
Luminous power or flux	ϕ_v	lumen (lm)
Luminous energy	Q_v	lumen . second (Talbot)
Luminous density	U_v	lumen . second per cubic metre $lm.s/m^3$
Luminous emittance (exitance)	M_v	lumen per square metre lm/m^2
Luminous intensity	I_v	lumen per steradian (candela) cd
Illuminance	E_v	lumen per square metre (lux) lx
Luminance (Photometric Brightness)	L_v	candela per square metre (nit) nt

Table (2.1) Radiometric and Photometric quantities, units and symbols

energy per unit volume dV is defined as. Refs(44,45,46):

$$U_e = dQ_e / dV \tag{2.33}$$

The radiant emittance defined as the power per unit area emitted by an extended source Refs.(42,44,46,47) :

$$M_e = d\phi_e / dA \tag{2.34}$$

The radiometric intensity I_e of a source is defined as the quantity of the radiant output power ϕ_e emitted per unit solid angle Ω Refs. (42,44, 45,46,47,48) :

$$I_e = d\phi_e / d\Omega \tag{2.35}$$

Where the solid angle Ω fig. (2.6) is subtended by an area dA on a surface of a given radius R and it equal to : Refs.[34,42,44,45,47]

$$\Omega = dA / R^2 \tag{2.36}$$

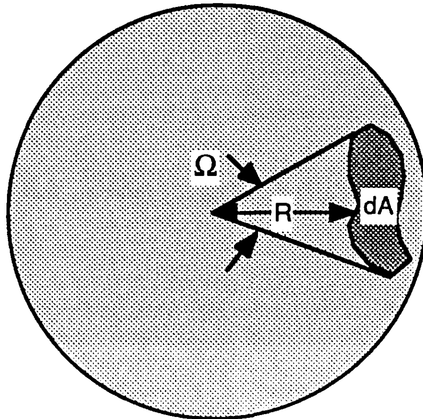

Figure (2.6) The solid angle Ω for the area dA on a sphere of radius R

2.3.2 Point Sources:

Starting with a point source that radiates uniformly, if a small element of area dA is positioned a distance R normal to the point source fig (2.7). The illumination of that element is given by the irradiance E_e which is defined as radiant power incident upon the element per unit area fig.(2.7) Refs.(34,42,44,45,47) :

$$E_e = d\phi_e / dA \tag{2.37}$$

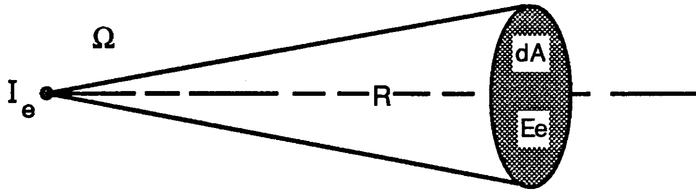

Figure 2.7 Radiant intensity of a point source with solid angle Ω

The irradiance of the element of area dA by the point source can be expressed in terms of its radiant intensity. (Since the intensity of a point source does not change with the angle, then) Ref.(34)

$$I_e = d\phi_e / d\Omega \quad \text{and} \quad \phi_e = I_e \Omega \tag{2.38}$$

At a distance R from the point source the area dA subtended by the solid angle dΩ

$$d\Omega = dA / R^2 \tag{2.39}$$

By substituting eqs.(2.38) and (2.39) in eq.(2.37) the result is :

$$E_e = I_e / R^2 \quad (2.40)$$

In this way, the irradiance E_e at a point on a surface varies directly with the radiated intensity I_e of the source and inversely as the square of the distance R between the source and the point fig.(2.7) (If the surface is normal to the direction of the incident light). This is one example of an inverse square law and is applicable when the source is a point source. However, if the light radiates from an extended source and the collection area is close to the illuminated area , a correction factor must be included.

The term, radiant intensity is restricted to point sources whilst for an extended sources the term radiance is used. The radiance L_e is defined as the amount of radiant power leaving a source of unit surface area and per unit solid angle. The radiance of an extended source in a direction normal to its surface is Refs(34,44) :

$$L_e = \phi_e / A_s \, \Omega \quad (2.41)$$

Where A_s is the area of finite source. In a direction making an angle θ between the normal to the finite source fig.(2.8) and the direction of propagation of the light the radiance will equal to: Refs.(34,45,46,47)

$$L_e(\theta) = \phi_e / A_s \cos\theta \, \Omega \quad (2.42)$$

$$L_e(\theta) = L_e(0) / \cos\theta \quad (2.43)$$

Here $L_e(0)$ is the radiance when $\theta = 0$. By substituting the eq.(2.38) in the eq.(2.42) the result is the radiance expressed in term of the radiant intensity:

$$L_e(\theta) = I_e / A_s \cos\theta \quad (2.44)$$

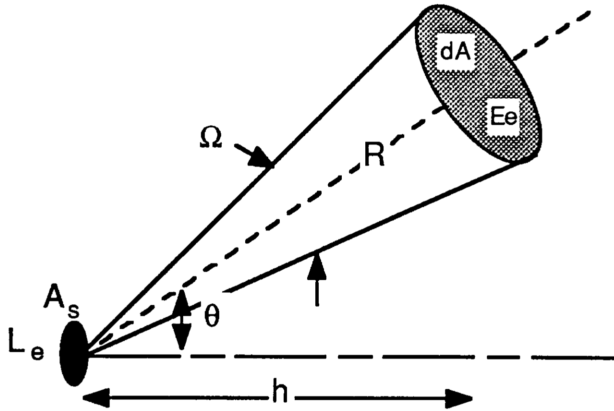

Figure 2.8 Radiance of an extended source to an area making an angle θ with the normal

The authors of Refs.(44,47) showed that:

$$L_e' = (n'/n)^2 L_e \tag{2.45}$$

Where L_e' is the new radiance for the medium with refraction index n', If the two indices of refraction (n,n') are the same then :

$$L_e' = L_e \tag{2.46}$$

2.3.3 Lambertian Sources:

When a uniform beam of light hits a surface, the spatial profile of the reflected light will depend on the surface. The reflection from a smooth surface is known as regular reflection, whilst, if the surface is rough or matt the reflection is termed diffuse.

For a perfect diffuse surface with an angle θ between the normal to the surface and the direction of the incident light. The lambert's cosine law can be applied. This law states that the irradiance of any surface varies as the cosine of the angle of incidence. As in Ref. (42) the radiant intensity varies according to the lambert's law fig. (2.9) : Ref.(42)

$$I_\theta = I_e \cos\theta \qquad (2.47)$$

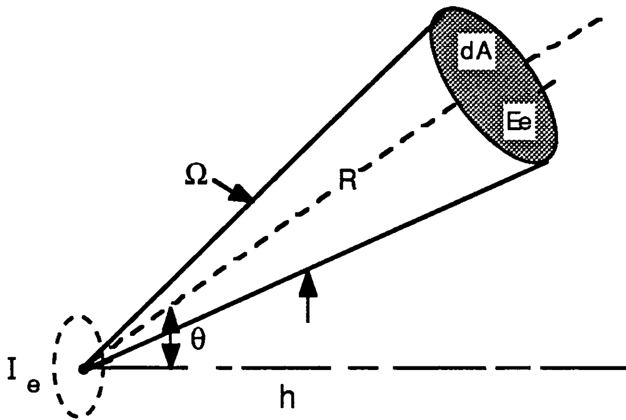

Figure 2.9 Radiant intensity from an elemental area source to an area making an angle θ with the normal

The total flux reflected from a perfectly diffuse surface (lambertian reflector) per unit solid angle is proportional to the cosine of the angle between the normal to the surface. Refs(45,46,47):

$$E_e = I_e \cos\theta / R^2 \qquad (2.48)$$

A lambert source or lambert emitter can be defined as the source which has the same directional properties as outlined above.

The lambert's cosine law can be extended to the cosine cubed law, by substituting $(h/\cos\theta)$ instead of R, from fig. (2.9) :

$$R = h / \cos\theta \qquad (2.49)$$

By substituting eq.(2.49) in (2.48)

$$E_e = I_e \cos^3\theta / h^2 \qquad (2.50)$$

Where h is the perpendicular distance between the source and the surface.

2.4 Summary of Theoretical Results:

Gaussian :

1. Beam radius at distance Z from the beam waist :

$$W_Z^2 = W_o^2 [1+(\lambda Z/\pi W_o^2)^2]$$

2. Rayleigh range :

$$Z_R = \pi W_o^2/\lambda$$

3. Magnification of a thin lens of focal length (f) :

$$m = f/[(d_1 - f)^2 + (Z_R)^2]^{0.5}$$

4. Radius of a new beam waist :

$$W_{o2} = m W_{o1}$$

5. Location of the new beam waist :

$$d_2 = f + m^2(d_1 - f)$$

6. Intensity at any radius from the beam axis :

$$I_r = I_o e^{-2(r^2/W^2)}$$

7. Total power propagated within a beam :

$$P_T = I_o \pi W^2/ 2$$

8. Total power passed by an aperture of radius ρ centred on the beam axis :

$$P = P_T [1 - e^{-2(\rho^2/w^2)}]$$

Radiometric :

1. Radiant power :

$$\phi_e = dQ_e / dt$$

2. Radiant intensity of a point source :

$$I_e = d\phi_e / d\Omega$$

3. Solid angle :

$$\Omega = dA / R^2$$

4. Irradiance :

$$E_e = d\phi_e / dA$$

5. Radiance of a finite source :

$$L_e = \phi_e / A_s \Omega$$

6. Inverse square law :

$$E_e = I_e / R^2$$

7. Lambert's cosine law :

$$E_e = I_e \cos\theta / R^2$$

CHAPTER 3
MATHEMATICAL MODELLING

CHAPTER 3: MATHEMATICAL MODELLING

3.1 Introduction:

According to the scheme chosen, which was detailed in chapter 1, the specific type of configuration selected for the non-contact sensor makes use of an on-axis optical system. By sensing the reflected beam using a differential photodiode method it is possible to generate a signal which varies with the distance from the focused beam waist to the workpiece in a predictable though non-linear fashion.

This chapter presents the measuring principle of the sensor together with two mathematical methods of analysis and associated computer programs generated for the purpose of design simulation. The first analysis uses modelling dependent only on the theory of gaussian beam propagation, whilst the second is a combination of gaussian and radiometric modelling.

Dobosz Ref.(21) and Fainman, Lenz and Shamir in Ref.(20) discuss a number of optical non-contact profilometers. The mathematical description by Dobosz is based on the theory of propagation of gaussian laser beams. The authors of Ref(.20) use specific operator algebra and the characteristics of the Wigner distribution function to perform their mathematical analysis.

3.2 Measuring Principle:

The measuring principle of the sensor is shown in fig.(3.1). A He-Ne laser [1] is used to generate a laser beam with initial beam waist $2W_{01}$ [14], which passes through a beam splitter B_1 [3] and is focused onto the workpiece surface by the main lens L_1 [5] to form a new beam waist $2W_{02}$ [15]. The light is reflected from the workpiece surface [6] and collected through L_1 the main lens and partially directed by B_1 into the image lens L_2 [7], to focus after beings split by B_2 [8] at beam waist planes $2W_{04}$ and $2W_{04}'$ [16,17].

These two parts are then detected by two photodiodes PH_1, PH_2 [10,12] each placed behind two pinholes of equal size PN_1 and PN_2 [9,11] respectively. If the two pinholes

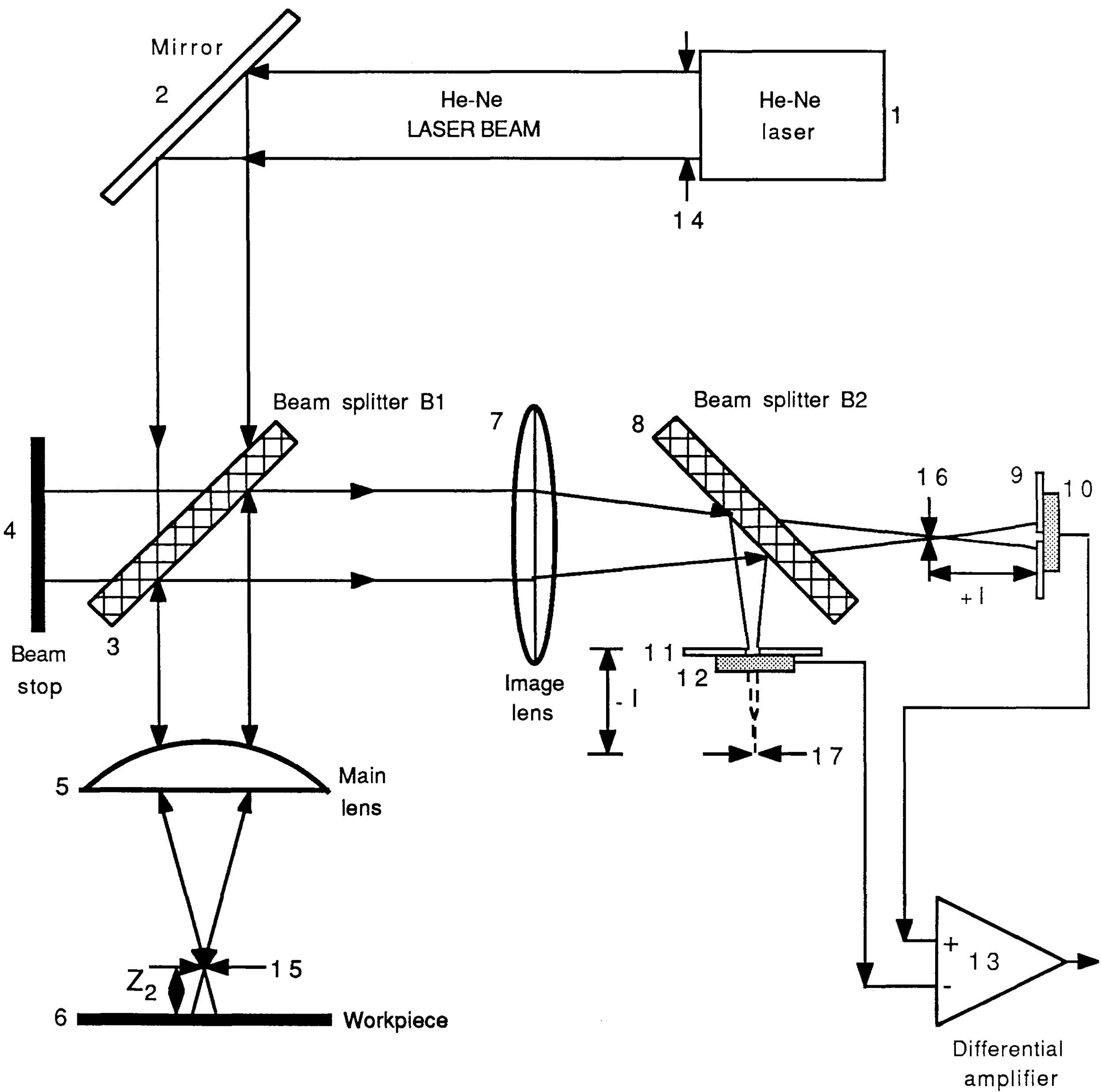

1. He-Ne laser
2. Mirror
3. First beam splitter B_1
4. Beam stop
5. Main lens L_1
6. Workpiece
7. Image lens L_2
8. Second beam splitter B_2
9. First pinhole PN_1
10. First photodiode PH_1
11. Second pinhole PN_2
12. Second photodiode PH_2
13. Differential amplifier
14. Plane of intial beam waist $2W_{o1}$
15. Plane of beam waist $2W_{o2}$
16. Plane of beam waist $2W_{o4}$
17. Plane of beam waist $2W_{o4'}$

Figure 3.1
The measurement principle

are positioned exactly at the beam waist planes $2W_{04}$, $2W_{04}'$, they would both pass the same amount of light for any position of the surface.

If pinhole PN_1 is placed at a distance (l) behind the $2W_{04}$ plane and PN_2 is placed at the same distance (l) in front of the $2W_{04}'$ plane. The radial intensity distributions in front of the two detectors are identical, but of different radii of curvature. Any displacement of the surface from the position of the plane $2W_{02}$ will then generate two different output signals. Consequently, the position of the surface can be determined by the differential photodiode method, which is described in detail in the next section.

3.2.1 The Differential Photodiode Method:

The translation of the workpiece surface, from the beam waist plane $2W_{02}$, produces a variation in the voltage from a photodiode detecting the reflected beam, (due to the variation in beam intensity) as in fig.(3.2a). This signal alone is not capable of explicitly representing the position and direction of the workpiece displacement, as two axial positions ($\pm Z$) are possible for any given voltage fig.(3.2a). However, if two such measuring systems are placed at symmetrical offset distances, their output voltage signal is as in fig.(3.2b). The subtraction of the two signals leads to the differential system performance shown in fig.(3.2c). From this output signal the position is still not uniquely described, but the sign of the displacment is given. It then becomes practical to use this as a control signal in a feed back servo mechanism to correct and maintain a fixed distance between lens and workpiece surface .

The optical operation of the system is illustrated in fig.(3.3a). When the workpiece surface is located at the focused beam waist $2W_{02}$ ($Z_2 = 0$), the light power passing through the two pinholes is equal. Thus the differential amplifier produces a zero value output voltage.

The effect of a small longitudinal displacement of the workpiece in the direction Z parallel to the beam axis will cause a larger shift of the planes $2W_{04}$ and $2W_{04}'$. As a

result the power detected by one photodiode will increase, while the second will decrease similarly. A differential amplifier is then used to identify the amount and direction of displacement Z_2 fig.(3.3b).

It can be seen in fig.(3.3b) that the relation between the distance and the output voltage is non-linear except for a portion between the positive and negative peaks. This linear range is determined by the size and position of lenses, pinholes and photodiodes and is perhaps the most important part of the output signal (for control purposes), as it characterises the response of the sensor when the stand-off sensor is following a surface.

The theoretical and experimental modelling are aimed at developing methods for optimising component position and size to improve the linearity and sensitivity of the device.

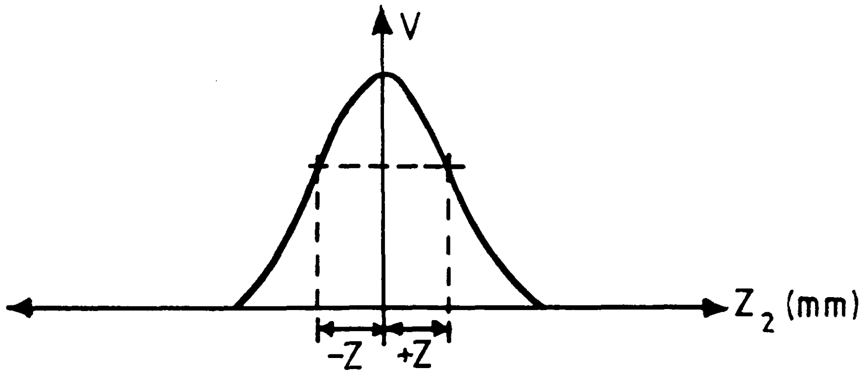

Figure 3.2a One photodiode output

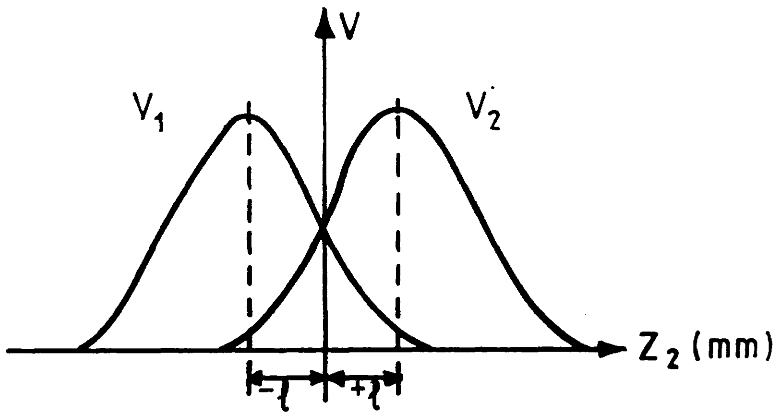

Figure 3.2b Output of two photodiodes offset from Z'=0 by a distance ±l

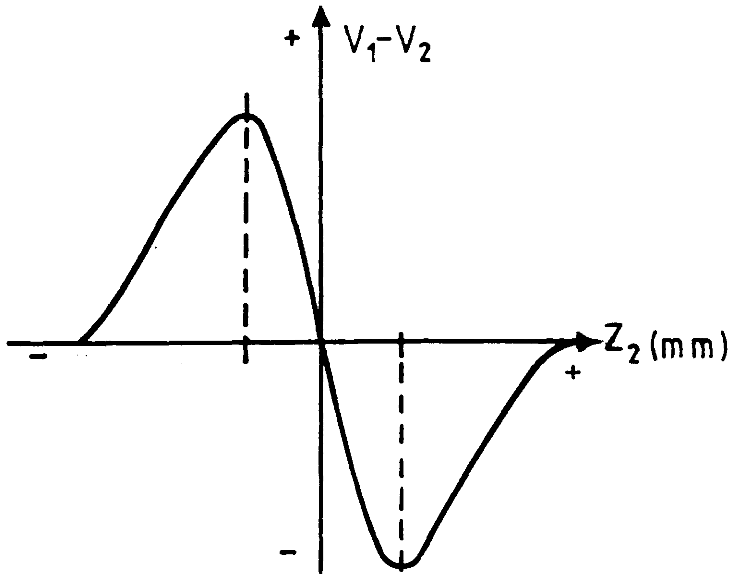

Figure 3.2c Output of photodiodes after amplification and subtraction

Laser beam
Beam splitter
Image lens
Beam splitter
Photodiode 1
$Z_2=0$
+l
Pinhole 1
Pinhole 2
Photodiode 2
-l
$Z_2=0$
Main lens
Ideal workpiece position
Z_2
Workpiece far away from the focussed beam wasit position
Differential amplifier
-
+

Figure 3.3a Principle of differential photodiode method

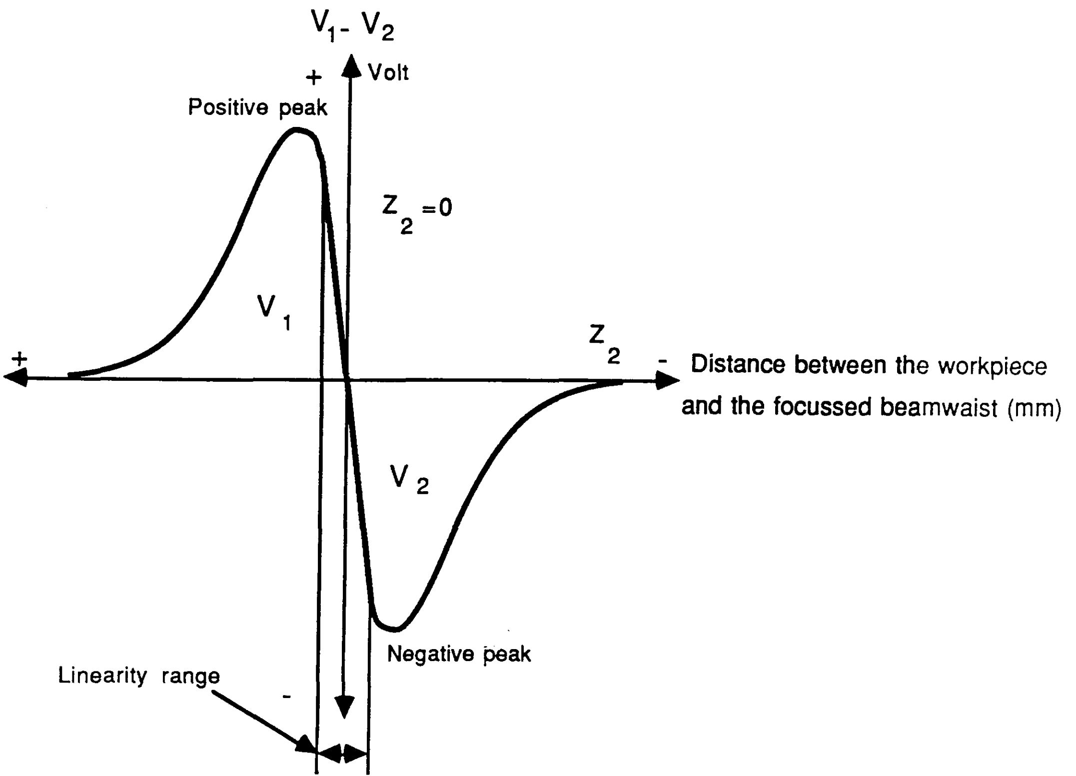

Figure 3.3b : The differential signal

3.3 Gaussian Modelling:

This modelling attempts to give quantitative results to the effect of the changing components within the measuring system. This analysis may then be used to optimize the position and selection of these components to enable fast accurate instrument response.

A mathematical simulation follows the beam path from the laser to the photodiodes. This describes the behavior of the beam through its path and finally calculates the output voltage. This output can then be used to determine the overall sensor response.

The theory is based on that of a propagating gaussian beam following the principles laid out by Dobosz Ref.(21), starting from basic gaussian theory. This considers the transmission of the beam through the optical system in a step by step fashion and calculates the detected power using the mathematical equations presented in the previous chapter.

3.3.1 Gaussian Analysis:

This section presents a description of the mathematical analysis of one arm of the optical system as depicted in fig.(3.4). This shows the progress of the gaussian beam path from the laser through : the main lens L_1, the image of the main lens L_2, the image lens L_3 and a pinhole of radius R_p.

If f and f' are the distances from the object and image focal points F and F' respectively to the centre of the lens, then from geometrical optics Ref.(54) :

$$f / f' = n / n' \quad (3.1)$$

Where n, n' are the refractive indices of the two media on either sides of the lens. If a thin lens in air is assumed then the index of refraction of the medium surrounding the lens is equal to one then from equation (3.1) for all the lenses ($f = f'$).

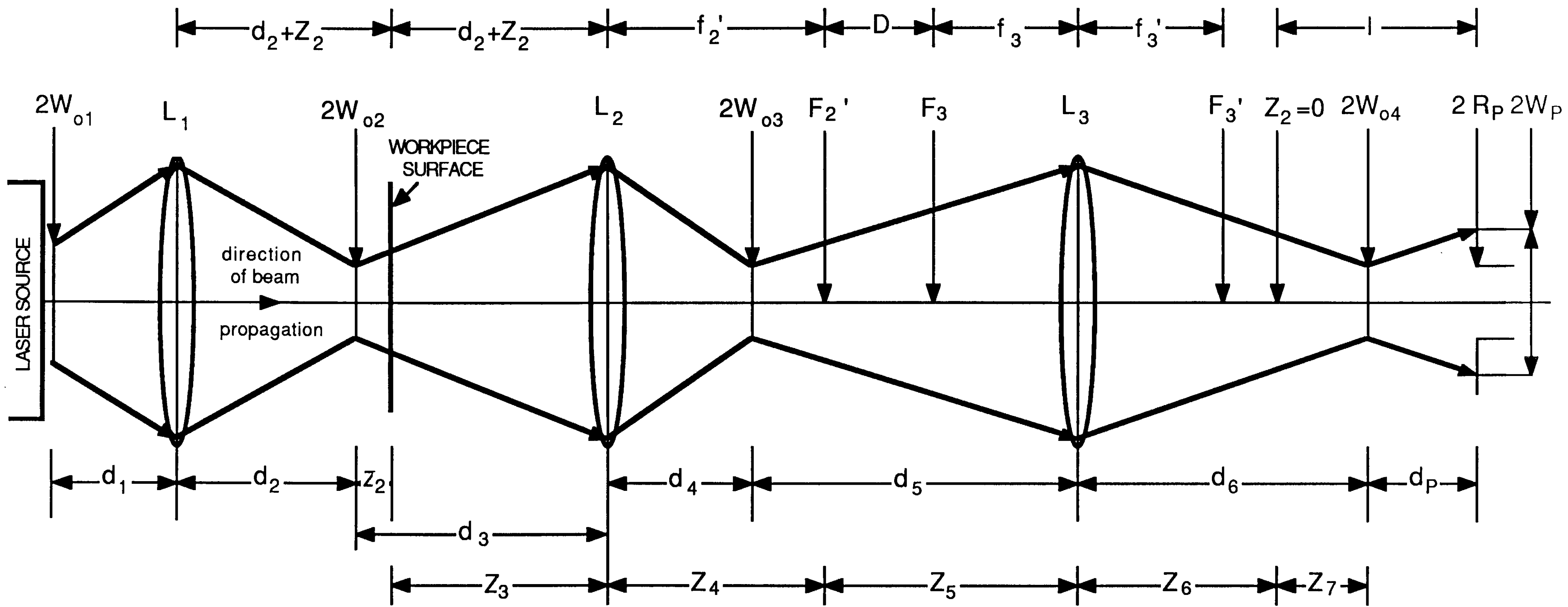

Figure 3.4 One arm of the optical system for the gaussian model

If a laser light source with beam waist radius W_{01} is situated a distance d_1 from a lens L_1, the beam will be focused by the lens to a spot size W_{02} at a distance d_2 from it. The magnification m_1 of the main lens L_1 can be calculated as:

$$m_1 = f_1 / [(d_1 - f_1)^2 + Z_{R1}{}^2]^{0.5} \qquad (3.2)$$

Where

$$Z_{R1} = \pi W_{01}{}^2 / \lambda \qquad (3.3)$$

so the focused spot size W_{02} :

$$W_{02} = m_1 W_{01} \qquad (3.4)$$

and the location of the new spot W_{02} can be determined from :

$$d_2 = f_1 + m_1{}^2(d_1 - f_1) \qquad (3.5)$$

As in fig.(3.4) the distance from the focused waist radius W_{02} to the lens L_2 is d_3 and from the law of reflection

$$d_3 = d_2 + 2 Z_2 \qquad (3.6)$$

So the translation of the workpiece parallel to the light axis gives an effective double translation of the waist W_{02} with respect to lens L_2. If Z_2 equal zero, then the surface and W_{02} are coincident and the distance Z_3 is d_2 .

Using the previous equation and the equations in the previous chapter to calculate W_{03}. Which is the image of the waist radius W_{02} through the lens L_2. The positions d_3 and Z_3 are transformed by the lenses L_2, to d_4 and Z_4 fig. (3.4).

$$m_2 = f_2 / [(d_3 - f_2)^2 + Z_{R2}{}^2]^{0.5} \qquad (3.7)$$

$$W_{o3} = m_2 W_{o2} \quad (3.8)$$

$$d_4 = f_2 + m_2^2(d_3 - f_2) \quad (3.9)$$

$$Z_4 = f_2 + m_2^2(Z_3 - f_2) \quad (3.10)$$

The distance between the lenses L_2 and L_3 is equal to :

$$DLN = f_2 + f_3 + D \quad (3.11)$$

Where f_3 and f_2 are the focal lengths of the lenses L_3 and L_2 respectively, D is the distance between the focal points F_2' and F_3 of the two lenses L_2 and L_3 respectively.

so $$d_5 = DLN - d_4 \quad (3.12)$$

and $$Z_5 = DLN - Z_4 \quad (3.13)$$

The same method is used to calculate: W_{04} which is the image of the waist radius W_{03} through the lens L_3 and the distances d_6 and Z_6 which are the result of transformation of the distances d_5 and Z_5 through the lens L_3 fig. (3.4).

If a pinhole is placed at a distance l behind the image plane [when ($Z_2 = 0$) as in fig.(3.3)], then the beam radius W_P in front of the pinhole may be calculated as :

$$W_P = W_{04}[\,1 + (\lambda\, d_P/ \pi\, W_{04}^2)^2\,]^{0.5} \quad (3.14)$$

Where d_P according to fig.(3.2) is :

$$d_{P1} = l - (d_6 - Z_6) \quad (3.15)$$

$$d_{P1} = l - Z_7 \quad (3.16)$$

Where Z_6 is the image distance of Z_3 through the lenses L_2,L_3 when (Z_2=0).

The total power transmitted through the pinhole is :

$$P_{P1} = P_n \, [1 - e^{-2(R_P{}^2/W_P{}^2)}] \qquad (3.17)$$

Where P_n is the total light power in front of the pinhole and R_P is the radius of the pinhole.

If the photodetector is assumed to be perfectly linear, then the output photodetector voltage V_{P1} as in Ref.(21) :

$$V_{P1} = K_P \, P_{P1} \qquad (3.18)$$

Where K_P is the photodetector sensitivity .

The second photodiode and pinhole is placed at a distance l before the image plane when $(Z_2=0)$:

$$d_{P2} = l + (d_6 - Z_6) \qquad (3.19)$$

$$d_{P2} = l + Z_7 \qquad (3.20)$$

The output voltage (V_{DA}) of the differential amplifier used to measure the photodiode output is :

$$V_{DA} = K_A \, [\, V_{P1} - V_{P2} \,] \qquad (3.21)$$

Where K_A is the amplifier gain and V_{P1} and V_{P2} are the photodiode output voltages. The subtraction of these two voltages will give a curve with the shape as in fig.(3.3b), through which the magnitude and direction of the error may be calculated.

Both simulation and device normalizes the output voltage as:

$$V_T = K_A \ V_{Ref} \frac{[V_{P1} - V_{P2}]}{[V_{P1} + V_{P2}]} \qquad (3.22)$$

Due to the irregular variation in reflected beam power from the workpiece as it is translated or from different workpieces. This is caused by the varying roughness and reflectivity of the workpiece surface. The output is multiplied by V_{Ref} to convert it to a voltage signal.

According to the previous analysis, if the focused beam radius W_{02} plane coincides with the plane of the workpiece surface, then ($Z_2 = 0$) and the the plane of W_{04} will occur at the distance Z_6 ($d_6 = Z_6$). Because both photodiodes are at the same distance from the beam waist W_{04} eqs. (3.16), (3.20), this condition will produce a zero value of the output voltage as a result of equal power being detected by the two photodiodes.

3.3.2 Gaussian Modelling Program:

The previous mathematical simulation was coded as a program on a VAX computer in the Mechanical Engineering department, using Fortran 77. The logical flow of the program is shown in fig.(3.5), while the program itself is included in appendix (A7).

The program simulates one particular configuration of the optical system. It calculates the variables mentioned in the previous section, for a variation in workpiece position, to produce a set of output results. These results are presented as graphs giving information as to the characteristics of the configuration. From this, understanding can be gained about the design. An analysis can be conducted by varying the size and position of components and observing the effect on the normalized output voltages. Thus the modelling program is an important tool for optimization.

The program presents the output as a group of three graphs of desired output parameters, which are controlled through a plotting control file, with each graph being supported by a title. Additionally, a list of the input data for the configuration simulated is given in the top left hand corner of the plot.

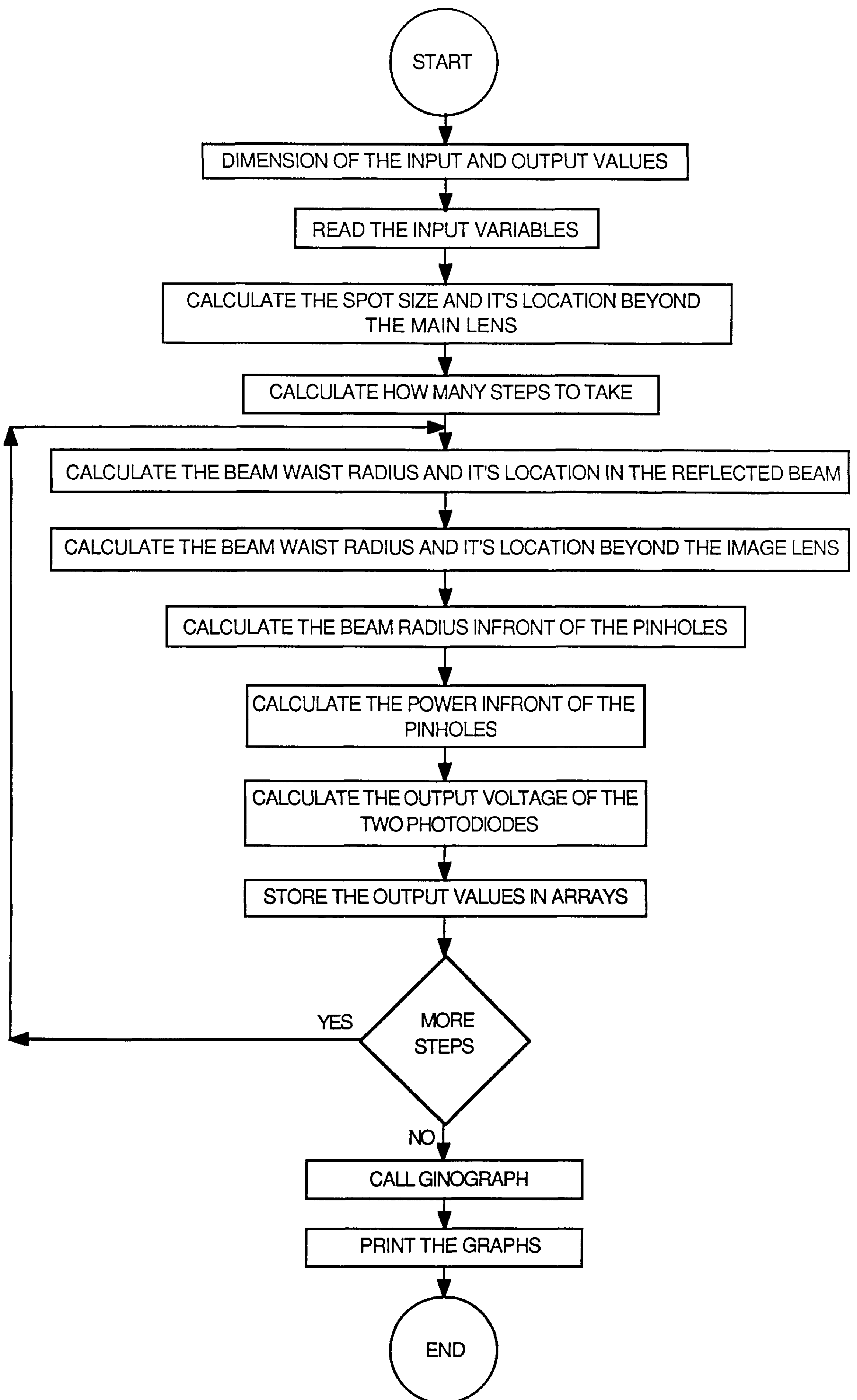

Figure 3.5 The flow chart of the gaussian modelling program

3.3.3 Results of Simulation:

Some of the results of the program are presented in graphical form (figs. 3.6, 3.7 and 3.8) for different input data. Figure 3.6 shows three graphs, which give some simulation results for the gaussian model program, for an optical system with a 75mm main lens focal length. The simulation input parameters are listed in the upper left hand box, while the lower left graph presents the beam spot size in front of the two pinholes, relative to the distance between the beam waist W_{02} and the surface. The solid line represents the spot size in front of pinhole PN_1, while the dashed line is for the second pinhole PN_2. The lower right graph shows output voltage as detected by the two photodiodes, whilst the top graph characterises the normalized output response of the system. This format is maintained for all simulation results presented in this chapter.

Figure 3.7 is similar to figure 3.6 but for a 120mm focal length main lens. Fig 3.8 presents the result of the gaussian model program for the optimum set-up presented previously by Dobosz in Ref.(21). The results are identical and gives some supporting evidence as to the program's correct function. The result of this model are compared with other simulation and experimental results in chapter 4.

Robot Sensor Simulation - Gaussian Design !!!

FIGURE(3.6)

LASER WAVELENGTH (mm)........................		-0.6330E -3
LASER BEAM WAIST RADIUS (mm)..............	-	0.31500
BEAM POWER (mW).................................		-0.4000E 1
FOCAL LENGTH OF THE MAIN LENS (mm)........	-	75.000
FOCAL LENGTH OF THE IMAGE LENS (mm).......	-	300.000
DIAMETER OF THE PINHOLE (mm)..............	-	0.200000
LASER TO MAIN LENS DISTANCE (mm)..........	-	1000.000
DISTANCE BETWEEN MAIN AND IMAGE LENS (mm).	-	0.000
PINHOLE OFFSET DISTANCE (mm)..............	-	5.000000
AMPLIFIER GAIN............................	-	4.000

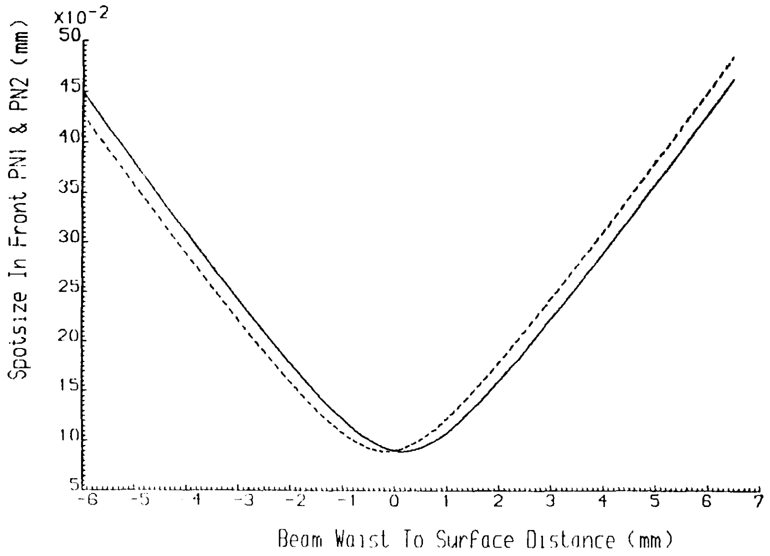

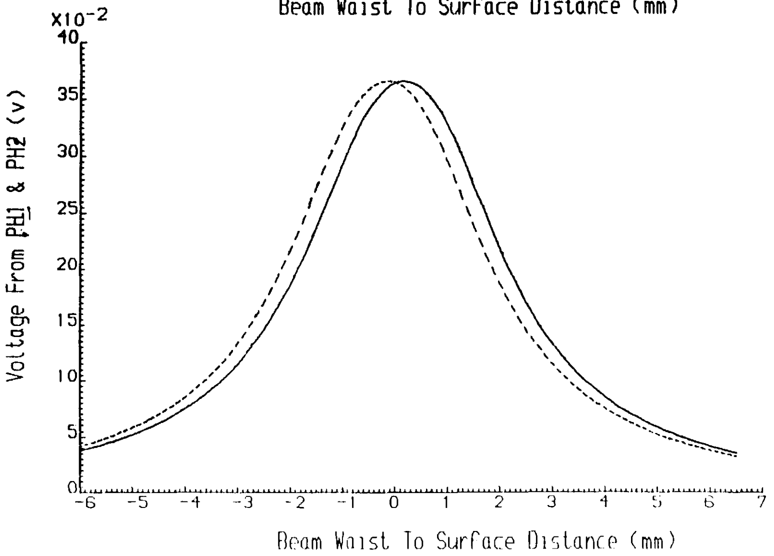

Figure 3.6 Gaussian simulation results for 75mm lens

Robot Sensor Simulation - Gaussian Design !!!

FIGURE(3.7)

LASER WAVELENGTH (mm).....................	-0.6330E -3
LASER BEAM WAIST RADIUS (mm)..............	- 0.31500
BEAM POWER (mW)...........................	-0.4000E 1
FOCAL LENGTH OF THE MAIN LENS (mm)........	- 120.000
FOCAL LENGTH OF THE IMAGE LENS (mm).......	- 300.000
DIAMETER OF THE PINHOLE (mm)..............	- 0.200000
LASER TO MAIN LENS DISTANCE (mm)..........	- 1000.000
DISTANCE BETWEEN MAIN AND IMAGE LENS (mm).	- 0.000
PINHOLE OFFSET DISTANCE (mm)..............	- 5.000000
AMPLIFIER GAIN............................	- 4.000

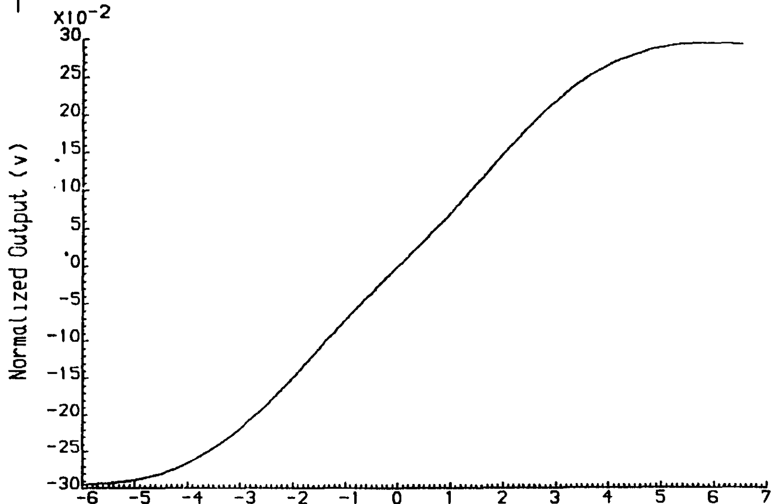

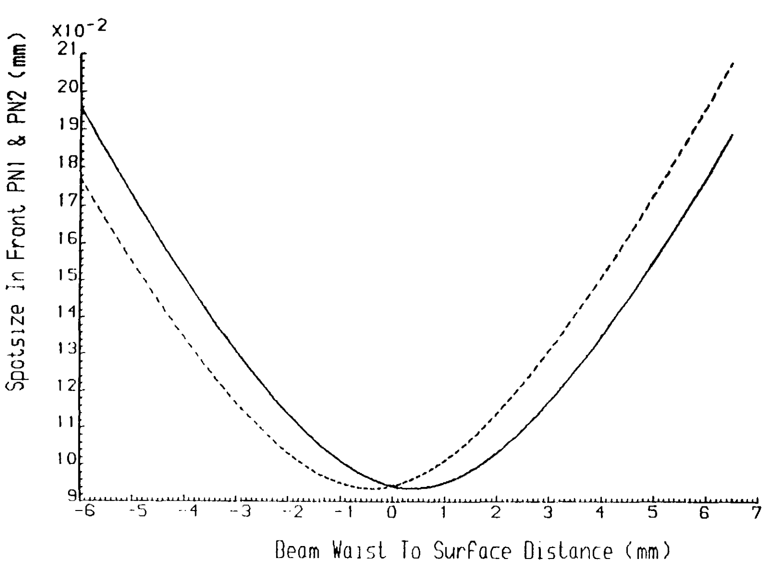

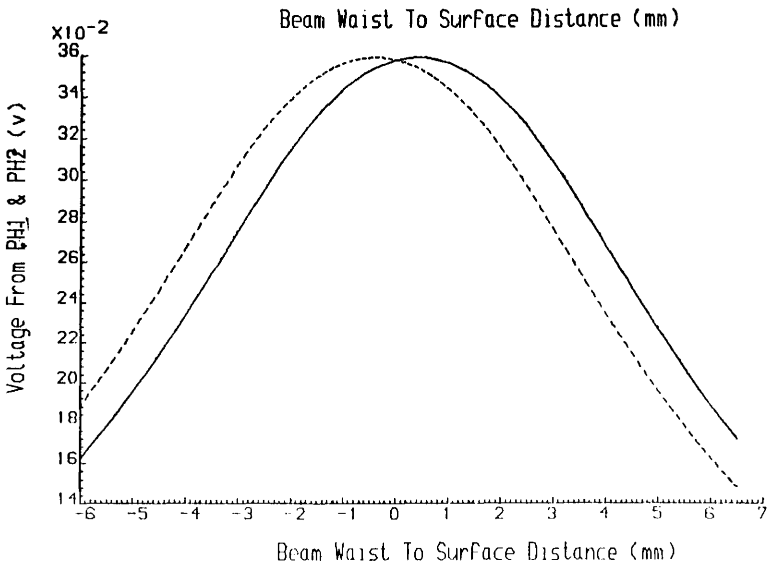

Plotted on 16-AUG-88 at 21:34:36

Figure 3.7 Gaussian simulation results for 120mm lens

Robot Sensor Simulation - Gaussian Design !!!

FIGURE(3.8)

Parameter	Value
LASER WAVELENGTH (m)	-0.6320E -6
LASER BEAM WAIST RADIUS (m)	- 0.00116
BEAM POWER (W)	-0.1250E -1
FOCAL LENGTH OF THE MAIN LENS (m)	- 0.003
FOCAL LENGTH OF THE IMAGE LENS (m)	- 0.135
DIAMETER OF THE PINHOLE (m)	- 0.000080
LASER TO MAIN LENS DISTANCE (m)	- 0.001
DISTANCE BETWEEN MAIN AND IMAGE LENS (m)	- 0.000
PINHOLE OFFSET DISTANCE (m)	- 0.004500
AMPLIFIER GAIN	- 1.000

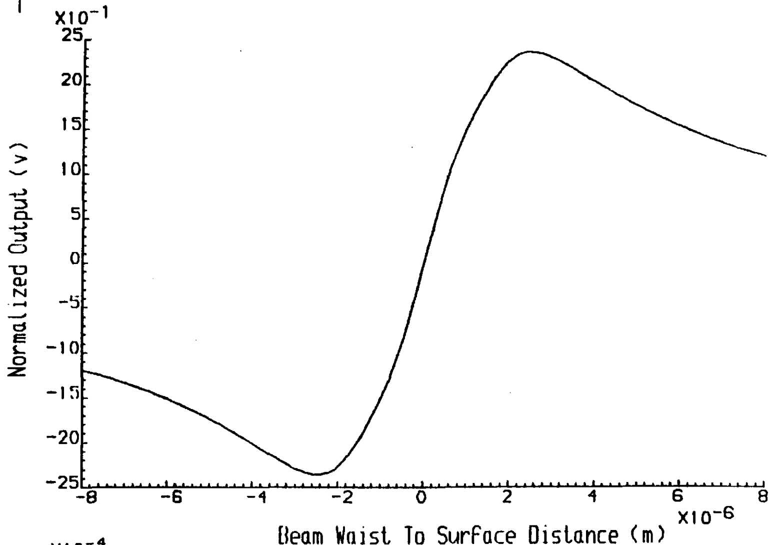

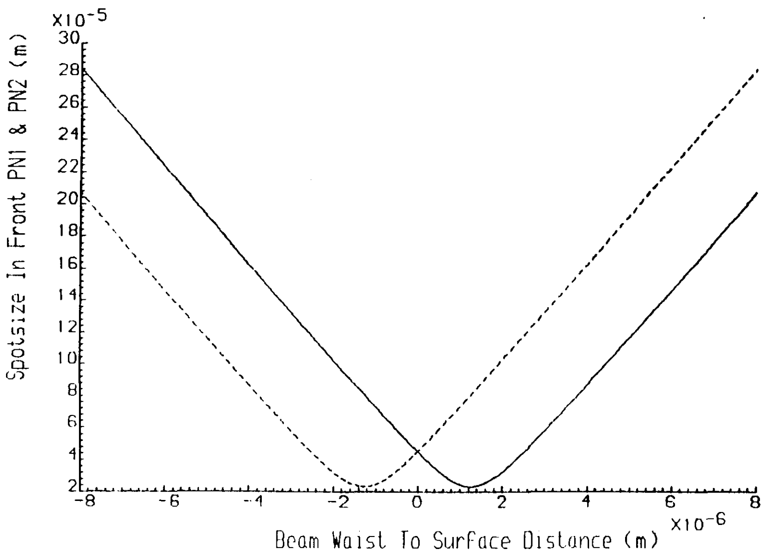

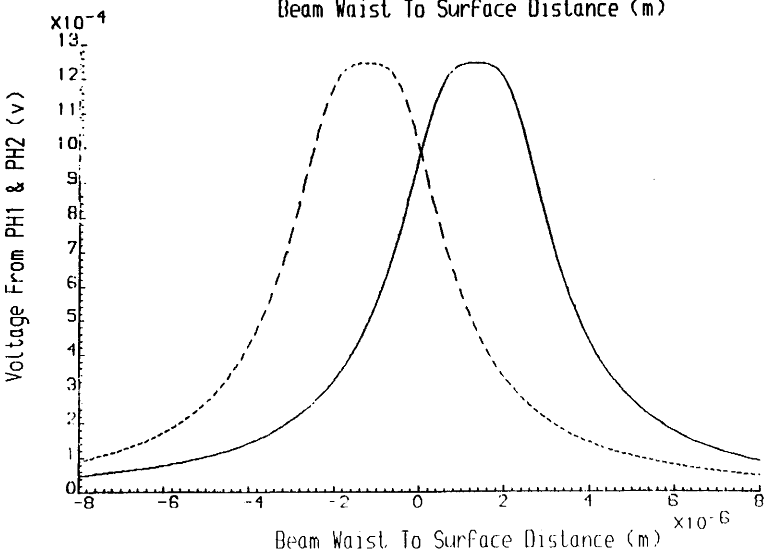

Figure 3.8 Gaussian simulation results for Dobosz parameters

3.4 Radiometric Modelling:

From the experimental procedure it was found that the laser beam upon reflection from the workpiece does not have a gaussian intensity distribution. This is due to the destruction of the gaussian profile by the roughness of the workpiece surface. As a consequence, a gaussian model of the reflected beam is not wholly correct and an alternative model was sought which would take account of this.

One possible way of modelling the optical system is to use geometric optical theory to calculate the radiometric intensity distribution in front of the two pinholes. In this case the surface beam spot is considered as a uniformly illuminated lambertian source of diffuse reflection, with a radius equal to the gaussian beam radius on the workpiece surface, which emits light according to the lambert cosine law. Whilst the assumption of uniform illumination ignores the gaussian intensity distribution, it is justified by the substantial improvement in the accuracy of the mathematical modelling.

The radiometric model assumes the laser beam is gaussian from the laser source to the point when it hits the surface fig.(3.9). It is then possible to model the two pinholes as being transformed from their initial position through the image lens L_3 and the unfolded image of the main lens L_2 fig. (3.9). Thus, two images of the pinholes are formed in front of the workpiece surface. The total power passing through the pinholes can then be calculated through use of the lambertian law.

3.4.1 Radiometric Analysis:

This section details the mathematical analysis of a radiometric model of one arm of the optical system [illustrated in fig. (3.9)]. A laser beam with beam waist radius W_{01} is focused by the main lens L_1 to a new beam waist radius W_{02}. L_2 is the reflected image of the main lens L_1, while L_3 is the image lens. Two pinholes PN_1 and PN_2 are positioned at a distances Z_{P1} and Z_{P2} from the reference beam waist W_{ref}.

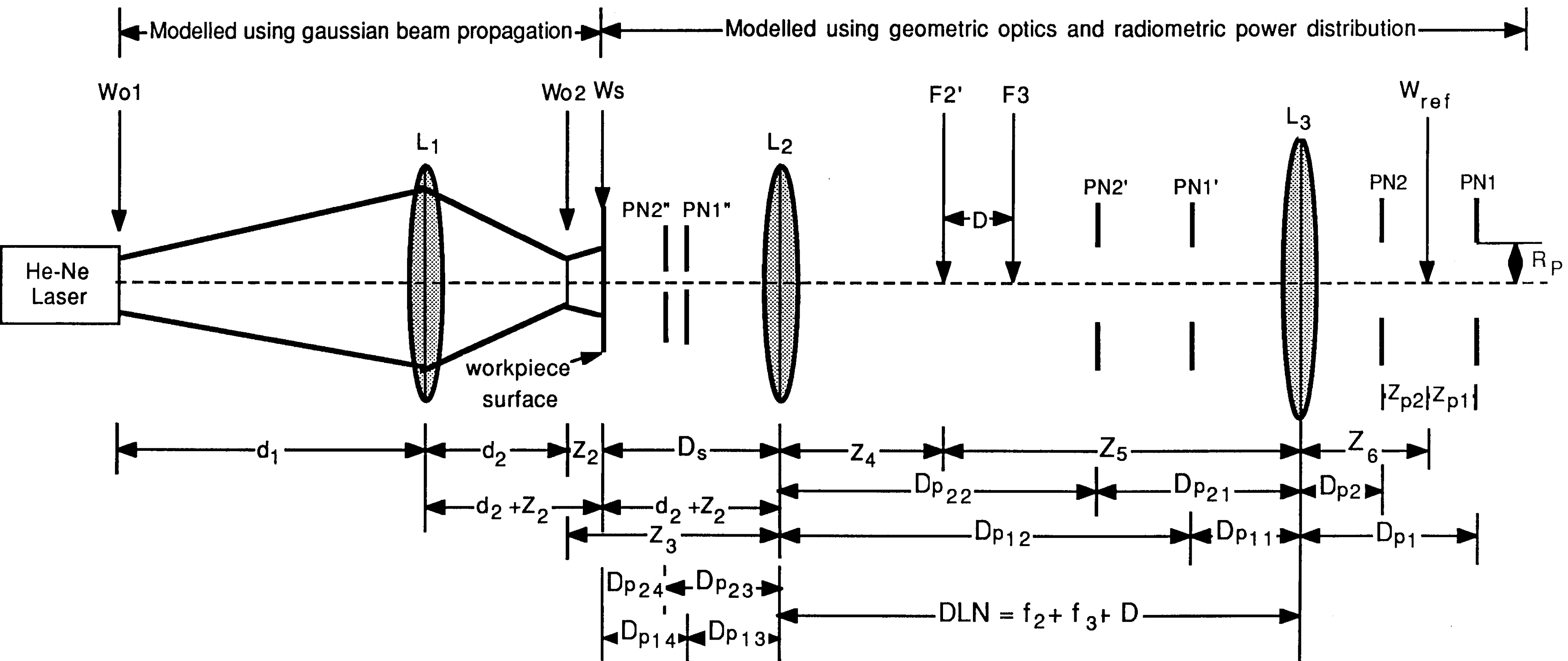

Figure 3.9 Diagram showing radiometric method of modelling

Since, the calculation of the size and position of the focused beam waist W_{o2} is similar to the procedure in section (3.3.1), using gaussian beam theory, the result of that section can be used.

To calculate the maximum intensity I_o at the focused beam waist :

$$I_o = 2 P_T / \pi W_{o2}^2 \tag{3.23}$$

The power of the beam spot (P_s) on the workpiece surface is :

$$P_s = \pi I_o W_s^2 /2 \tag{3.24}$$

Where W_s is the beam radius on the workpiece surface:

$$W_s = W_{o2}[1 + (\lambda Z_2 / \pi W_{o2}^2)^2]^{0.5} \tag{3.25}$$

The position of the W_{ref} is calculated by setting ($Z_3 = d_2 + 2 Z_2$) see fig. (3.9), d_2 is calculated using the thin lens equation as in section (3.3.1).:

$$1/Z_4 = 1/f_2 - 1/Z_3 \tag{3.26}$$

Where Z_4 is the position of a beam waist formed between the L_2 and L_3, and f_2 is the focal length of the lens L_2 . The distance between the two lenses L_2 and L_3 is (DLN) and it is equal to :

$$DLN = f_2 + f_3 + D \tag{3.27}$$

Where f_3 is the focal length of the image lens L_3 and D is the distance between the focal points F_2' and F_3 of the two lenses L_2 and L_3. The position of the beam waist relative to the image lens L_3 is Z_5 and equal to :

$$Z_5 = DLN - Z_4 \quad (3.28)$$

After passing the image lens the position of the reference beam waist W_{ref} is Z_6 and can be calculated from :

$$1/Z_6 = 1/f_2 - 1/Z_5 \quad (3.29)$$

The positions of the two pinholes PN_1 and PN_2 with respect to the reference beam waist W_{ref} are Z_{P1} beyond it and Z_{P2} before it. In this way the distance between the two pinholes and the image lens L_3 are DP_1 and DP_2 respectively and may be calculated as :

$$DP_1 = Z_6 + Z_{P1} \quad (3.30)$$

$$DP_2 = Z_6 - Z_{P2} \quad (3.31)$$

If the two pinholes have equal radius R_P, but at different distances from the image lens L_3. Two images of the pinholes are formed PN_1' and PN_2' with respect to L_2. By using the thin lens equation for the image lens :

$$1/DP_{11} = 1/f_3 - 1/DP_1 \quad (3.32)$$

$$1/DP_{21} = 1/f_3 - 1/DP_2 \quad (3.33)$$

Here DP_{11} and DP_{21} are the position of the pinholes image PN_1' and PN_2' respectively. The radius of the two images (according to the magnification of the thin lens) are equal to :

$$PN_1' = MP_1 \; R_P \quad (3.34)$$

$$PN_2' = MP_2 \; R_P \quad (3.35)$$

Where PN_1' and PN_2' are the new radii of the pinholes, R_P is the initial pinholes radius,

MP_1 and MP_2 are the magnification of the pinholes PN_1 and PN_2 through L_3 respectively and according to the geometrical optics they are equal to :

$$MP_1 = DP_{11} / DP_1 \quad (3.36)$$

$$MP_2 = DP_{21} / DP_2 \quad (3.37)$$

This causes the nearest pinhole to the lens to have an image of smaller size.

The two images are then transformed through the lens L_2 to form the images PN_1'' and PN_2'' in front of the workpiece surface. The distance between the images and L_2 is :

$$DP_{12} = DLN - DP_{11} \quad (3.38)$$

$$DP_{22} = DLN - DP_{21} \quad (3.39)$$

The size of the new images are :

$$PN_1'' = PN_1' \;\; MP_{11} \quad (3.40)$$

$$PN_2'' = PN_1' \;\; MP_{21} \quad (3.41)$$

Where MP_{11} and MP_{21} are magnifications through the lens L_2 :

$$MP_{11} = DP_{13} / DP_{12} \quad (3.42)$$

$$MP_{21} = DP_{23} / DP_{22} \quad (3.43)$$

The two pinholes PN_1 and PN_2 form two images at different distances in front of the workpiece surface. The distance D_s between the surface and L_2 is :

$$D_s = d_2 + Z_2 \quad (3.44)$$

so the distance between the photodiodes PN_1" and PN_2" and the surface are equal to :

$$DP_{14} = D_s - DP_{13} \quad (3.45)$$

$$DP_{24} = D_s - DP_{23} \quad (3.46)$$

If the surface is considered as a lambertian source, the total power transmitted through the pinholes can be calculated using lambert's cosine law. As in fig. (3.10) the power $d\phi$ reaches the pinhole from the surface can be written as : Ref. (45,46,47)

$$d^2\phi = L\, dS\, d\Omega\, \cos\theta \quad (3.47)$$

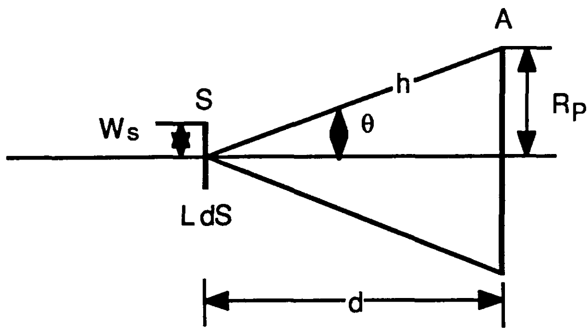

Figure 3.10: The total power emitted from the beam spot on the workpiece surface toward a pinhole

From fig (3.10) :

$$d\Omega = dA \cos\theta / h^2 \quad (3.48)$$

so

$$d^2\phi = L\, dS\, dA\, \cos\theta^2 / h^2 \quad (3.49)$$

Where dS is the projected area of the source element and dA is the projected area of the pinhole. After the integration detailed in appendix (A8) :

$$P_T = \pi^2 L W_s^2 \left[\frac{R_P^2}{R_P^2 + d^2} \right] \quad (3.50)$$

Where P_T is the total power transmitted through the pinhole, L is the radiance of the source, W_s is the laser beam radius on the workpiece surface, R_P is the radius of the pinhole, d is the perpendicular distance between the source and the pinhole. So for the pinholes PN_1" and PN_2" the total transmitted powers :

$$P_{PN1"} = \pi^2 L W_s^2 \left[\frac{PN_1"^2}{PN_1"^2 + DP_{14}^2} \right] \quad (3.51)$$

$$P_{PN2"} = \pi^2 L W_s^2 \left[\frac{PN_2"^2}{PN_2"^2 + DP_{24}^2} \right] \quad (3.52)$$

The output photodetector voltages V_{P1} and V_{P2} [which are positioned immediately after the pinholes PN_1 and PN_2] are :

$$V_{P1} = K_P P_{PN1"} \quad (3.53)$$

$$V_{P2} = K_P P_{PN2"} \quad (3.54)$$

Where K_P is the sensitivity of the photodetector.

The output voltage (V_{DA}) of the differential amplifier used to measure the photodiode output is :

$$V_{DA} = K_A [V_{P1} - V_{P2}] \quad (3.55)$$

Where K_A is the amplifier gain.

The normalized output V_T of the deferential amplifier is :

$$V_T = K_A \ V_{Ref} \frac{[V_{P1} - V_{P2}]}{[V_{P1} + V_{P2}]} \qquad (3.56)$$

3.4.2 Radiometric Modelling Program:

The modelling program was written in Fortran 77 on a VAX computer in the Mechanical Engineering Department. The program coded the analysis of section (3.4.1) in a similar fashion to the gaussian modelling program. The logical flow of the program is shown in fig.(3.11), while the program itself is given in appendix (A9).

The output data of the program is again presented as three graphs to enable the effects of design parameter change to be seen. The program uses the normalized output method presented in section (3.3.1). The title "Radiometric Modelling" is given at the top of the input parameter list to distinguish the results from the Gaussian Modelling.

3.4.3 Results of Simulation:

Some of the modelled results are shown as graphs in this chapter for the same input data as the gaussian modelling results. Figure 3.12 shows the results of the radiometric model for an 75mm main lens. It can observed that the distance between the two peaks is reduced when compared to the gaussian results. The lower left graph represents the power in front of the pinholes. Figure 3.13 gives the power, voltage and the normalized output for a main lens with 120mm focal length. As in the 75mm case the slope of the normalized curve is less than the one for the gaussian model. Figure 3.14 is plotted for the optimum parameters, as analyzed by Dobosz in Ref.(21). The results of this model will be compared with the other simulated and experimental results in chapter 4.

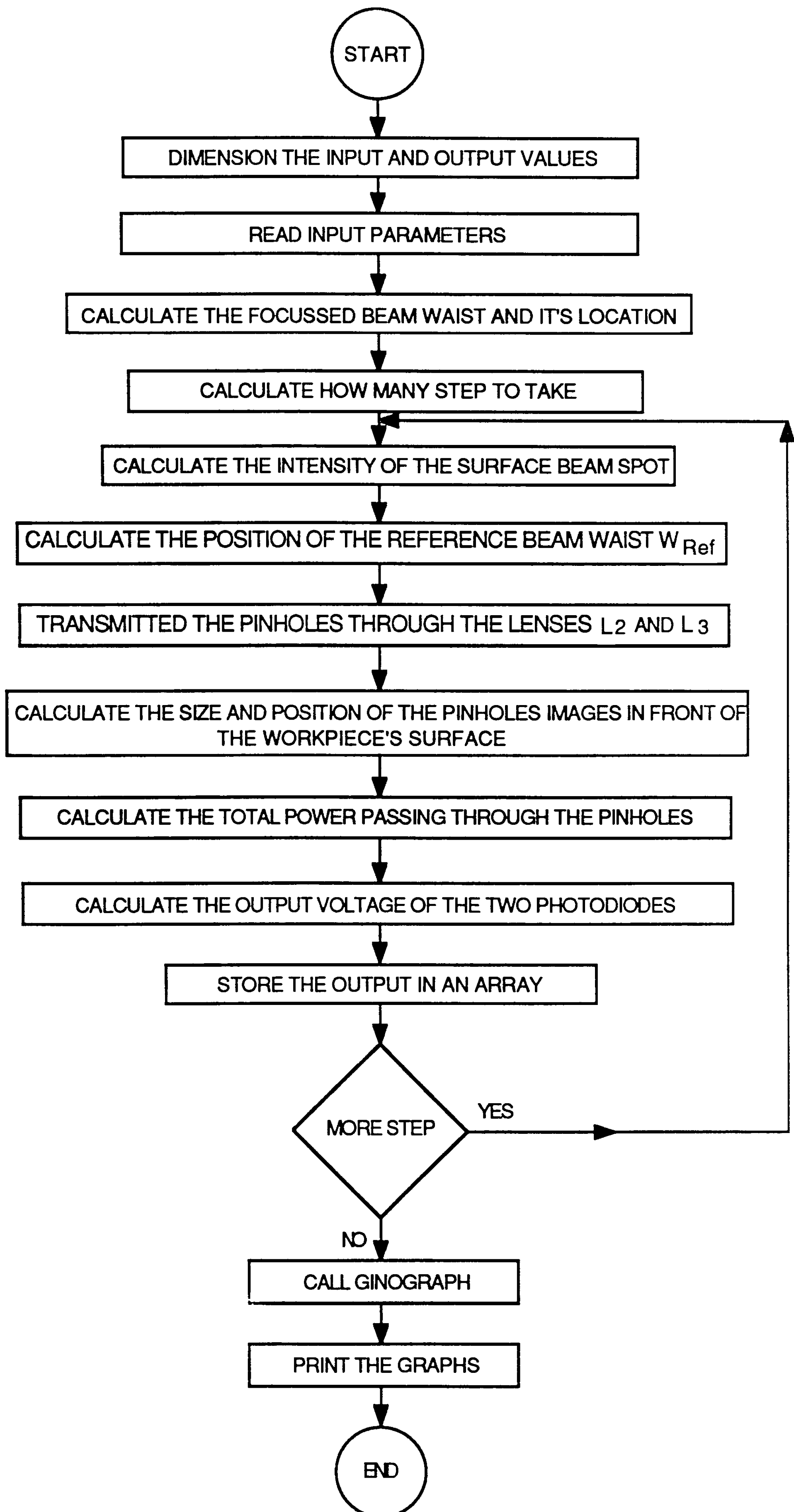

Figure 3.11 The flow chart of the radiometric modelling program

Robot Sensor Simulation - Radiometric Design !!

FIGURE(3.12)

LASER WAVELENGTH (mm)......................	-0.6330E -3
LASER BEAM WAIST RADIUS (mm).............	- 0.31500
BEAM POWER (mW)...........................	-0.4000E 1
FOCAL LENGTH OF MAIN LENS (mm)..........	- 75.000
FOCAL LENGTH OF IMAGE LENS (mm).........	- 300.000
DIAMETER OF THE PINHOLE (mm).............	- 0.200000
LASER TO MAIN LENS DISTANCE (mm).........	- 1000.000
DISTANCE BETWEEN MAIN AND IMAGE LENS (mm)	- 0.000
PINHOLE OFFSET DISTANCE (mm).............	- 5.000000
AMPLIFIER GAIN............................	- 4.000

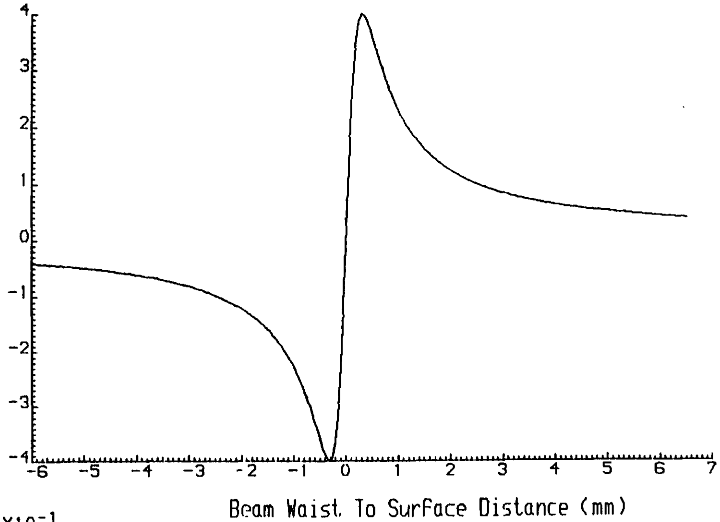

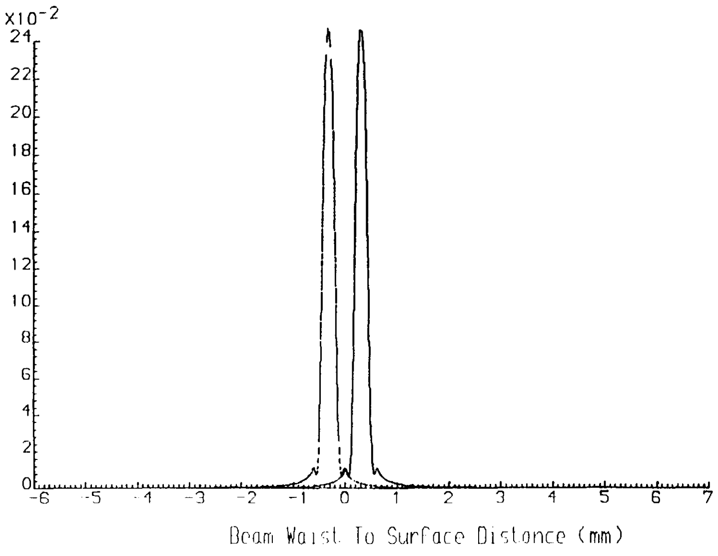

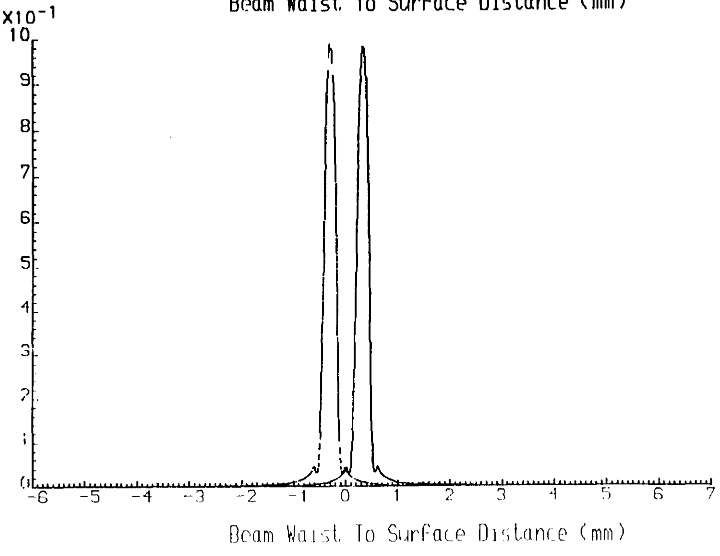

Plotted on 9-SEP-88 at 12:55:35

Figure 3.12 Radiometric simulation results for 75mm lens

Robot Sensor Simulation - Radiometric Design !!

FIGURE(3.13)

LASER WAVELENGTH (mm)......................	-0.6330E -3
LASER BEAM WAIST RADIUS (mm).............	- 0.31500
BEAM POWER (mW)...........................	-0.4000E 1
FOCAL LENGTH OF MAIN LENS (mm)...........	- 120.000
FOCAL LENGTH OF IMAGE LENS (mm)..........	- 300.000
DIAMETER OF THE PINHOLE (mm).............	- 0.200000
LASER TO MAIN LENS DISTANCE (mm).........	- 1000.000
DISTANCE BETWEEN MAIN AND IMAGE LENS (mm)	- 0.000
PINHOLE OFFSET DISTANCE (mm).............	- 5.000000
AMPLIFIER GAIN...........................	- 4.000

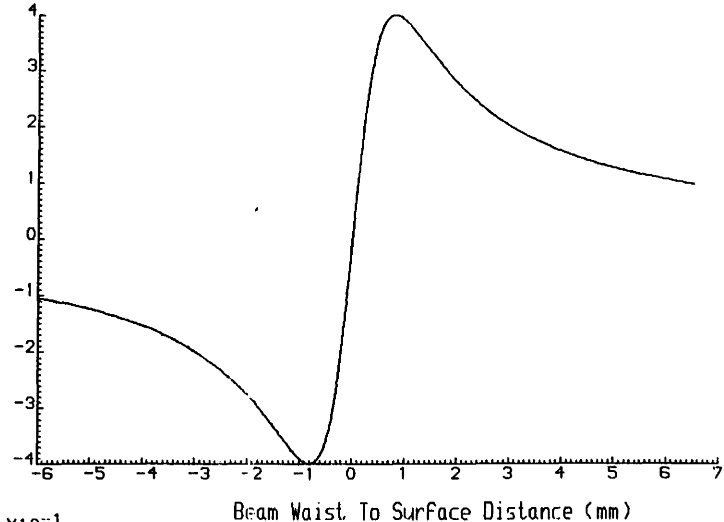

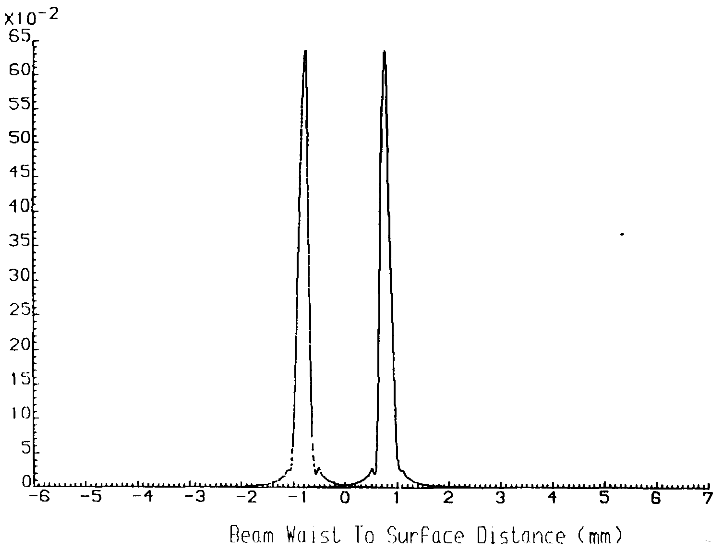

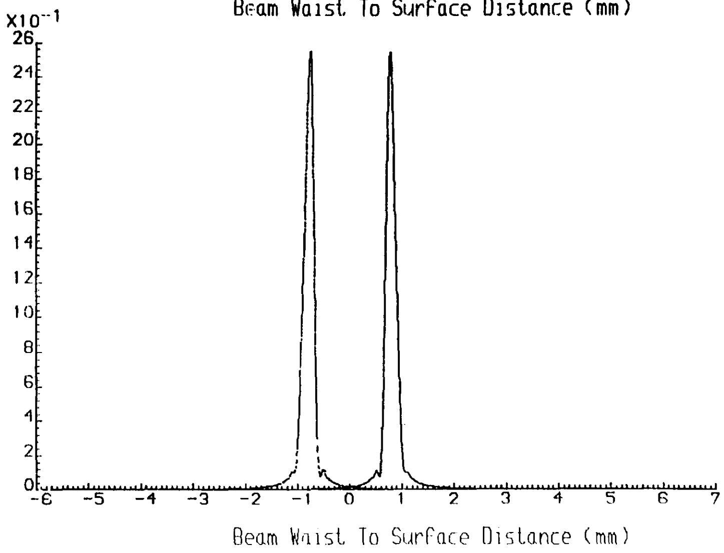

Plotted on 9-SEP-88 at 12:58:59

Figure 3.13 Radiometric simulation results for 120mm lens

Robot Sensor Simulation - Radiometric Design !!

FIGURE(3.14)

LASER WAVELENGTH (m)....................	-	-0.6320E -6
LASER BEAM WAIST RADIUS (m)............	-	0.00116
BEAM POWER (W)...........................	-	-0.1250E -1
FOCAL LENGTH OF MAIN LENS (m)..........	-	0.003
FOCAL LENGTH OF IMAGE LENS (m).........	-	0.135
DIAMETER OF THE PINHOLE (m)............	-	0.000080
LASER TO MAIN LENS DISTANCE (m)........	-	0.001
DISTANCE BETWEEN MAIN AND IMAGE LENS (m)	-	0.000
PINHOLE OFFSET DISTANCE (m)............	-	0.004500
AMPLIFIER GAIN..........................	-	4.000

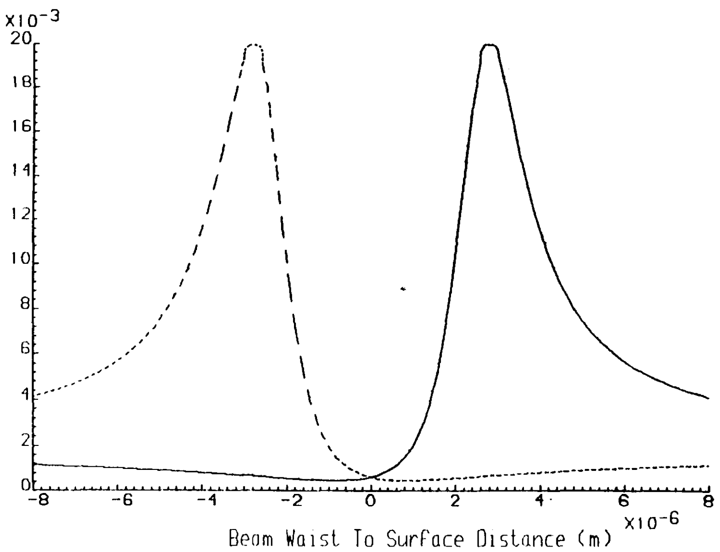

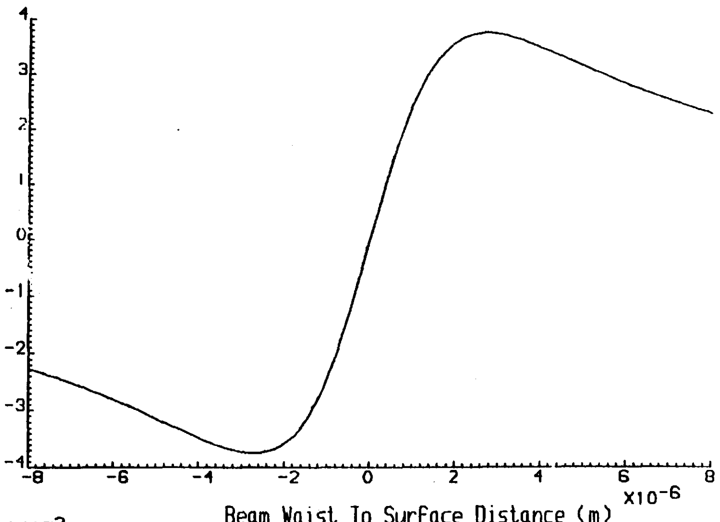

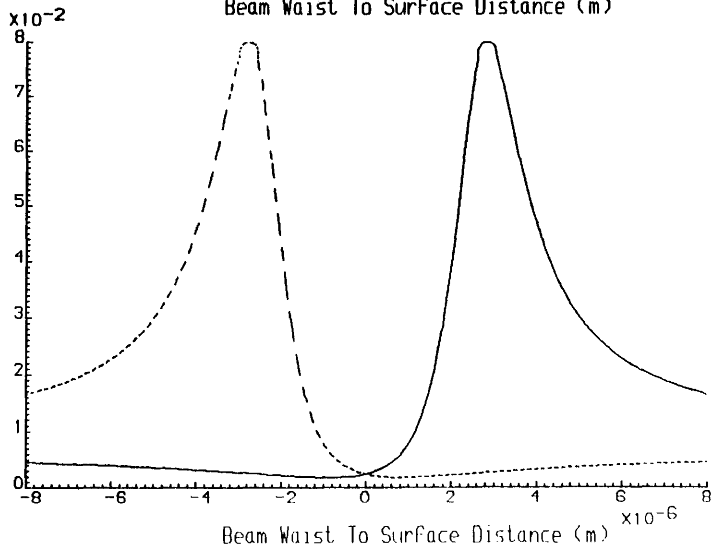

Plotted on 9-SEP-88 at 13:02:58

Figure 3.14 Radiometric simulation results for Dobosz parameters

CHAPTER 4
EXPERIMENTAL MODELLING

CHAPTER 4: EXPERIMENTAL MODELLING

4.1 Introduction:

In order that the performance of the designed system may be analyzed, a comparison is required between the performance predicted in chapter 3 and recorded operational characteristics. Therefore this chapter presents the operational characteristics of the optical system recorded through an experimental procedure. The experimental work was performed to confirm design principles for a general class of opto-electronic stand-off sensor, which could then be used as a guide, to select and design particular sensor configuration optimized to a desired function.

A description of the experimental apparatus and procedure is given. The experimental apparatus is divided into optical apparatus and transducing and conditioning system. The results of 13 experiments, presented in graphical form, are used to show the effects of changing the size and position of selected components on the output voltage signal. The results of gaussian, gaussian-radiometric and experimental modelling are discussed later in this chapter.

4.2 Experimental Apparatus:

The experimental apparatus can be sub-divided into two sub-systems.

An optical system which transmits an image of the reflected laser beam to form a spot in front of the photodiodes. This spot size being related to the spot size of the focused beam on the workpiece surface and hence the stand-off distance.

A transducing and signal conditioning system, which effectively measures this spot size by transducing the laser spot power falling through the pinholes into an electrical signal. This signal is then conditioned and amplified to determine the axial displacement of the workpiece.

4.2.1 Optical System:

A Helium - Neon laser [1] fig.(4.1) (Uniphase model 1103) with an output power of approximately = 4 mW (rated class 3b) and wavelength λ=0.633 µm is used to provide a bright, highly directional light source. A square flat mirror [2] (101.6 x 101.6mm) of utility quality is mounted at an angle of 45° to change the direction of the beam, to allow a variation in the distance between the laser and the main lens, due to the limited size of the optical table.

The beam is then split by the first beam plate splitter B_1 [3] (78 x78 x1mm) into two parts. One part is absorbed by a beam stop [4], the other is modified and focused onto the workpiece by the main lens L_1 [5] (plano-convex crown glass lens). In the experiment two different focal length lenses were employed 75mm and 120mm with diameters of 40mm and 50mm respectively, to evaluate the effect of focal length and clear aperture upon the output.

The reflected beam is collected through the main lens L_1, then split into two parts again by B_1. One returning along the path of the main beam, the other turned towards the image lens L_2 [7] (Biconvex crown glass lens) with a focal length of 300mm and diameter of 50mm. This beam is again split by means of a beam splitter B_2 [8] (50 x 50 x1mm) into two equal parts, each going to a circular pinhole mounted in front of a photodiode. Three pinhole diameters were used (100, 200, 300 µm) to investigate the effect of pinhole size on the output signal.

The distance between the photodiodes and the pinholes was made as small as possible, to reduce truncation and perturbation effects. Optical components were mounted on low profile bench carriers with transverse and vertical slides for alignment. These slides were fixed onto the optical to avoid vibration and movement of optical components.

Moreover, the components were fixed at known distances for each configuration. In the first configuration the distance between main lens and the laser was (1m), while the distance between the main and image lenses was fixed so that, the focal points of the two

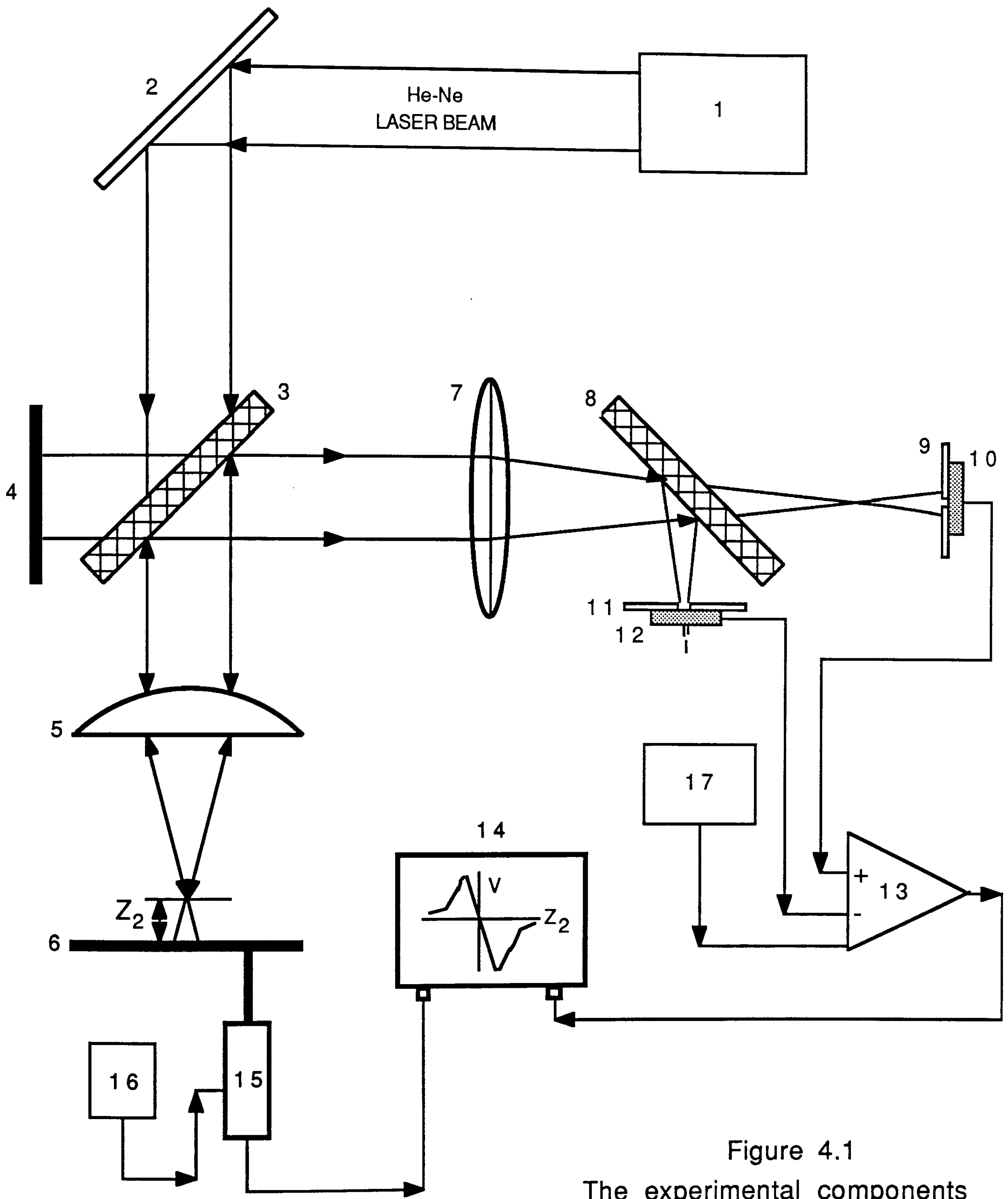

Figure 4.1
The experimental components

1. He-Ne laser
2. Mirror
3. First beam splitter B_1
4. Beam stop
5. Main lens L_1
6. The workpiece
7. Image lens L_2
8. Second beam splitter B_2
9. First pinhole PN_1
10. First photodiode PH_1
11. Second pinhole PN_2
12. Second photodiode PH_2
13. Differential amplifier
14. X-Y recorder
15. LVDT
16. LVDT DC-supply
17. Amplifier DC-supply

lenses were coincident. The mirror and the beam splitters were positioned at suitable distances to modify the beam direction. In effect the configuration can be seen as a microscope.

4.2.1.1 Alignment of Optical Components:

This task is one of importance as alignment of the optical components affects the experimental result. It needs time and practice to perfect and must be carried out for each optical configuration, this process is outlined in appendix (A10).

One of the problems encountered in the experiment is the determination of the position of the beam waist planes ($2W_{02}$, $2W_{04}$, $2W_{04}'$). This is done after alignment of the laser,main lens, beam splitters, mirror and the image lens.

4.2.2 Transducers and Signal Conditioning System:

Two general purpose photodiodes PH_1 and PH_2 (RS 305-462) are placed behind two pinholes PN_1 and PN_2. These transform light power to an analog current by means of photosensitive area located at the centre of the photodiode frame. The diode induced current is a function of the intensity of light falling on the sensitive area. The output current from the two photodiodes is fed into a differential amplifier through two input sockets, to be converted to a voltage signal, amplified and output to the Y axis of an X-Y recorder.

The axial displacement of the workpiece from the plane $2W_{02}$ is transduced to a voltage signal by a DC-LVTD (linear voltage displacement transducer), fed by a DC-power supply. This has a linear range of 12.5mm, so calibration is required to ensure working in this range of core displacement. The output is connected to the X axis of the X-Y recorder.

The X-Y recorder (Hewlett-Packard 7045A) was employed as a device to plot the amplifier signal in volts versus the workpiece displacement in mm.

4.2.2.1 The Differential Amplifier:

The amplifier was one of the most problematical components of the experimental apparatus, many modifications were required to improve its performance, accuracy and reliability. After many experiments it was found that the original amplifier, was incapable of providing the required improvement in signal and the decision was taken to design and build a new amplifier to the following specification :

. independent amplification and balance of each photodiode channel.

. two outputs to allow the measurement of the photodiode currents directly.

. two outputs giving the quantities (V_1-V_2) and (V_1+V_2).

. a polarity switch on the input.

. an improved circuit for the division $[(V_1-V_2)/(V_1+V_2)]$ with an independent adjustment of V_{Ref} (V_{Ref} is a voltage multiplying the division quantity to convert it to a voltage).

. three LEDs showing the position of the workpiece.

A circuit diagram is shown in fig.(4.2), while a front view of the amplifier is shown in fig.(4.3).

For the purpose of describing the schematic circuit of the amplifier and its function, the main circuit is sub-divided into eight sub-circuits as in fig.(4.2). The photodiode signal currents are fed to circuits No.1 and 2, these being two stage amplifiers which convert the current signal from the photodiodes to a voltage signal, with potentiometers to adjust the gain and balance of the signal. The output of the two amplifiers are connected through a polarity switch No.3. The two voltages are then fed to the sum and difference circuits No.4 and 5 to produce the quantities (V_1+V_2) and (V_1-V_2).

The output of the sum and difference circuits are connected to the division circuit No.6 to perform the division $(V_1-V_2)/(V_1+V_2)$. This is multiplied by V_{Ref} to convert it to a voltage (circuit No.7 has an independent amplification) for output. Three lights are nested in circuit No.8 fig.(4.2) to indicate the presence of a valid

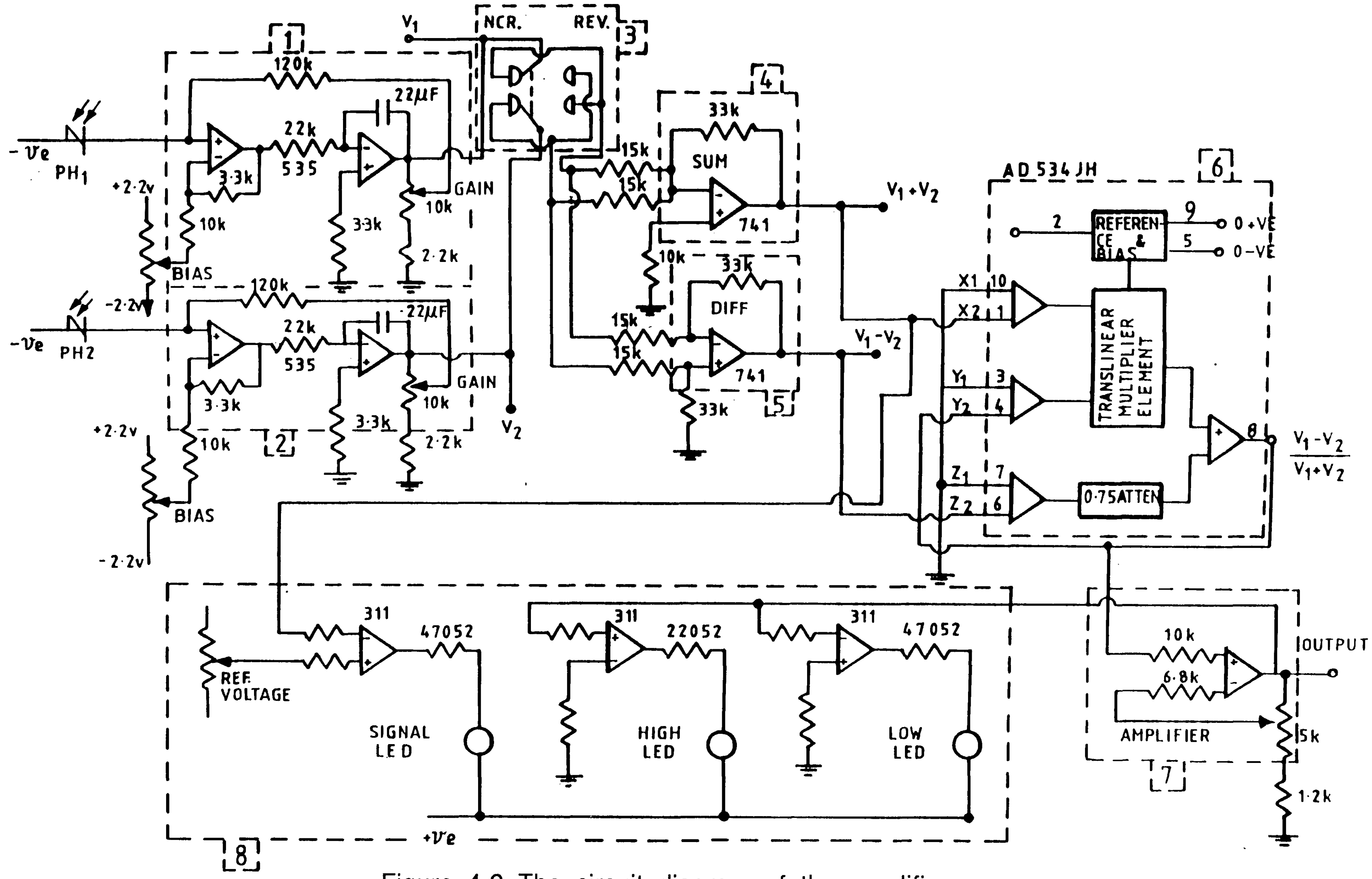

Figure 4.2 The circuit diagram of the amplifier

signal and the position of the workpiece fig.(4.3).

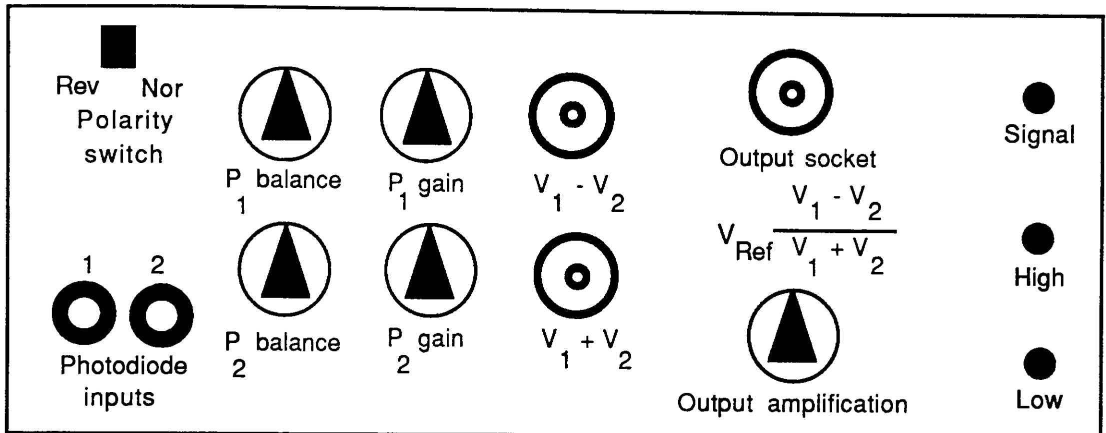

Figure 4.3 The front view of the amplifier

4.3 Experimental Procedure:

Two main series of experiments were conducted using 75mm and 120mm main lens focal lengths. Each series of experiments attempted to determine the effect of changing the following parameters: pinhole size, pinhole offset distance, distance between the main and image lenses and workpiece surface.

Two measured parameters were taken as representing the output response of the sensor. Firstly the sensitivity of the signal (the distance between the positive and negative peaks of the signal output), was though important for the system design because the characteristics of the control output response are dependent on it and the effective range of the device is characterized by it.

Secondly the linearity of the line between the two peaks was examined, as one of the aims in optimizing the sensor configuration is to utilize linear control system technology. The magnitude of the output voltage was not considered important as it can be controlled by the gain of the amplifier and the magnitude of V_{Ref}.

The experimental results were recorded using an X-Y recorder, by moving the

workpiece with a limit of 6.5mm before the focused beam waist $2W_{02}$ plane and 6mm after it, this being the linear range of the LVDT. The X and Y axes of the recorder were calibrated to fit the graph paper.

Careful alignment(4.2.1.1) was required for each experiment (see appendix A10).

4.4 Results:

The results were recorded in graphical form for all experiments. The X axis of each graph recorded the deviation of the workpiece surface from the beam waist in millimeters, while the Y axis recorded the normalized output voltage from the sensor. Each graph was then annotated with a list of main experimental parameters.

From graphs 4.1 and 4.2 (pages 82 and 83) it can be seen that the pinhole offset distance (l) (the symmetrical distance between the pinholes and the planes of beam waist $2W_{04}$ and $2W_{04}'$) affects the characteristics of the output signal. From the results it can be seen that, for a given pinhole size, the linearity and the sensitivity of the normalized output increases and the peak output voltage decreases, when the offset distance is reduced. These phenomena occurred for both configurations.

This occurs because the pinhole offset distance ($\pm l$) controls the overlap of the voltage signals V_1 and V_2. This can be seen in fig.(4.4). The differential amplifier produces a summation of these two voltages as a normalized output voltage. At 100% overlap the normalized output voltage is zero fig.(4.4a). The output increases as the percentage ratio of the overlap decreases, until it reaches a maximum output at 0% overlap fig(4.4c). Any further increase in the distance ($\pm l$) forms a section with no overlap between the signals and a consequent loss in linearity.

After many experiments it was estimated that the optimum distance for the pinhole offset in the configurations studied was about ±5mm and this value was held constant throughout the rest of the experiments.

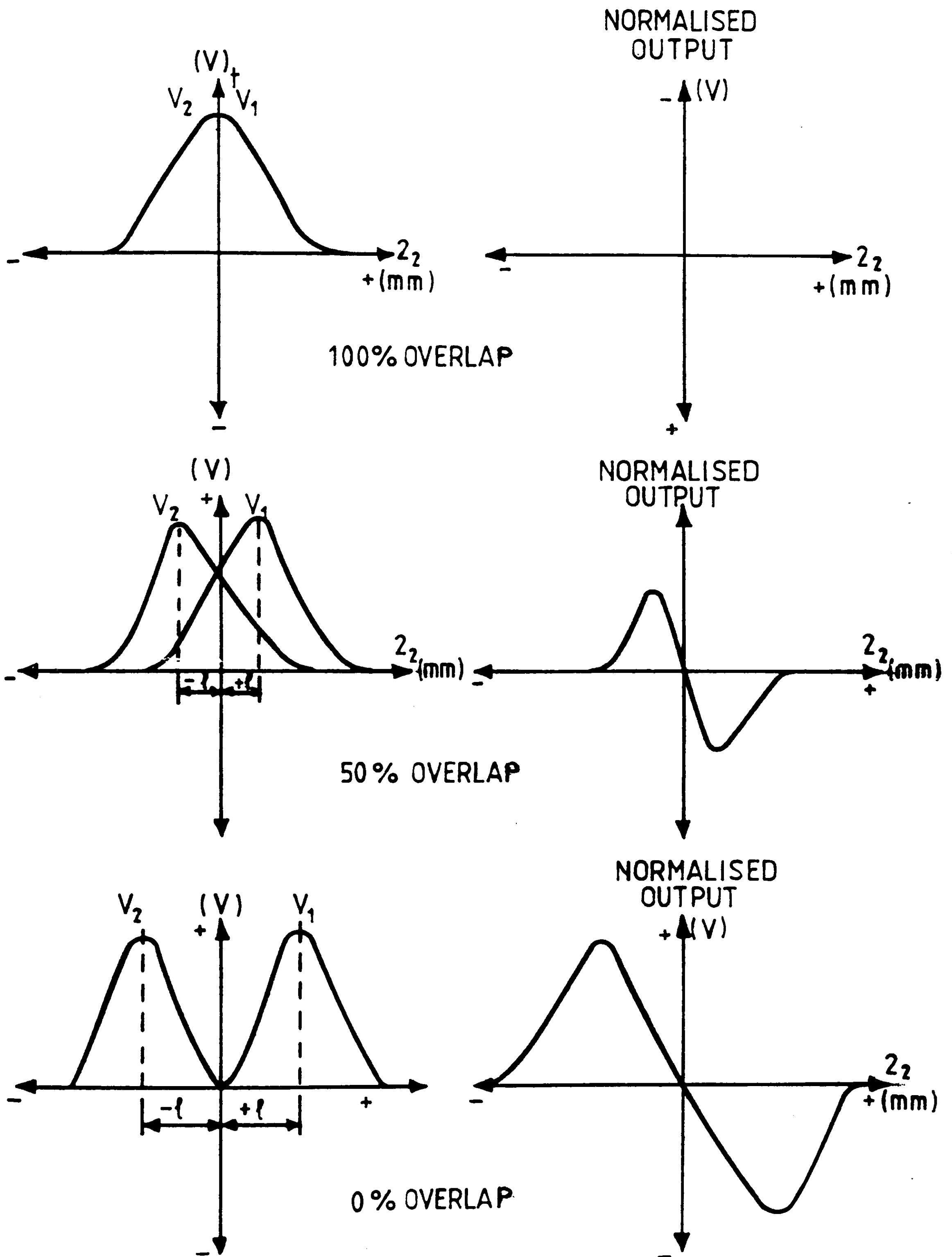

Figure 4.4 Overlapping of photodiode output voltages

The results in graphs 4.3 and 4.4 (page 84 and 85) show that the pinhole size has an important effect on output signal. A pinhole of 100μm diameter (curve No.3 on both graphs) gives the smallest distance between peaks leading to the most sensitive output, but suffers from a large noise effects due to of the interaction of speckle and truncation effects. A 300μm diameter (curve No.1 on both graphs) gives a larger distance between the peaks (reduced sensitivity), but with less noise due to its larger size as speckle noise is integrated out. A pinhole size of 200μm gives results (Curves No.2 on both graphs) placed between the previous curves and appeared to be the best compromise for pinhole size (for this particular combination of main and image lens focal lengths). Consequently, the later experiments were performed utilizing this pinhole size.

The graphs 4.5 and 4.6 (pages 86 and 87), show the effect of changing the distance between the laser and main lens on sensor output. This shows that as the laser is moved away from the main lens, that the sensitivity and the magnitude of the output increases. This is because, the focused beam has greater divergence and consequently a more rapid change in intensity is seen at the pinholes. From the previous graphs it can be seen that this effect has less influence on the output signal in comparison to the pinhole size and offset distance.

The curve No.1 on graphs 4.7 and 4.8 (pages 88 and 89) were plotted for an incident angle of 0.0° as a reference signal. Curve No.2 on both graphs were shown the output signal after the workpiece was turned through 5 and 10 degrees clockwise, while Curves No.3 were produced by a turn of 10 and 15 degrees counter clockwise.

The sensitivities exhibited are nearly identical for each group of curves in both graphs and the magnitude of the output voltages are almost constant. The shifting position of the output curves occurred because the rotational axis of the workpiece was not coincident with the focused spot on the workpiece surface. From these results it can be seen that sensor output is largely independent of the angle of the incident beam.

The effects of variation in the distances between the main and image lenses are recorded in graphs (4.9), (4.10), (4.11) and (4.12). The graphs (4.9) and (4.10) illustrate the effect

of extending the distance between the main and image lenses. It can be seen that by increasing this distance that the sensitivity is increased. The curves 2a and 2b in the graph (4.9) are plotted for the same set-up, but in curve 2b the gain of the second photodiode PH_2 was reduced.

The graphs (4.11) and (4.12) to present the effect of reducing the distance between the main and image lenses, by moving the image lens toward the main lens. This results in decreased sensitivity and magnitude of the normalized output voltage.

A more sensitive output is recorded when the distance between the main and image lenses is increased, because the beam diameter in front of the image lens changes more rapidly. Different magnitudes of the output voltage in graphs (4.9) and (4.10) were probably due to misalignment or the division circuit of the amplifier not working properly.

To show the effect of the focal length of the main lens upon the output an experiment was conducted, the results of which are presented in graph (4.13) (page 94). It can be seen that curve No.2 records a more sensitive output than curve No.1. This indicates a reduction in the focal length of the main lens produces a more sensitive signal but with less output voltage. This occurs due to the increased magnification of the system (any small movement of the surface from the focused position will cause a large change in beam spot diameter in front of the pinholes). In curves No.3 and 4 the same main lenses are utilized but without any image lens. This shows a significant drop in output voltage, signifying that an image lens is required to recollect the reflected light beam.

The results of the effect of changes in workpiece surface are not presented because, a factor of four was found between the peak output voltages for mild and galvanised steel workpieces. This made the presentation of results on the same paper with calibrated axes impossible. It was thought that this result was due to the divider within the amplifier not working correctly.This effect was to be seen in the performance of the control experiments presented later.

4.5 Comparison Between Mathematical and Experimental Modelling:

At this stage three models together with representative results have been presented. It is important to compare these in order that an analysis can be made and conclusions drawn which are useful for a designer wanting to optimize the components and sensor geometry for a given application. This section compares the two mathematical models (gaussian and gaussian-radiometric) with the experimental model. Additionally it discusses the predictions resulting from the use of the analysis presented by Dobosz Ref.(21).

The gaussian and gaussian-radiometric model programs outlined earlier were fused into one program, in order that both predicted normalized output voltage signals would be plotted on the same graph. The results of this program are compared with the experimental models in the form of a overlay placed over experimental results. In the graphs presented gaussian implies the output produced by the gaussian model, whilst radiometric implies the output from the gaussian- radiometric model.

Graph 4.1T shows the gaussian and radiometric normalized outputs for the optimum set-up of the configuration using a 75mm main lens. These results can be compared with the experiment output signal for the 75mm configuration (curve No.1 graph 4.1). It can be seen from the two graphs, that the experimental output lies between the radiometric and gaussian models and that the radiometric model results are a closer prediction of actual performance.

Graphs 4.4T presents the gaussian and radiometric normalized output signals for a configuration with a main lens of 120mm focal length, sharing the same parameters as those in the experiment. By comparing these curves with the experiment result (graph 4.4 curve No.2). It can again be seen that the experimental result fell between the two models with the radiometric model proving the more accurate response. It should also be noticed that, the difference between the gaussian and experimental results increases as the focal length of the main lens increases. Generally, the results of the radiometric model are closer to the experiment results presented in this study.

To analyze and discuss the response of the three models (gaussian, radiometric and experimental) to changes in input parameters detailed in section (4.3) and to deduce the relationship between these models. A more concise method of presentation of results is required. This is achieved by Graphs 4.14 to 4.17 inclusive, which present the peak to peak distance (sensitivity of the output signal), with respect to various input parameters.

From these graphs it may be concluded that :

.The behavior of the beam is neither totally gaussian nor totally radiometric.

.The radiometric model is closer to the experimental model in comparison to the gaussian model for the cases discussed in this section.

.The experimental results are bounded between the gaussian and the radiometric models.

Consequently, to build a sensor the designer should compare both the gaussian and radiometric output signals for specific input parameters, in order to estimate the behavior of a particular design.

Graph 4.18 (page 99) is plotted for the parameters presented by Dobosz in Ref.(21). This shows an unexpected result, that is the coincidence of the linear part of the gaussian and radiometric models and the approximate coincidence of the two peaks. This interesting result indicates that by reducing of the focal length of the main lens and by changing the ratio between the main and image lens focal lengths, a coinciding of the output of the two models is obtained.

This result encouraged the running of the simulation program over a wider range of input parameters to investigate their effects on sensor response. Some of these results are presented in this chapter for input parameters annotated on the same graph.

From graph 4.19 it can be seen that for a main lens with a focal length of 10mm and image lens of 30mm, that the gaussian and radiometric peaks of the normalized output and the linear part are nearly coincident. Graph 4.20 simulated a different ratio between the main and image lens focal length. The main lens is 10mm, while the image lens is 230mm. Both linear sections and the two peaks are perfectly coincident .

These results mean that for devices with a small measuring range using a small focal length main lens and wider initial beam waist, that the difference between results of the two

models becomes negligibly small. This indicates that the beam behaves equally gaussian and radiometric for these specific configurations. This might answer the question as to why previous works limited their range of measurement for a part of millimeter or for a few millimeters.

Graph 4.21 presents the effect of changing only the wavelength of light source on the sensitivity of the output signal for the optical system detailed in graph (4.1). It can be seen from the graph that the peak to peak distance for the gaussian model decreases (shows increased sensitivity) as the wavelength increases. The radiometric model shows no response to this change in wavelength.

Graph 4.22 shows that the sensitivity of the gaussian model is increased as the initial beam waist of the light source is increased. Again the radiometric model shows no response to this effect.

As can be seen in graph 4.23 separating the laser from the main lens causes increasing sensitivity of the output signal.

From these three graphs it can be concluded that, the initial beam waist, wavelength and distance between the light source and the main lens, have no effect on the performance of the radiometric model because they affect both output voltages equally and the normalization of the voltages excludes these effects (see section 3.3.1 and 3.4.1). These results indicate that a wider set of experiments is required to determine which model proves more correct, although the radiometric model currently appears to be more generally applicable.

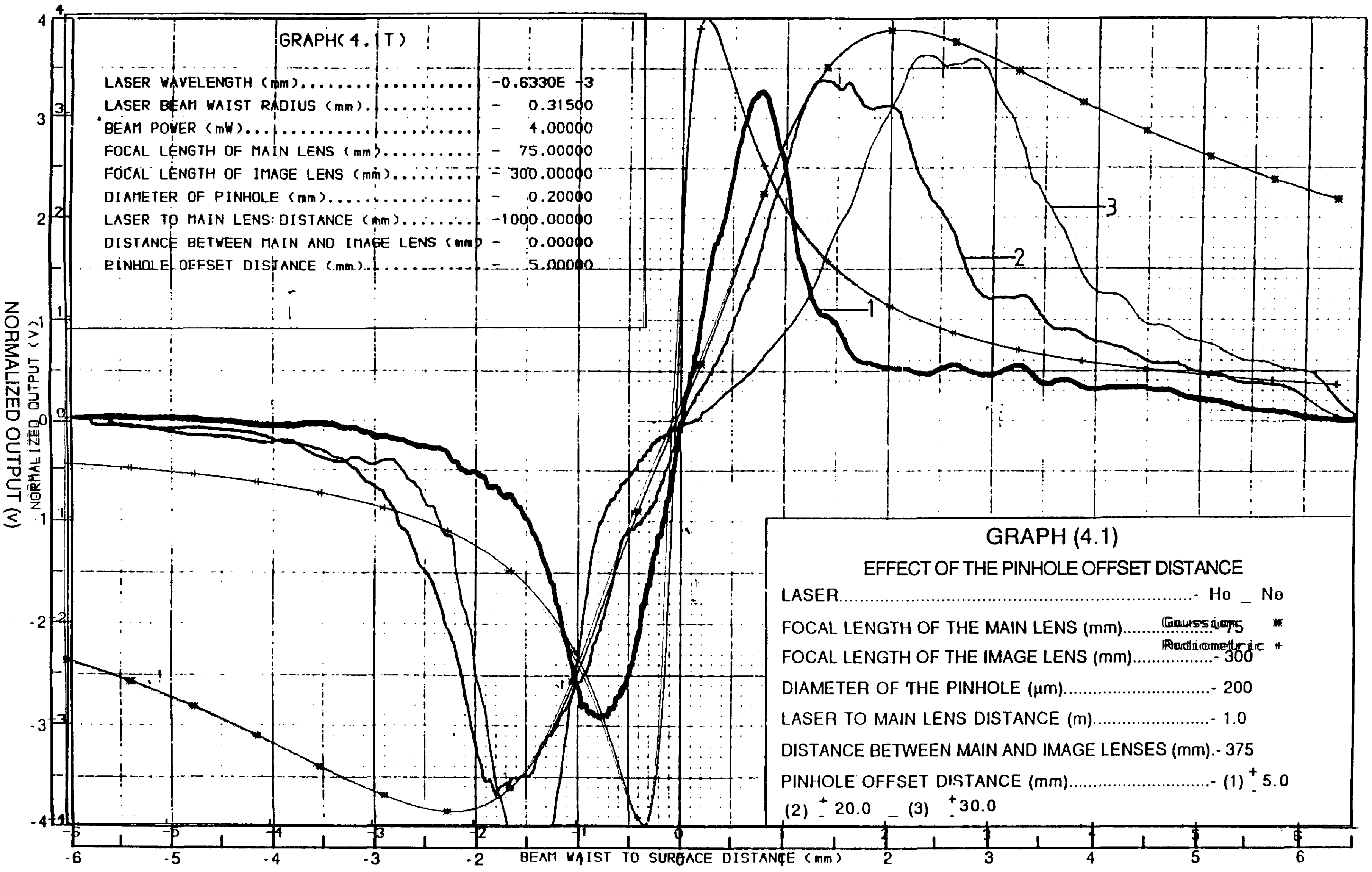

GRAPH (4.1)

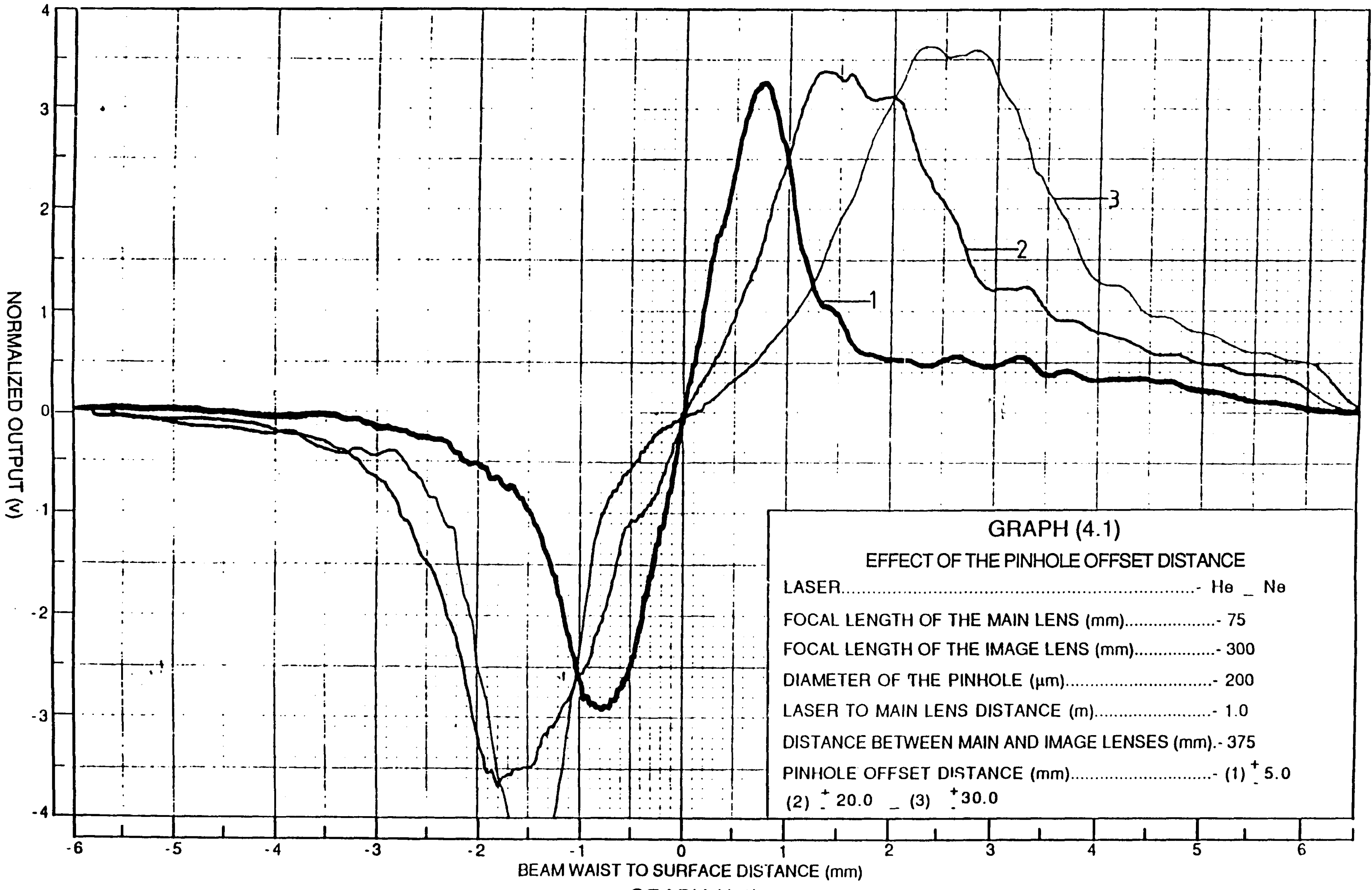

GRAPH (4.1)

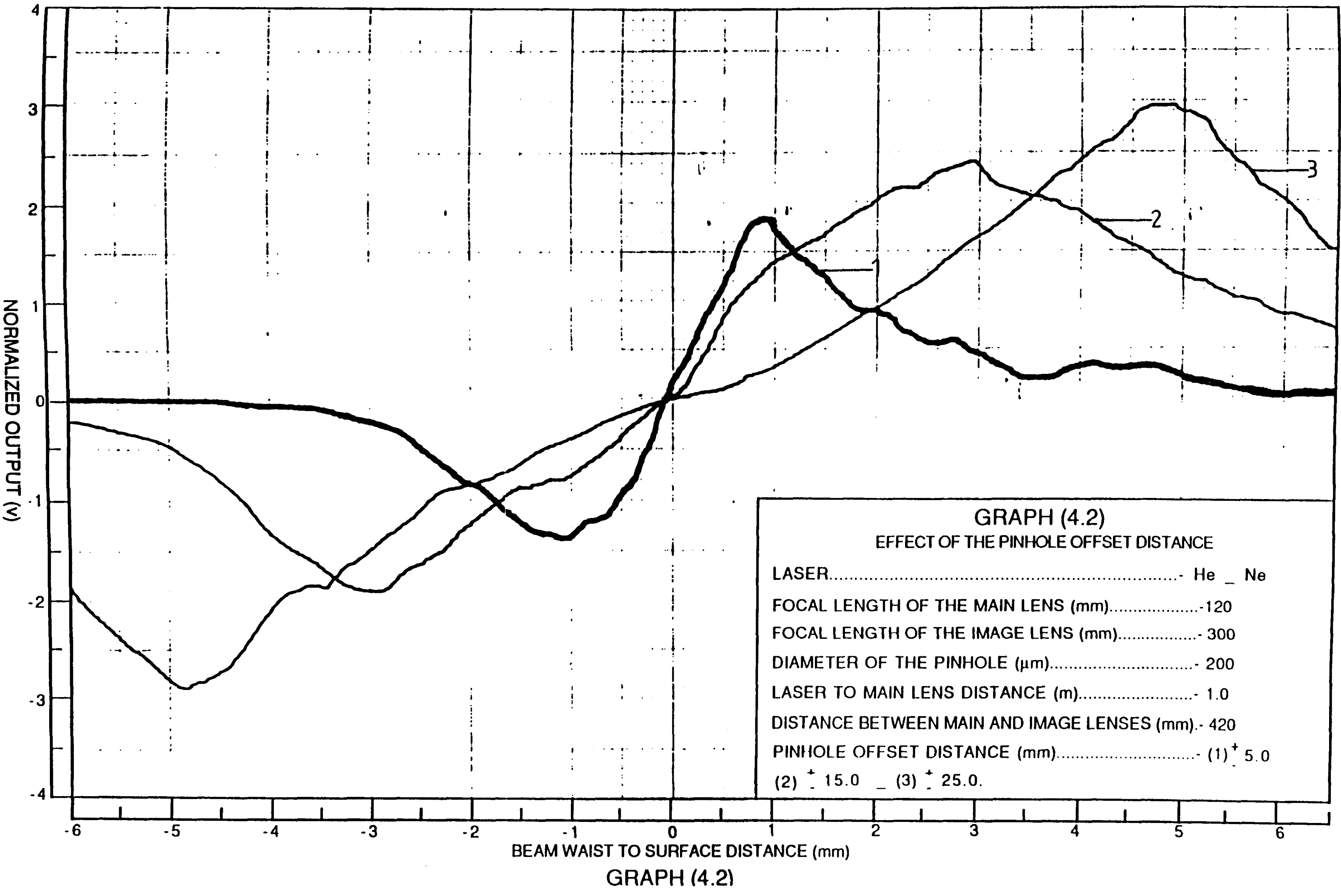

GRAPH (4.2)

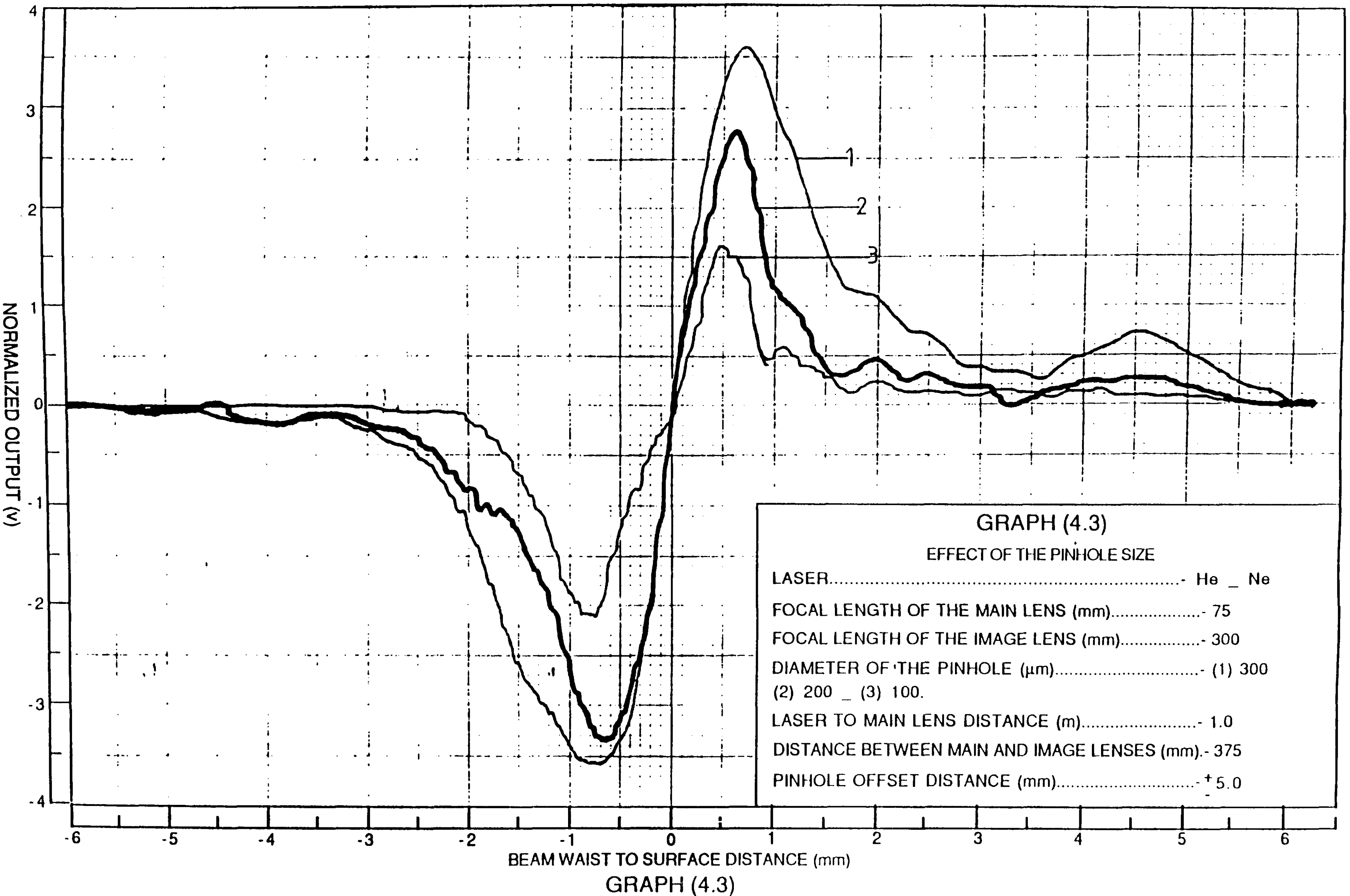

GRAPH (4.3)

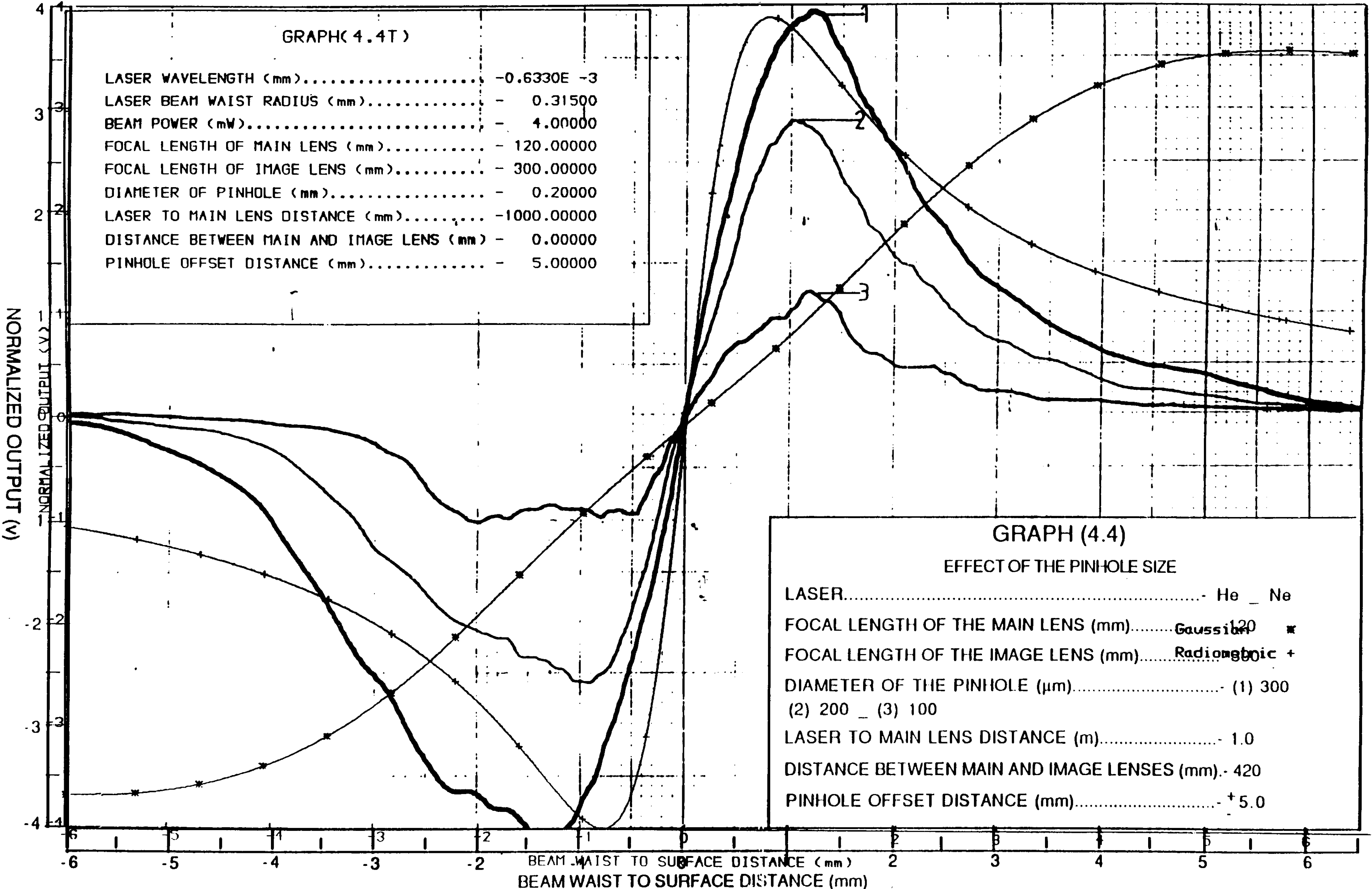

GRAPH (4.4)

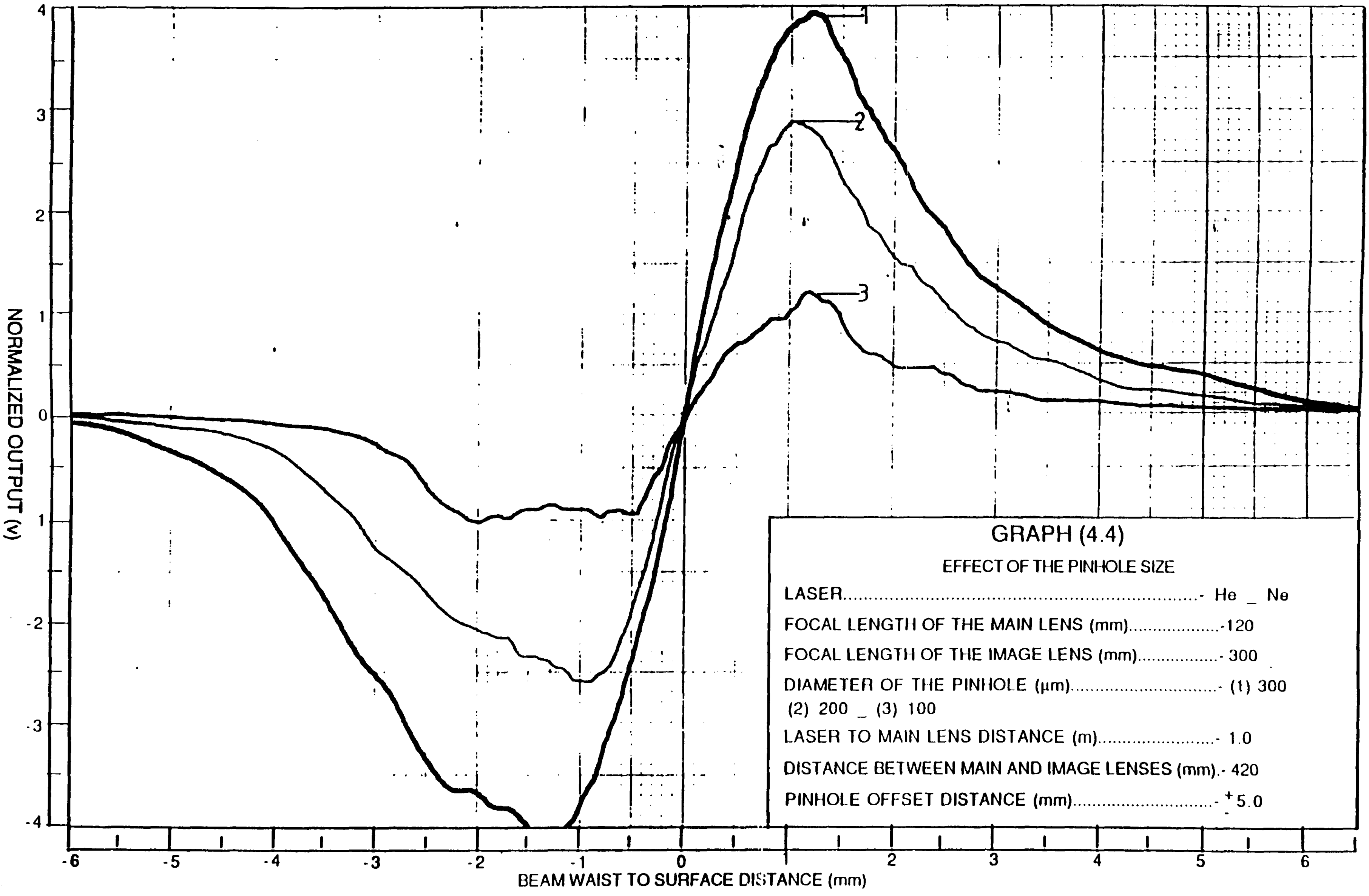

GRAPH (4.4)

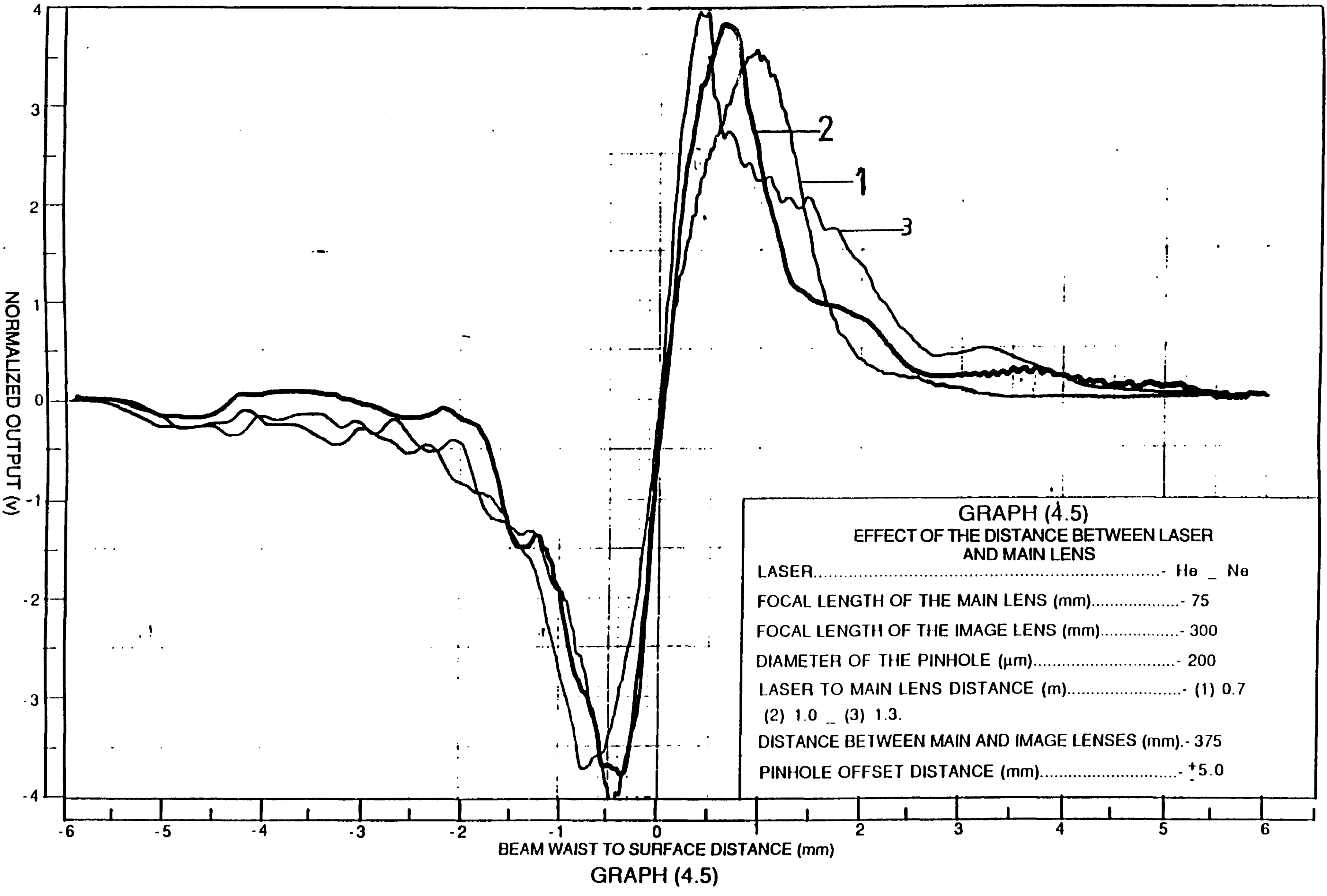

GRAPH (4.5)

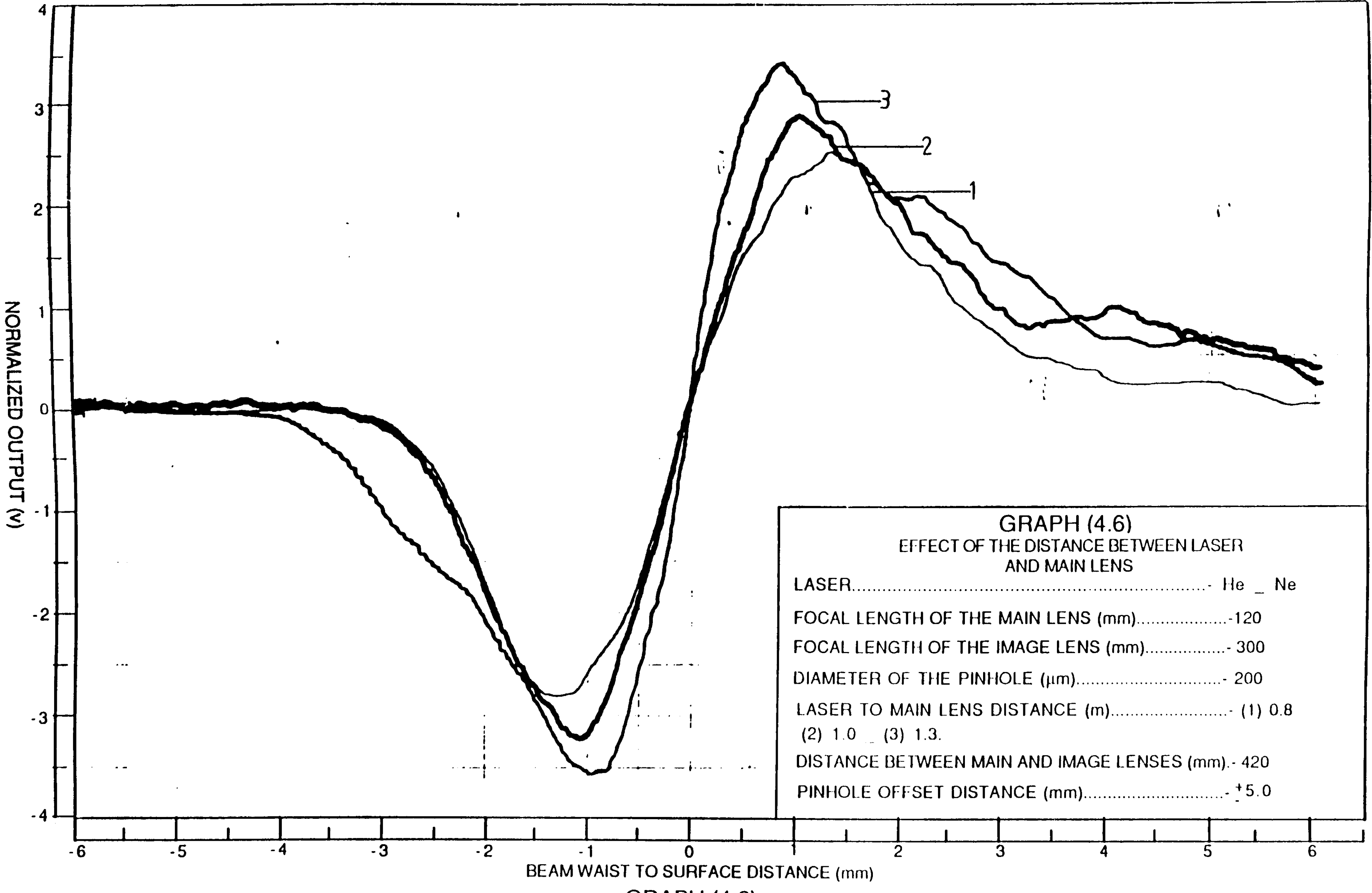

GRAPH (4.6)

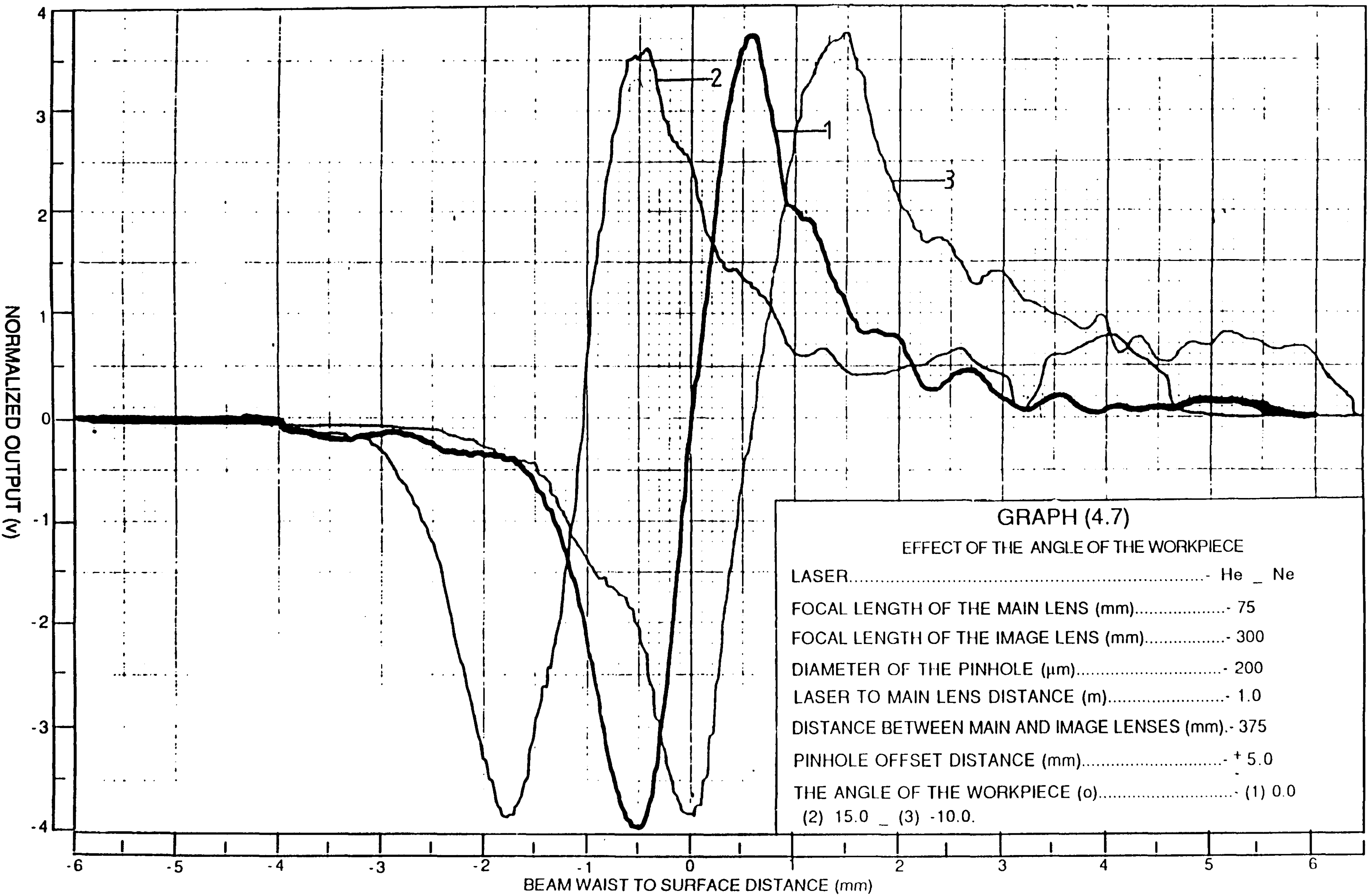

GRAPH (4.7)

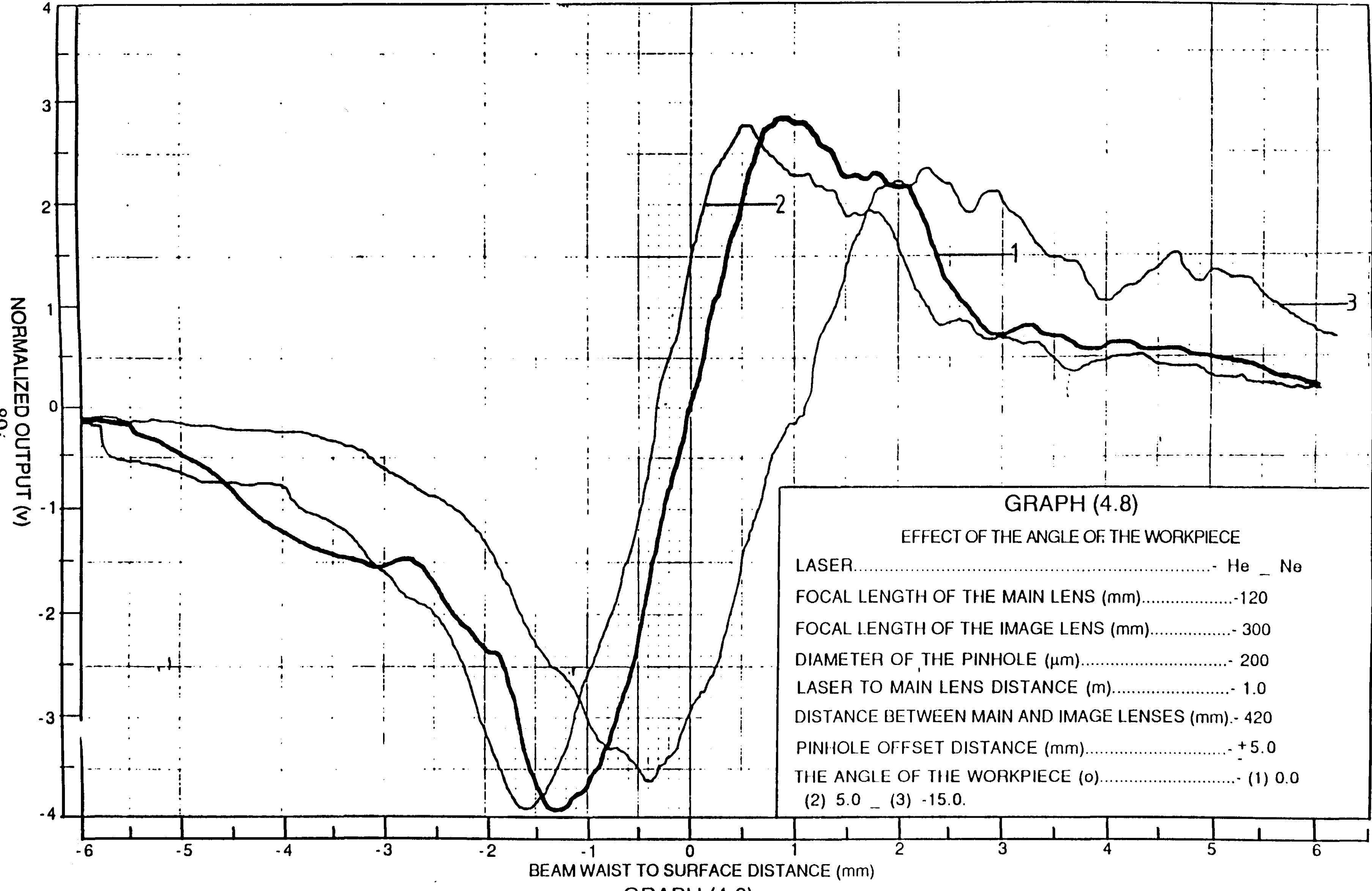

GRAPH (4.8)

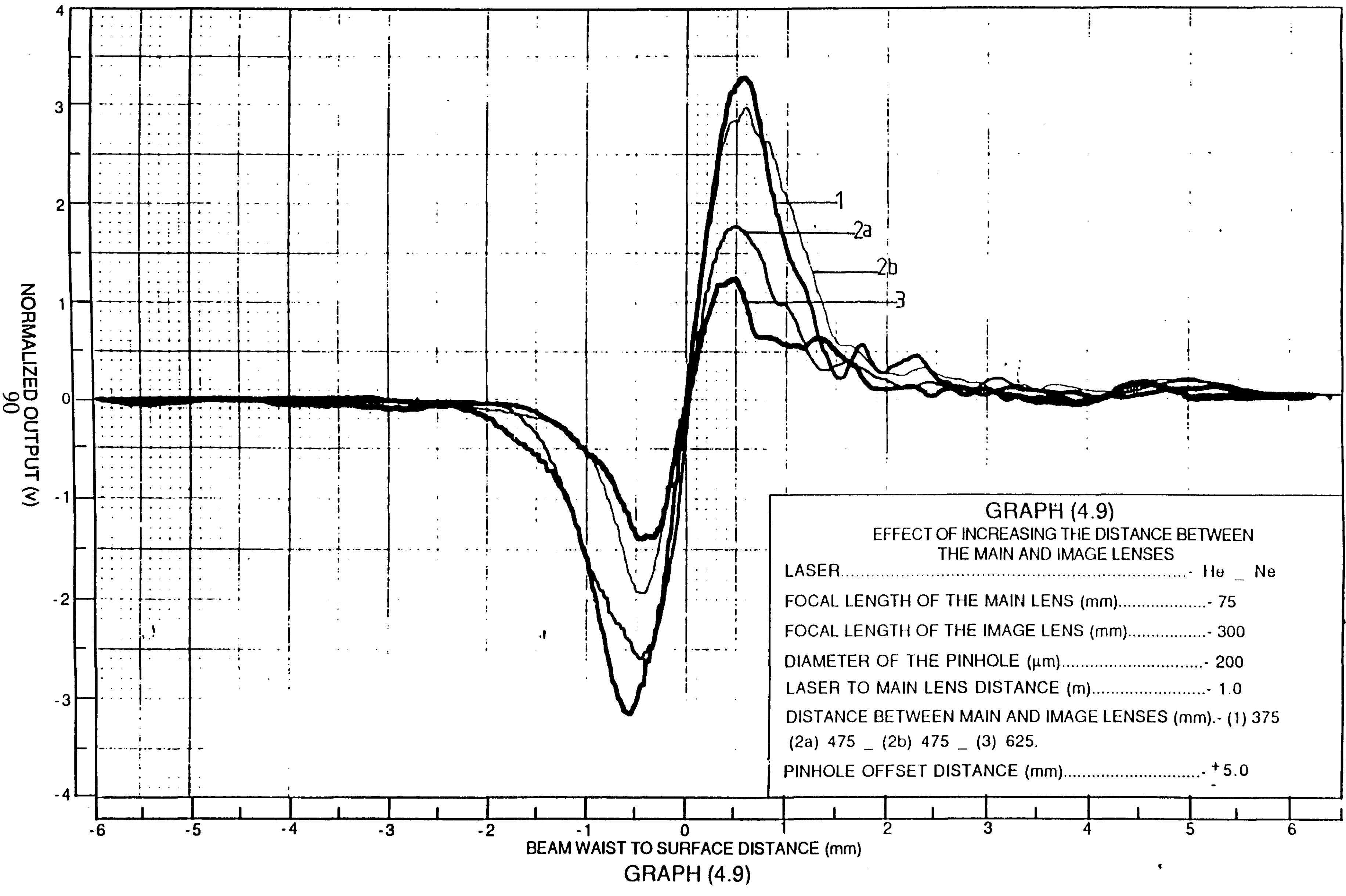

GRAPH (4.9)

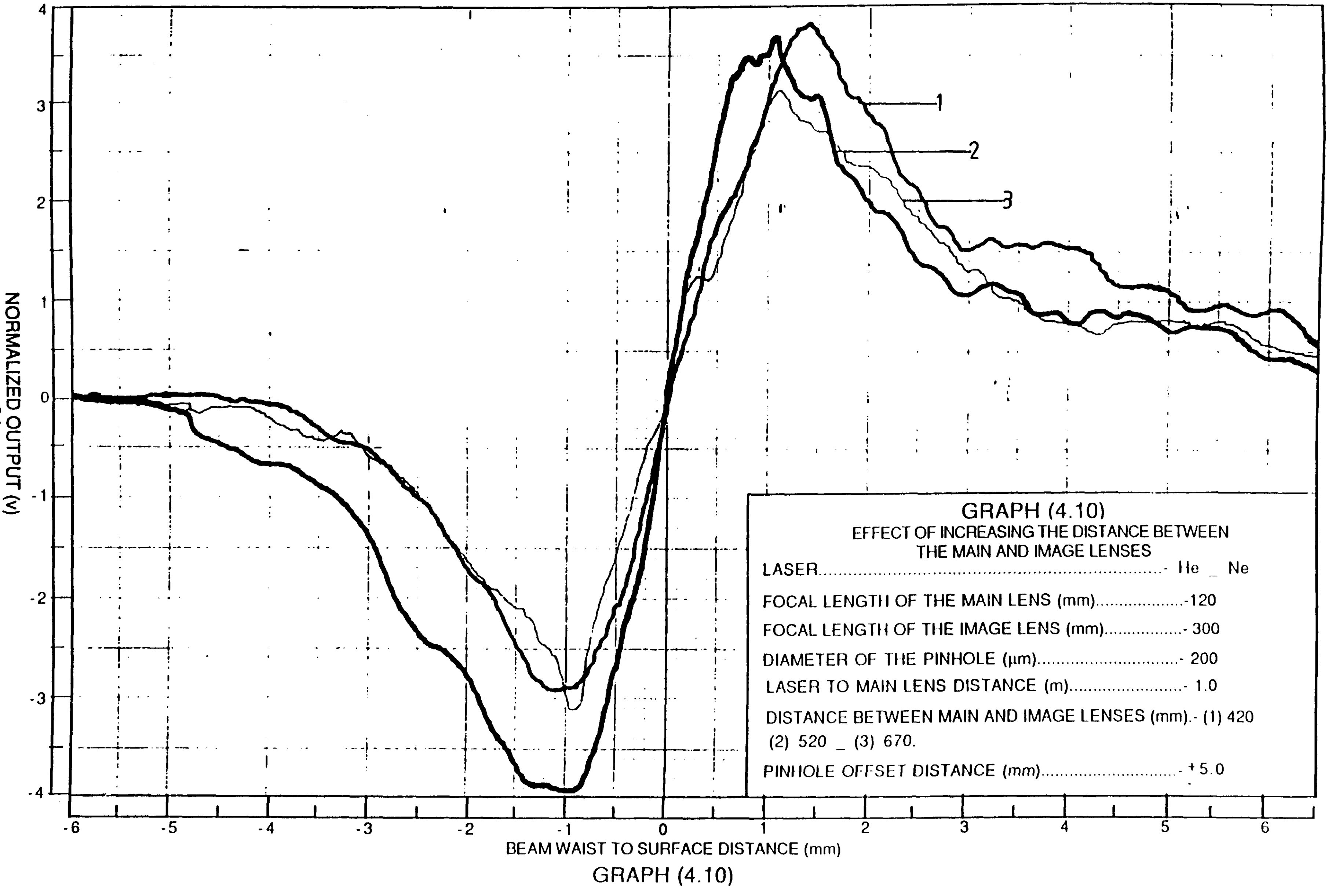

GRAPH (4.10)

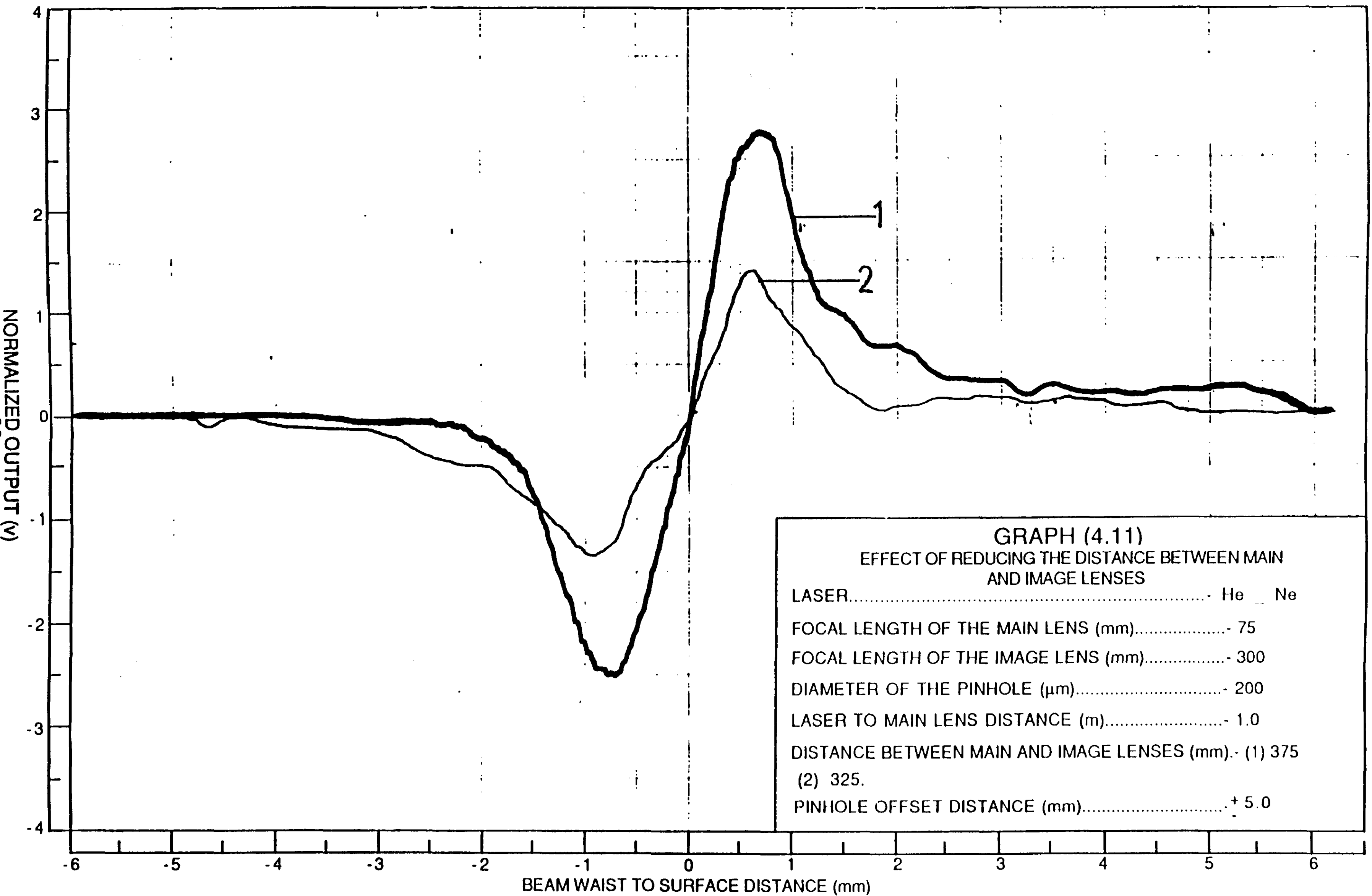

GRAPH (4.11)

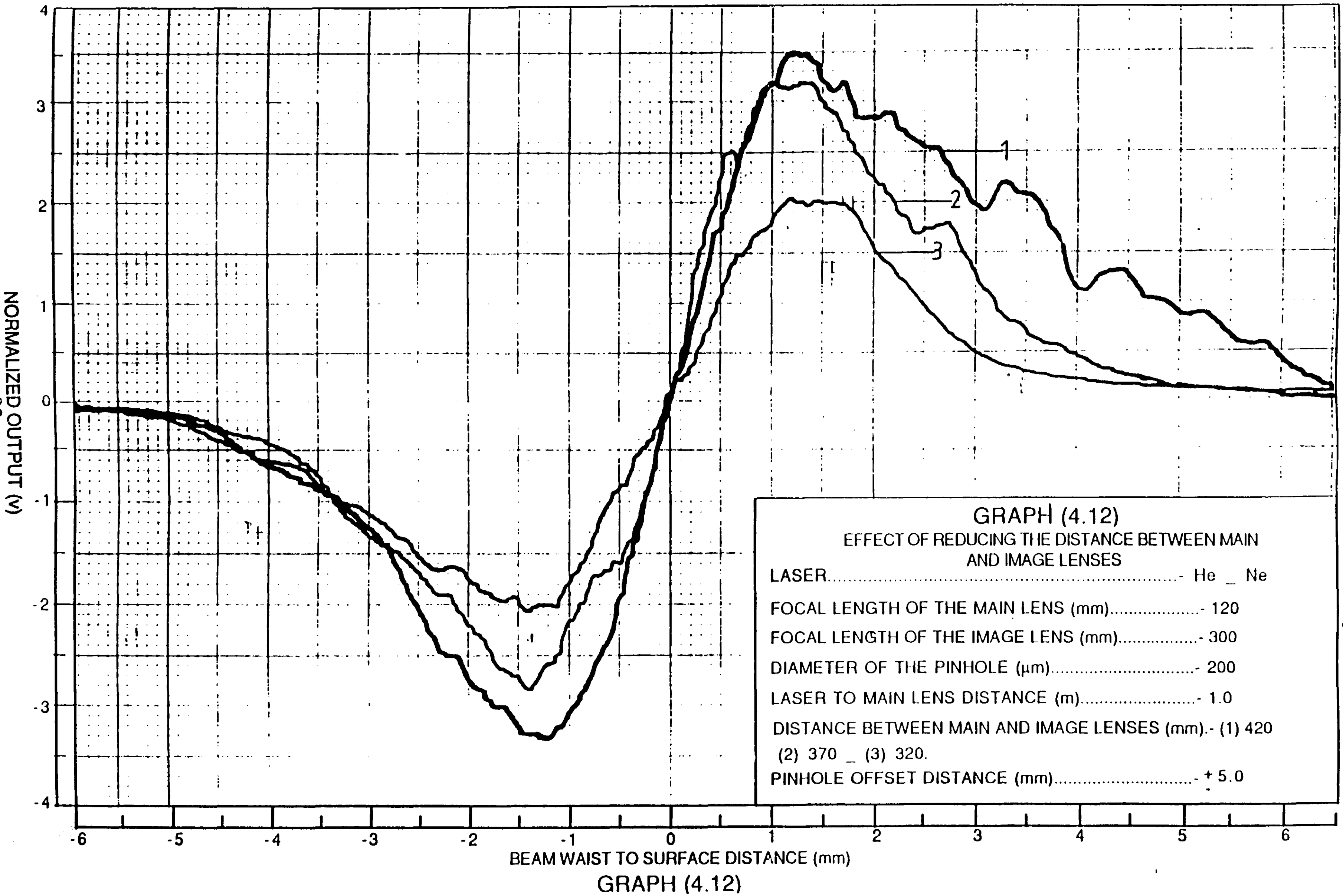

GRAPH (4.12)

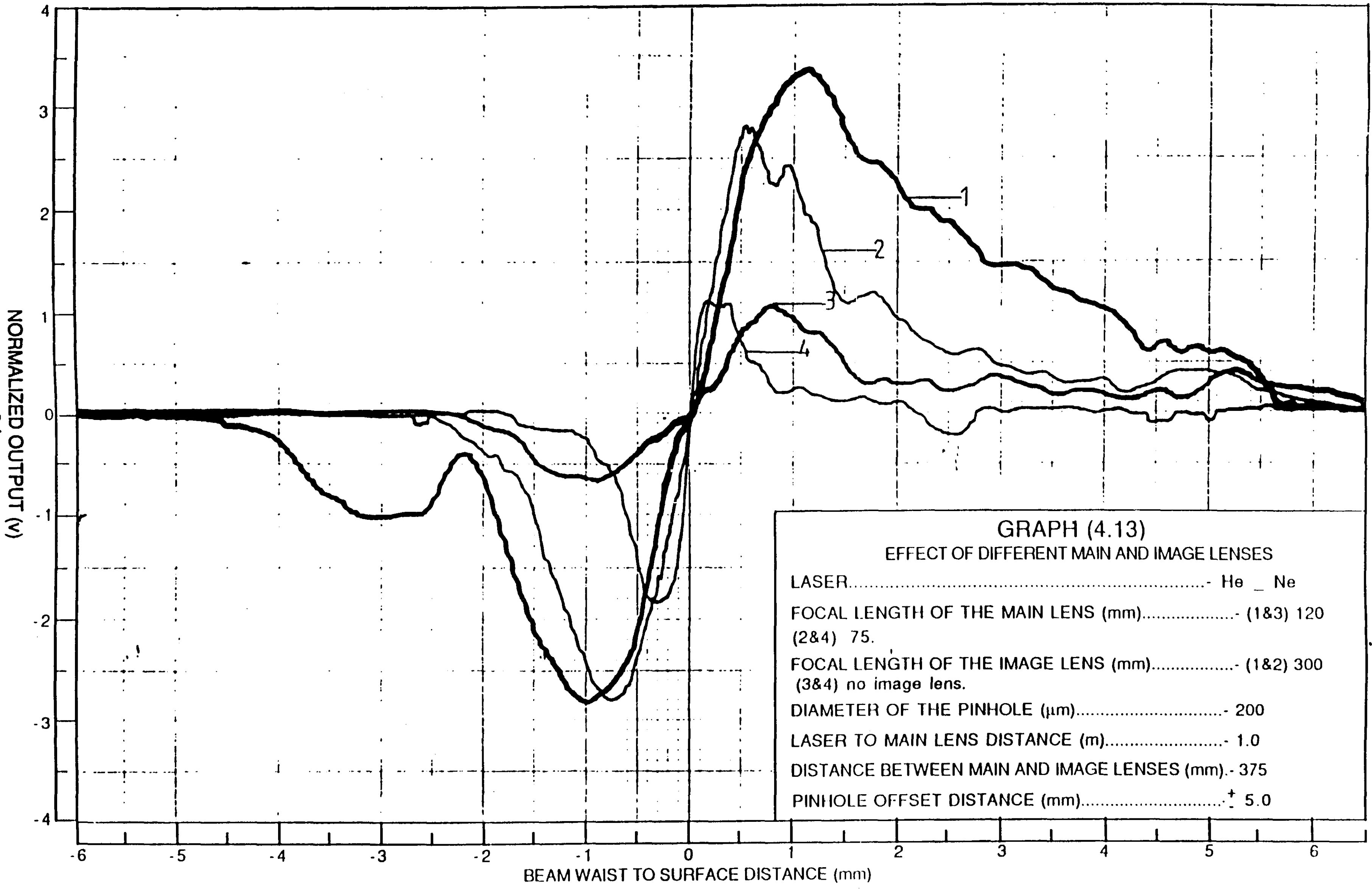

GRAPH (4.13)

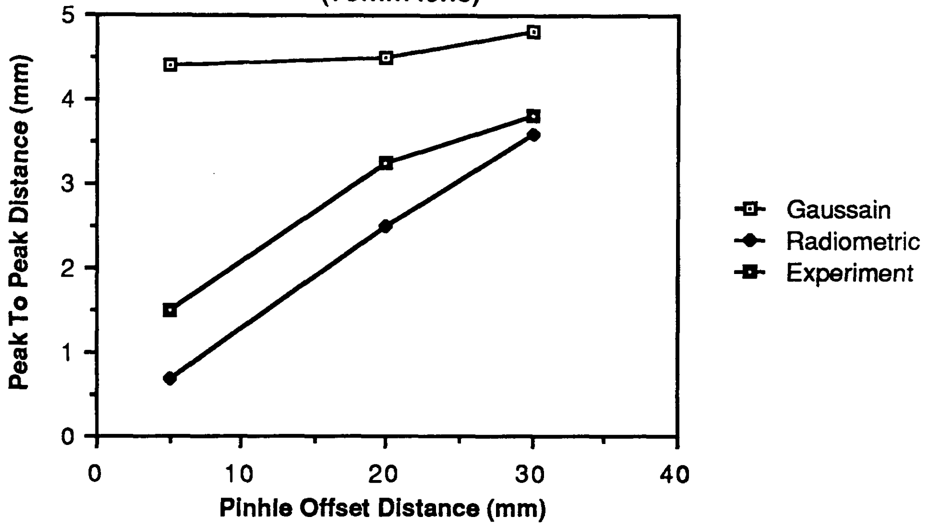
GRAPH 4.14a Effect Of Pinhole Offset Distance
(75mm lens)
Peak To Peak Distance (mm)
5
4
3
2
1
0
0
10
20
30
40
Pinhle Offset Distance (mm)
Gaussain
Radiometric
Experiment

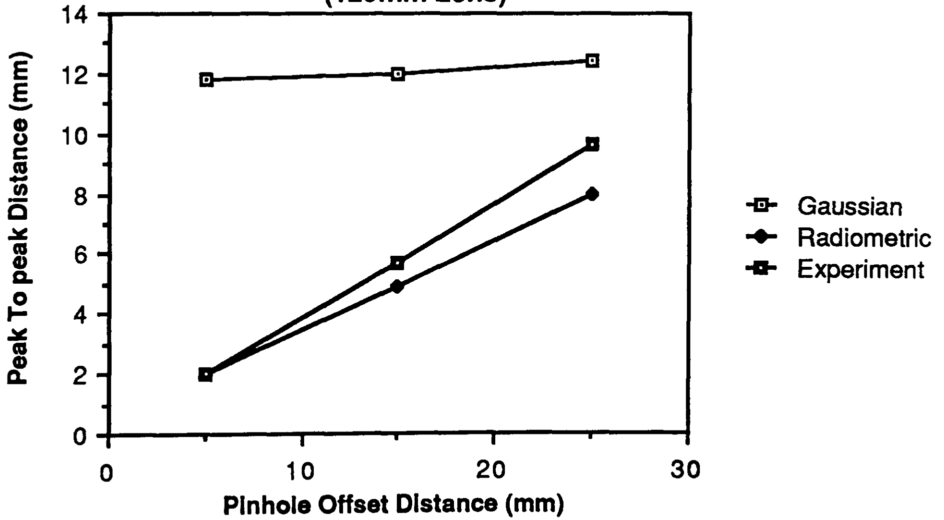
GRAPH 4.14b Effect Of Pinhole Offset Distance
(120mm Lens)
Peak To peak Distance (mm)
14
12
10
8
6
4
2
0
0
10
20
30
Pinhole Offset Distance (mm)
Gaussian
Radiometric
Experiment

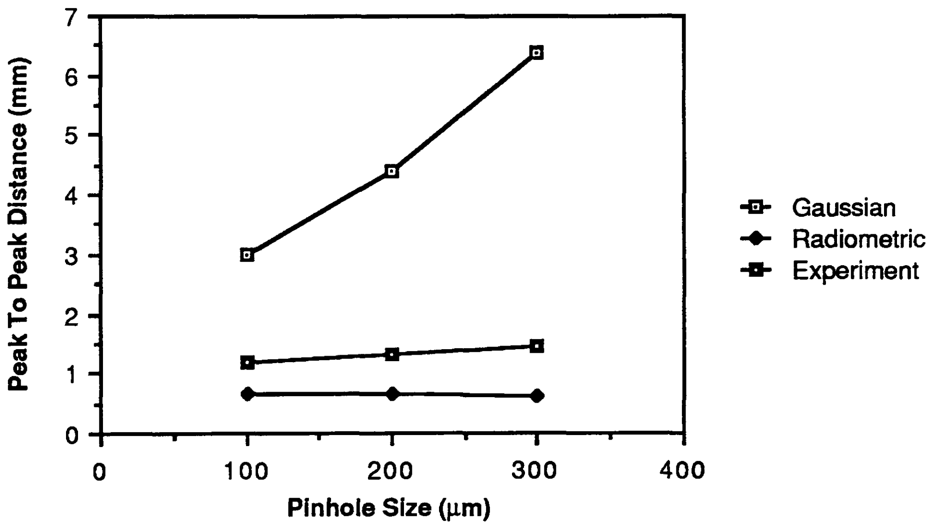
GRAPH 4.15a Effect Of Pinhole Size (75mm lens)
Peak To Peak Distance (mm)
Pinhole Size (μm)
0
1
2
3
4
5
6
7
0
100
200
300
400
Gaussian
Radiometric
Experiment

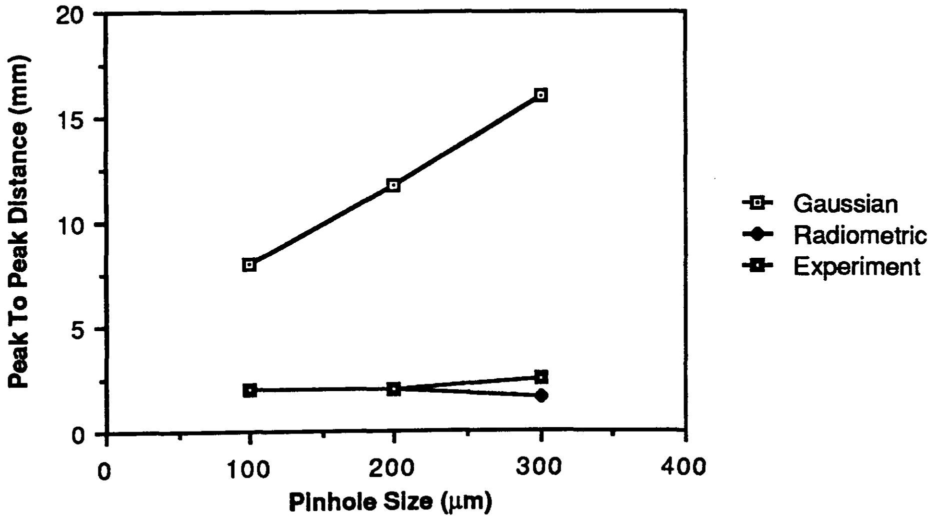
GRAPH 4.15b Effect Of Pinhole Size (120mm lens)
Peak To Peak Distance (mm)
Pinhole Size (μm)
0
5
10
15
20
0
100
200
300
400
Gaussian
Radiometric
Experiment

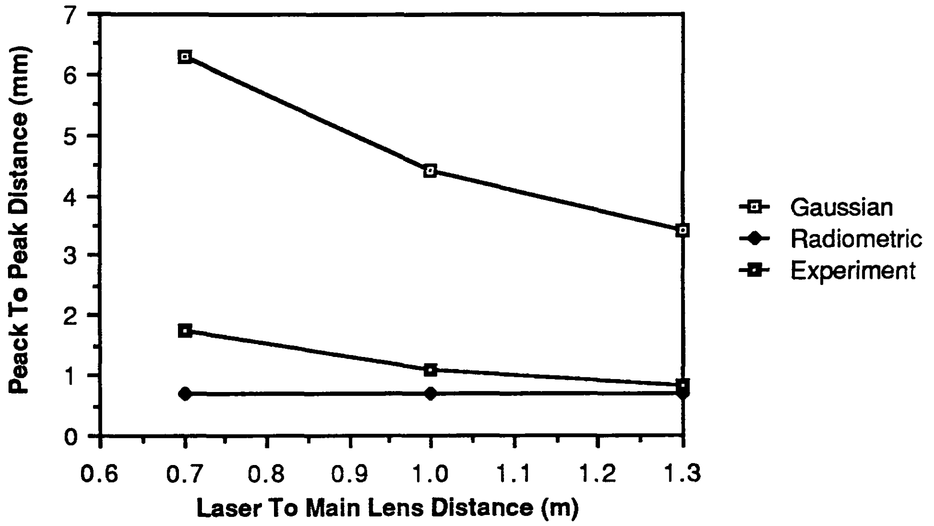
GRAPH 4.16a Effect Of Distance Between Laser
And Main Lens (75mm Lens)
Peack To Peak Distance (mm)
7
6
5
4
3
2
1
0
0.6
0.7
0.8
0.9
1.0
1.1
1.2
1.3
Laser To Main Lens Distance (m)
Gaussian
Radiometric
Experiment

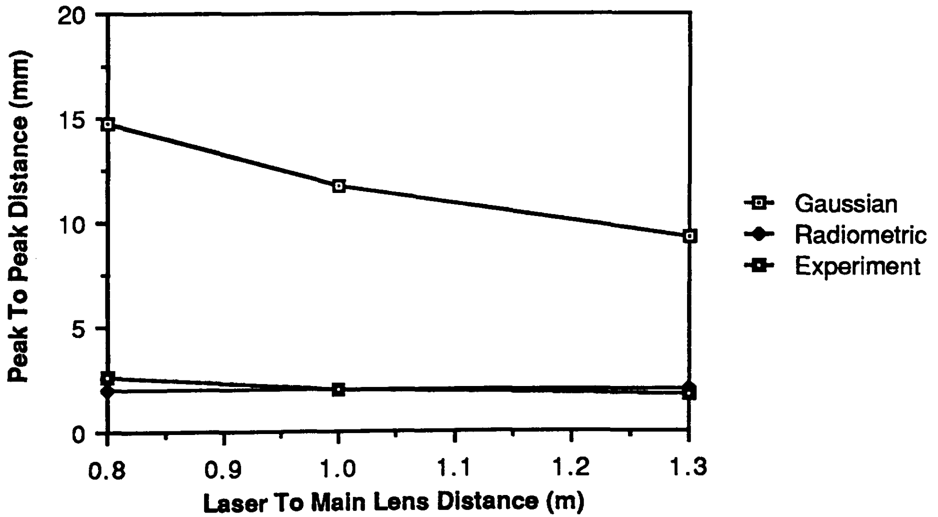
GRAPH 4.16b Effect Of Distance Between Laser
And Main Lens (120mm Lens)
Peak To Peak Distance (mm)
20
15
10
5
0
0.8
0.9
1.0
1.1
1.2
1.3
Laser To Main Lens Distance (m)
Gaussian
Radiometric
Experiment

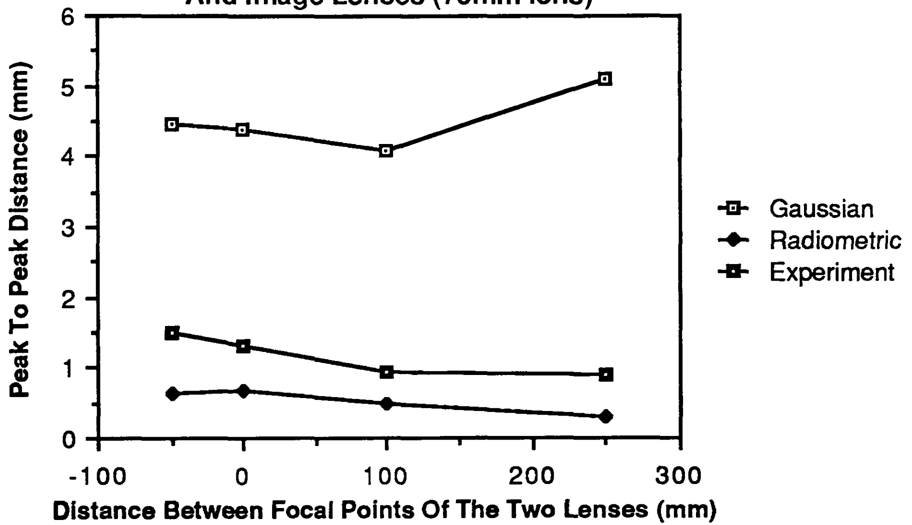
GRAPH 4.17a Effect Of Distance Between The Main And Image Lenses (75mm lens)
Peak To Peak Distance (mm)
0
1
2
3
4
5
6
-100
0
100
200
300
Distance Between Focal Points Of The Two Lenses (mm)
Gaussian
Radiometric
Experiment

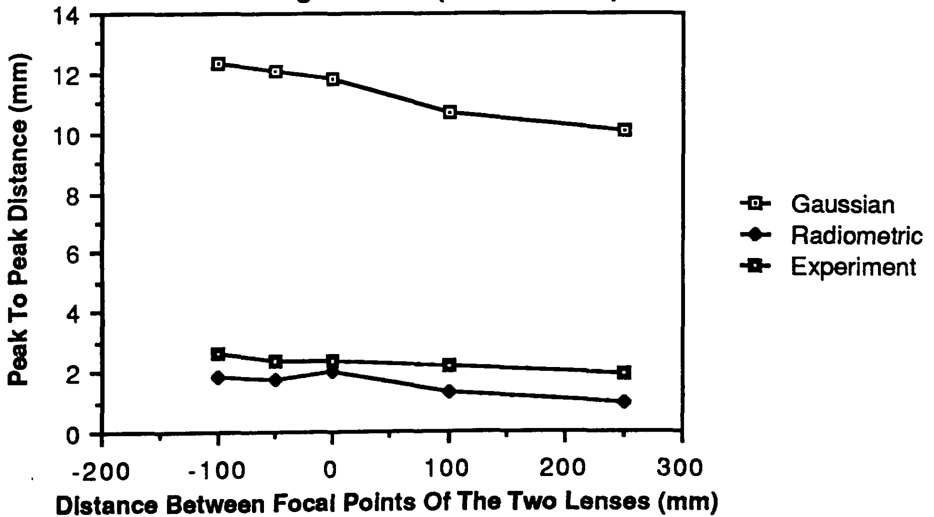
GRAPH 4.17b Effect Of Distance Between The Main And Image Lenses (120mm Lens)
Peak To Peak Distance (mm)
0
2
4
6
8
10
12
14
-200
-100
0
100
200
300
Distance Between Focal Points Of The Two Lenses (mm)
Gaussian
Radiometric
Experiment

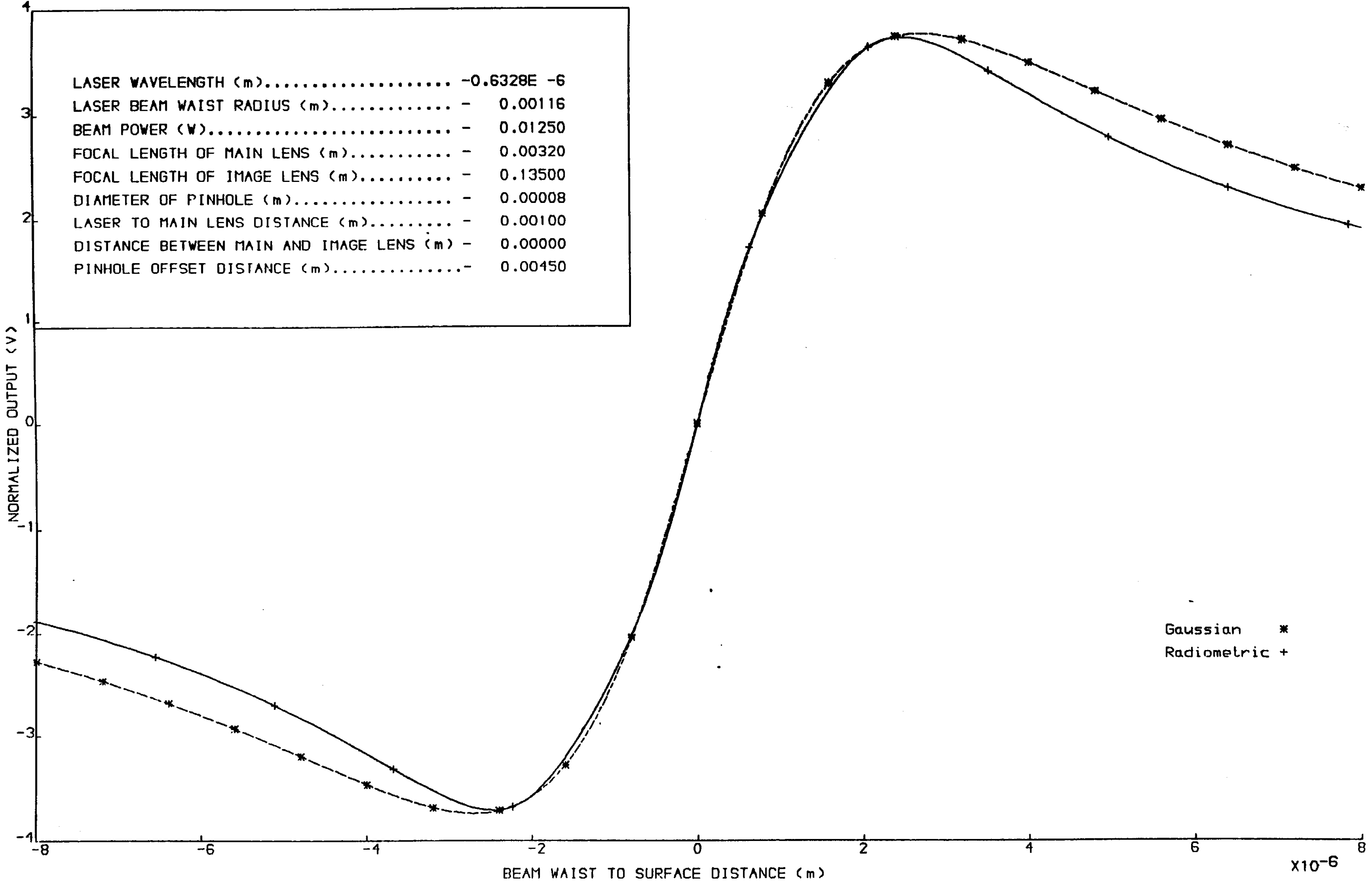

Graph 4.18 Gaussian and radiometric normalized output for Dobosz parameters

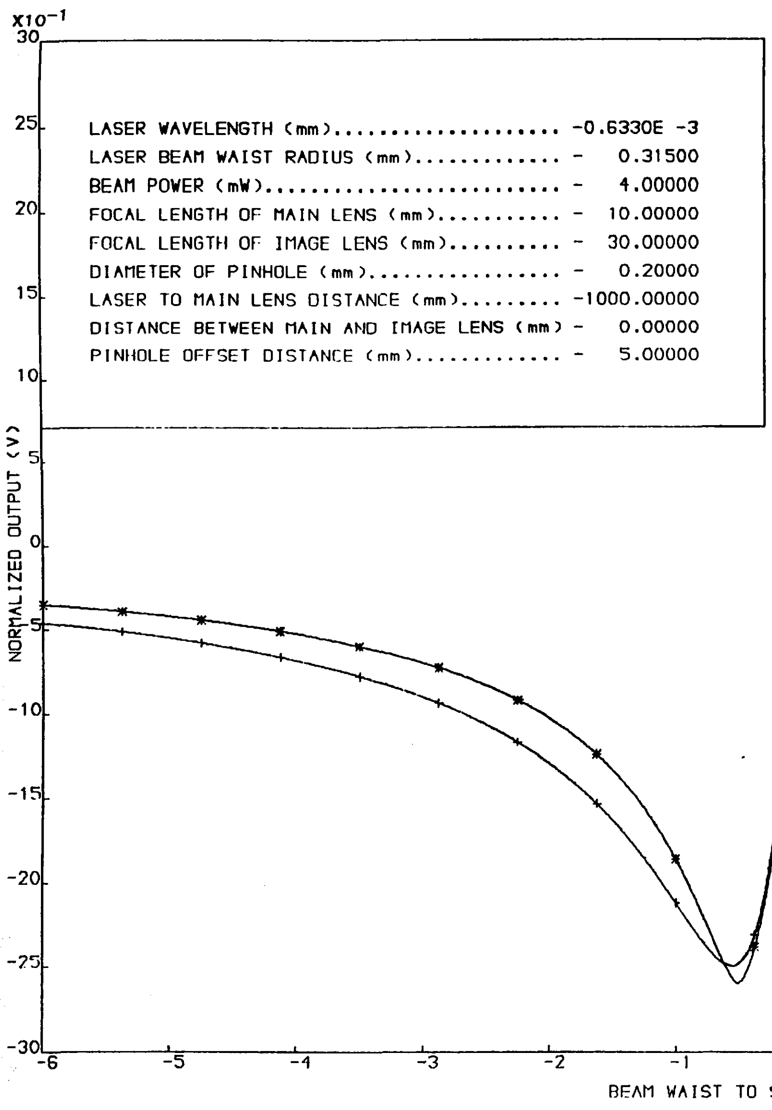

Graph 4.19 Gaussian and radiometric normalized output for 10mm main lens and 30mm image lens

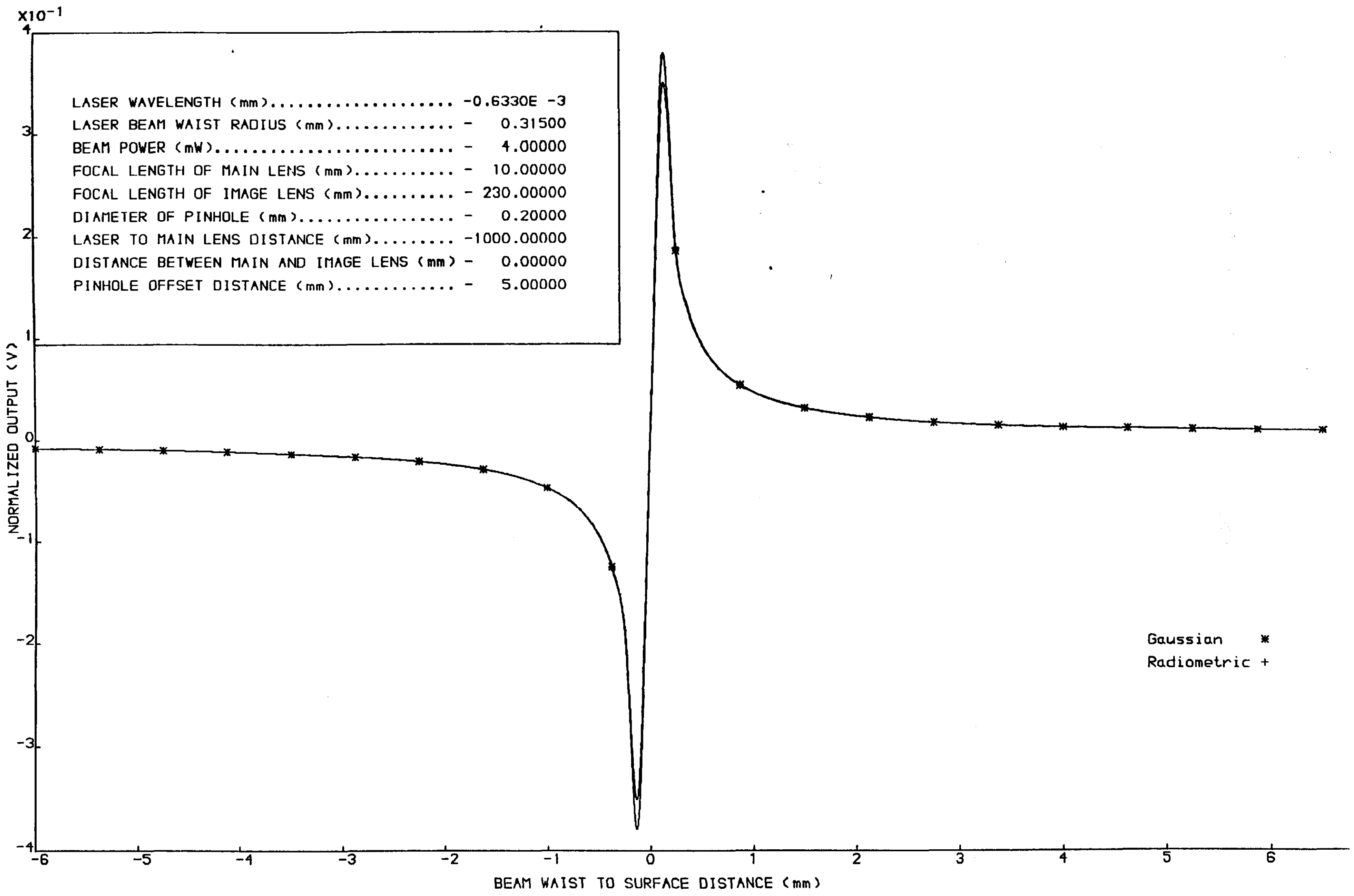

Graph 4.20 Gaussian and radiometric normalized output for 10mm main lens and 230mm image lens

GRAPH 4.21 Effect Of Laser Wavelength

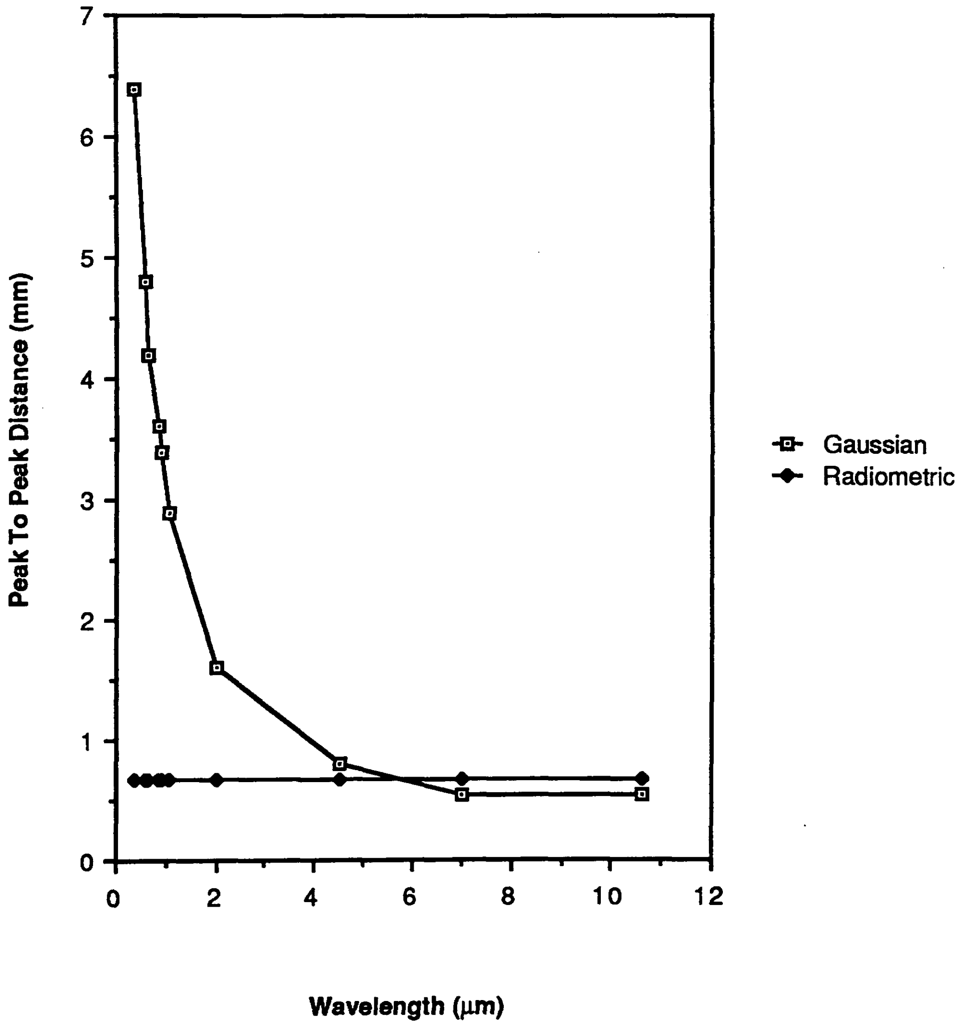

GRAPH 4.22 Effect of Initial Beam Waist Radius

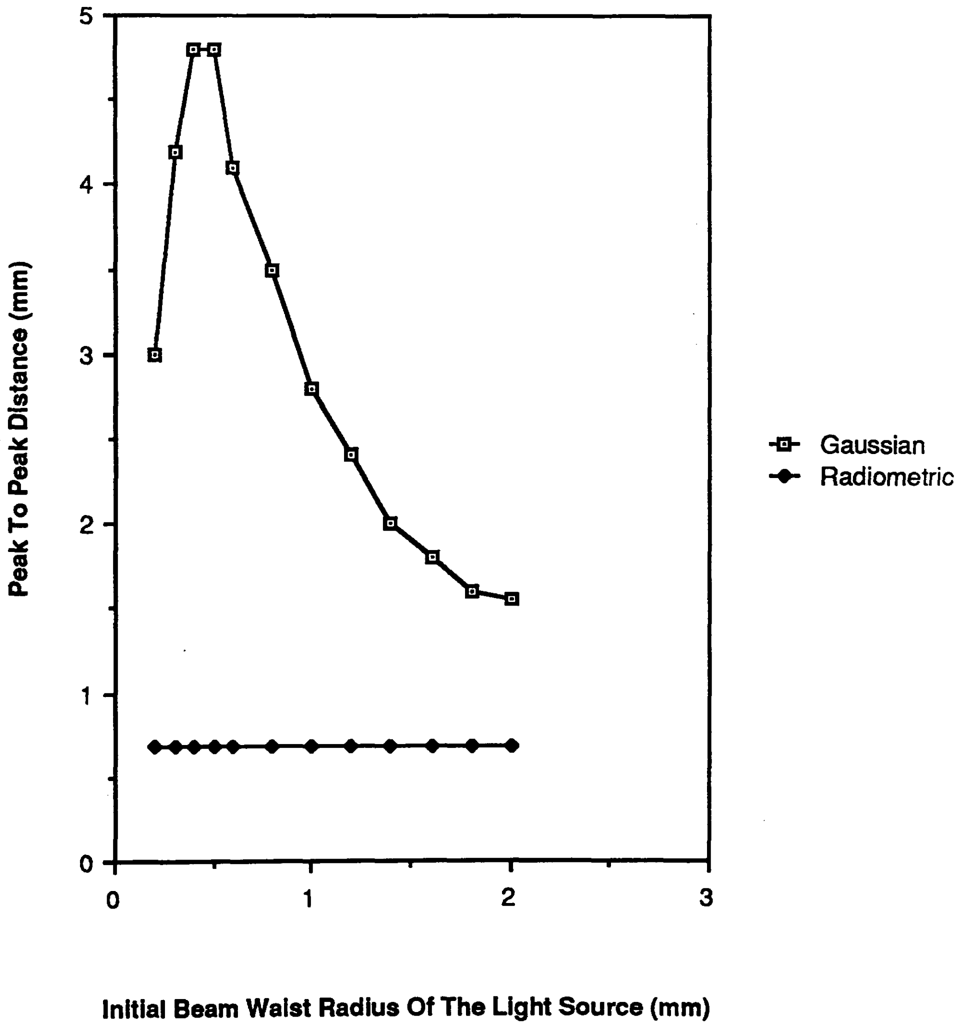

GRAPH 4.23 Effect of Changing The Distance Between Laser and Main Lens

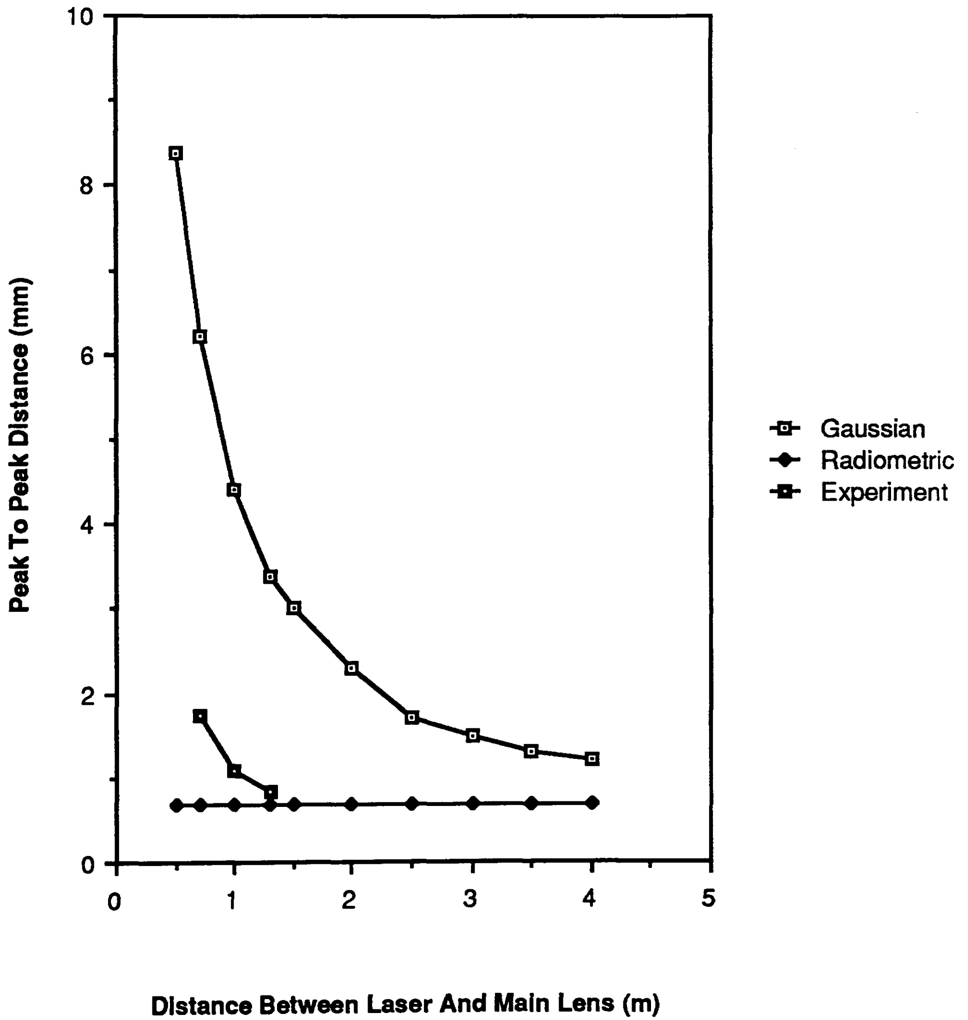

CHAPTER 5
CLOSED LOOP STAND-OFF SYSTEM DESIGN AND OPERATIONAL CHARACTERISTICS

CHAPTER 5: CLOSED LOOP STAND-OFF SYSTEM DESIGN AND OPERATIONAL CHARACTERISTICS

5.1 Introduction:

The previous chapters discussed and analyzed the optimization of an opto-electronic stand-off sensor, through the use of theoretical and experimental models. This sensor output is important as it plays a critical role in the performance of a closed loop stand-off system, as it provides a feed back control signal.

Generally, to optimize the control of a physical system, it is necessary to obtain a good mathematical model of the system. Once the output response of the model is optimized, then a comparison can be made between actual and theoretical response. Consequently, conclusions may be drawn as to the design and performance of the complete stand-off control system.

This chapter centres on designing a complete stand-off system through modelling of its predicted performance and operational characteristics. A brief literature review highlights relative control issues and methods of presenting control systems. The control circuit chosen for the actual system is introduced. Additionally, a review of the common actuators used in robotics systems, with particular attention paid to solenoids, (which was chosen as the actuator for the experiment) is given. The predicted and actual output responses for different input steps and materials and an analysis of the performance of the stand-off system are presented.

5.2 Control Issues:

A control system may be defined as a device or combination of components, which regulates the flow of resources of energy to obtaining a desired goal. In general control systems can be categorized as open or closed-loop. The main difference between them is the use of feedback comparison for closed-loop operation.

In a closed-loop control system, the controlled variable , is fed back and compared with a reference input. This is shown in the block diagram fig.(5.1). More detail of block

diagram representation, methods of mathematical modelling and transfer function is given in appendix (A11). The system can then drive the output until it equals the input by making the error signal equal to zero. Any differences between the actual and desired status will be automatically corrected in a well designed closed-loop control system.

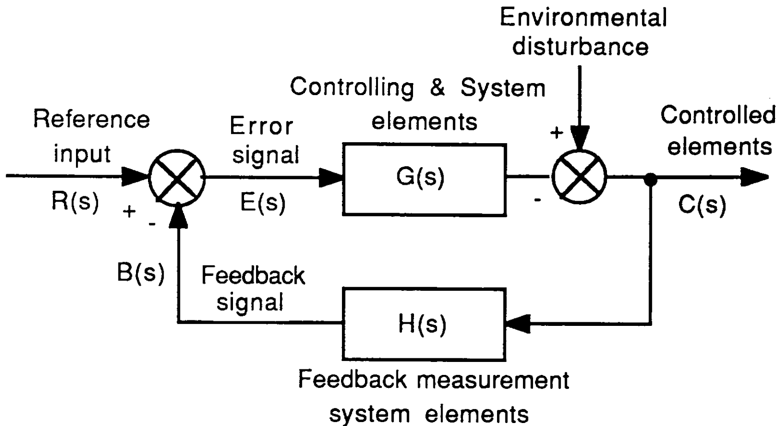

Figure 5.1 Block diagram of a closed-loop control system

A typical Feed-back control system is shown in fig.(5.1) . The term G(s) represents controlling and system elements , H(s) represents a feedback measurement system (used to convert the control signal into a form suitable for the comparator), R(s) is a reference input, E(s) is an error signal and B(s) is a feedback signal. A special type of feed-back system is the unity-feedback control system, Which has the feedback element equal to one fig.(5.2).

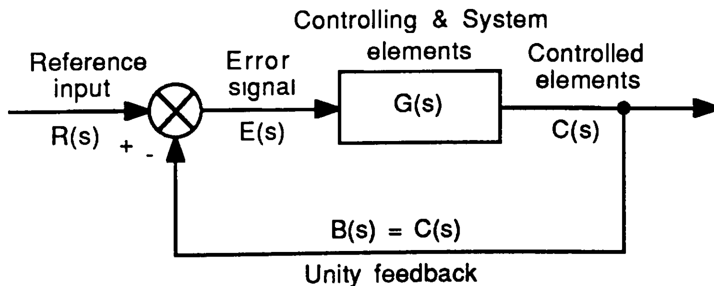

Figure 5.2 Block diagram of a unity feed-back control system

Lists of the ANSI standard nomenclature and symbols for use in control engineering can be found in Ref.(4).

In open-loop systems no comparison of the controlled variable with the reference input is made fig.(5.3). Consequently, it is a simpler and less complex structure of control, but is unable to respond to changes in the environment.

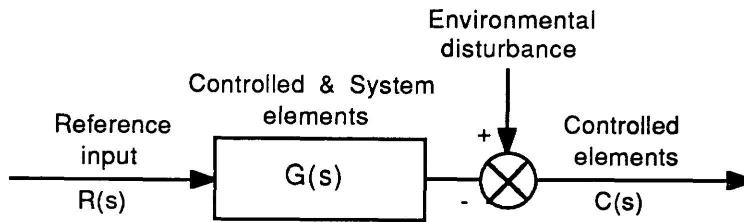

Figure 5.3 Block diagram of open-loop control system

Since, the laser based stand-off system under consideration must work within a constantly changing environment (constantly changing surface position), a closed loop control system is the only option.

This chapter goes onto discuss the design synthesis and analysis of an appropriate control system.

5.3 Actuation:

Mechanical actuators are devices that exert a motive force to drive loads, such as robot manipulator to a given position. These may be classified as two types: angular actuators which provide a rotary motion and linear actuators, which have linear motion of extension and retraction. The classification of actuators may also be related to the type of the power used: hydraulic, pneumatic and electric. All mechanical actuators convert one form of power into a form of mechanical motion. Appendix (A12) highlights the more common types of actuator employed in robotic systems. This part focuses upon the modelling of a solenoid, which was employed in the system designed.

A solenoid is a coil of wire or conductor with a length that is large compared with its

diameter. When it carries a current, a magnetic field is induced within the coil. If an iron or steel core is positioned in the coil fig.(5.4), it becomes magnetized with identical poles. As a result, the core is repelled from the coil.

The magnitude of the force generated by a solenoid F depends on the current I flowing in it and the length of the conductor L. As a result, a larger current produces a stronger magnetic field, with a consequent increase in force. The force can be expressed as Ref.(58) :

$$F = f_d \; I \; L \sin \alpha \tag{5.1}$$

Where f_d is the magnetic induction or flux density in the field, I is the current in the coil, L is the length of the conductor and α is the angle between the conductor and the field.

It is experimentally difficult to measure the magnetic induction and calibration of solenoids may be achieved by lumping the length and magnetic induction into an experimentally determined solenoid constant:

$$F = K_{sol} \; I \tag{5.2}$$

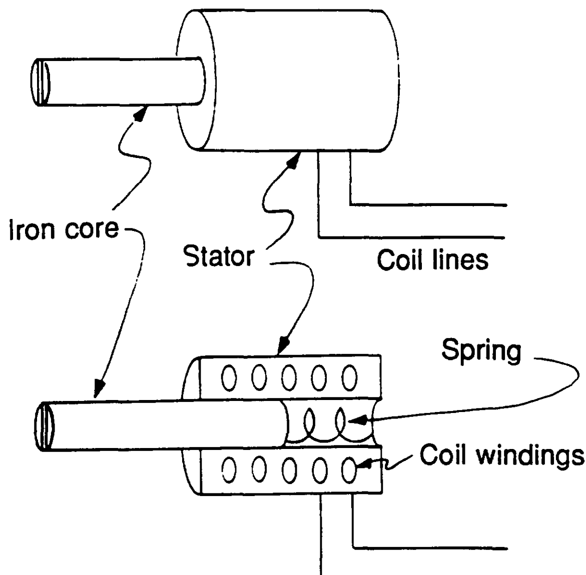

Figure 5.4 Schematic diagram for solenoid Ref.(1)

5.4 The Control Circuit:

A block diagram of the closed-loop control system used is shown in fig.(5.5). This represents the relationships between the system components by their laplace transfer functions. The components of the circuit are a proportional controller with gain K_c, which amplifies an error voltage V_e to a control signal V_c. This signal is fed to a DC actuator, in this design a solenoid. This signal energizes the solenoid winding, resulting in a magnetic field in the steel core directly proportional to the amount of current flowing in the solenoid winding. This magnetic field exerts a force F upon the core of the solenoid. Which is in mechanical contact with a moving lens mechanism (a combination of a main lens carriage, return spring and a damper). When the current is reduced, the magnetic field collapses and the core returns inside the solenoid due to a return spring. Damping is achieved by a viscous coating around the close fitting solenoid core.

The moving lens mechanism is moved by an actuating force F to achieve a desired position X. If the system is disturbed by movement of the workpiece to a new position X_c the error distance to be corrected X_e is equal to :

$$X_e = X_c - X \qquad (5.3)$$

This error distance is sensed and transduced to an error voltage by means of the stand-off sensor presented earlier. This signal is then conditioned by a differential amplifier, to a convenient level for the proportional controller. In this situation a closed-loop or feed-back control system has been achieved.

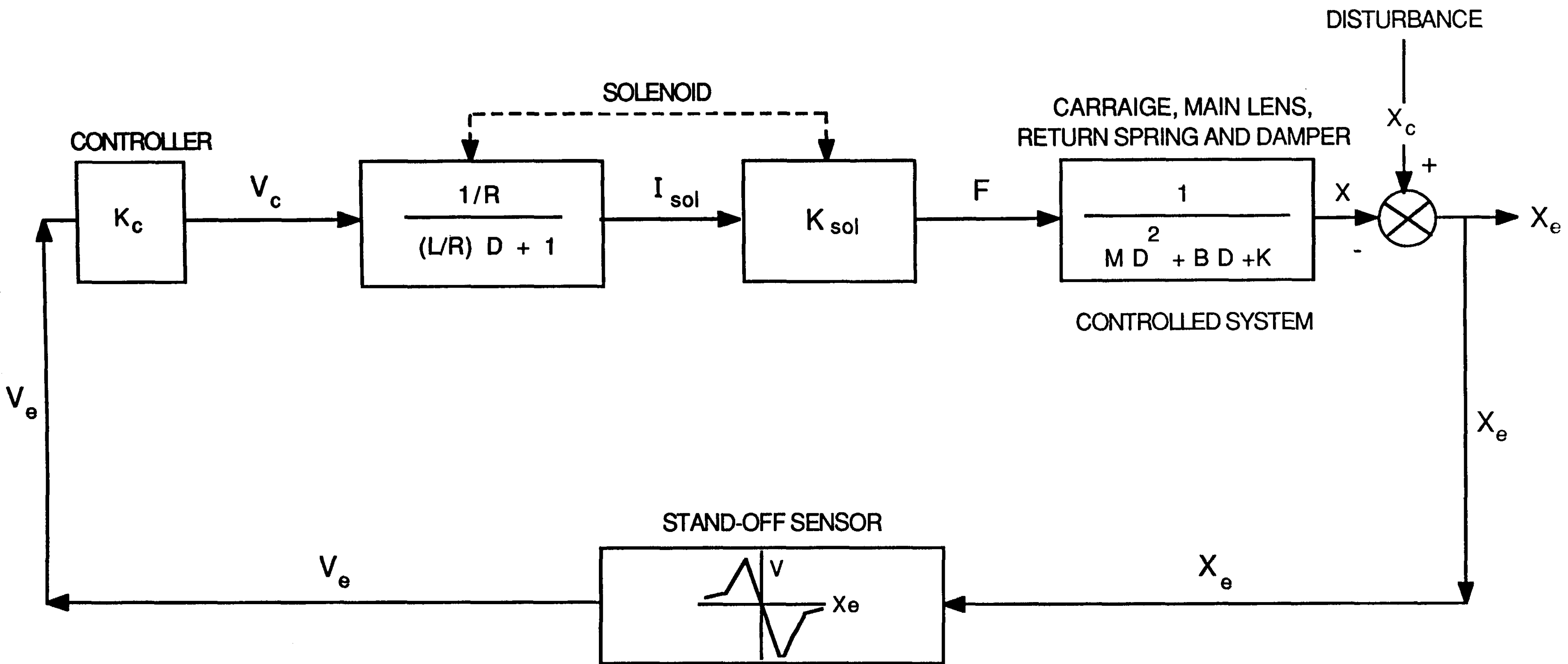

Figure 5.5 Block diagram of the control system using a solenoid

5.4.1 System Model:

This is a mathematical representation of the system in which the block diagrams are lumped together. The mathematical simulation of the control system considering each component individually is as follow:

A proportional controller of gain Kc amplifies its input (an error voltage Ve) to an output (control voltage signal Vc) as :

$$Vc = Kc\ Ve \tag{5.4}$$

A solenoid actuator is used to exert a linear force to correct the position of the workpiece. This converts the control voltage signal to a linear force in two stages. Firstly a current flows through the solenoid coil and generates a magnetic field which is proportional to the current. This current is calculated using the inductance and resistance of the solenoid coil fig.(5.6):

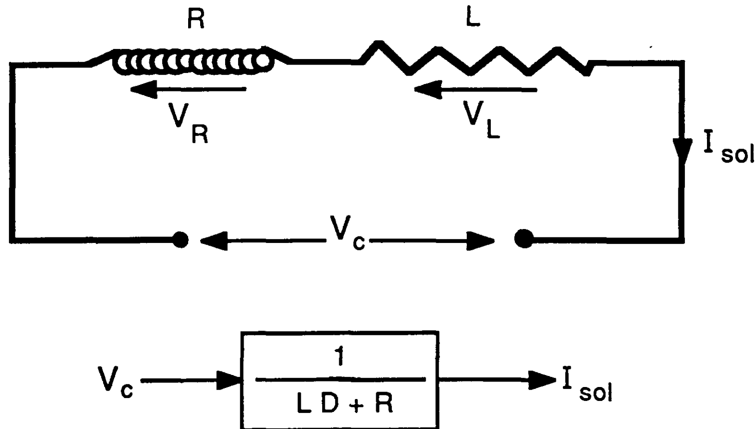

Figure 5.6 The solenoid current model

$$Vc - L\ (dI/dt) = I\ R \tag{5.5}$$

$$Vc - L\ DI = I\ R \tag{5.6}$$

$$V_c = (L\,D + R)\,I \qquad (5.7)$$

$$I_{sol} = V_c/(L\,D + R) \qquad (5.8)$$

Secondly, the current I_{sol} is converted to a force F as shown in fig.(5.5) as :

$$F = K_{sol}\ I_{sol} \qquad (5.9)$$

Where K_{sol} was experimentally determined, by applying a variable current to the solenoid and measuring the output force. K_{sol} was found about 112 newtons per ampere, but not perfectly linear, being a function of coil position.

The controlled system is a mechanical system containing: the main lens and its holder, carriage, return spring and damper, taking the lumped form of a mass-spring-damper combination. The relationship between the input and the output is defined by the second order transfer function fig.(A11.8) appendix (A11) :

$$X = [\ 1/\ (\ m\ D^2 + B\ D + K\ )]\ F \qquad (5.10)$$

Where m is the sum of the masses of the main lens, holder, carriage and solenoid core. B is the damping coefficient of the damper and K is the spring stiffness measured as 0.45 N/mm.

The damping coefficient of the solenoid was estimated experimentally as 3.5 Ns/mm, by determining the speed of the solenoid relative to the amount of the current provided by a DC power supply.

If the workpiece is moved away from the beam waist W_{02} position (fig.(3.1) chapter 3), the error distance through the comparator is equal to :

$$X_e = X_c - X \qquad (5.11)$$

The error signal is the actuating signal and is converted to an error voltage V_e by the stand-off sensor. By using the gaussian-radiometric model described in section (3.4), it is then possible to determine the error voltage.

5.5 Predicted Performance:

A computer program was written to simulate the system model presented in section (5.4.1). The program was written in the Advanced Continuous Simulation Language (ACSL), on a VAX computer in the Mechanical Engineering Department, a copy of which is given in appendix (A13). The program simulates the effects of varying system parameters on the output for a step input disturbance. The program can then be used to optimize system operation.

The program calls a subroutine which simulates the action of the sensor. This is similar to the gaussian-radiometric modelling program presented in section (3.4.2) and a copy is given in appendix (A14). The ACSL program feeds the sensor subroutine with the error distance X_e. This parameter is translated to an error voltage through the mathematical operations in the subroutine and returned to the main program. The subroutine can be used to estimate the effect of size and geometry of the optical apparatus upon the system output as in section (3.4).

A sample of the output of the control program is shown in fig.(5.7), showing the input step X_c in mm and the output response is X in mm versus the time T in seconds, which characterizes the performance of the system.

The simulation results are presented together with experimental results in a later section, where a comparison and discussion of results is also presented.

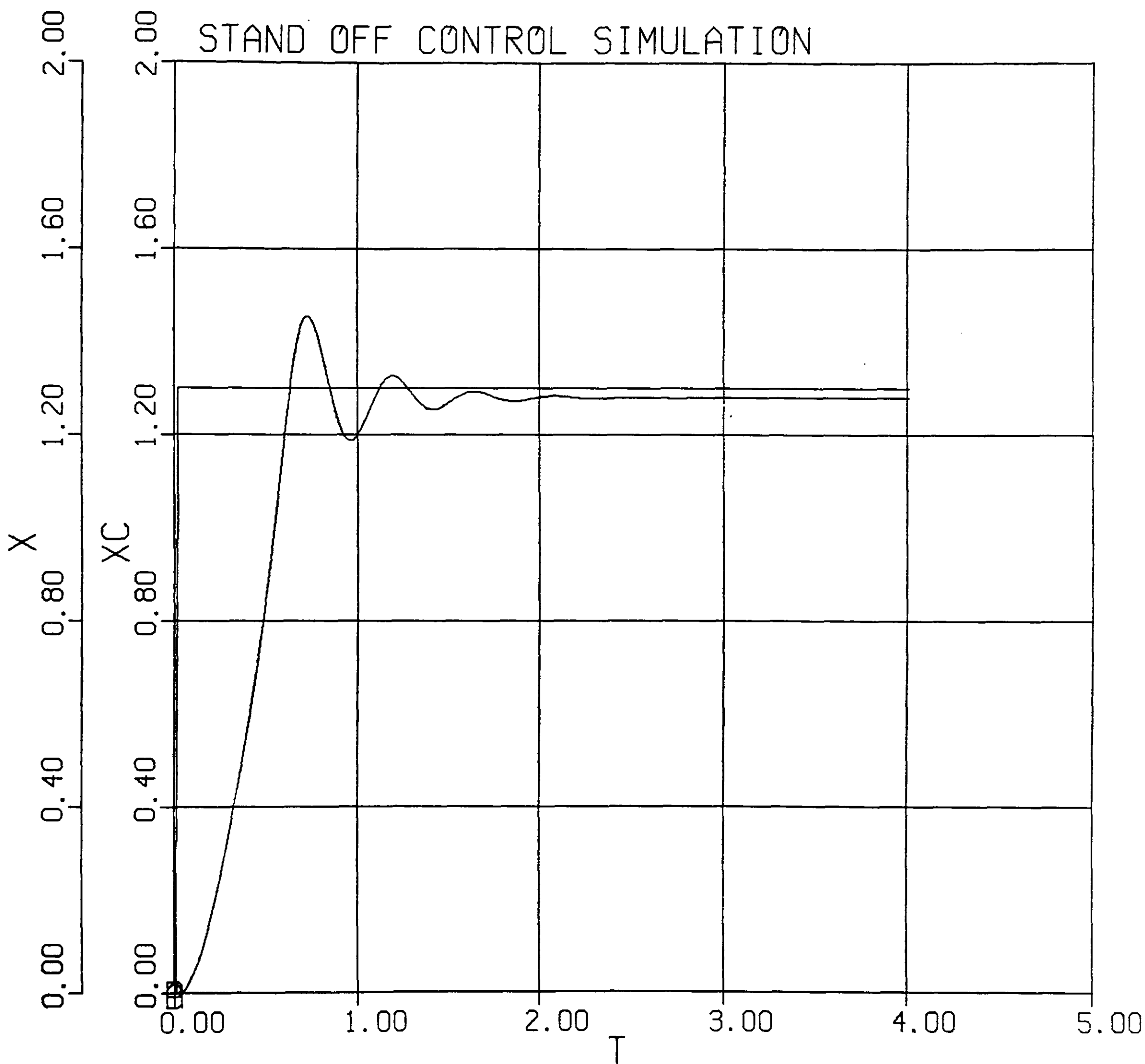

Figure 5.7 Output results of the predicted performance

5.6 Operational Characteristics:

A diagram of the experimental apparatus used to investigate stand-off control is shown in fig.(5.8). Optical components and the error measuring principle are detailed in chapter 4 and 3 respectively. The main components used are :

A differential amplifier used as an error signal conditioning stage producing the error voltage signal V_e. This is described in more detail in section (4.2.2.1).

Controller, a proportional controller with one channel input and one output (RDK9) sold by Stafa Control System was tried. This controller was found through experimental procedure to be unsuitable, due to its slow response.

A proportional controller was then built for use with the solenoid chosen. This has a gain variable between 0.4 and 4.0. Additionally, a bias voltage varying between 0 and 6 volts is used to preload the spring and centre the solenoid within it limits of travel. The circuit diagram of the controller is given in fig.(5.9).

A DC solenoid acts as the actuator in the designed system. The characteristics of the solenoid were found experimentally. The maximum travel of the core is 3.4mm and consequently the experiment step input is limited to this travel. The inductance of the solenoid coil was measured and found equal to 256 mH, whilst the resistance was 48.625 ohms. The damping coefficient and the solenoid constant K_{sol} were introduced in section (5.4.1)

The controlled system, consists of the main lens (focal length of 75mm) mounted on a carriage in contact with the solenoid core and connected to a return spring. A dial gauge was used to accurately record and calibrate the displacement transducer which was positioned in contact with the solenoid core fig.(5.8) to acquire the movement of the carriage.

The displacement transducer, A Sagamo Schlurnberger transducer type C31 was used to sense, convert and condition the carriage movement to an analog voltage signal.

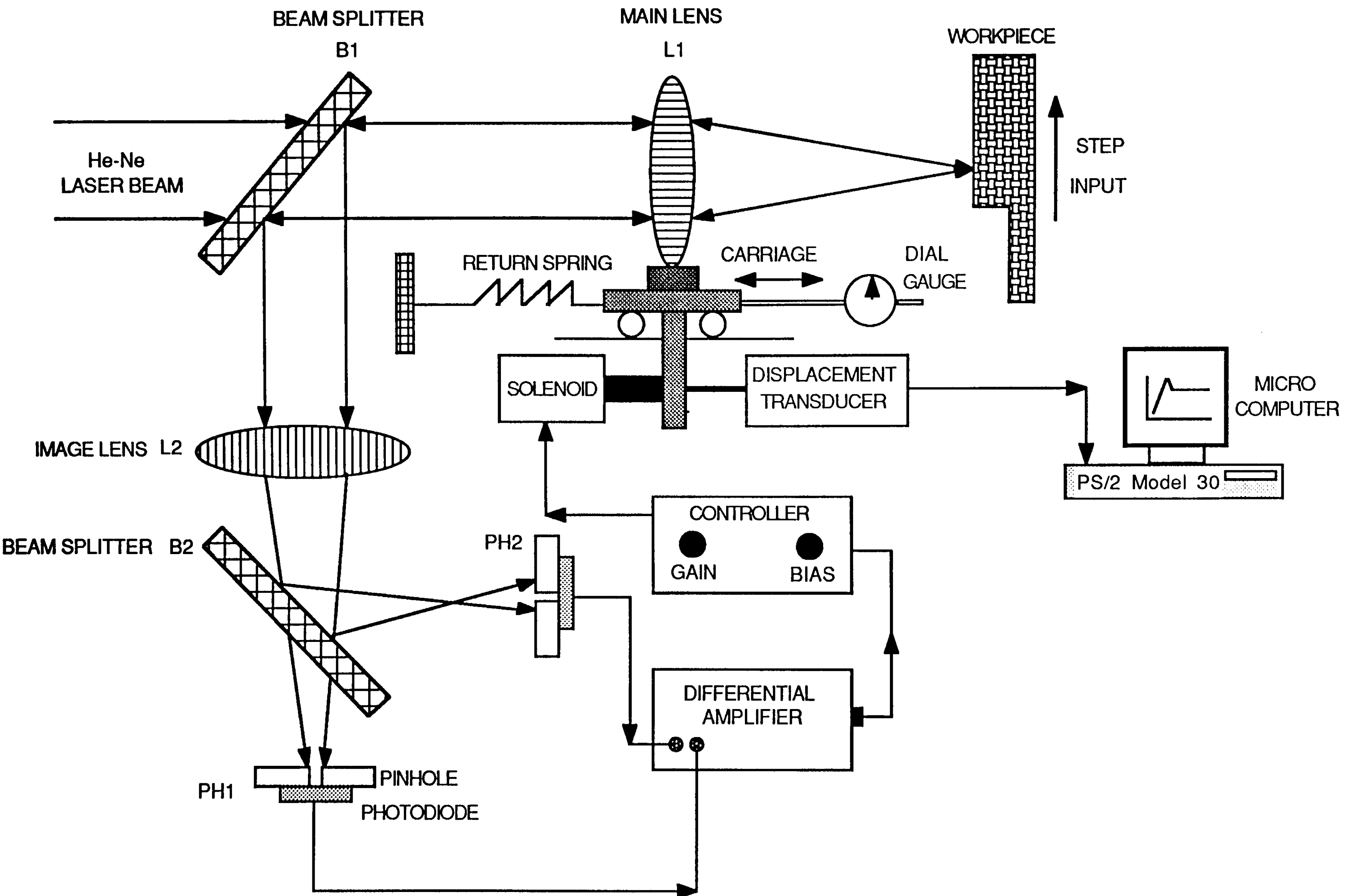

Figure 5.8 Schematic diagram of apparatus used in control experiments

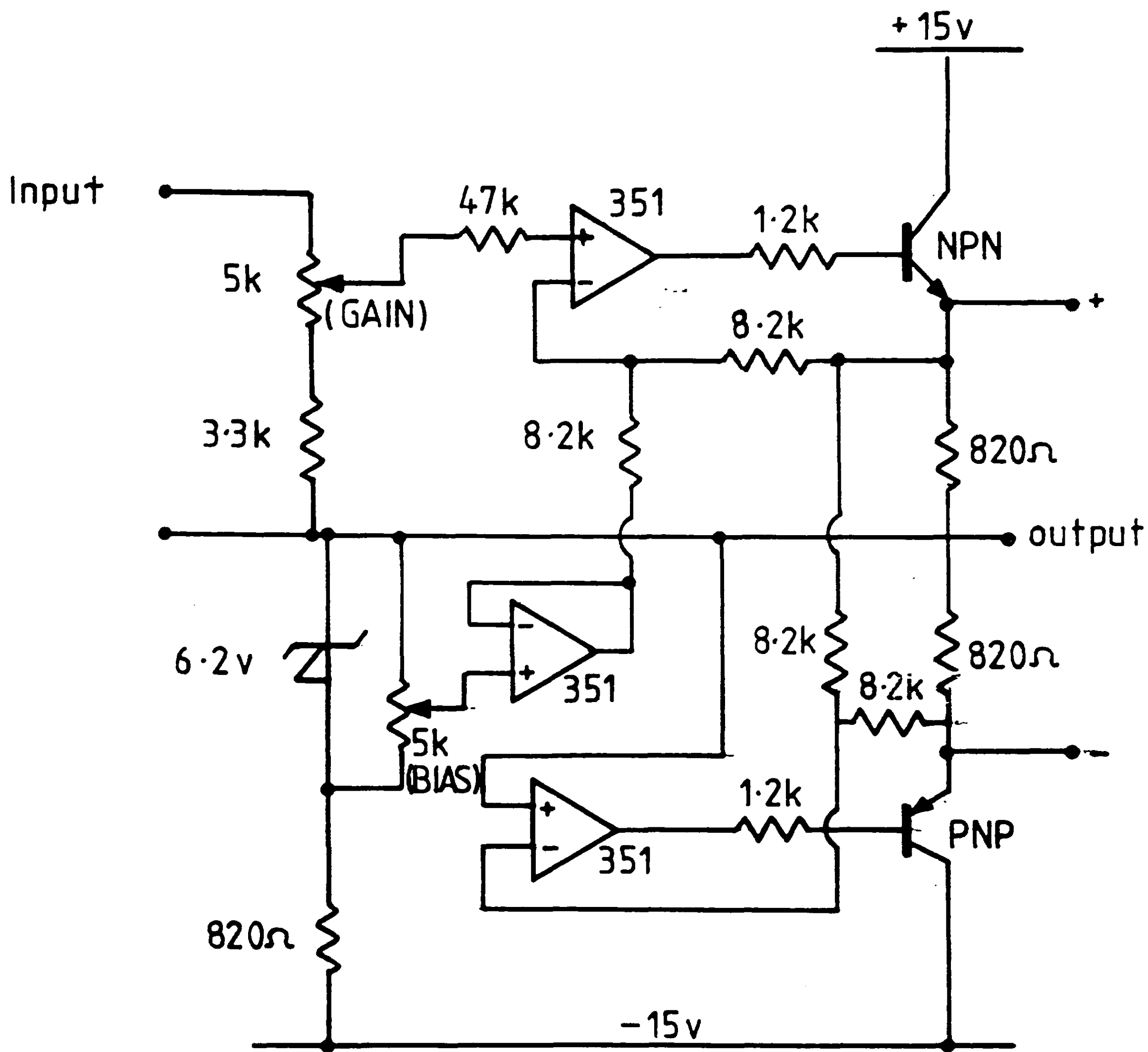

Figure 5.9 Circuit diagram of the proportional controller

The micro computer, IBM PS2 model 30 was utilized in the experimental procedure to record the output response of the system, after converting it to a digital format by means of an A/D converter card. At the same time the micro computer was connected to the VAX computer, which allowed the transfer of the simulation results for every experiment to the micro computer, thus allowing direct comparison with the experimental results.

Alignment of the optics and amplifier adjustment was performed to optimize signal output. The experiment was then conducted and results plotted together with theoretical results, which are presented in the next section.

5.6.1 Results:

In order to analyze the behaviour characteristics of the system and to compare operational characteristics to predicted performance, the output response was recorded for varying: step size, material, controller gain and for forward and backward steps. The results can then be used to analyze the effect of changing any of the previous parameters on the performance of the control system. The graphs presented are described and discussed in groups designed to show the effect of changing one parameter.

All the experiments were performed using a He-Ne laser as a light source, with focal lengths of the main and image lenses equal to 75mm and 300mm respectively.

Graphs 5.1, 5.2 and 5.3 show the system response for three different materials : Mild steel, Galvanised steel and Formica. They have the same controller gain and bias, but slightly different step sizes. As can be seen from these graphs, the response time for the galvanised steel is fastest, in second place is the mild steel and finally the formica. The experimental response is faster than the theoretical for the mild and galvanised steel, however for the formica is less. The steady state error for the galvanised is less than the others and its overshoot is bigger. The formica appears to be over damped. Therefore it can be deduced that the amount of the back reflection affects the response of the system. The

colour and roughness of the workpiece surface alters the amount and distribution of reflected light. On this basis, the performance of the system varies with the type of the workpiece in use.

Since, the previous experiment in chapter 4 made use of mild steel as a standard workpiece, it was chosen to perform the rest of the experiments using this material.

Graphs 5.4, 5.1 and 5.5 shows the effect of variation in controller gain. Gain of 0.8, 1.6, 3.2 are given for the same step size, bias and material. It can be seen from the three graphs that the both experimental and theoretical responses become faster, steady state errors reduce and oscillation in the response increases as the gain is increased. Table 5.1 and graphs 5.10 and 5.11 give the experimental and theoretical response time and steady state error for a number of gain. It can be seen that the gap between the theoretical and experimental results is decreased as the gain is increased.

Gain	Response time sec		Steady state error mm	
	Theoretical	Experimental	Theoretical	Experimental
0.8	1.9	1.1	0.0343	0.09
1.6	1.4	0.8	0.0172	0.095
3.2	0.9	0.59	0.0087	0.016

Table 5.1 Response time and steady state error for mild steel

Graph 5.6 displays the output response for forward and backward steps for a mild steel workpiece with an input step size of 1.62mm. The experimental backward response is slower and without over shoot, due to the time for the magnetic field to collapse in the coil

and non-linear effects in the solenoid.

Graphs 5.7 and 5.8, show the effect of different disturbance step size on the system performance. Graph 5.7 shows the experimental and theoretical output responses for 1.27mm and 1.62mm step sizes for mild steel. Graph 5.8 shows the variation of the simulated output for step sizes of 1mm, 2mm and 3mm, due to the restriction of the core movement to 3.4mm. From these graphs it can be seen that the non-linearity in the sensor output (graph 4.1.1) has a significant effect on the system response. Thus to achieve optimum response, the system requires to operate in the linear portion of the output signal, see (graph 4.4.1).

From graph 5.9, it can be concluded that variation in the surface reflectivity affects the response of the system. This variation in the reflectivity of the materials causes the device to exhibit a total noise range of 500μm for Galvanised steel, about 200μm for Mild steel and about 20μm for Formica. Accordingly, this suggests that the division circuit in the amplifier does not work perfectly, although the results are acceptable for a large number of applications.

A number of conclusions can be drawn from these results:

Firstly, the difference between theoretical and experimental output responses. The parameter which had most effect on these results is the non-linearity of the solenoid, (the simulation assumed that it was a linear). As a result the term K_{sol} actually varies in a non-linear fashion.

Secondly an experiment was applied to the return spring, which showed that the stiffness of the spring was not constant.

Thirdly the division of the photodiode output voltages in the simulation is conducted numerically in the computer, while the actual analog division circuit in the differential amplifier does not work perfectly. This leads to a change in the output response when the workpiece material changes, while the theoretical response remains the same.

Fourthly a steady state error was observed in the output response due to two effects. The first one is the inherent limitations of a proportional controller and the second is the

difficulty of controlling the non-linear movement of the solenoid.

Consequently to improve the system attention should be given to the division circuit in the differential amplifier, by adding an integration stage to the controller and by replacing the solenoid by a DC servomotor.

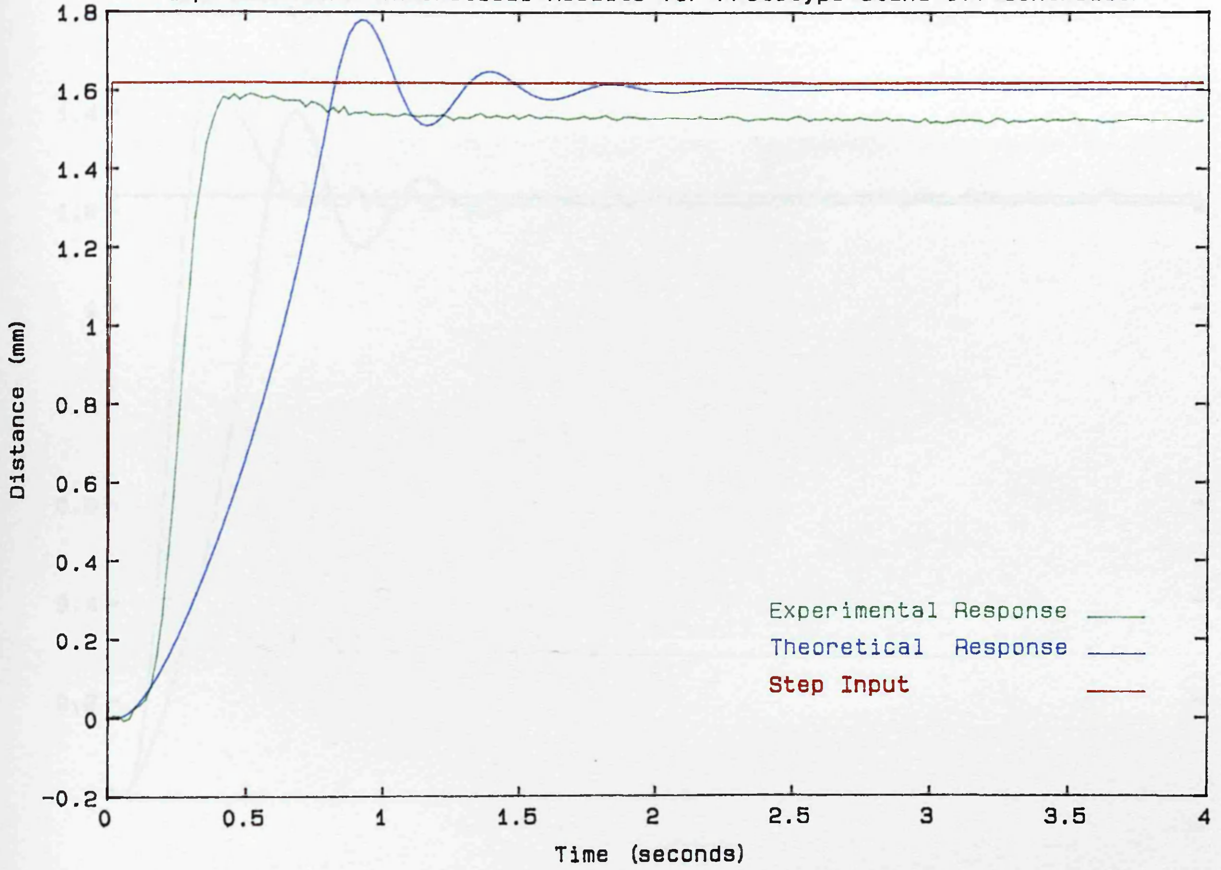

Material	: Mild steel	Light source	: He-Ne laser
Gain	: 1.6	Main lens	: 75mm
Bias	: 1.4 v	Image lens	: 300mm
Step size	: 1.62mm		

Graph 5.1 Step response for mild steel

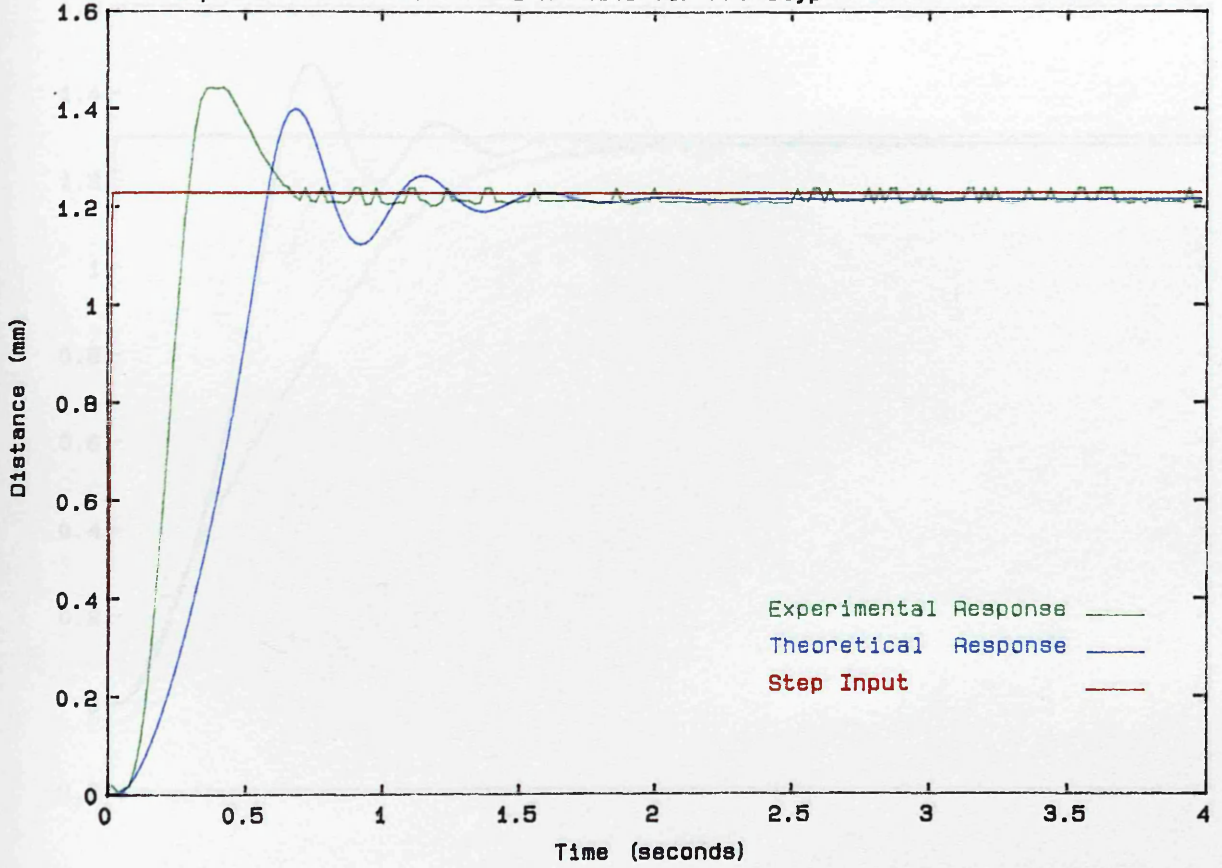

Material	: Galvanised steel	Light source	: He-Ne laser
Gain	: 1.6	Main lens	: 75mm
Bias	: 1.4 v	Image lens	: 300mm
Step size	: 1.23mm		

Graph 5.2 Step response for Galvanised steel

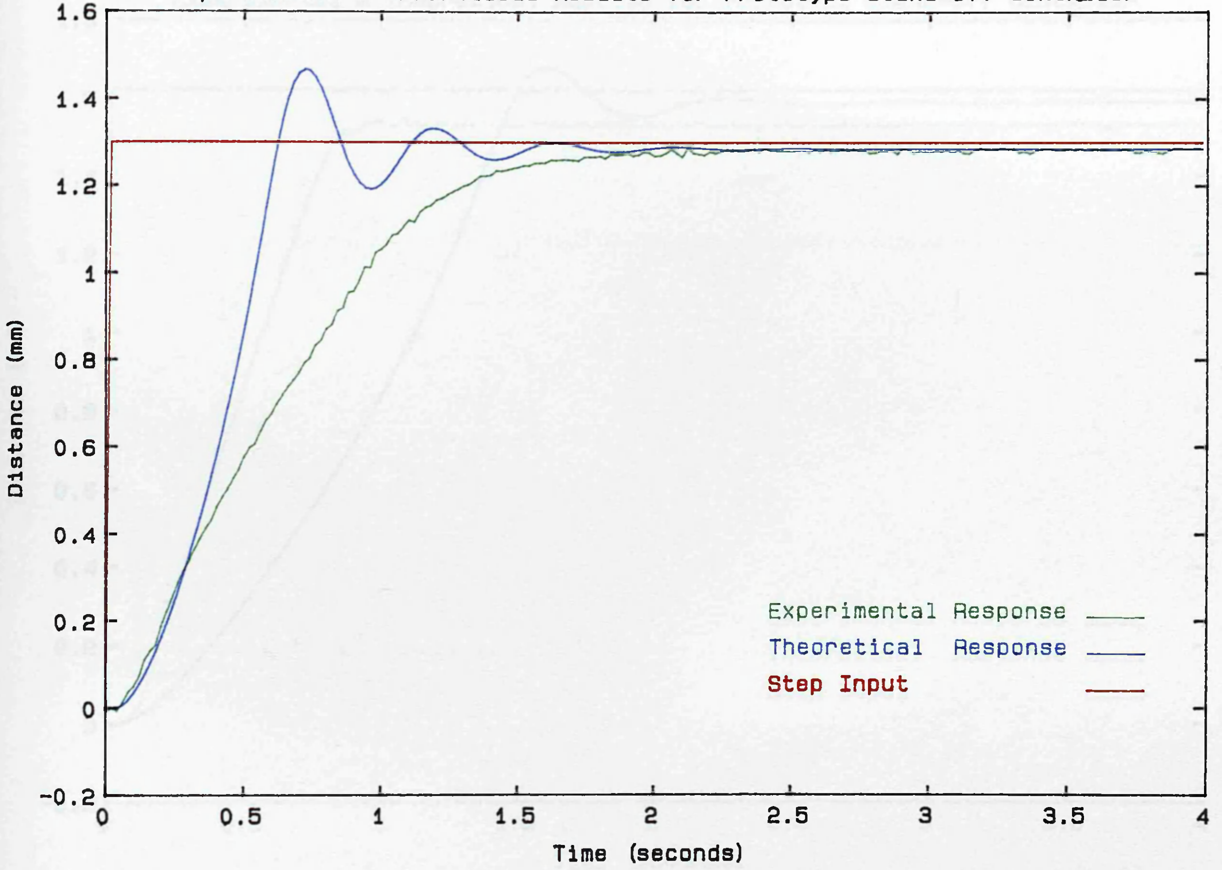

Material : Formica	Light source : He-Ne laser
Gain : 1.6	Main lens : 75mm
Bias : 1.4 v	Image lens : 300mm
Step size : 1.3mm	

Graph 5.3 Step response for Formica

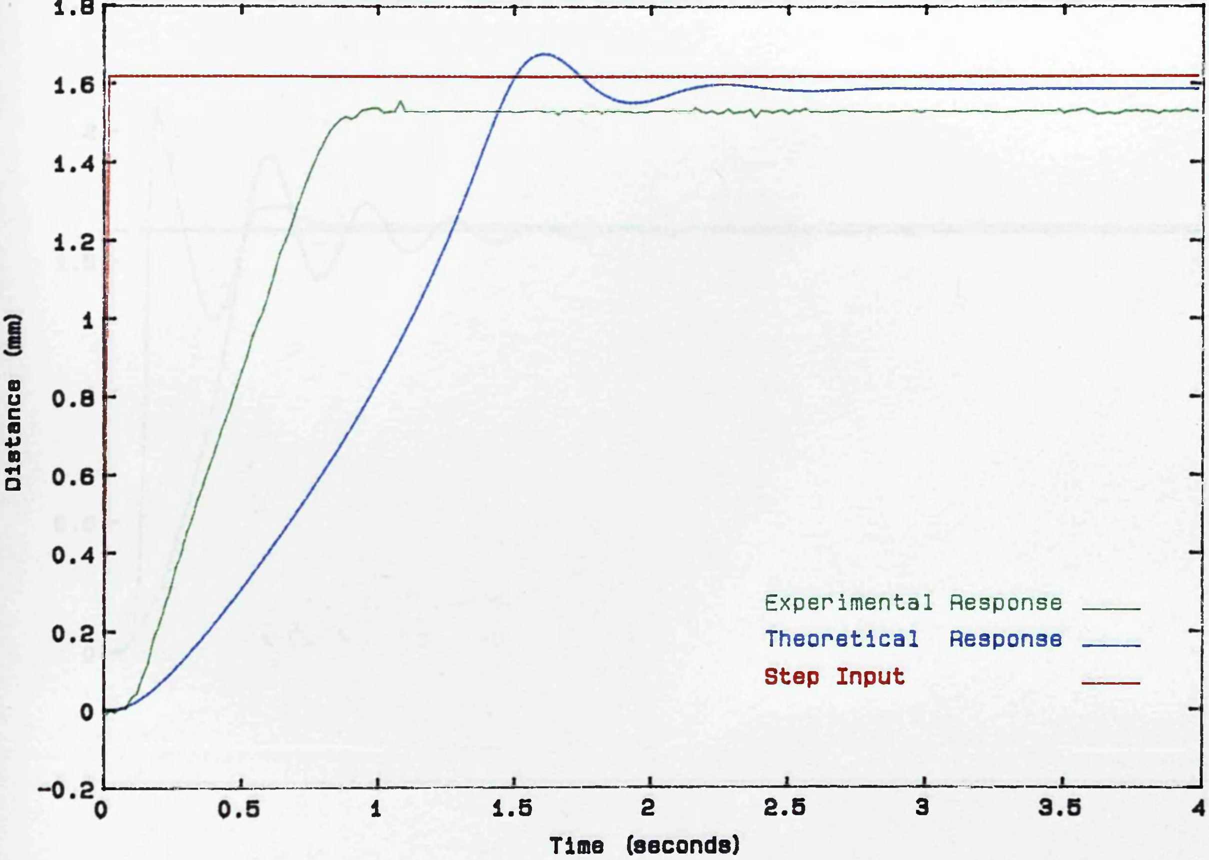

Material : Mild steel	Light source : He-Ne laser
Gain : 0.8	Main lens : 75mm
Bias : 1.4 v	Image lens : 300mm
Step size : 1.62mm	

Graph 5.4 Step response for mild steel

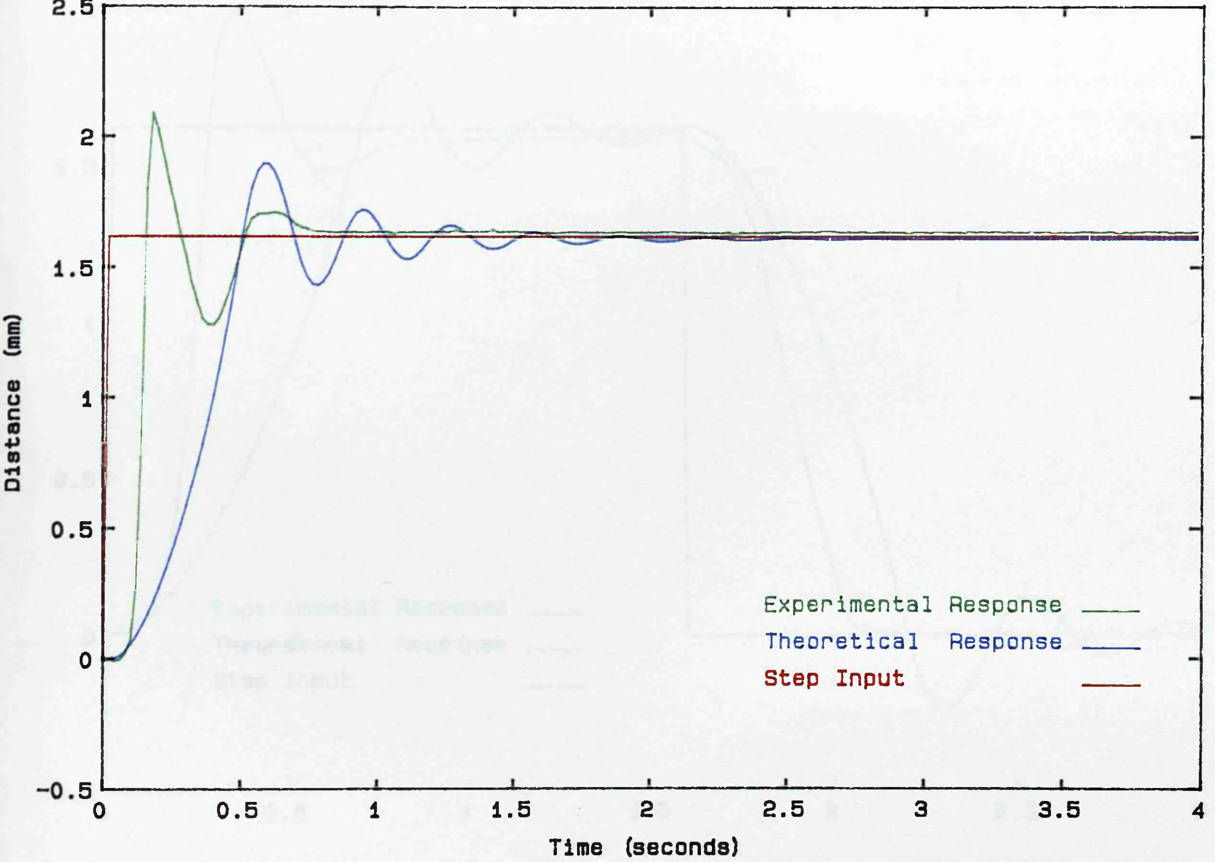

Material : Mild steel	Light source : He-Ne laser
Gain : 3.2	Main lens : 75mm
Bias : 1.4 v	Image lens : 300mm
Step size : 1.62mm	

Graph 5.5 Step response for mild steel

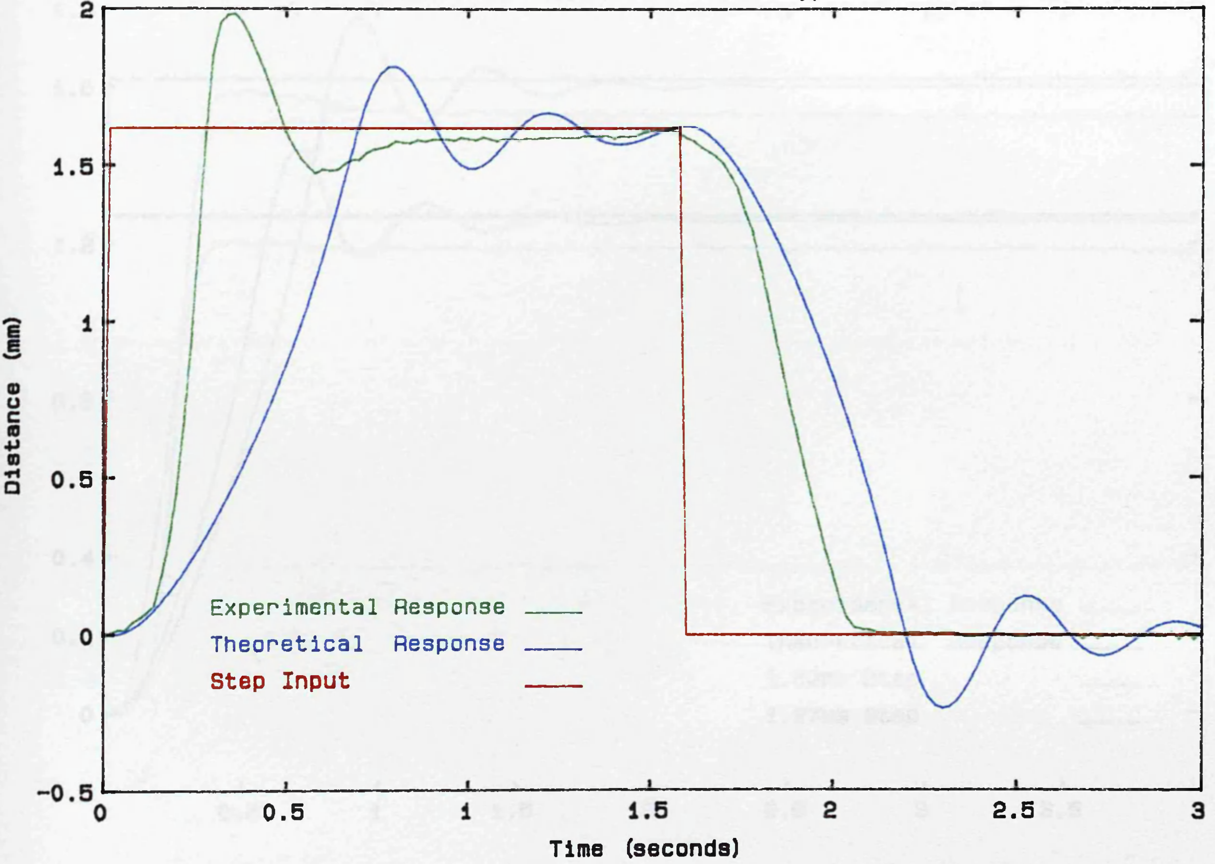

Material	: Mild steel	Light source	: He-Ne laser
Gain	: 2.0	Main lens	: 75mm
Bias	: 1.4 v	Image lens	: 300mm
Step size	: 1.62mm		

Graph 5.6 Forward and backward step responses for mild steel

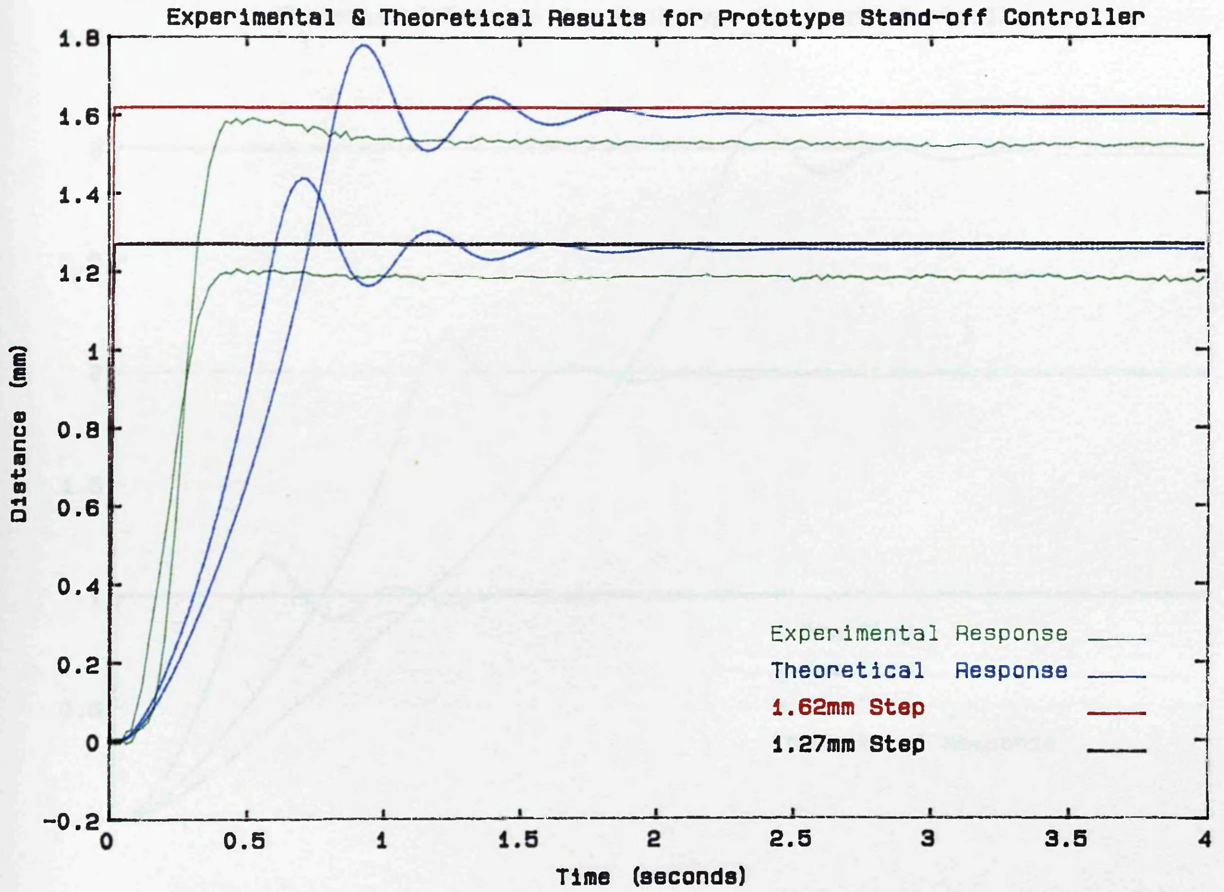

Material	: Mild steel	Light source	: He-Ne laser
Gain	: 1.6	Main lens	: 75mm
Bias	: 1.4 v	Image lens	: 300mm
Step size	: 1.62mm & 1.27mm		

Graph 5.7 Different step responses for mild steel

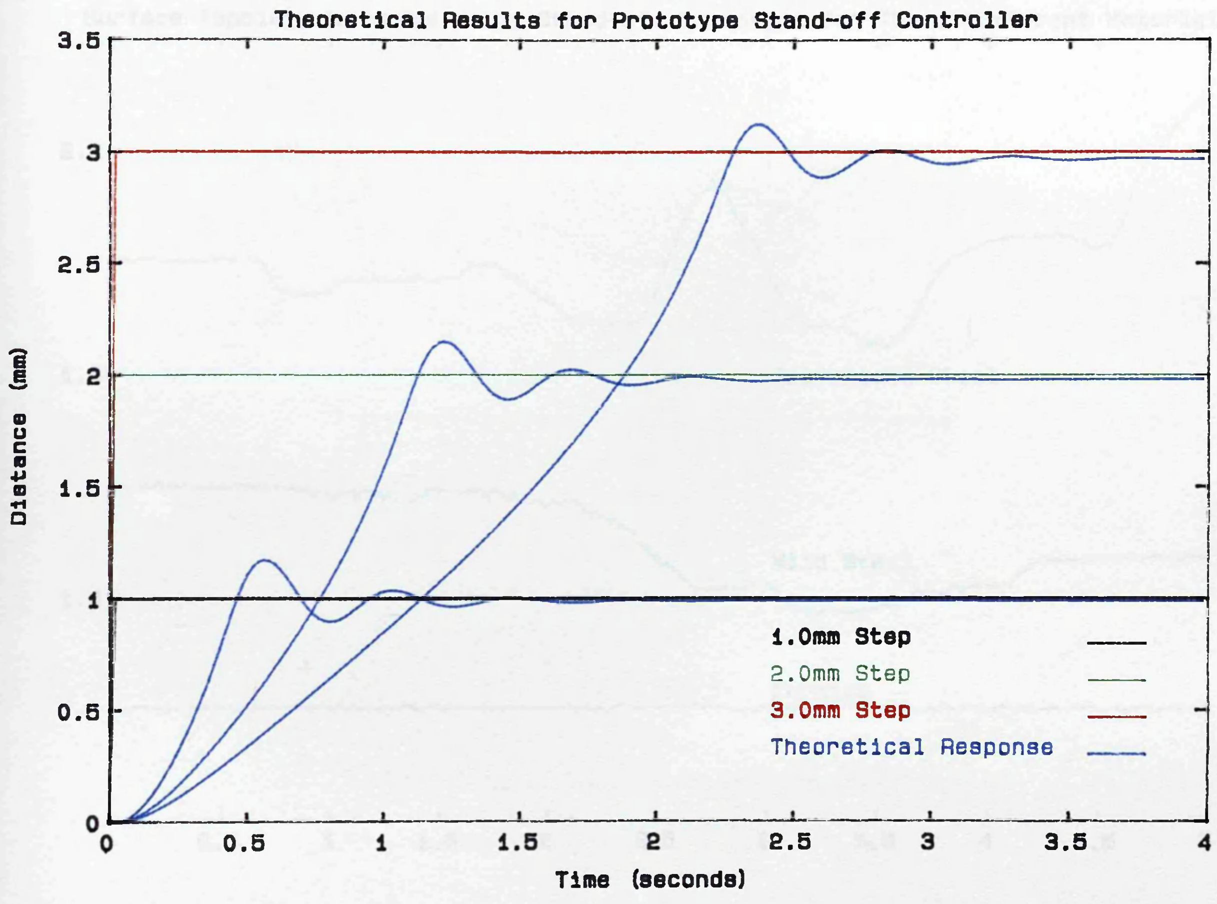

Material : Mild steel	Light source : He-Ne laser
Gain : 1.6	Main lens : 75mm
Step size : 1mm, 2mm & 3mm	Image lens : 300mm

Graph 5.8 Different theoretical step responses

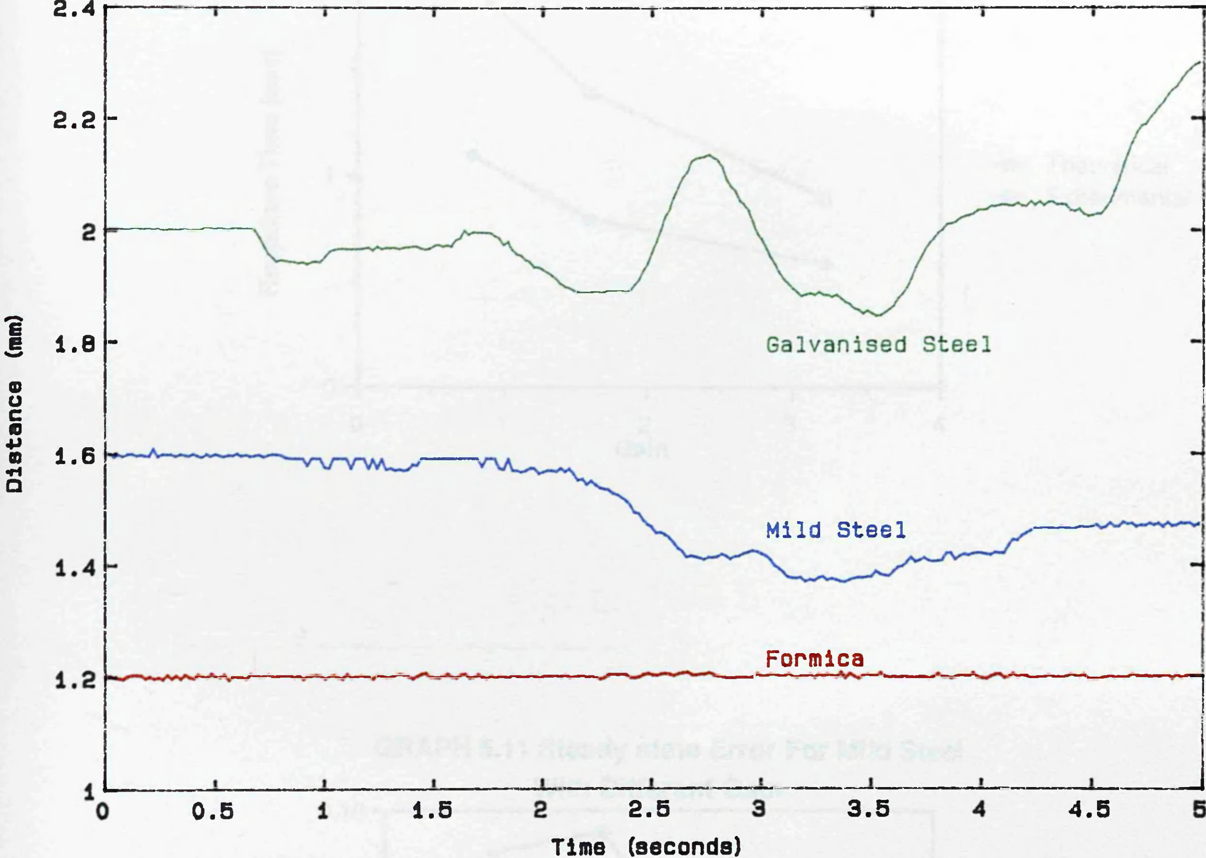

Material	: Galvanised steel, Mild steel&Formica	Light source	: He-Ne laser
Gain	: 1.6	Main lens	: 75mm
Bias	: 1.4 v	Image lens	: 300mm

Graph 5.9 Profile of three different materials

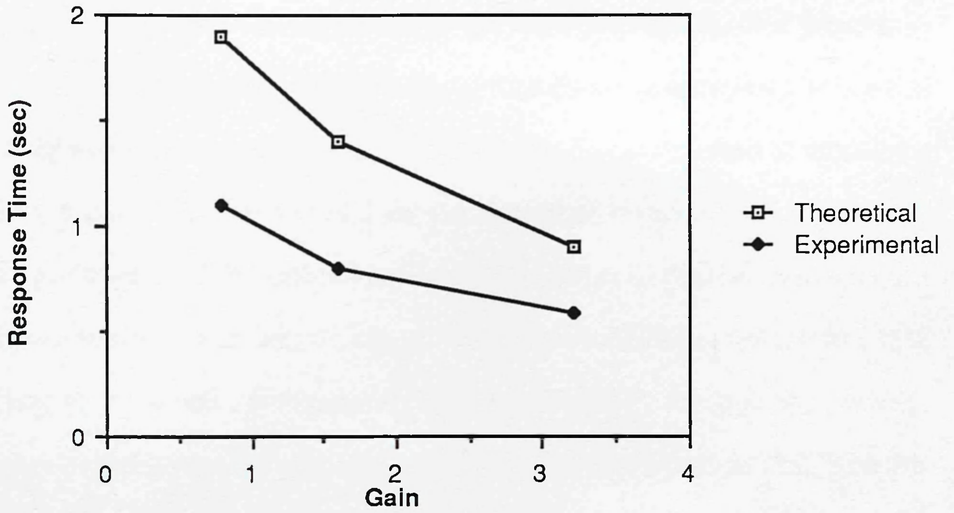
GRAPH 5.10 Response Time For Mild Steel
With Different Gain
Response Time (sec)
2
1
0
0
1
2
3
4
Gain
Theoretical
Experimental

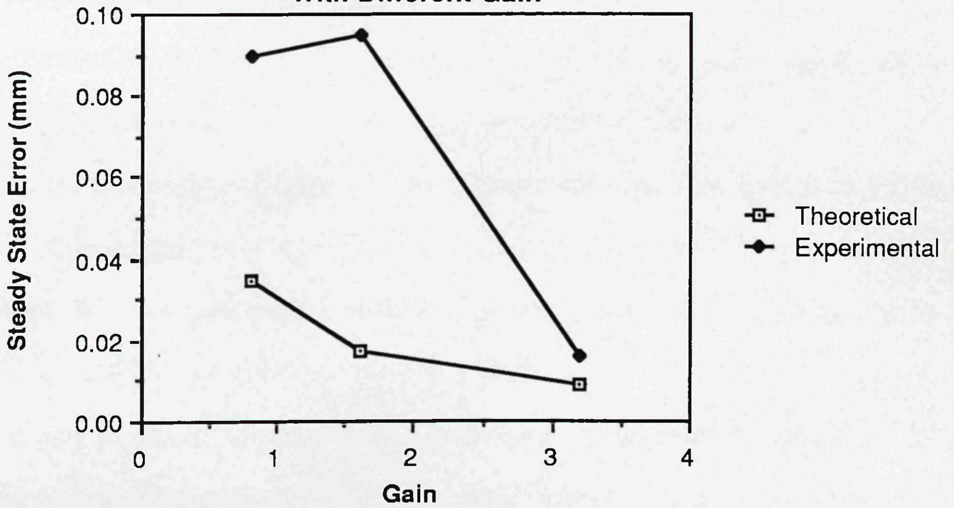
GRAPH 5.11 Steady state Error For Mild Steel
With Different Gain
Steady State Error (mm)
0.10
0.08
0.06
0.04
0.02
0.00
0
1
2
3
4
Gain
Theoretical
Experimental

CHAPTER 6
CONCLUSION

CHAPTER 6: CONCLUSION

6.1 Discussion and Conclusions:

An on-axis noncontact opto-electronic sensor and actuation system was presented, capable of sensing, measuring and keeping a prescribed distance between a robot end effector and workpiece surface. Two mathematical models were presented to model the sensor. The first, a gaussian model based on the theory of propagation of gaussian beams extended previous work by Dobosz to include the effect of the distance between the laser and main lens and main lens to image lens separation. Dobosz work Ref.(21) used a coefficient to described approximately the loss of energy through the pinhole, while the gaussian model presented utilized a normalized voltage equation (3.22). In this way the effects of reflectivity, colour, profile and texture for different materials may be neglected.

It was found that the workpiece surface destroyed the gaussian intensity distribution of the laser beam upon reflection, therefore the reflected beam could not be considered to be gaussian. Thus, a gaussian-radiometric model was formulated using geometric optical theory and a radiometric intensity distribution. This produced a normalized output signal with a large reduction in the distance between the two peaks of the output signal, when compared to the gaussian model.

The radiometric model proved generally to be more accurate however, it failed to show the effect of the initial beam waist, wavelength and the distance between the laser and the main lens. Whereas both experimental and gaussian modelling agreed at least in trend.

The experiments produced output voltage signals bounded between the gaussian and the radiometric models. Generally, the beams can be considered as behaving as neither totally gaussian nor totally radiometric for the experiments performed in this research. The radiometric model is a closer approximation to the experimental results for the cases presented in this work.

It can be concluded from the experimental and theoretical results presented and their

analyses in chapter 3 and 4, that a large number of parameters affect the sensitivity and the magnitude of the output signal.

. Reducing the offset distance of the pinholes will increase the linearity between the two peaks of the output signal and the sensor sensitivity. On the other hand, the peak output voltage will decrease.

. As the pinhole size is decreased the sensitivity of the sensor increases. This however, leads to a noisy signal due to speckle and the optimum size for a particular design is arrived at by compromising between output signal and truncation, fluctuation and noise effects.

. Extending the distance between main and image lenses results in increased output sensitivity. The peak output voltage increased for the experimental set-up using the 120mm lens, while it reduced for the 75mm lens. This may have been due to the balance of the amplifier not being correct or misalignment.

Reducing the distance between the main and image lenses results in a loss of linearity between the two peaks and decreased sensitivity and peak voltage. In general the best configuration of the optical system, is one where the focal points of the two lenses coincide. This allows the optical part of the sensor to be kept to a reasonable size. It should be noted that for configurations other than this, the gaussian model shows a loss of symmetry between the positive and negative parts of the output signal,

. Using a main lens with shorter focal length increases sensitivity, but reduces the peak normalized output voltage.

The distribution of the reflected beam power appears as a random pattern of speckle points. The image lens concentrates these to a focused spot, highlighting the need to use an image lens as a collector of the reflected light beam.

The gaussian and radiometric models were fused into one program and when programmed with Dobosz optical parameters, to test both models against his results Ref.(21), the gaussian model gave the same result as the radiometric and had very good agreement with the results presented by Dobosz.

By reducing the main lens focal length the two models produce similar results and in some cases these were coincident. The reasons for this are currently unknown and further experimental and theoretical work is required to answer this.

The positioning of the pinholes is currently performed by eye estimation and is subject to positional error. The output signal is sensitive to this parameter and further investigation is needed to improve this operation.

The operational characteristics of the servo system showed that, the experimental (actual) time response was faster than the predicted performance of the system. It is though that this is due to the non-linearity of the solenoid, which was assumed to be linear in the simulation. The actual responses for different materials were different. Whilst, the theoretical responses were the same. This was caused by the division circuit of the differential amplifier not working correctly.

The time response of the servo system increased in a non-linear fashion as the step size of an induced disturbance became larger. This being due to the non-linear nature of the normalized output signal from the sensor.

Generally, there is a proportional error, which results in an output response greater or less than the input step disturbance, this would suggest that an integration term should be added to the proportional controller.

6.2 Further work and development:

Throughout this work, some areas requiring further investigation and development came to light. In order to improve the design and performance of the sensor and associated servo system, the following list of tasks require to be addressed :

. A detailed study of the effect of the surface on the reflected beam and its effect on system performance.

. Further development of the division circuit in the amplifier to overcome the influence of surface characteristics and make the sensor work more effectively with different materials.

. An investigation and experimental study into the effect of reducing the size of optical elements and inter-component distance, in order that the system may be integrated into robot end effectors.

. More experiments to be conducted using shorter main and image focal length lenses to demonstrate the theoretical results of coincidence of both models.

. A servo motor should be substituted for the solenoid which has difficulties in stalling between limits of its motion.

. A study of the interaction between the working of the sensor and its industrial environment.

APPENDICES

Appendix (A1) General Definition, Classification and Application of Robots:

A robot has been defined as Refs.(1,2,3) : a reprogrammable and multifunctional manipulator, designed to move materials, parts, tools or specialized devices through various programmed motions in the performance of a variety of tasks. Reprogrammable means that the a robot can be directed or programmed to perform different tasks. Multifunctional defines the capability of a robot to be appropriately retooled to a specific task. Whilst the concept of manipulator implies an articulated mechanical system allowing the movement of objects or tools in the performance of its programmed task.

From this perspective, a robot can be considered as a special class of automated machine, differentiated from other automatic devices by its programmability and versatility. Whilst its capability to physically manipulate the real world separates it from a computer.

The science encompassing the design, building and application of robots is robotics. This is a branch of engineering in which subjects as diverse as remote control, artificial intelligence and mechanical engineering are merged.

The basic components of any robot are : manipulator, end effector, power source, controller, sensors and actuation system. All of these components can be engineered together to form a mechanical system capable of robotic tasks.

These elements can be examined in more detail :

- A **manipulator** is a mechanically actuated skeleton of the robot which provides support for tools or objects being manoeuvred in space. It comprises links and rigid and moving joints to allow motion in different directions. A closely packed combination of joints, termed a wrist, is often mounted on the end of two or more links to provide anthropomorphic like movement to an end effector or gripper.

- An **end effector or gripper** is effectively a tool interacting with the robotic environment. These can be special tools designed to weld, paint, mill or perform other machining operations, or be hand like to achieve assembly tasks.

- The **power source** provides the driving force required to move the robot. There are

three main types : hydraulic, electric and pneumatic. Hydraulic sources are generally used in large payload or high speed applications. Electric sources are best suited for medium weight applications where high accuracy is required. Pneumatically powered robots are generally limited to pick and place applications, where travel can be limited by mechanical stops.

- The **controller** organizes the movement of the manipulator in accordance with a list of instructions and in response to sensory information. These instructions are written as programs and control action is supported by data acquired by sensors. A controller has a memory to permit storage and execution of instructions, but is incapable of coping with environmental conditions that are not provided for within the programmed algorithms.

- **Sensors** are devices that transduce information as to the robot's environment into a form amenable to the control unit. These are used to provide feedback which is used to control the speed and position of the manipulator, or to detect the presence or absence of a workpiece and to ensure safe operation.

- The **actuation** system is a combination of actuators and transmission components taking the form of motors, cables, bands, belts, gears, etc.. Its function is to translate data provided by the controller into actuator movements and to link the actuators with the manipulators.

There are four common method of classification of robotic systems Ref.(1) : Method of control, pathway, morphology and level of technology.

Robots may be classified by their morphology or configuration. There are four basic types, described by the motion of their axes :

1- **Cartesian**, rectangular coordinate or gantry configuration: the manipulator moves in three perpendicular axes X, Y and Z. As a consequence, the work volume takes shape like a rectangular box fig.(A1.1).

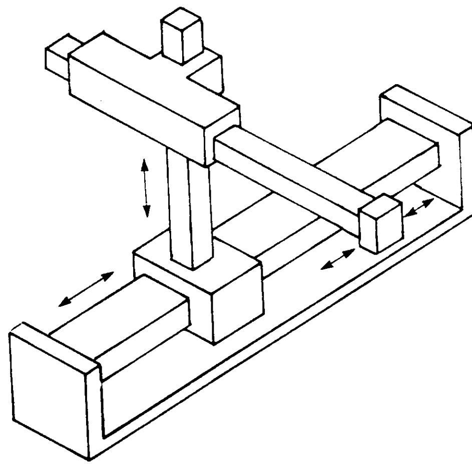

Figure A1.1 Cartesian configuration

2- A **spherical** or polar configuration having two rotary and one linear motion. The manipulator pivots about both horizontal and vertical axes. This coupled with the ability to extend and retract in a linear motion produces a work volume in the shape of a section of a sphere fig.(A1.2).

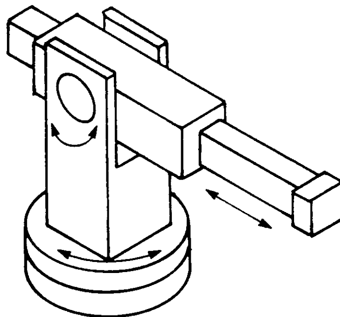

Figure A1.2 Spherical configuration

3- In the **Cylindrical** configuration the manipulator arm pivots on its base and moves up and down around a vertical axis, extending and retracing horizontally. This combination of two linear and one rotary motion leads to a cylindrical work volume fig.(A1.3).

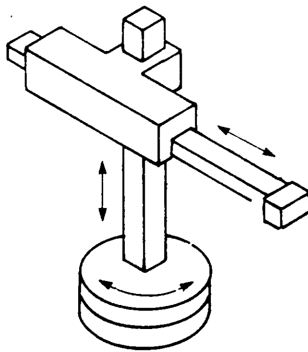

Figure A1.3 Cylindrical configuration

4- **Jointed arm configuration**, this configuration may be divided into vertically jointed arms (anthropomorphic configuration) and horizontally jointed arms. The common **anthropomorphic** configuration uses a revolute system of coordinates having three rotary motions, one about the vertical axis of the base and another two, pivoting about horizontal axes. The gripper can be extended and retracted by movement of these joints, so the work volume is the same as the spherical robot fig.(A1.4). Several commercially available robots possess an anthropomorphic configuration, eg. Cincinnati Milacron and Unimation PUMA robots.

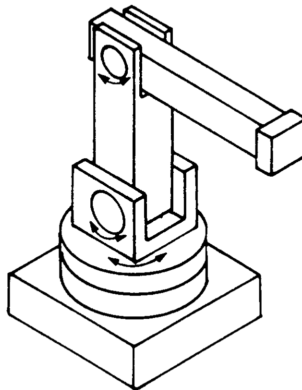

Figure A1.4 Anthropomorphic configuration

Horizontal jointed robots are often referred to as SCARAs (selectively compliant assembly robot arm) and are predominantly used in assembly tasks. The gripper is kept vertical and rotates with the shoulder, elbow and wrist about vertical axes fig.(A1.5). Additionally the end effector of the manipulator has a linear vertical motion.

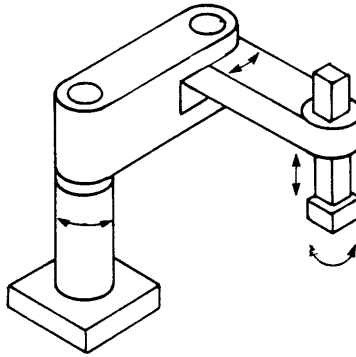

Figure A1.5 SCARA configuration

Each of these configurations have inherent advantages and disadvantages in the performance of specific tasks and for more detail the reader is directed to Refs.(4,5).

Industrial robots are increasingly used in manufacturing and commercial applications for several reasons including:

- Improved product quality.
- Reduced cost of production.
- Increased productivity.
- Ability to work in hazardous and hostile environments.

These advantages arise from the properties inherent of robots: the ability to perform tasks repetitively without tiring whilst maintaining levels of performance, accuracy, the ability to work in toxic or hazardous environments and the ability to conduct a variety tasks by changing end effector.

Robot applications can be classified as follows : Refs.(1,3,4,5)

1. **Materials handling**: moving workpieces from one location to another within a work cell, loading and unloading parts from a machine, packing and palletizing operations and other transfer operations.

2. **Material processing**: where the robot performs one or more manufacturing processes in the work cell, such as: spot or arc welding, fettling of castings, drilling, grinding and deburring of components.

3. **Assembly** of components: a growing and important application area is the assembly of products using robots. The process is usually made up of the sequential addition of components to a basic part to create a more complex sub-assembly or complete product. The difference between assembly tasks and other material handling tasks is that value is added to the product through the assembly operation.

4. **Painting and finishing**: such as, swarf removal or spray painting of components or assembles.

5. **Inspection** through the use of sensors, to gauge and measure quality characteristics of manufactured products.

6. **Transportation**: specialized robots may be used to transport parts or loads from one location to another. These are normally known as Automatically Guided Vehicles (AGVs).

Appendix (A2) Robot Internal Sensors:

Internal sensors can be divided into the following categories : force or torque sensors and movement or position sensors. These sensors are used to provide control information on robot status during the performance of tasks, such as: the force or torque applied to joints or the speed, movement and acceleration of an end effector.

Force and torque sensors, are utilized to determine whether safe loading limits are being exceeded and to sense the force exerted on a workpiece by an end effector. Force sensors employ piezoelectrical or strain gauge transducers, to provide a signal proportional to the force applied at the point of contact and may be sub-divided into three classes based on their location within the manipulator.

Wrist force, sensors measure three components of force (F_x, F_y and F_z) or three components of torque (T_x, T_y and T_z) applied to a wrist. Generally these make use of compliant structures and strain gauges to measure deflections proportional to applied forces.

Joint sensors, are used to directly measure the force or torque acting at each joint of a manipulator. If the joint is driven by dc servomotor, then torque can be estimated by measuring the current flowing through the armature. If the joint is driven by a hydraulic motor then sensing can be accomplished by determining back pressure.

A Pedestal force sensors, employs strain gauge or piezoelectric transducers to measure the three components of force and torque acting on the base of a robot.

Movement or position sensors, measure either rectilinear (translational) or angular (rotational) movement and are employed to measure position and dynamic motion of manipulator, wrist and robot arm. There are many types of position sensors available the most commonly used being: potentiometers, encoders and resolvers.

Potentiometers, are mechanically variable resistors, which are analog devices, whose output voltage is proportional to the position of a wiper on a resistive element. There are two types of potentiometer: linear and rotary. In the linear type the resistance element is mounted so that the slide elements move in a straight line. Whilst in the rotary type the

resistance element is bent into a circle or helix, fig.(A2.1) shows a rotary type.

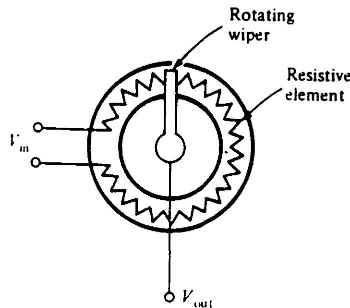

Figure A2.1 A rotary potentiometer

Encoders, are available in two basic forms: incremental and absolute. Incremental encoders are less expensive and simpler than absolute encoders, utilizing two or four photocells to sense the individual steps and the direction of motion. Absolute encoders are usually high precision rotary or linear devices, mounted on rotary or linear joints to identify the exact position through the use of grey scales coded onto a sensing scale.

Linear variable differential transducers (LVDTs), consist of three coils and moving core. An a.c. or d.c. voltage is supplied to the input coil which then generates an output voltage across the secondary coil, which is a linear function of the displacement of a magnetic core within the coils fig.(A2.2).

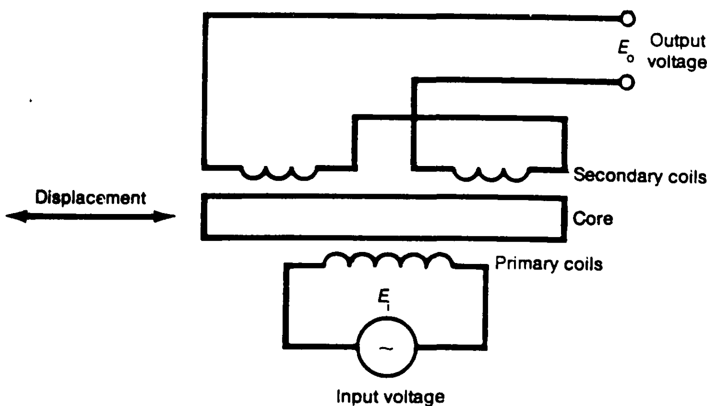

Figure A2.2 A linear variable differential transformer (LVDT) Ref.(4)

Resolvers, are generally rotational position measuring devices with analog or digital output, working on electro-magnetic principles. The output being proportional to the position of a moving element with respect to a fixed element. Further details of these position sensors can be found in Refs.(3,4,10).

There are other type of sensors like velocity and acceleration sensors. Velocity sensors measure translational and rotational velocity, such device is a dc tachometer, which is essentially a dc generator providing an output voltage proportional to the angular velocity of an armature.

Acceleration sensors transduce linear translation and consequently angular acceleration by the integration of speed measurement, or by the force created by the acceleration on a known mass.

Appendix (A3) Robot External Sensors:

These may be classified as noncontact or contact on the basis of their method of information acquisition see fig.(1.1). Noncontact sensors operate without requiring physical contact with the object being sensed. As a result, noncontact sensors are less exposed to the risk of physical damage.

Noncontact sensors can be divided into vision, range, proximity and optical sensors.

- A **vision sensor** system is tasked with the sensing, acquisition and interpretation of vision data taken from the robot environment. This process may be sub-divided into six principle tasks Ref.(8) sensing, preprocessing, segmentation, description, recognition and interpretation. A vision system is generally made up of: television camera, digitizing hardware, illuminator, digital computer and preprocessor see fig.(A3.1). Machine vision has had limited employment in robot systems for manufacturing applications, such as inspection, welding and assembly see Ref.(3,5).

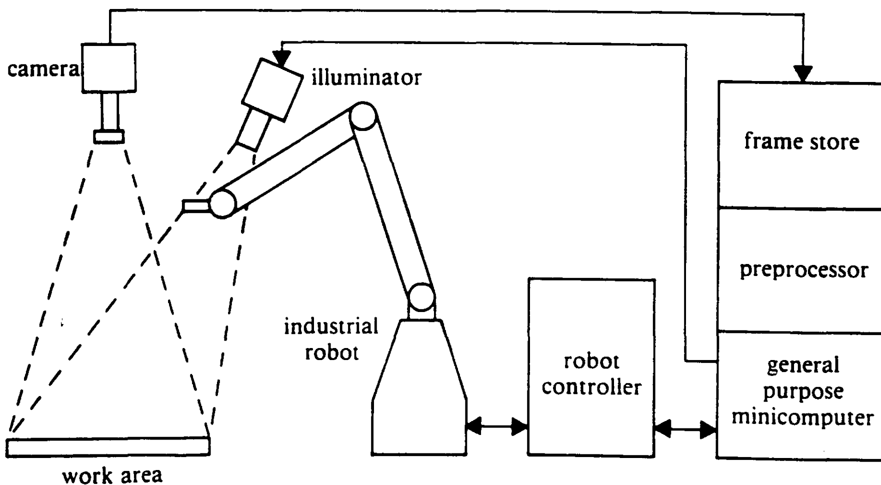

Figure A3.1 The organization of a robot vision system (Ref. 5)

-**Range sensors** are used to measure the distance between a reference point on the sensor and an object within the range of the sensor. Several range sensing techniques have

been applied to scene analysis, Some of these being :

Triangulation based on the trigonometry of triangulation see fig.(A3.2).

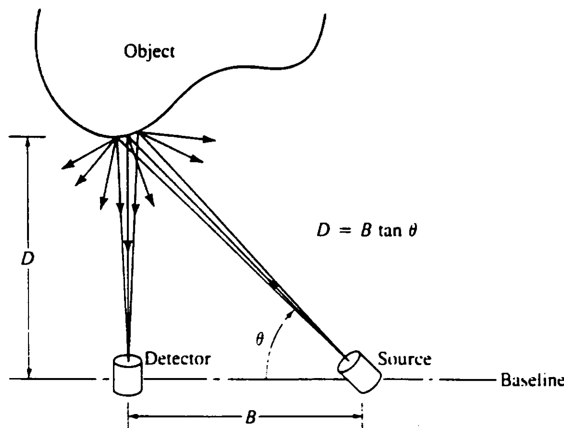

Figure A3.2 Range sensing by triangulation (Ref. 8)

Time of flight of light or sound where a pulsed beam of light or sound is used and the delay between the outgoing and returning beams is sensed by phase shift measurement see fig.(A3.3).

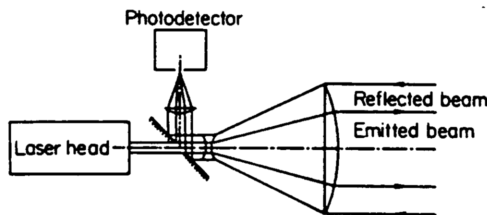

Figure A3.3 The design of a time flight sensor

Structured lighting is an approach based on projecting a sheet of light onto a set of objects and recording the image of the reflected light by a camera . By trigonometry the distortion of the reflected sheet can be used to calculate range see fig.(A3.4).

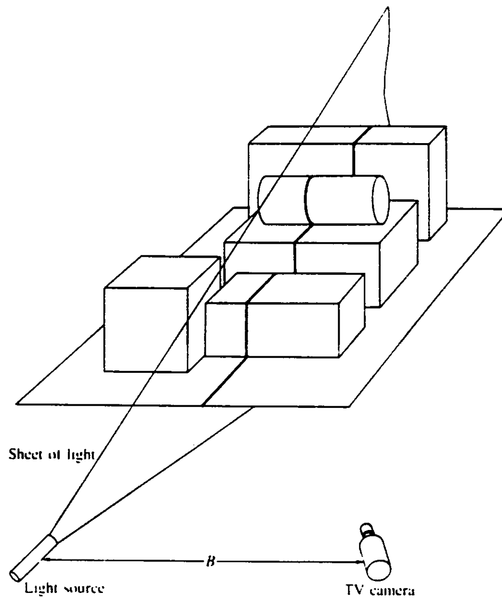

Figure A3.4 Sensor utilizing a structured light approach (Ref. 8)

-**Proximity sensors**, are bi-stable devices used to sense the presence or absence of an object near the sensor. They are normally placed on the wrist or the inner or outer surfaces of an end effector of the robot, or at specific locations in the work volume. A variety of effects are used in proximity sensors including: ultrasonic, capacitive, inductive and hall-effect.

Contact sensors, vary in level of sophistication, from simple bi-stable micro-switches to more complex systems of tactile arrays. They can only be used to supply data after physical contact has been made between the robot and its surrounding. Contact sensors may be sub-divided into touch and force sensors.

Touch sensors indicate only that contact has been made between the robot end effector and an object or between two objects in the work space. This technique is used to indicate the presence or absence of objects at certain location, or to stop the motion of a robot when its end effector makes contact with an object. Touch sensors are normally mounted on the outer or inner surface of gripper jaws. Touch sensors may be sub-divided into three classes: bi-stable, analog and tactile array.

A digital or bi-stable sensor is made up of a switch with two positions, open and closed positioned on an appropriate surface of an end effector or at a specific location in the work volume Refs.(8,9,10).

An analog sensor gives an output is proportional to local movement. Analog touch sensors are usually mounted on the robot fingers to measure deflection of grippers Refs.(8,9,10). A combination of bi-stable or analog sensors can be used to form a matrix sensor Ref.(10).

Tactile array sensors, are used to provide sufficient information to allow an object's shape and orientation to be acquired. Generally these are positioned on the inner surfaces of a robot gripper in a form of a pad. The output signals each being proportional to the amount of deflection of each pad sensor fig.(A3.5).

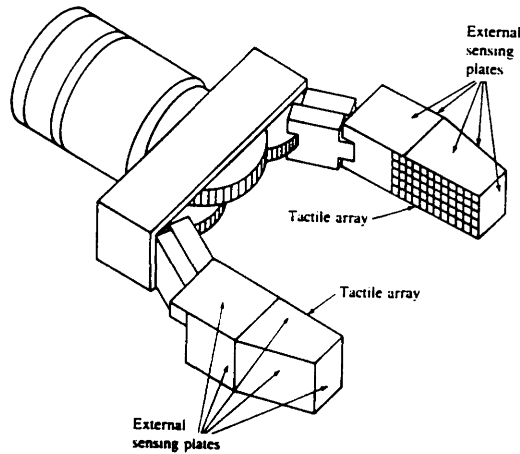

Figure A3.5 Tactile array sensor (Ref. 8)

Force sensors, are generally used as internal sensors. However, some force sensors are positioned on end effectors and are used to extract information from the environment. These can be sub-divided into two groups : slip and grip sensors.

Slip sensors, are positioned on the inner surface of each gripper finger to detect workpiece slipping during gripping. The motion of the object between the two jaws of the gripper generates an output signal which can then be used to automatically increase gripper force until motion stops. One of the available techniques used is spring-loaded friction

wheels driving angular sensors fig. (A3.6).

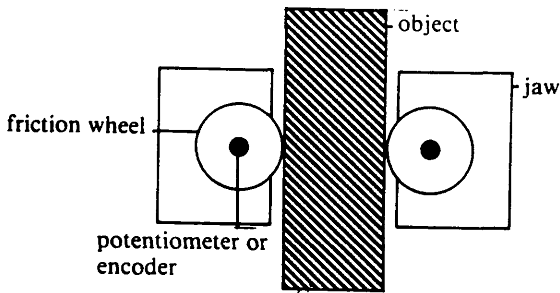

Figure A3.6 Slip sensor (Ref. 5)

Grip sensors, are used to control the gripping force of the robot on an object. A large gripping force may damage the object, whilst a light gripping force may allows the object to slip. These sensors are normally positioned within each gripper finger, thus must be small in size.

Appendix (A4) Review of Work Conducted in the Field of a Gaussian Beam Generation, Transmission and Modification

The propagation of gaussian beams was first properly detailed by Fox and Li in 1961 Ref.(49). The following year Kogelnik and Rigord discussed the modes of optical resonators Ref.(50) and later in the same year Kogelnik and Boyd further developed the theory of confocal resonators to include the effect of unequal aperture and radii of curvature of resonator reflectors Ref.(51). Kogelnik gave an explanation in 1964 of the matching transformation of a gaussian beam performed by the insertion of a lens Ref.(41). This was followed in 1965 by a more detailed discussion of the modes of an optical resonator and specifically the generation of gaussian beams Ref.(39). In the same year he published a paper describing the propagation of a spherical gaussian beam through lenslike media including loss or gain effects Ref.(52). In 1966 he and Li Ref.(38) gave a comprehensive review of the theory of laser beam and resonators.

Other researchers including Chu Ref.(40) investigated the various properties of gaussian beams and their propagation through free space and thin lenses. Erik Stingns in 1979 Ref.(32) described some nomographs which could be used to calculate the radius, power and peak intensity of a gaussian beam. Four years later Self Ref.(33) presented, an alternative formulation of the transformation of a gaussian beam through a thin lens which gives the location of the new beam waist. In 1985 Donald O'Shea published his book Ref.(34) and in which he describes in some detail the characteristics of gaussian beams, their modification and laser beam illumination.

Appendix (A5) Derivation of Formula for the Total Power with in a Gaussian Beam:

The radial intensity profile of a gaussian beam of radius W is :

$$I = I_o \, e^{-2(r^2/W^2)}$$

At a cross section of the gaussian beam the power may be calculated by the integration of the intensity over the cross sectional area :

$$P = \int_A I \, dA$$

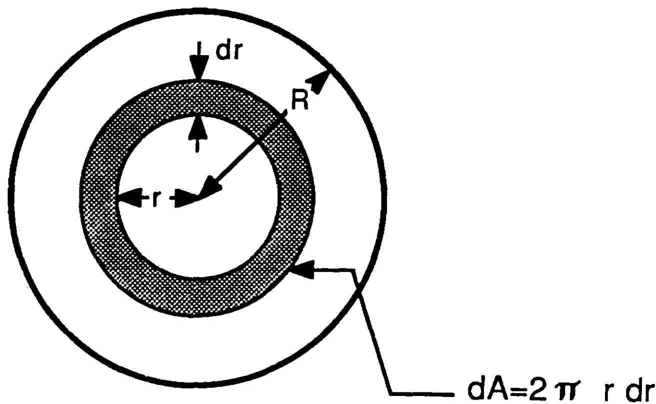

Figure A5.1 On axis view of a gaussian beam intensity distribution

By using an elemental area as in fig.(A2.1) and substituting the radial distribution of I in the equation :

$$P = \int_0^R I_o \, e^{-2(r^2/W^2)} \, 2\pi r \, dr$$

Multiplying and dividing the right hand side by $(-2W^2)$:

$$P = I_o \pi \int_0^R \{(-4\ r\ W^2/2\ W^2)[e^{-2(r^2/W^2)}]\ dr\}$$

$$P = (I_o \pi\ W^2/2)\ [-\ e^{-2(r^2/W^2)}]_0^R$$

$$P = (I_o \pi\ W^2/2)\ [1\ -\ e^{-2(R^2/W^2)}]$$

To calculate the total power (P_T) substitute ($R = \infty$) :

$$P_T = I_o \pi\ W^2/2$$

The total power transmitted by an aperture with radius = ρ :

$$P = P_T\ [\ 1\ -\ e^{-2(\rho^2/W^2)}]$$

Appendix (A6) Derivation of Gaussian Beam Divergence :

From equation (2.12) the beam waist radius equal:

$$W_z^2 = W_o^2 \, [\, 1+ (\lambda Z/\pi W_o^2)^2 \,]$$

In the far field distance when Z is large fig.(2.3) $[(\lambda Z/\pi W_o^2)$ is large$]$ it can be said that :

$$W_z \approx (\lambda Z/\pi W_o)$$

The differential of W_z relative to the distance z is the radial divergence of the beam:

$$dW_z/dz = \lambda/\pi W_o = \theta_h$$

When the diameter of the beam is considered, the full divergence can be expressed as:

$$\therefore \theta_f = 4\lambda / \pi d_o$$

Appendix (A7) Gaussian Beam Simulation Program:

This appendix contains the gaussian simulation program for the gaussian model

```
      PROGRAM SENSOR
C     GAUSSIAN MODEL
C ****************************************************************
C       This program was written and developed by Hussein Ali Abdullah and Finlay
C       Buchan between February and April 1987. It simulates an optical chain for a
C       stand-off sensor for use in robotic systems. The program uses gaussian beam
C       theory to model the progress of a laser beam to the point where it is reflected
C       from a workpiece surface and the interaction of the reflected beam with two
C       photodiodes. Further details relating to the program are given in the M.Sc. thesis
C       of H.A.Abdullah, "Mechanical Engineering, Glasgow University, Glasgow G12
C       8QQ".
C ****************************************************************
      IMPLICIT DOUBLE PRECISION(D,V)
      REAL INTST,MAG1,MAG2,MAG3,LNRAD1,LNRAD2,LNRAD3
      LOGICAL*1 TITLEY(25), TITLEX(25), QTITLE(80), DAT(15), TIM(10)
      DIMENSION ARRAY(0:500,20), ISTART(10,3), IEND(10,3),
     1          NPOINT(10,3), NCOLY(10,3),NCOLX(10,3), ISTEP(10,3),
     2          A(10,0:500), B(10,0:500),BPOSX(3),BPOSY(3),APOSX(3),
     3   APOSY(3),BTPOSX(3),BTPOSY(3),ATPOSX(3),ATPOSY(3),
     4   AMAX(10),AMIN(10),BMAX(10),BMIN(10),NLINE(10),
     5   A2(0:500), B2(0:500),A3(0:500), B3(0:500),
     6   A4(0:500), B4(0:500),A1(0:500), B1(0:500),XAMAX(10),
     7   XAMIN(10)
      CHARACTER*40 TITLEL,INDATA,OUTDATA,EXDATA
   87 WRITE(6,*)'PLEASE INPUT THE NAME OF YOUR INPUT DATAFILE......'
      READ(5,100)INDATA
      IF (INDATA .EQ. ' ') GOTO 87
   88 WRITE(6,*)'PLEASE INPUT THE NAME OF YOUR OUTPUT DATAFILE ...'
      READ(5,100)OUTDATA
      IF (OUTDATA .EQ. ' ') GOTO 88
C     IF (EXDATA .EQ. ' ') GOTO89
C
C
```

```
C     ****************************************************************
C     READ INPUT VARIABLES FROM**data file**
C     READ FROM**UNIT=15**
C     ****************************************************************
      OPEN(UNIT=15,FILE=INDATA,STATUS='OLD',ERR=90)
      OPEN(UNIT=6,FILE=OUTDATA,STATUS='NEW',ERR=91)
       OPEN(UNIT=30,FILE='SEN.DAT',STATUS='OLD',ERR=92)
      READ(15,*)WALEN
      READ(15,*)WSRAD1
      READ(15,*)POWR
      READ(15,*)FOCLL1
      READ(15,*)FOCLL3
      READ(15,*)LNRAD1
      READ(15,*)LNRAD3
      READ(15,*)FOCLDS
      READ(15,*)PNDIA
      READ(15,*)ZEDPN1
      READ(15,*)ZEDPN2
      READ(15,*)SENSPH
      READ(15,*)DIS0
      READ(15,*)DIS1
      READ(15,*)ZED0
      READ(15,*)ZED1
      READ(15,*)RESOL
      READ(15,*)REFLCT
      READ(15,*)AMPLI
      READ(15,*)VREF
      READ(15,100)TITLEL
C     ****************************************************************
C     *********************VARIABLE LIST***************************
C     ****************************************************************
C     WALEN     WAVELENGHT OF THE LASER BEAM
C     WSRAD     WAIST RADIUS OF THE LASER BEAM
C     RANG      RAYLEIGH RANGE OF THE LASER BEAM
C     POWR      POWER OF THE LASER
C     INTST     THE AXIAL INTENSITY OF THE BEAM
C     FOCLL1    FOCAL LENGTH OF THE MAIN LENS1
C     FOCLL2    FOCAL LENGTH OF THE IMAGE OF THE MAIN LENS1
```

```
C   FOCLL3     FOCAL LENGTH OF THE IMAGE LENS2
C   FOCLDS     DISTANCE BETWEEN FOCAL POINTS OF LENS1 AND LENS2
C   MAG        MAGNIFICATION OF A LENS
C   LNRAD      RADIUS OF A LENS
C   BRDLN      BEAM RADIUS AT THE LENS
C   POWRPN     POWER IN FRONT OF THE PHOTODIODE'S PINHOLE
C   PNRAD      PINHOLE RADIUS AT THE PHOTODIODE
C   PNDIA      PINHOLE DIAMETER AT THE PHOTODIODE
C   ZEDPN      DISTANCE FROM IMAGE WAIST RADIUS TO THE PINHOLE
C   SENSPH     SENSITIVITY OF THE PHOTODIODE
C   VOLT       PHOTODIODE OUTPUT VOLTAGE
C   DIS        DISTANCE BETWEEN THE WAIST RADIUS AND LENS
C   ZED        DISTANCE BETWEEN MAIN LENS AND WORKPIECE
C   DSTEP      INCREMENT OF DISTANCE BETWEEN LENS1 AND
               WORKPIECE
C   RESOL      NUMBER OF DISTANCE CALCULATION STEPS
C   REFLCT     SURFACE REFLECTIVITY
C   AMPLI      THE AMPLIFIER GAIN
C   VOLTT      NORMALIZED OUTPUT VOLTAGE
C   VREF       REFERENCE VOLTAGE
C   ************************************************************
C   *                  *** MAIN CALCULATION ***                *
C   ************************************************************
    WRITE(6,101)
    WRITE(6,*)TITTLEL
C   ************************************************************
C   **CALCULATE THE SPOT SIZE ON THE SURFACE(WSRAD2) AND ITS***
C   *                        LOCATION                          *
C   ************************************************************
 100 FORMAT(A)
 101 FORMAT(1H ,T15,' RESULT OF MODELLING')
    PI=3.1415926
    RANG1=(PI*WSRAD1**2)/WALEN
    MAG1=FOCLL1/(SQRT((DIS1-FOCLL1)**2+RANG1**2))
    WSRAD2=MAG1*WSRAD1
    DIS2=FOCLL1+(MAG1**2*(DIS1-FOCLL1))
C   ************************************************************
    WRITE(6,107)
```

```
      WRITE(6,108)
      WRITE(6,109)
      WRITE(6,110)
      WRITE(6,*)'*****************************************************'
  107 FORMAT(1H ,'  DISTANCE        VOLTAGE    VOLTAGE       THE')
  108 FORMAT(1H ,'  BETWEEN            OF          OF        TOTAL')
  109 FORMAT(1H ,'LENS1&SURFACE  PHOTODIOD1 PHOTODIOD2  VOLTAGE')
  110 FORMAT(1H ,'    (m)                (v)          (v)          (v)')
C     ************************************************************
C
C     ************************************************************
C        CALCULATE THE STAND-OFF DISTANCE,THE DISTANCE(DIS3)
C        BETWEEN THE SPOT ON THE SURFACE(WSRAD2)TO THE IMAGE OF
C        THE MAIN LENS(L2), THE DISTANCE(ZED3)WHEN (ZED2=0),THE
C        NEW WAIST RADIUS (WSRAD3)AND IT'S LOCATION
C     ************************************************************
      J=0
      DSTEP=(ZED1-ZED0)/RESOL
      DO 400,ZED2=ZED0,ZED1,DSTEP
      J=J+1
      DIS3=DIS2+(2*ZED2)
     BMRAD2=WSRAD2*SQRT(1+((0.318309*WALEN*ZED2)/(WSRAD2**2))**2)
      ZED3=DIS2
      RANG2=(PI*WSRAD2**2)/WALEN
      FOCLL2=FOCLL1
      LNRAD2=LNRAD1
      MAG2=FOCLL2/(SQRT((DIS3-FOCLL2)**2+RANG2**2))
      WSRAD3=MAG2*WSRAD2
      RANG3=(PI*WSRAD3**2)/WALEN
      DIS4=FOCLL2+((MAG2**2)*(DIS3-FOCLL2))
      ZED4=FOCLL2+((MAG2**2)*(ZED3-FOCLL2))
      DISTAN=DIS4-ZED4
  BMRAD3=WSRAD3*SQRT(1+((0.318309*WALEN*DISTAN)/(WSRAD3**2))**2)
C     ************************************************************
C   CALCULATE:THE DISTANCE BETWEEN MAIN AND IMAGE LENSES, THE
      NEW  WAIST RADIUS(WSRAD4) BEYOND THE IMAGE LENS AND ITS  C
                              LOCATION
```

```
C   ****************************************************************
      DISLEN=FOCLL2+FOCLL3+FOCLDS
      DIS5=DISLEN-DIS4
      ZED5=DISLEN-ZED4
      MAG3=FOCLL3/(SQRT((DIS5-FOCLL3)**2+RANG3**2))
      WSRAD4=MAG3*WSRAD3
      RANG4=(PI*WSRAD4**2)/WALEN
      DIS6=FOCLL3+((MAG3**2)*(DIS5-FOCLL3))
      ZED6=FOCLL3+((MAG3**2)*(ZED5-FOCLL3))
C   ****************************************************************
C   *   CALCULATE:THE OFFSET DISTANCE OF THE PINHOLES AND THE   *
C   *              BEAM RADIUS IN FRONT OF THE PINHOLES           *
C   ****************************************************************
      ZED7=DIS6-ZED6
     BMRAD4=WSRAD4*SQRT(1+((0.318309*WALEN*ZED7)/(WSRAD4**2))**2)
      DISPN1=ZEDPN1+ZED7
      DISPN2=ZEDPN2-ZED7
   BRDPN1=WSRAD4*SQRT(1+((0.318309*WALEN*DISPN1)/(WSRAD4**2))**2)
   BRDPN2=WSRAD4*SQRT(1+((0.318309*WALEN*DISPN2)/(WSRAD4**2))**2)
C   ****************************************************************
C    CALCULATE:THE LOSS OF THE POWER THROUGH THE APERTURE OF
C        THE LENSES (POWR2,POWR4,POWR6) AND THE BEAM SPLITTER
C        (POWR1,POWR5), THE REFLECTED POWER FROM THE SURFACE
C        (POWR3).CALCULATE THE POWER IN FRONT OF THE PINHOLES
C                                (POWRPN)
C   ****************************************************************
      POWR1=0.5*POWR
      BRDLN1=WSRAD1*SQRT(1+((0.318309*WALEN*DIS1)/(WSRAD1**2))**2)
      BE1=(LNRAD1/BRDLN1)**2
      POWR2=POWR1*(1-(EXP(-2*BE1)))
      POWR3=REFLCT*POWR2
      BRDLN2=WSRAD2*SQRT(1+((0.318309*WALEN*DIS3)/(WSRAD2**2))**2)
      BE2=(LNRAD2/BRDLN2)**2
      POWR4=POWR3*(1-(EXP(-2*BE2)))
      POWR5=0.5*POWR4
      BRDLN3=WSRAD3*SQRT(1+((0.318309*WALEN*DIS5)/(WSRAD3**2))**2)
      BE3=(LNRAD3/BRDLN3)**2
      POWR6=POWR5*(1-(EXP(-2*BE3)))
```

```
      POWRPN=0.5*POWR6
      PNRAD=0.5*PNDIA
C     ****************************************************************
C     *CALCULATE:THE OUTPUT VOLTAGE OF THE PHOTODIODES AND THE*
C      ************OUTPUT OF THE DIFFERENTIAL AMPLIFIER***********
C     ****************************************************************
      POWRP1=POWRPN*(1-(EXP(-2*((PNRAD/BRDPN1)**2))))
      POWRP2=POWRPN*(1-(EXP(-2*((PNRAD/BRDPN2)**2))))
      RATIO1=COF*(PNRAD/WSRAD4)
      RATIO2=COF*(PNRAD/WSRAD4)
      VOLT1=SENSPH*POWRP1*ampli
      VOLT2=SENSPH*POWRP2*ampli
      VOLTT=((VOLT1-VOLT2)/(VOLT1+VOLT2))*VREF
      WRITE(6,111)ZED2,FOCLL3,VOLT1,VOLT1,WSRAD4
  111 FORMAT(1H ,4X,E15.5,5X,E15.5,3X,E12.3,2X,E12.3,2X,F10.8)
       ARRAY(J,4)=ZED2
       ARRAY(J,5)=VOLT1
       ARRAY(J,6)=VOLT2
       ARRAY(J,7)=VOLTT
       ARRAY(J,8)=BRDPN1
       ARRAY(J,9)=BRDPN2
 400  CONTINUE
       WRITE(6,*)'*******************************************************'
C
       CLOSE(UNIT=15,STATUS='KEEP')
       CLOSE(UNIT=6,STATUS='KEEP')
C
 JCOUNT=J
NARRAY=9  ! Nos of cols in ARRAY
C
C     ****************************************************************
C Write into output file LOUTPUT.OUT
C     ****************************************************************
       WRITE (35,666) ((ARRAY(L,M),M=1,NARRY),L=1,J)
  666  format(' ',F4.0,6E15.6)        !Remember to change format
C     ****************************************************************
C     ***************** START OF GRAPH ROUTINE ******************
C     ****************************************************************
```

```
DATA BPOSX/20,160.,160./ ! X coord of start of X-axis
DATA BPOSY/20.,20.,115./ ! Y coord of start of X-axis
DATA APOSX/20.,160.,160./ ! X coord of start of Y-axis
DATA APOSY/20.,20.,115./ ! Y coord of start of Y-axis
DATA BTPOSX/55.,195.,195./ ! X coord of start of X-title
DATA BTPOSY/10.,10.,105./ ! Y coord of start of X-title
DATA ATPOSX/10.,150.,150./ ! X coord of start of Y-title
DATA ATPOSY/40.,40.,135./ ! Y coord of start of Y-title
C
C   **************************************************************
NNODE=J
NC=8
C   **************************************************************
C
DO 60 K=1,3 !For each graph
READ (30,*)NLINE(K)
DO 50 N=1,NLINE(K) !For each line
READ(30,*) NCOLY(N,K),NCOLX(N,K)
NPOINT(N,K)=JCOUNT
C (number of points to be plotted later on.)
C
 50 CONTINUE
 60 CONTINUE
C
C   **************************************************************
C                     * - SELECT OUTPUT DEVICE - *
C   **************************************************************
62    WRITE (5,*)'? SELECT NO ? 1=4010,2=BENSON,3=VERSATEC,4=LA100'
      READ (5,*) KTER
      IF (KTER .EQ. 1)THEN
        CALL T4010
   CALL CHASWI(1)
        CALL PICCLE
        CALL SCALE(0.6)
      ELSE IF (KTER .EQ. 2)THEN
        CALL B1302
      ELSE IF (KTER .EQ. 3) THEN
        CALL V1200
```

```
   CALL DEVPAP(210.,280.,0)
   CALL CHASWI(1)
   CALL SCALE(0.9)
   CALL ROTAT2(90.)
   CALL SHIFT2(0.,-210.)
     ELSE IF (KTER .EQ. 4) THEN
       CALL LA100
 ELSE
   GOTO 62
     ENDIF
C     ************************************************************
C                          * -- SHEET OF A4 DRAWN -- *
C     ************************************************************
 179  CALL MOVTO2(0.,0.)
      CALL LINTO2(297.,0.)
      CALL LINTO2(297.,210.)
      CALL LINTO2(148.5,210.)  ! These three lines draw the
      CALL LINTO2(148.5,200.)  ! small tick in the middle
      CALL MOVTO2(148.5,210.)  ! of top line
      CALL LINTO2(0.,210.)
      CALL LINTO2(0.,0.)
C     ***************************************************************
C     *  CONVERT TWO DIM ARRAY INFO INTO ONE DIM FOR GINO AND   *
C       *     DETERNINE MIN AND MAX FOR AXIS SCALING (AXISCA)     *
C     ***************************************************************
      DO 70,L=1,3
 AMAXT=-1.E20
 BMAXT=-1.E20
      AMINT=-AMAXT
 BMINT=-BMAXT
      DO 67,N=1,NLINE(L)
 AMAX(N)=-1.E20
 BMAX(N)=-1.E20
 AMIN(N)=-AMAX(N)
 BMIN(N)=-BMAX(N)
 J=0
      DO 65,I=1,JCOUNT
```

```
C
 A(N,J)= ARRAY(I,NCOLY(N,L))
 IF(N.EQ.1)A1(J)=A(N,J)
 IF(N.EQ.2)A2(J)=A(N,J)
 IF(N.EQ.3)A3(J)=A(N,J)
 IF(N.EQ.4)A4(J)=A(N,J)
C
 B(N,J)= ARRAY(I,NCOLX(N,L))
 IF(N.EQ.1)B1(J)=B(N,J)
 IF(N.EQ.2)B2(J)=B(N,J)
 IF(N.EQ.3)B3(J)=B(N,J)
 IF(N.EQ.4)B4(J)=B(N,J)
C
 IF(A(N,J).GT.AMAX(N)) THEN
   AMAX(N)=A(N,J)
        XAMAX(N)=B(N,J)
 ENDIF
 IF(A(N,J).LT.AMIN(N)) THEN
     AMIN(N)=A(N,J)
   XAMIN(N)=B(N,J)
  ENDIF
C
  IF(B(N,J).GT.BMAX(N))BMAX(N)=B(N,J)
  IF(B(N,J).LT.BMIN(N))BMIN(N)=B(N,J)
  J=J+1
 65    CONTINUE
 IF(AMAX(N).GT.AMAXT)AMAXT=AMAX(N)
 IF(AMIN(N).LT.AMINT)AMINT=AMIN(N)
     IF(BMAX(N).GT.BMAXT)BMAXT=BMAX(N)
 IF(BMIN(N).LT.BMINT)BMINT=BMIN(N)
 67    CONTINUE
 CALL CHASIZ(2.,2.)
     CALL AXIPOS(1,BPOSX(L),BPOSY(L),120.,1)
 CALL AXISCA(1,10,BMINT,BMAXT,1)
     CALL AXIDRA(-2,1,1)
     CALL AXIPOS(1,APOSX(L),APOSY(L),80.,2)
     CALL AXISCA(1,10,AMINT,AMAXT,2)
     CALL AXIDRA(2,-1,2)
```

```
      CALL GRAPOL(B1,A1,NPOINT(1,L))
 IF(NPOINT(2,L).EQ.0)GOTO69
  CALL DASHED(1,3.5,2.,0.)
  CALL GRAPOL(B2,A2,NPOINT(2,L))
 IF(NPOINT(3,L).EQ.0)GOTO69
  CALL DASHED(1,2.5,2.,0.)
  CALL GRAPOL(B3,A3,NPOINT(3,L))
 IF(NPOINT(4,L).EQ.0)GOTO69
  CALL DASHED(1,1.5,1.,0.)
  CALL GRAPOL(B4,A4,NPOINT(4,L))
69  CALL DASHED(0)
 CALL CHASIZ(2.,3.)
C      CALL MOVTO2(APOSY(L),XAMAX(L))
C  CALL LINTO2(APOSY(L)+5,XAMIN(L))
      CALL MOVTO2(ATPOSX(L),ATPOSY(L))
  CALL CHAANG (90.)
  CALL TITLE(TITLEY)
      CALL CHAHOL(TITLEY)
  CALL CHAANG (0.)
      CALL MOVTO2(BTPOSX(L),BTPOSY(L))
  CALL TITLE(TITLEX)
      CALL CHAHOL(TITLEX)
C WRITE (5,*)'AMIN,AMAX',AMIN,AMAX
 70 CONTINUE
C    ***************************************************************
C    *  READ MAIN TITLE FROM FILE CONTROL.DAT - DRAW BOX IN     *
C              *              TOP LEFT HAND CORNER               *
C    ***************************************************************
     CALL MOVTO2(10.,200.)
     CALL TITLE(QTITLE)
     CALL CHAHOL(QTITLE)
     CALL MOVTO2(10.,197.)
      CALL CHAHOL('--------------------------------------------*.')
     CALL MOVTO2(5.,185.)
     CALL LINTO2(140.,185.)
     CALL LINTO2(140.,120.)
C     CALL LINTO2(80.,120.)
C     CALL LINTO2(80.,185.)
```

```
C     CALL MOVTO2(80.,120.)
      CALL LINTO2(5.,120.)
      CALL LINTO2(5.,185.)
      CALL MOVTO2(15.,180.)
C     ****************************************************************
C     **************** WRITES PLOT DATE AND TIME ******************
C     ****************************************************************
 DAT(10)=' '
 DAT(11)='a'
 DAT(12)='t'
 DAT(13)=' '
 DAT(14)='*'
 DAT(15)='.'
 TIM(9)='*'
 TIM(10)='.'
 CALL CHASIZ (2.,2.)
 CALL MOVTO2 (225.,1.)
 CALL ITALIC (30.)
 CALL CHAHOL ('Plotted on *.')
 CALL DATE (DAT)
 CALL TIME (TIM)
 CALL CHAHOL (DAT(1))
 CALL CHAHOL (TIM(1))
 CALL ITALIC (0.)
C     ****************************************************************
C     *READ INFORMATION FOR TYPING WITHIN THE CLOSED BOX IN THE*
C                  *        TOP LEFT HAND CORNER              *
C     ****************************************************************
    CALL CHASIZ (2.,2.)
 C=180.
 700 READ (30,181,END=1000)NCHAR,QTITLE
 181 FORMAT (Q,80A1)
 QTITLE (NCHAR+1) ='*'
 QTITLE (NCHAR+2) ='.'
 CALL MOVTO2 (10.,C)
 CALL CHAHOL (QTITLE)
 C=C-3.
```

```
GOTO 700
1000 CALL MOVTO2 (10.,178.)
 CALL CHAHOL ('                FIGURE(3.9)       *.')
CALL MOVTO2 (10.,173.)
 CALL CHAHOL ('LASER WAVELENGTH (mm)..................... -*.')
CALL CHAFLO (WALEN,10)
CALL MOVTO2 (10.,168.)
 CALL CHAHOL ('LASER BEAM WAIST RADIUS (mm).............. -*.')
CALL CHAFIX (WSRAD1,10,5)
CALL MOVTO2 (10.,163.)
 CALL CHAHOL ('BEAM POWER (mW)........................... -*.')
CALL CHAFLO (POWR,10,6)
CALL MOVTO2 (10.,158.)
 CALL CHAHOL ('FOCAL LENGTH OF THE MAIN LENS (mm)........ -*.')
CALL CHAFIX (FOCLL1,10,3)
CALL MOVTO2 (10.,153.)
 CALL CHAHOL ('FOCAL LENGTH OF THE IMAGE LENS (mm)....... -*.')
CALL CHAFIX (FOCLL3,10,3)
CALL MOVTO2 (10.,148.)
 CALL CHAHOL ('DIAMETER OF THE PINHOLE (mm).............. -*.')
CALL CHAFIX (PNDIA,10,6)
CALL MOVTO2 (10.,143.)
 CALL CHAHOL ('LASER TO MAIN LENS DISTANCE (mm).......... -*.')
CALL CHAFIX (DIS1,10,3)
CALL MOVTO2 (10.,138.)
CALL CHAHOL ('DISTANCE BETWEEN MAIN AND IMAGE LENS (mm). -*.')
CALL CHAFIX (FOCLDS,10,3)
CALL MOVTO2 (10.,133.)
      CALL CHAHOL ('PINHOLE OFFSET DISTANCE (mm)...............-*.')
     CALL CHAFIX (ZEDPN1,10,6)
     CALL MOVTO2 (10.,128.)
       CALL CHAHOL ('AMPLIFICATION GAIN.......................-*.')
     CALL CHAFIX (AMPLI,10,3)
C    ****************************************************************
C    *                    - END OF MAIN PROGRAM -                   *
C    ****************************************************************
     CALL DEVEND
     STOP
```

```
C     ERRORS DURING OPENING
 90   WRITE(5,*)'UNABLE TO OPEN INDATA FILE'
      STOP
 91   WRITE(5,*)'UNABLE TO OPEN STANDOFF.OUT FILE'
      STOP
 92   WRITE(5,*)'UNABLE TO OPEN FL2G.DAT FILE'
      STOP
 93   WRITE(5,*)'UNABLE TO OPEN EXP.DAT FILE'
      END
C
C     ***************************************************************
C     * SUROUTINE FOR READING AXIS TITLES FROM FILE CONTROL.DAT *
C     ***************************************************************
 SUBROUTINE TITLE(QTITLE)
 LOGICAL*1 QTITLE(80)
C WRITE(5,*)'$ INPUT TITLE FOR THE Y  AXIS '
 READ (30,181) NCHAR, QTITLE
 QTITLE(NCHAR+1)='*'
 QTITLE(NCHAR+2)='.'
 181 FORMAT(Q,80A1)
 RETURN
 END
```

Appendix (A8) **Derivation of Total Power Transmitted Through a Pinhole:**

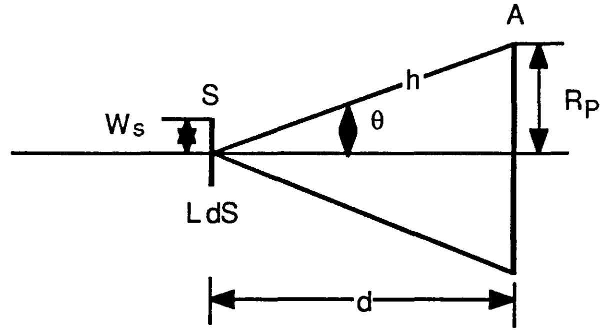

Figure A8.1

From equation (3.49) :

$$d^2\phi = L\, dS\, dA \frac{\cos^2\theta}{h^2}$$

As in figure A8.1 ϕ equal to:

$$\phi = L \int_0^{Ws} dS \int_0^{Rp} dA \frac{\cos^2\theta}{h^2}$$

By substitutting the magnituade of dS and dA as described in figures A8.2 and A8.3, the power falling through a pinhole at A is giving by :

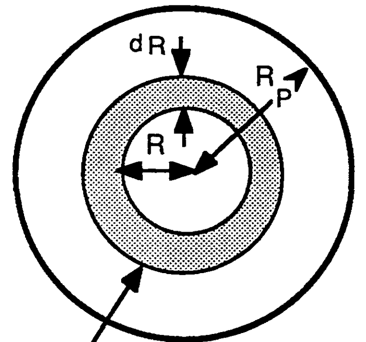

dA=2 π R dR

The pinhole elemental cross sectional area dA

Figure A8.2

$$\cos\theta = \frac{d}{\sqrt{(d^2 + R^2)}}$$

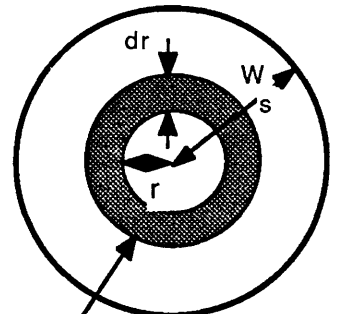

dS=2 π r dr

The source elemental cross sectional area dS

Figure A8.3

$$\phi = L \int_0^{Ws} 2\pi\, r\, dr \int_0^{Rp} 2\pi\, R\, dR \frac{\cos^2\theta}{h^2}$$

$$= L\pi^2 \left[r^2 \right]_0^{Ws} \int_0^{Rp} \frac{\frac{d^2}{(d^2 + R^2)}}{(d^2 + R^2)} 2R\, dR$$

$$= L\pi^2 Ws^2 \int_0^{Rp} \frac{d^2}{(d^2 + R^2)^2} 2R\, dR$$

$$= L\pi^2 Ws^2 \left[- \frac{d^2}{(d^2 + R^2)} \right]_0^{Rp}$$

$$= L\pi^2 Ws^2 \left[- \frac{d^2}{(d^2 + Rp^2)} + \frac{d^2}{d^2} \right]$$

$$= L\pi^2 Ws^2 \left[1 - \frac{d^2}{d^2 + Rp^2} \right]$$

$$= L \pi^2 Ws^2 \left[\frac{d^2 + Rp^2 - d^2}{d^2 + Rp^2} \right]$$

$$= L \pi^2 Ws^2 \left[\frac{Rp^2}{d^2 + Rp^2} \right]$$

Appendix (A9) Gaussian-Radiometric Simulation Program:

This appendix contains the simulation program for the gaussian-radiometric model.

```
      PROGRAM SENSOR
C     GAUSSIAN AND RADIOMETRIC MODEL
C
C **********************************************************************
C       This program was written and developed by Hussein Ali Abdullah, between
C       September and October 1987. It simulates an optical chain for a stand-off sensor
C       for use in robotic systems.The program uses  gaussian beam theory for models
C       the progress of a laser beam to the point where it is reflected from a workpiece
C       surface. Geometrical Optics and radiometric theory is then used to model the
C       interaction of the reflected beam with two photodiodes. Further details relating
C       to the program are given in the M.Sc. thesis of  H.A.Abdullah "Mechanical
C       Engineering Department,Glasgow University, Glasgow G12 8QQ".
C **********************************************************************
      IMPLICIT DOUBLE PRECISION (F,D,V,E,T,P,W,Z)
      REAL INTST,MAG1,MAG2,MAG3,LNRAD1,LNRAD2,LNRAD3,MPN1,MPN2
      LOGICAL*1 TITLEY(25), TITLEX(25), QTITLE(80), DAT(15), TIM(10)
      DIMENSION ARRAY(0:500,20), ISTART(10,3), IEND(10,3),
     1          NPOINT(10,3), NCOLY(10,3),NCOLX(10,3), ISTEP(10,3),
     2          A(10,0:500), B(10,0:500),BPOSX(3),BPOSY(3),APOSX(3),
     3   APOSY(3),BTPOSX(3),BTPOSY(3),ATPOSX(3),ATPOSY(3),
     4   AMAX(10),AMIN(10),BMAX(10),BMIN(10),NLINE(10),
     5   A2(0:500), B2(0:500),A3(0:500), B3(0:500),
     6   A4(0:500), B4(0:500),A1(0:500), B1(0:500),XAMAX(10),
     7   XAMIN(10)
      CHARACTER*40 TITLEL,INDATA,OUTDATA,EXDATA
 87   WRITE(6,*)'PLEASE INPUT THE NAME OF YOUR INPUT DATAFILE......'
      READ(5,100)INDATA
      IF (INDATA .EQ. ' ') GOTO 87
 88   WRITE(6,*)'PLEASE INPUT THE NAME OF YOUR OUTPUT DATAFILE ...'
      READ(5,100)OUTDATA
      IF (OUTDATA .EQ. ' ') GOTO 88
C
C
```

```
C     *************************************************************
C     READ INPUT VARIABLES  FROM **data file**
C     READ FROM **UNIT=15**
C     *************************************************************
      OPEN(UNIT=15,FILE=INDATA,STATUS='OLD',ERR=90)
      OPEN(UNIT=6,FILE=OUTDATA,STATUS='NEW',ERR=91)
      OPEN(UNIT=30,FILE='OPTO.DAT',STATUS='OLD',ERR=92)
      READ(15,*)WALEN
      READ(15,*)WSRAD1
      READ(15,*)POWR
      READ(15,*)FOCLL1
      READ(15,*)FOCLL3
      READ(15,*)LNRAD1
      READ(15,*)LNRAD3
      READ(15,*)FOCLDS
      READ(15,*)PNDIA
      READ(15,*)ZEDPN1
      READ(15,*)ZEDPN2
      READ(15,*)SENSPH
      READ(15,*)DIS0
      READ(15,*)DIS1
      READ(15,*)ZED0
      READ(15,*)ZED1
      READ(15,*)RESOL
      READ(15,*)REFLCT
      READ(15,*)AMPLI
      READ(15,*)VREF
      READ(15,100)TITLEL
C     *************************************************************
C     ***********************VARIABLES LIST*************************
C     *************************************************************
C     WALEN     WAVELENGHT OF THE LASER BEAM
C     WSRAD     WAIST RADIUS OF THE LASER BEAM
C     RANG      RAYLEIGH RANGE OF THE LASER BEAM
C     POWR      POWER OF THE LASER
C     FOCLL1    FOCAL LENGTH OF THE MAIN LENS1
C     FOCLL2    FOCAL LENGTH OF THE IMAGE OF THE MAIN LENS1
C     FOCLL3    FOCAL LENGTH OF THE IMAGE LENS2
```

```
C    FOCLDS   DISTANCE BETWEEN FOCAL POINTS OF LENS1 AND LENS2
C    MAG      MAGNIFICATION OF A LENS
C    LNRAD    RADIUS OF A LENS
C    BRDLN    BEAM RADIUS AT THE LENS
C    PNRAD    PINHOLE RADIUS AT THE PHOTODIODE
C    PNDIA    PINHOLE DIAMETER AT THE PHOTODIODE
C    PN       RADIUS OF THE PINHOLE IMAGE
C    ZEDPN    DISTANCE FROM IMAGE WAIST RADIUS TO THE PINHOLE
C    DP       DISTANCE FROM THE PINHOLE IMAGE TO THE LENS
C    PM       MAGNIFICATION OF THE PINHOLE IMAGE
C    TE11     POWER EMITTED FROM THE SURFACE SPOT
C    EP       POWER TRANSMITTED BY THE PINHOLE
C    SENSPH   SENSITIVITY OF THE PHOTODIODE
C    VOLT     PHOTODIODE OUTPUT VOLTAGE
C    DIS      DISTANCE BETWEEN THE WAIST RADIUS AND LENS
              (GAUSSIAN)
C    DI       DISTANCE BETWEEN THE WAIST RADIUS AND LENS
              (RADIOMETRIC)

C    ZED      DISTANCE BETWEEN MAIN LENS AND WORKPIECE
C    DSTEP    INCREMENT OF DISTANCE BETWEEN LENS1 AND
              WORKPIECE
C    RESOL    NUMBER OF DISTANCE CALCULATION STEPS
C    REFLCT   SURFACE REFLECTIVITY
C    AMPLI    AMPLIFIER GAIN
C    VOLTT    NORMALIZED OUTPUT VOLTAGE
C    VREF     REFERENCE VOLTAGE
C
C    ****************************************************************
C    *                    *** MAIN CALCULATION ***                  *
C    ****************************************************************
     WRITE(6,101)
     WRITE(6,*)TITLEL
C    ________________
C    * GAUSSIAN PART *
C    ****************************************************************
C  CALCULATE THE FOCUSSED BEAM WAIST (WSRAD2) AND ITS LOCATION
*******************************************************************
```

```
C   *  CALCULATE THE BEAM RADIUS ON THE WORKPIECE SURFACE AND
C   *                    THE POWER IN THAT REGION                    *
C   ******************************************************************
 100 FORMAT(A)
 101  FORMAT(1H ,T15,' RESULT OF MODELLING')
    PI=3.1415926
    RANG1=(PI*WSRAD1**2)/WALEN
    BMRAD1=WSRAD1*SQRT(1+((0.318309*WALEN*DIS1)/(WSRAD1**2))**2)
    MAG1=FOCLL1/(SQRT((DIS1-FOCLL1)**2+RANG1**2))
    WSRAD2=MAG1*WSRAD1
    DIS2=FOCLL1+(MAG1**2*(DIS1-FOCLL1))
    POWR1=POWR*(1-(EXP(-2*(LNRAD1/BMRAD1)**2)))
    TE0=(0.636*POWR1)/(WSRAD2**2)
C
    WRITE(6,*)'*********************************************************'
C
C   ******************************************************************
    WRITE(6,107)
    WRITE(6,108)
    WRITE(6,109)
    WRITE(6,110)
    WRITE(6,*)'*********************************************************'
 107  FORMAT(1H ,'  DISTANCE        VOLTAGE    VOLTAGE       THE')
 108  FORMAT(1H ,'  BETWEEN            OF          OF         TOTAL')
109 FORMAT(1H ,'LENS1&SURFACE  PHOTODIOD1  PHOTODIOD2  VOLTAGE')
 110  FORMAT(1H ,'    (m)                (v)          (v)          (v)')
C   ******************************************************************
C
C   ******************************************************************
C   CALCULATE THE STAND-OFF DISTANCE,THE DISTANCE(DI3) BETWEEN
    THE SPOT ON THE SURFACE (WSRAD2)TO THE IMAGE OF THE MAIN
     LENS(L2), THE DISTANCE(ZD3) WHEN (ZED2=0).
C   ******************************************************************
    J=0
    DSTEP=(ZED1-ZED0)/RESOL
    DO 400,ZED2=ZED0,ZED1,DSTEP
    J=J+1
```

```
      FOCLL2=FOCLL1
      LNRAD2=LNRAD1
      ZD3=DIS2+2*ZED2
C
C   *******************************************************************
C   *     CALCULATE THE INTENSITY OF THE SURFACE BEAM SPOT           *
C   *******************************************************************
      WS=WSRAD2*SQRT(1+((0.318309*WALEN*ZED2)/(WSRAD2**2))**2)
      TE1=POWER1*0.632/WS**2
      TEMP=-2*(WS*WS)/(WSRAD2*WSRAD2)
C      TE11=TE0*DEXP(TEMP)
      TE11=TE0*REFLCT/PI
C   -------------------------------
C
C   *GEOMETRICAL & RADIOMETRIC PART*
C   *******************************************************************
C   ** CALCULATE THE POSITION OF THE REFERENCE BEAM WAIST Wref **
C   *******************************************************************
      DISLEN=FOCLL2+FOCLL3+FOCLDS
      ZD4=(1/FOCLL2)-(1/ZD3)
      Z4=1/ZD4
      Z5=DISLEN-Z4
      ZD6=(1/FOCLL3)-(1/Z5)
      Z6=1/ZD6
      DP1=Z6+ZEDPN1
      DP2=Z6-ZEDPN2
C
C   *******************************************************************
C    CALCULATE THE PINHOLE'S IMAGE THROUGH THE LENSES L2 AND L3
C   *******************************************************************
      DP111=(1/FOCLL3)-(1/DP1)
      DP11=1/DP111
      DP211=(1/FOCLL3)-(1/DP2)
      DP21=1/DP211
      DP12=DISLEN-DP11
      DP22=DISLEN-DP21
      DP133=(1/FOCLL2)-(1/DP12)
      DP13=1/DP133
```

```
      DP233=(1/FOCLL2)-(1/DP22)
      DP23=1/DP233
      DP12=DISLEN-DP11
      DP22=DISLEN-DP21
      DP133=(1/FOCLL2)-(1/DP12)
      DP13=1/DP133
      DP233=(1/FOCLL2)-(1/DP22)
      DP23=1/DP233
C
C   ****************************************************************
C     *    CALCULATE THE SIZE AND POSITION OF THE PINHOLES      *
C       *       IMAGES IN FRONT OF THE WORKPIECE SURFACE       *
C   ****************************************************************
      PM1=DP11/DP1
      PM2=DP21/DP2
      PNRAD=0.5*PNDIA
      PN1=PM1*PNRAD
      PN2=PM2*PNRAD
      PM12=DP13/DP12
      PM22=DP23/DP22
      PN11=PM12*PN1
      PN21=PM22*PN2
      PNAR=PI*PNRAD**2
      DP14=(DIS2+ZED2)-DP13
      DP24=(DIS2+ZED2)-DP23
      WSAR=PI*WS**2
C
C   ****************************************************************
C   **CALCULATE THE TOTAL POWER PASSING THROUGH THE PINHOLES **
C   ****************************************************************
      TEE1=TE11
      TEE2=TE11
      EP11=PI*TEE1*PN11**2/(PN11**2+DP14**2)
      EP22=PI*TEE2*PN21**2/(PN21**2+DP24**2)
      EP1=(EP11)*PI*WS**2
      EP2=(EP22)*PI*WS**2

C   ****************************************************************
```

```
C    ***CALCULATE THE OUTPUT VOLTAGE OF THE TWO PHOTODIODES ***
C    ****************************************************************
     VOLT1=EP1*AMPLI
     VOLT2=EP2*AMPLI
     VG=((VOLT1-VOLT2)/(VOLT1+VOLT2))*VREF
     WRITE(6,111)ZED2,VOLT1,VOLT2,VG
 111 FORMAT(' ',E10.4,3E14.4)
      ARRAY(J,4)=ZED2
      ARRAY(J,5)=VOLT1
      ARRAY(J,6)=VOLT2
      ARRAY(J,8)=EP1
      ARRAY(J,9)=EP2
      ARRAY(J,10)=VG
C
 400 CONTINUE
      WRITE(6,*)'************************************************************'
C
      CLOSE(UNIT=15,STATUS='KEEP')
      CLOSE(UNIT=6,STATUS='KEEP')
C
 JCOUNT=J
 NARRAY=10  ! Nos of cols in ARRAY
C
C    ****************************************************************
C     Write into output file LOUTPUT.OUT
C    ****************************************************************
      WRITE (35,666) ((ARRAY(L,M),M=1,NARRY),L=1,J)
 666 format(' ',F4.0,6E15.6)       !Remember to change format
C
C    ****************************************************************
C    ***************** START OF GRAPH ROUTINE **********************
C    ****************************************************************
 DATA BPOSX/20,160.,160./ ! X coord of start of X-axis
 DATA BPOSY/20.,20.,115./ ! Y coord of start of X-axis
 DATA APOSX/20.,160.,160./ ! X coord of start of Y-axis
 DATA APOSY/20.,20.,115./ ! Y coord of start of Y-axis
 DATA BTPOSX/55.,195.,195./ ! X coord of start of X-title
 DATA BTPOSY/10.,10.,105./ ! Y coord of start of X-title
```

```
 DATA ATPOSX/10.,150.,150./ ! X coord of start of Y-title
 DATA ATPOSY/30.,40.,135./ ! Y coord of start of Y-title
C
C     ****************************************************************
      NNODE=J
      NC=8
C     ****************************************************************
C
 DO 60 K=1,3 !For each graph
 READ (30,*)NLINE(K)
 DO 50 N=1,NLINE(K) !For each line
 READ(30,*) NCOLY(N,K),NCOLX(N,K)
 NPOINT(N,K)=JCOUNT
C (number of points to be plotted later on.)
 50 CONTINUE
 60 CONTINUE
C
C
C     ****************************************************************
C                    * - SELECT OUTPUT DEVICE - *
C     ****************************************************************
62     WRITE (5,*)'? SELECT NO ? 1=4010,2=BENSON,3=VERSATEC,4=LA100'
     READ (5,*) KTER
     IF (KTER .EQ. 1)THEN
       CALL T4010
   CALL CHASWI(1)
       CALL PICCLE
       CALL SCALE(0.6)
     ELSE IF (KTER .EQ. 2)THEN
       CALL B1302
     ELSE IF (KTER .EQ. 3) THEN
       CALL V1200
   CALL DEVPAP(210.,280.,0)
   CALL CHASWI(1)
   CALL SCALE(0.9)
   CALL ROTAT2(90.)
    CALL SHIFT2(0.,-210.)
```

```
      ELSE IF (KTER .EQ. 4) THEN
        CALL LA100
   ELSE
    GOTO 62
      ENDIF
C
C     ****************************************************************
C     * -- SHEET OF A4 DRAWN -- *
C     ****************************************************************
 179  CALL MOVTO2(0.,0.)
      CALL LINTO2(297.,0.)
      CALL LINTO2(297.,210.)
      CALL LINTO2(148.5,210.)  ! These three lines draw the
      CALL LINTO2(148.5,200.)  ! small tick in the middle
      CALL MOVTO2(148.5,210.)  ! of top line
      CALL LINTO2(0.,210.)
      CALL LINTO2(0.,0.)
C
C     ****************************************************************
C       *  CONVERT TWO DIM ARRAY INFO INTO ONE DIM FOR GINO AND   *
C         *     DETERNINE MIN AND MAX FOR AXIS SCALING (AXISCA)     *
C     ****************************************************************
      DO 70,L=1,3
   AMAXT=-1.E20
   BMAXT=-1.E20
       AMINT=-AMAXT
   BMINT=-BMAXT
      DO 67,N=1,NLINE(L)
   AMAX(N)=-1.E20
   BMAX(N)=-1.E20
   AMIN(N)=-AMAX(N)
   BMIN(N)=-BMAX(N)
   J=0
      DO 65,I=1,JCOUNT
C
  A(N,J)= ARRAY(I,NCOLY(N,L))
  IF(N.EQ.1)A1(J)=A(N,J)
  IF(N.EQ.2)A2(J)=A(N,J)
```

```
IF(N.EQ.3)A3(J)=A(N,J)
IF(N.EQ.4)A4(J)=A(N,J)
B(N,J)= ARRAY(I,NCOLX(N,L))
IF(N.EQ.1)B1(J)=B(N,J)
IF(N.EQ.2)B2(J)=B(N,J)
IF(N.EQ.3)B3(J)=B(N,J)
IF(N.EQ.4)B4(J)=B(N,J)
C
IF(A(N,J).GT.AMAX(N)) THEN
  AMAX(N)=A(N,J)
      XAMAX(N)=B(N,J)
ENDIF
IF(A(N,J).LT.AMIN(N)) THEN
    AMIN(N)=A(N,J)
  XAMIN(N)=B(N,J)
ENDIF
IF(B(N,J).GT.BMAX(N))BMAX(N)=B(N,J)
IF(B(N,J).LT.BMIN(N))BMIN(N)=B(N,J)
J=J+1
65    CONTINUE
IF(AMAX(N).GT.AMAXT)AMAXT=AMAX(N)
IF(AMIN(N).LT.AMINT)AMINT=AMIN(N)
    IF(BMAX(N).GT.BMAXT)BMAXT=BMAX(N)
IF(BMIN(N).LT.BMINT)BMINT=BMIN(N)
67    CONTINUE
CALL CHASIZ(2.,2.)
     CALL AXIPOS(1,BPOSX(L),BPOSY(L),120.,1)
CALL AXISCA(1,10,BMINT,BMAXT,1)
     CALL AXIDRA(-2,1,1)
     CALL AXIPOS(1,APOSX(L),APOSY(L),80.,2)
     CALL AXISCA(1,10,AMINT,AMAXT,2)
     CALL AXIDRA(2,-1,2)
     CALL GRACUR(B1,A1,NPOINT(1,L))
IF(NPOINT(2,L).EQ.0)GOTO69
CALL DASHED(1,4.,2.,0.)
CALL GRACUR(B2,A2,NPOINT(2,L))
IF(NPOINT(3,L).EQ.0)GOTO69
CALL DASHED(1,4.,2.,0.)
```

```
 CALL GRACUR(B3,A3,NPOINT(3,L))
 IF(NPOINT(4,L).EQ.0)GOTO69
  CALL DASHED(1,4.,2.,0.)
 CALL GRACUR(B4,A4,NPOINT(4,L))
69  CALL DASHED(0)
      CALL CHASIZ(2.,3.)
C      CALL MOVTO2(APOSY(L),XAMAX(L))
C  CALL LINTO2(APOSY(L)+5,XAMIN(L))
     CALL MOVTO2(ATPOSX(L),ATPOSY(L))
 CALL CHAANG (90.)
 CALL TITLE(TITLEY)
     CALL CHAHOL(TITLEY)
 CALL CHAANG (0.)
     CALL MOVTO2(BTPOSX(L),BTPOSY(L))
 CALL TITLE(TITLEX)
     CALL CHAHOL(TITLEX)
C WRITE (5,*)'AMIN,AMAX',AMIN,AMAX
 70 CONTINUE
C
C     ************************************************************
C     *   READ MAIN TITLE FROM FILE CONTROL.DAT - DRAW BOX IN     *
C     *                 TOP LEFT HAND CORNER                 *
C     ************************************************************
     CALL MOVTO2(10.,200.)
     CALL TITLE(QTITLE)
     CALL CHAHOL(QTITLE)
     CALL MOVTO2(10.,197.)
     CALL CHAHOL('--------------------------------------------*.')
     CALL MOVTO2(5.,185.)
     CALL LINTO2(140.,185.)
     CALL LINTO2(140.,120.)
C     CALL LINTO2(80.,120.)
C     CALL LINTO2(80.,185.)
C     CALL MOVTO2(80.,120.)
     CALL LINTO2(5.,120.)
     CALL LINTO2(5.,185.)
     CALL MOVTO2(15.,180.)
```

```
C
C     ******************************************************************
C     **************** WRITES PLOT DATE AND TIME ********************
C     ******************************************************************
 DAT(10)=' '
 DAT(11)='a'
 DAT(12)='t'
 DAT(13)=' '
 DAT(14)='*'
  DAT(15)='.'
 TIM(9)='*'
 TIM(10)='.'
 CALL CHASIZ (2.,2.)
 CALL MOVTO2 (225.,1.)
 CALL ITALIC (30.)
 CALL CHAHOL ('Plotted on *.')
 CALL DATE (DAT)
 CALL TIME (TIM)
 CALL CHAHOL (DAT(1))
 CALL CHAHOL (TIM(1))
 CALL ITALIC (0.)
C
C     ******************************************************************
C     * READ INFORMATION FOR TYPING WITHIN THE CLOSED BOX IN THE *
C                    *          TOP LEFT HAND CORNER              *
C     ******************************************************************
     CALL CHASIZ (2.,2.)
 C=180.
700 READ (30,181,END=1000)NCHAR,QTITLE
181 FORMAT (Q,80A1)
 QTITLE (NCHAR+1) ='*'
 QTITLE (NCHAR+2) ='.'
 CALL MOVTO2 (10.,C)
 CALL CHAHOL (QTITLE)
 C=C-3.
 GOTO 700
1000 CALL MOVTO2 (10.,178.)
     CALL CHAHOL ('                FIGURE(3.15) *.')
```

```
      CALL MOVTO2 (10.,173.)
      CALL CHAHOL ('LASER WAVELENGTH (mm)................... -*.')
      CALL CHAFLO (WALEN,10)
      CALL MOVTO2 (10.,168.)
      CALL CHAHOL ('LASER BEAM WAIST RADIUS (mm)............. -*.')
      CALL CHAFIX (WSRAD1,10,5)
      CALL MOVTO2 (10.,163.)
      CALL CHAHOL ('BEAM POWER (mW)......................... -*.')
      CALL CHAFLO (POWR,10)
      CALL MOVTO2 (10.,158.)
      CALL CHAHOL ('FOCAL LENGTH OF MAIN LENS (mm)........... -*.')
      CALL CHAFIX (FOCLL1,10,3)
      CALL MOVTO2 (10.,153.)
      CALL CHAHOL ('FOCAL LENGTH OF IMAGE LENS (mm).......... -*.')
      CALL CHAFIX (FOCLL3,10,3)
      CALL MOVTO2 (10.,148.)
      CALL CHAHOL ('DIAMETER OF THE PINHOLE (mm)............. -*.')
      CALL CHAFIX (PNDIa,10,6)
      CALL MOVTO2 (10.,143.)
      CALL CHAHOL ('LASER TO MAIN LENS DISTANCE (mm)......... -*.')
      CALL CHAFIX (DIS1,10,3)
      CALL MOVTO2 (10.,138.)
      CALL CHAHOL ('DISTANCE BETWEEN MAIN AND IMAGE LENS (mm) -*.')
      CALL CHAFIX (FOCLDS,10,3)
      CALL MOVTO2 (10.,133.)
      CALL CHAHOL ('PINHOLE OFFSET DISTANCE (mm)..............-*.')
      CALL CHAFIX (ZEDPN1,10,6)
      CALL MOVTO2 (10.,128.)
      CALL CHAHOL ('AMPLIFICATION GAIN......................-*.')
      CALL CHAFIX (AMPLI,10,3)
C     ****************************************************************
C              *              - END OF MAIN PROGRAM -            *
C     ****************************************************************
      CALL DEVEND
      STOP
C     ERRORS DURING OPENING
 90   WRITE(5,*)'UNABLE TO OPEN INDATA FILE'
      STOP
```

```
 91  WRITE(5,*)'UNABLE TO OPEN OUTPUTDATA FILE'
     STOP
 92  WRITE(5,*)'UNABLE TO OPEN OPTO.DAT FILE'
     STOP
 93  WRITE(5,*)'UNABLE TO OPEN EXP.DAT FILE'
     STOP
     END
C
C    ********************************************************************
C    * SUROUTINE FOR READING AXIS TITLES FROM FILE CONTROL.DAT  *
C    ********************************************************************
 SUBROUTINE TITLE(QTITLE)
 LOGICAL*1 QTITLE(80)
C WRITE(5,*)'$ INPUT TITLE FOR THE Y  AXIS '
 READ (30,181) NCHAR, QTITLE
 QTITLE(NCHAR+1)='*'
 QTITLE(NCHAR+2)='.'
 181 FORMAT(Q,80A1)
 RETURN
 END
```

Appendix (A10) Alignment Procedure:

Stage 1: Alignment of the main laser beam to the main lens

This stage is performed by firstly aligning the laser parallel to the experimental table to ensure that the laser beam remains at the same height above the table along the beam path. Once this horizontal alignment has been performed, it is then necessary to align the main lens. This can be done by marking the position of the raw laser spot beyond the main lens position and then manoeuvring the main lens so that, the new beam spot after it has passed through the main lens returns to the marked position. This alignment can be checked by seeing the reflected spot from the front face of the lens falls centrally on the laser output aperture.

Stage 2: Alignment of the reflected beam with the image lens:

The part of the reflected beam which is redirected by the beam splitter B_1 to the image lens is aligned by utilizing a disk which has a diameter equal to the diameter of the lens to be mounted. This disk is placed immediately in front of the lens and the lens moved vertically and horizontally until the centre of the beam coincides with the centre of the disk.

Stage 3: Alignment of the photodiodes with the pinholes

This is performed by positioning the photodiode [10] fig.(4.1) perpendicular to the beam plane and allowing the beam to hit the sensitive area of the photodiode. A careful adjustment in the plane is then made to maximize the output voltage from the photodiode. The pinhole is then placed immediately in front of the photodiode. A fine adjustment of the pinhole with respect to the photodiode is then made again to maximize the photodiode output.

To find the position of the focused beam spot on the workpiece ($2W_{02}$ in fig.(3.1)) the workpiece is moved back and forwards until the reflected spot coincides with the laser output aperture. This position indicates that the plane of the workpiece corresponds to the $2W_{02}$ plane.

After the $2W_{02}$ plane has been found, the next step is to find the position of the $2W_{04}$

and $2W_{04}'$ planes see fig.(3.1), in order to position the pinhole and photodiode assemblies a distance (±l) from them. The workpiece is fixed at the $2W_{02}$ ($Z_2 = 0$). A black disk is inserted in the beam path after the second beam splitter B_2 , Moving the disk forwards and backwards to find the smallest beam spot, indicates the position of $2W_{04}$. A similar procedure is carried out to estimate the position of $2W_{04}'$ plane.

Appendix (A11) Block Diagram Representation and Mathematical Modelling:

Block Diagram Representation :

A block diagram is a convenient and simple method of representing and describing a control system. It is used to indicate the operation of the components of the control system by their transfer functions. The basic components of the block diagram are :

- Blocks containing a mathematical representation of the control components relating fig.(A11.1) the input and the output :

$$C(s) = G(s)\ E(s) \tag{A11.1}$$

Where G(s) represent their operation of control elements represented within the block, E(s) is the actuating signal and C(s) is the controlled variable.

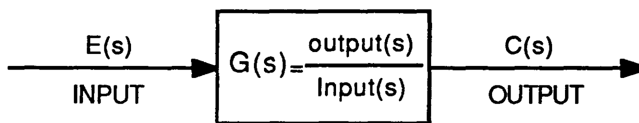

Figure A11.1 Block diagram representation

- Signal arrows, denoting the direction of signal flow within the system fig.(A11.2).

Figure A11.2 Signal arrows

- Junction points, to indicate shared signal flow fig.(A11.3) :

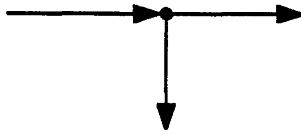

Figure A11.3 A junction point

- Comparators, where signals are added or subtracted (algebraically). A crossed circle symbol is used to denote this component and its operation fig(A11.4).

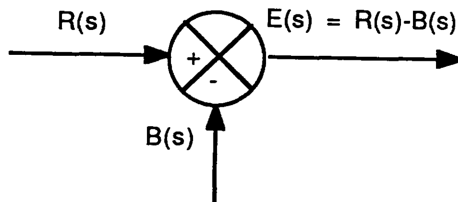

Figure A11.4 Block diagram of a comparator

System analysis and block diagram transformations can be found in Ref.(4,55,56).

Mathematical Modelling:

In order to study and investigate the performance of a control system, it is convenient to create a mathematical or numerical analog of it. This section considers the mathematical representations of mechanical and electrical components, which are used in the system model.

To model a simple mechanical system, it is required to represent three basic characteristics of a mechanical translation system. They are stiffness, damping and mass.

For the operation of a spring, Hooke's law may be used :

$$F_s = K X \qquad (A11.2)$$

Where F_s is the spring force to deflect a spring distance X from its free length

fig.(A11.5a), K is the spring constant (stiffness). The block diagram of this case is shown in fig.(A11.5b), with the input to the system (spring) being the force applied F_s and the output its displacement X.

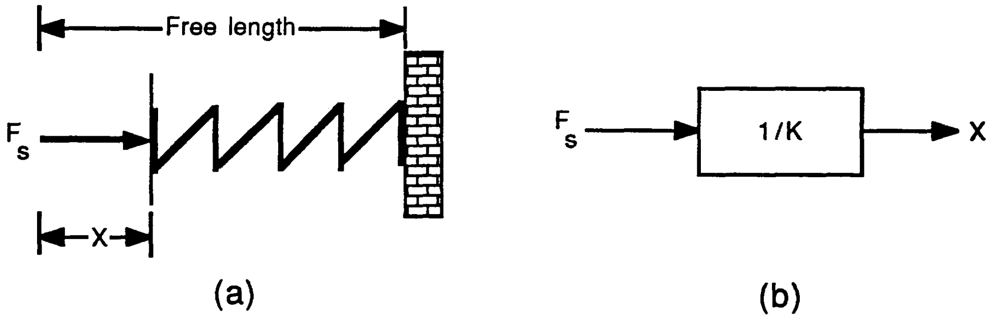

Figure A11.5 Spring characteristics

A viscous damper is illustrated in fig.(A11.6a), the force F_d is applied to move the piston at velocity V relative to the other end. It is equal to the product of the damping coefficient and the velocity :

$$F_d = B\ V = B\ (dx/dt) \qquad \text{(A11.3)}$$

The block diagram is shown in fig.(A11.6b), with the force F_d as input and the displacement X as output.

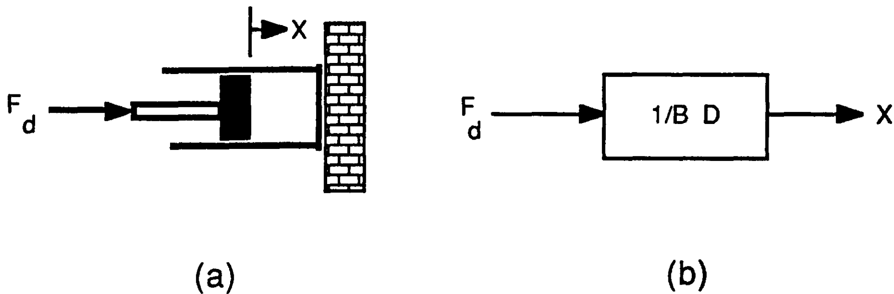

(a) (b)

Figure A11.6 Viscous damper characteristics

Newton's second law states that :

$$F_m = m\ a = m\ (d^2x/dt^2) = m\ D^2X \qquad \text{(A11.4)}$$

Where m is the mass, a is acceleration, D is the differential operator. This is denoted diagrammatically in fig.(A11.7a) and the block diagram is showed in fig.(A11.7b).

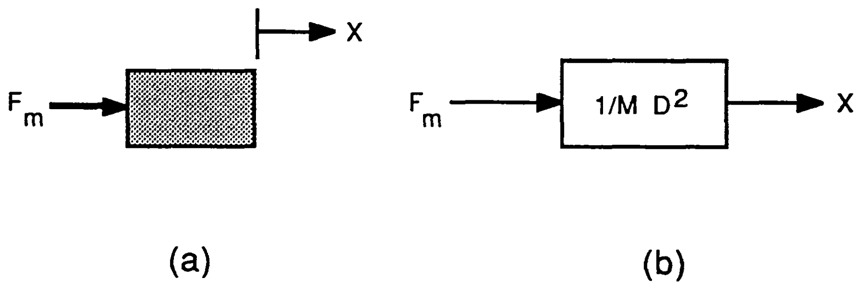

Figure A11.7 Inertial characteristics of an accelerating mass

Fig.(A11.8a) shows a combination system of mass, spring and damper. Using Newton's second law of motion the forces acting on the mass are:

$$F = F_m + F_d + F_s \qquad \text{(A11.5)}$$

$$F = m\ D^2X + B\ DX + K\ X \qquad \text{(A11.6)}$$

$$F = (\ m\ D^2 + B\ D + K\ )\ X \qquad \text{(A11.7)}$$

In this system the input is F and the output is the displacement X fig.(A11.8b). The system has been described by a second-order linear differential equation.

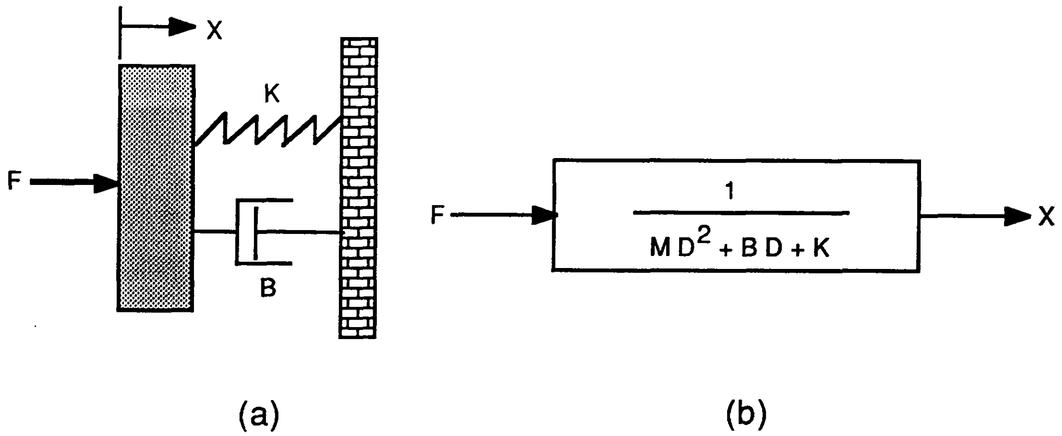

Figure A11.8 Mass-spring-damper combination

Similarly, electrical components such as resistors, inductors and capacitors (RLC) may be similarly represented. These are the three basic components of electric circuits. The voltage drops V_R across a resistor fig.(A11.9a) is :

$$V_R = R\ I \qquad (A11.8)$$

Where R is the resistance in ohm and I is the current flowing through the resistor in ampere. The block diagram is presented in fig.(A11.9b).

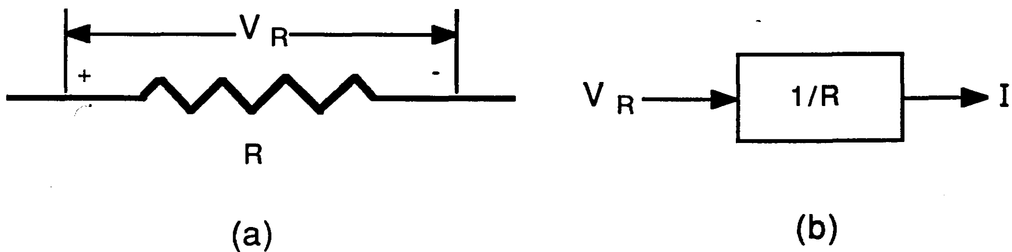

Figure A11.9 Representation of resistor

The voltage drop V_L for an inductor fig.(A11.10a) is :

$$V_L = L\ (dI/dt) = L\ DI \qquad (A11.9)$$

Where L is the inductance in henry and D is the time derivative operator. Fig.(A11.10b) is illustrated the block diagram of this element.

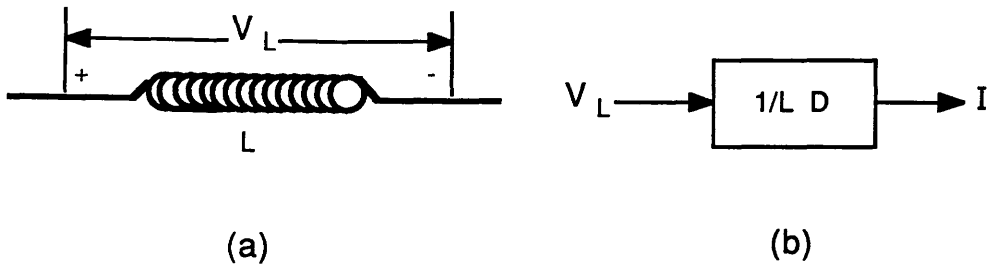

Figure A11.10 Representation of inductor

For a capacitor the voltage drop V_C across it is fig.(A11.11a) :

$$V_C = (1/CD)\ I \qquad (A11.10)$$

Where C is the capacitance in farads.

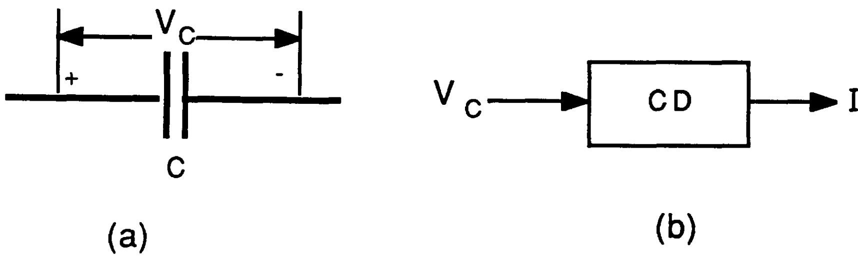

Figure A11.11 Representation of capacitor

For the series combination of (RLC) circuit fig.(A11.12a), the total voltage drop V is equal to the sum of the drop voltage across the inductor, resistor and capacitor.

$$V = V_L + V_R + V_C \qquad (A11.11)$$

$$= [\ L\ D\ I + R\ I + (1/C\ D)\ I\ ] \qquad (A11.12)$$

$$= [\ L\ D + R + (1/C\ D)\ ]\ I \qquad (A11.13)$$

The block diagram of the system is shown in fig.(A11.12b).

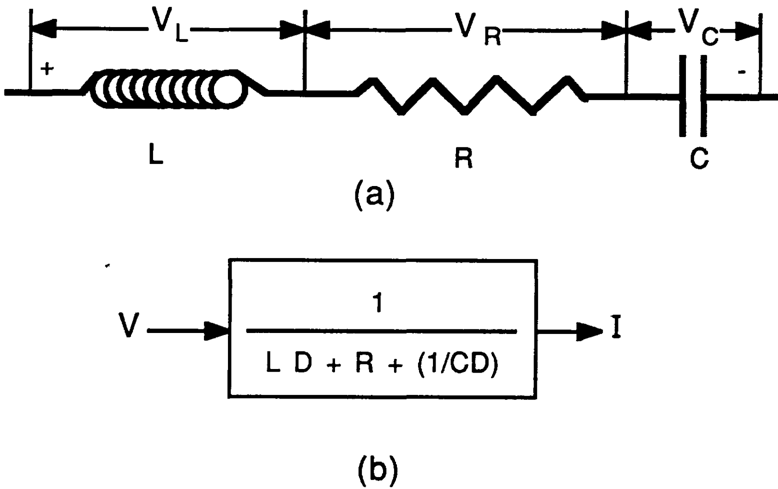

Figure A11.12 Resistor, inductor and capacitor series circuit

The charge Q is the time integral of current and it is equal to Ref.(57) :

$$Q = (1/D)\, I \quad \text{so} \quad I = Q\, D \tag{A11.14}$$

By substituting the eq.(A11.14) in the eq.(A11.13) the result is :

$$V = [\, L\, D^2 + R\, D + (1/C)\,]\, Q \tag{A11.15}$$

The block diagram of the circuit is illustrated in fig(A11.13).

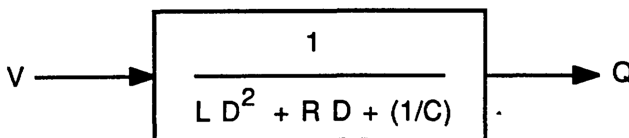

Figure A11.13 Block diagram of the charge Q for series RLC circuit

The mathematical representation of more complex systems which are connected in series or parallel, are presented in Ref.(56,57).

Transfer Function:

This is a method of mathematically describing components of a linear control system. The term linear means that the change in output is directly proportional to the change in input that caused it. The laplace transform method converts difficult differential and integral functions to equivalent algebraic functions presenting its operation as algebraic equations. A variable s or D is used to denote the mathematical derivative of a time dependent variable with respect to time. As a result functions which are variables of time like $F(t)$, $X(t)$ become functions of variable s. For more details see Ref.(4,55,56,57), useful laplace transforms for standard functions are presented widely.

Appendix (A12) Robotic Actuators:

Each type of actuator has its advantages and disadvantages. These need to be carefully considered with respect to the desired application.

Hydraulic actuation:

This utilizes a hydraulic fluid to generate a mechanical motion as an angular or linear output. Hydraulic power is supplied to the actuation system by a pump, which forces liquid (normally oil) into a ram. The liquid inside the cylinder by virtue of pressure applies a force on a piston, which in turn will exert a mechanical force. Fig.(A12.1) shows a simple hydraulic ram, (a double-action cylinder actuator). When a fluid under pressure is applied to port P and drainage is provided to port T the piston will extend. The opposite will occur if the fluid is directed to port T and drained from P. Rotary hydraulic actuators use the fluid to force a vane to produce a rotary movement.

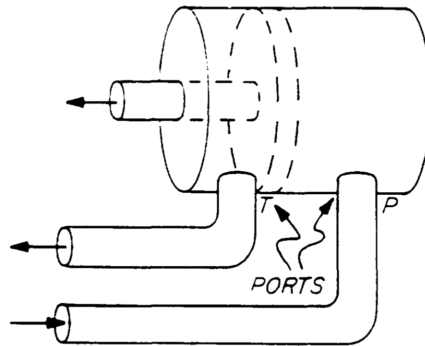

Figure A12.1 Double action hydraulic actuator Ref.(1)

Hydraulic actuators are particularly desirable in some robotics applications for of a number of unique advantages. Their ability to stall or hold their position without damage gives an advantage over some type of electrical actuator. Similarly, they can be quickly reversed at full load with consequent high accelerations. They are often preferred for driving large loads and can work in environments demanding spark free operation. On the other hand, they suffer from problems of leakage and in addition their drive units like their

pumps are expensive and noisy.

Pneumatic actuators:

These are similar to hydraulic actuators in principle, but make use of dried and filtered compressed air as their motive fluid. They are simple, clean and spark free, lightest in weight and often preferred in factories because of the availability of the compressed air. In contrast they are limited to relatively small payloads, have poor control due to compressibility effects and like hydraulic actuators their support devices, such as pumps are noisy and expensive.

Electrical Actuators:

These transduce electrical power into a mechanical movement. They are widely used in industrial robots. As they provide a fast, accurate actuation with excellent controllability. They are also relatively quiet in operation and easy to procure and replace. On the other hand, they often require a mechanical transmission system and brushes and other components need to be serviced due to wear and tear.

There are a variety of types of electrical actuators solenoid, DC servomotor, brushless DC motor, stepper motor and AC motors.

Appendix (A13) ACSL Control Program:

This appendix contains the ACSL control program, which was used to simulate the control system model, section (5.5).

```
PROGRAM POSITION
"******************"
"                                                                                  "
" This program was written and developed by Hussein Ali Abdullah during December  "
" 1987 and January 1988. It simulates a control circuit for the system design of a "
"  stand-off sensor for robotic systems, using ACSL language. Further details relating "
" to the program are given in the M.Sc. thesis of H. A. Abdullah, Mechanical      "
"  Engineering Department, Glasgow University, Glasgow G12 8QQ.                    "
"                                                                                  "
   "----------------------DEFINE PRESET VARIABLE"
      CONSTANT  Kc= 1.6 , Ks =1.0, ZSTEP=1.27 ...
          , TSTP =3.14 ,  Tm = 0.446 , B= 3.0 ...
          , TZ=0.02 , Ksol= 112.0 , R=48.625  ...
         , L =0.256
   CINTERVAL      CINT=0.02
   "------------------------FORCING FUNCTION"
   CC     = STEP(TZ)
   Xc     = CC*ZSTEP
   Xe     = Xc-X
   "------------------------MEASUREMENT DEVICE"
   PROCEDURAL (Ve=Xe,T,Xc,X)
   CALL SENSOR(Xe,T,XC,X,Ve)
   END $"OF PROCEDURAL"
   "------------------------CONTROLLER OUTPUT"
   Vc     = Ve * Kc
   "------------------------SOLENOID OUTPUT CURRENT"
   C      =L/R
```

```
    Isol    =(1/R)*REALPL(C, VC, 0.0)
    "--------------------------SOLENOID OUTPUT FORCE"
    F       = Ksol * Isol
    "--------------------------DEFINE ACTUATOR OUTPUT"
    A       = (Tm / Ks)
    E       = (B / Ks)
    X       = 1/Ks*CMPXPL (A, E, F, 0.0, 0.0)
TERMT (T.GT.TSTP)
END $ "OF PROGRAM"
```

Appendix (A14) **Gaussian Radiometric Subroutine for Control Simulation:**

This appendix contains the subroutine sensor, which is called by the ACSL program in the predicted performance of the system, section (5.5).

```
      SUBROUTINE SENSOR (ZED2,TIME,XC,X,VG)
C     ****************************************
C      GAUSSIAN AND RADIOMETRIC DESIGN
C     ************************************
C ******************************************************************
C        This subroutine was written and developed by Hussein Ali Abdullah, between
C        September and October 1987. It is called by the predicted modelling program
C        (program position) listed in appendix A13. It simulates an optical chain for a stand-
C        off sensor for use in robotic systems.The subroutine uses  gaussian beam theory
C        for the progress of a laser beam to the point where it is reflected from a workpiece
C        surface. Geometrical optics and radiometric theory is then used to model the
C        interaction of the reflected beam with two photodiodes. Further details relating to
C        the subroutine are given in the M.Sc. thesis of  H.A.Abdullah "Mechanical
C        Engineering Department,Glasgow University, Glasgow G12 8QQ".
C ******************************************************************

      REAL  INTST,MAG1,MAG2,MAG3,LNRAD1,LNRAD2,LNRAD3,MPN1,
     1          MPN2
      CHARACTER*40 TITLEL,INDATA,OUTDATA,EXDATA
      IF(NTST.EQ.1) GOTO 999
 87   WRITE(6,*)'PLEASE INPUT THE NAME OF YOUR INPUT DATAFILE...'
      READ(5,100)INDATA
      IF (INDATA .EQ. ' ') GOTO 87
C 88 WRITE(6,*)'PLEASE SUPPLY THE NAME OF OUTPUT DATAFILE ...'
C   READ(5,100)OUTDATA
C   IF (OUTDATA .EQ. ' ') GOTO 88
      100  FORMAT (A)
C     ******************************************************************
C     Read input variables from**data file**
C     Read from **UNIT=15**
C     ******************************************************************
      OPEN(UNIT=15,FILE=INDATA,STATUS='OLD',ERR=90)
```

```
C     OPEN(UNIT=6,FILE=OUTDATA,STATUS='NEW',ERR=91)
      READ(15,*)WALEN
      READ(15,*)WSRAD1
      READ(15,*)POWR
      READ(15,*)FOCLL1
      READ(15,*)FOCLL3
      READ(15,*)LNRAD1
      READ(15,*)LNRAD3
      READ(15,*)FOCLDS
      READ(15,*)PNRAD
      READ(15,*)ZEDPN1
      READ(15,*)ZEDPN2
      READ(15,*)SENSPH
      READ(15,*)DIS0
      READ(15,*)DIS1
      READ(15,*)ZED0
      READ(15,*)ZED1
      READ(15,*)RESOL
      READ(15,*)REFLCT
      READ(15,*)AMPLI
      READ(15,*)VREF
      READ(15,100)TITLEL
C     ******************************************************************
C     *                    *** MAIN CALCULATION ***                    *
C     ******************************************************************
      ******************************************************************
C     CALCULATE THE STAND-OFF DISTANCE,THE DISTANCE(DI3) BETWEEN
      THE SPOT ON THE SURFACE (WSRAD2)TO THE IMAGE OF THE MAIN
      LENS(L2), THE DISTANCE(ZD3) WHEN (ZED2=0).
C     ******************************************************************
      NTST=1
      PI=3.1415926
  999 RANG1=(PI*WSRAD1**2)/WALEN
      MAG1=FOCLL1/(SQRT((DIS1-FOCLL1)**2+RANG1**2))
      WSRAD2=MAG1*WSRAD1
      DIS2=FOCLL1+(MAG1**2*(DIS1-FOCLL1))
      BMRAD1=WSRAD1*SQRT(1+((0.318309*WALEN*DIS1)/(WSRAD1**2))**2)
      WS=WSRAD2*SQRT(1+((0.318309*WALEN*ZED2)/(WSRAD2**2))**2)
```

```
      POWR1=POWR*(1-(EXP(-2*(LNRAD1/BMRAD1)**2)))
      TE0=(0.632*POWR1)/(WS**2)
      TE1=TE0*REFLCT
      FOCLL2=FOCLL1
      LNRAD2=LNRAD1
      DISLEN=FOCLL2+FOCLL3+FOCLDS
      DI3=DIS2+2*ZED2
      ZD3=DIS2
C     ****************************************************************
C      ** CALCULATE THE POSITION OF THE REFERENCE BEAM WAIST Wref **
C     ****************************************************************

      D4=(1/FOCLL2)-(1/DI3)
      DI4=1/D4
      Z4=(1/FOCLL2)-(1/ZD3)
      ZD4=1/Z4
      TE1=TE0*REFLCT
      ZD5=DISLEN-ZD4
      DI5=DISLEN-DI4
      D6=(1/FOCLL3)-(1/DI5)
      DI6=1/D6
      Z6=(1/FOCLL3)-(1/ZD5)
      ZD6=1/Z6
      DP1=DI6+ZEDPN1
      DP2=DI6-ZEDPN2
C     ****************************************************************
C      CALCULATE THE PINHOLE'S IMAGE THROUGH THE LENSES L2 AND L3
C     ****************************************************************
      DP111=(1/FOCLL3)-(1/DP1)
      DP11=1/DP111
      DP211=(1/FOCLL3)-(1/DP2)
      DP21=1/DP211
      PM1=DP11/DP1
      PM2=DP21/DP2
      PN1=PM1*PNRAD
      PN2=PM2*PNRAD
      DP12=DISLEN-DP11
      DP22=DISLEN-DP21
```

```
      DP133=(1/FOCLL2)-(1/DP12)
      DP13=1/DP133
      DP233=(1/FOCLL2)-(1/DP22)
      DP23=1/DP233
C     *****************************************************************
C       *      CALCULATE THE SIZE AND POSITION OF THE PINHOLES        *
C         *         IMAGES IN FRONT OF THE WORKPIECE SURFACE          *
C     *****************************************************************
      PM12=DP13/DP12
      PM22=DP23/DP22
      PN11=PM12*PN1
      PN21=PM22*PN2
      PNAR=PI*PNRAD**2
      DP14=(DIS2+ZED2)-DP13
      DP24=(DIS2+ZED2)-DP23
      WSAR=PI*WS**2
C     *****************************************************************
C     ***CALCULATE THE OUTPUT VOLTAGE OF THE TWO PHOTODIODES ****
C     *****************************************************************
      TEE1=TE1
      TEE2=TE1
      EP11=PI*TEE1*PN11**2/(PN11**2+DP14**2)
      EP22=PI*TEE2*PN21**2/(PN21**2+DP24**2)
      EP1=(EP11)*PI*WS**2
      EP2=(EP22)*PI*WS**2
      VOLT1=EP1*AMPLI
      VOLT2=EP2*AMPLI
      VG=((VOLT1-VOLT2)/(VOLT1+VOLT2))*VREF
       RETURN
C     *****************************************************************
C     *                 - END OF MAIN CACULATION -                    *
C     *****************************************************************
 90   WRITE(5,*)'UNABLE TO OPEN INDATA FILE'
      STOP
C 91  WRITE(5,*)'UNABLE TO OPEN OUTPUTDAT FILE'
C     STOP
      END
```

REFERENCES

REFERENCES

1. Burns JR. W. C. and Worthington J. E., "Practical robotics systems,interfacing and applications", 1986, Prentice-Hall, Englewood Cliffs.

2. Hall E. L. and Hall B. C., " Robotics a user-friendly introduction", 1985, CBS College Publishing, Holt, Rinehart and Winston.

3. Groover M. P., Weiss M., Nagle R. N. and Odrey N. G., " Industrial Robotics technology, programming and applications, 1986, McGraw-Hill, Inc.

4. Critchlow A. J., "Introduction to robotics", 1985, Macmillan Publishing Company.

5. Todd D. J., "Fundamentals of robot technology (an introduction to industrial robots, teleoperators and robot vehicles)", 1986, Kogan Page Ltd.

6. Nitzan D., "Assessment of robotic sensors", Proc. robot vision and sensory control, 1981, pp.1, Stratford-Upon-Avon, United Kingdom.

7. Nitzan D., Barrouil C., Cheeseman P. and Smith R., "Use of sensors in robot systems", International conference on advanced robotics (ICAR), Sept. 1983, pp. 123, Tokyo, Japan.

8. Fu K. S., Gonzales R. C. and Lee C.S.G., "Robotics: control, sensing, vision and intelligence", 1987, McGraw-Hill, Inc.

9. Rosen C.A. and Nitzan D., "Use of sensors in programmable automation", Computer, December 1977, pp. 12.

10. Coiffet P. and Chirouze M., "An introduction to robot technology", First published 1982, Hermes Publishing (France), English language edition first published 1983, Kogan Page Ltd.

11. Lane J.D., "robotic welding", 1987, IFS (Publication) Ltd.

pp. 157- Porsander T. and Sthen T., "An adaptive torch positioner system".

pp. 167- Bjorkelund M., "A true seam-tracker for arc welding".

12. Shoham M., Fainman Y. and Lenz E., " An optical sensor for real-time positioning, tracking and teaching of industrial robots", IEEE Transactions on Industrial Electronics, Vol. IE-31, No. 2, May 1984, pp. 159.

13. Kanade T. and Sommer T. M., "An optical proximity sensor for measuring surface position and orientation for robot manipulation", Proc. SPIE Int. Soc. Opt. Eng., Vol 449, no. 2, 1984, pp. 667.

14. Kino G. S., Corle T. R., Hobbs P.C.D. and Xiao G. Q., "Optical sensors for range and depth measurement", Proceeding of the 5th international congress on applications of lasers and electro-optics, ICALEO 86, edited by Penney C. M. and Caulfield H. J., 10-13 November 1986, pp. 93, Virginia.

15. Sibayama K., Kubo M. and Itani K., "Sensory characteristics of the 'Melcut 3DCM'", Laser welding, machining and materials processing, 11-14 November 1985, pp. 113 , San Francisco.

16. Anderson R. P., Carr M. F. and Grieve R. J., "Feasibility study into use of laser scanning measuring device and robot as flexible inspection station", Advance in manufacturing technology (proceedings of the first national conference on production research), edited by McGoldrick P.F., September 1985, pp. 270, Kogan Page Ltd.

17. Vavreck A. N. and Watson H. E., "An intelligent robotic inspection system (IRIS), Proceeding of the 5th international congress on applications of lasers and electro-optics, ICALEO 86, edit by Penney C. M. and Caulfield H. J., 10-13 November 1986, pp. 111 , Virginia.

18. Molesini G., Pedrini G., Poggi P. and Quercioli F., " Focus-wavelength encoded optical profilometer", Optics Communication, Vol. 49, No. 4, March 1984, pp. 229.

19. Simon J., "New noncontact devices for measuring small microdisplacments", Applied Optics, Vol. 9, No.10, October 1970, pp.2337.

20. Fainman Y., Lenz E. and Shamir J., "Optical profilometer: a new method for high sensitivity and wide dynamic range", Applied Optics, Vol.21, No.17, September 1982, pp. 3200.

21. Dobosz M., "Optical profilometer: a practical approximate method of analysis", Applied Optics, Vol. 22, No. 24, December 1983, pp. 3983.

22. Kleinknecht H. P. and Meier H., "Optical profilometer for measuring surface contours of 1 to 150 microns depth", RCA Review, Vol. 46, No.1, March 1985, pp. 34.

23. Arecchi F. T., Bertani D. and Ciliberto S., "A fast versatile optical profilometer", Optics Communications, Vol. 31, No. 3, December 1979, pp. 263.

24. Whitefield R. J., "Noncontact optical profilometer", Applied Optics, Vol. 14, No. 10, October 1975, pp. 2480.

25. Cohen D. K., Gee W. H., Ludeke M. and Lewkowicz J., "Automatic focus control: the astigmatic lens approach", Applied Optics, Vol. 23, No. 4, February 1984, pp. 565.

26. Lee W. H., "Optical technology for compact disk pickups (disk players use quadrant detectors to maintain optical alignment)", Laser and Optronics, September 1987, pp. 85.

27. Quercioli F., Tiribilli B. and Molesini G., "Optical surface profile tranducers", Vol. 27, No. 2, 1988, pp. 135

28. Bertani D., Cetica M. and Ciliberto S., "A fast optical profilometer", Optics Communications, Vol. 46, No.1, June 1983, pp.1.

29. Melles Griot, "Optics Guide 3", pp.339.

30. Hitz C. B., "Review of laser modes", Laser and applications, November 1985, pp.79.

31. Stijns E., "Some nomographs for gaussian beams", Applied Optics, Vol.18, No.16, August 1979, pp.2827.

32. Dickson L. D., "Characteristics of a propagating gaussian beam", Applied Optics,Vol. 9,No. 8, August 1970, pp.1854.

33. Self S. A., "Focusing of spherical gaussian beams", Applied Optics, Vol. 22, No. 5, March 1983, pp.658.

34. O'Shea D. C., "Elements of modern optical design", 1985, John Wiely and Sons, Inc.

35. Herman R. M., Pardo J. and Wiggins T. A., "Diffraction and focusing of gaussian beams", Applied Optics,Vol. 24,No. 9, May 1985, pp.1346.

36. James T.,Parker D. E. and Karkheck J., "Waist location and rayleigh range for higher-order mode laser beams", Applied Optics, Vol. 23, No.13, July 1984, pp. 2088.

37. Marcuse D., "Light transmission optics", Bell laboratories series, chapter 6, 1972, Van Nostrand Reinhold Company.

38. Kogelnik H. and Li T., "Laser beams and resonators",Proceedings of the IEEE Journal, Vol. 54, No.10, October 1966, pp.1312.

39.Kogelnik H., "Imaging of optical modes-resonators with internal lenses", Bell System Technical Journal, Vol. 44, March 1965, pp.455.

40. Chu .T.S, "Geometrical representation of gaussian beam propagation", Bell System Technical Journal, Vol. 45, February 1966, pp. 287.

41. Kogelnik H., "Matching of optical modes", Bell System Technical Journal, Vol. 43, January 1964, pp.334.

42. Levi L., "Applied optics", "A guide to optical system design", Vol. 1, 1968, John Wily and Sons, Inc.

43. Kingslake R., "Applied Optics and Optical Engineering", Volume I, chapter 1, Teele R. P.,1965, Academic press Inc. (London) LTD.

44. Klein M.V., "Optics", 1970, John Wiley and Sons, Inc.

45. Meyer-Arendt J. R., " Introduction to Classical and Modern Optics", 1972, Prentice-Hall INC., Englewood Cliffs, N.J.

46. Thoms JR. W., "SPSE Handbook of photographic science and engineering", section 2 (Radiometry and Photometry), 1973, John Wiley and Sons, Inc

47. Young M., "Optics and Lasers", Second edition, 1984, Springer-verlag Berlin Heidelberg.

48. Shortley G. and Williams D., "Principles of College Physics", 1959, Prentice-Hall, INC., Englewood Cliffs, N.J.

49. Fox A. G. and Li T., "Resonant modes in a maser interferometer", Bell System Technical Journal, Vol. 40, March 1961, pp. 453.

50. Kogelnik H. and Rigrod W. W.,"Visual display of isolated optical resonator modes",Proceeding IRE,Vol. 50, February 1962, pp.220.

51. Boyd G. D. and Kogelnik H., "Generalized confocal resonator theory", Bell System Technical Journal, Vol. 41, July 1962, pp.1347.

52. Kogelnik H., "On the propagation of gaussian beams of light through lenslike media including those with a loss or gain variation", Applied Optics, Vol. 4, No.12, December 1965, pp.1562.

53. Hull D. M. and Stewart A., "Laser beam profiles-principles and definitions", Laser and applications, October 1985, pp.75.

54. Jenkins F. A. and White H. E., "Fundamentals of optics", Fourth edition, 1981, McGraw-Hill Book Company Japan, Ltd.

55. Dorf R. C., "Modern control systems", 1970, Addison-Wesly Publishing Company, Inc.

56. Shinners S. M., "Modern control system theory and application", Second edition, 1978, Addison-Wesly Publishing Company, Inc.

57. Raven F. H., "Automatic control engineering", Third edition, 1978, McGraw-Hill International Book Company, Inc.

58. Nelkon M. and Parker P., "Advanced level physics", Third edition, 1971, Heinemann Educational Books Ltd.